An investigation into the roles of Talpid3 and primary cilia in the developing brain

Bashford, Andrew

Award date:
2015

Awarding institution:
University of Bath

An investigation into the roles of *Talpid3* and primary cilia in the developing brain

Volume 1 of 3

Andrew Luke Bashford

A thesis submitted for the degree of Doctor of Philosophy

University of Bath

Department of Biology and Biochemistry

May 2015

Table of Contents

Page

List of figures

List of tables

Acknowledgements

I wish to express my sincere thanks my supervisors Dr Vasanta Subramanian and Professor Ravi Acharya. Without their hard work, guidance and patience this project would not have been possible. The research was funded by a Doctoral Training Grant provided by the Medical Research Council and I am grateful for the opportunity to complete this work at the University of Bath. I would like to extend my thanks to all of the support staff in the Department of Biology and Biochemistry, especially those involved in the animal housing facility. I am grateful for their kindness and commitment to ensuring the best possible standards of animal welfare.

My time in the laboratory was made considerably more enjoyable thanks to the support and friendship of all lab members past and present. Special thanks go to Ross Ferguson, Paul Sazinas, Eleni Serafeimidou-Pouliou, Alexandra Webster, Jacintha Sugnaseelan, Antje Kuhrs and all of the undergraduate project students who have joined us along the way. Particular thanks go to Ross for his constant advice, help and unending patience. In addition, I am very grateful for the kind contributions of work included in this project from both Ross and project student Fay Stafford.

Finally, very special thanks go to my family and friends for their continuous support, encouragement and always helping me to maintain a positive frame of mind.

Dedication

For Liz,

without whose love and encouragement

this work would never have been possible.

Abstract

The developing brain requires an intricate network of signals to direct proliferation, differentiation and cell fate decisions. Primary cilia are vital organelles with an emerging role regulating several major signalling cascades, in particular the Hedgehog pathway. Talpid3 (Ta3) is 166.7 kD protein found at the distal tip of centrioles. It has been shown to interact with a number of key centriolar proteins and is essential for the formation of primary cilia. A recent mouse model has been designed to conditionally target the highly conserved coiled-coil domain of *Ta3* using the Cre/loxP system.

This project uncovers the role of Ta3 in the developing brain. It characterises in detail the phenotype of mice with conditional loss of *Ta3* in the central nervous system using the *Nestin-Cre* deleter strain. Morphological and histological analyses demonstrate that significant defects occur postnatally with mice developing severe ataxia and hydrocephaly. Immunohistochemical techniques further characterise the distinct phenotypes of three key brain regions including the cerebellum, cortex and hippocampus. $Ta3^{fl/fl;NesCre}$ mutant mice exhibit defects in the proliferation, organisation, morphology and migration of both neuronal and glial cells. We have shown the mechanistic cause to be the result of widespread loss of primary cilia and a concomitant disruption in the transduction of the Hedgehog signalling pathway.

The neural roles of Ta3 are explored further through the optimisation of an *in vitro* neurosphere system to culture postnatal hippocampal progenitors. The use of a tamoxifen inducible strain allows the timely recombination of *Ta3* to study its role in a controlled environment. The cultured cells recapitulate many of the *in vivo* defects showing loss of primary cilia and reduced migration.

Finally, characterisation of the phenotypes seen in the $Ta3^{fl/fl;NesCre}$ mice were shown to resemble neurological traits seen in human conditions with loss of Primary cilia, known as 'human ciliopathies'. Through clinical collaboration this project demonstrated a human ciliopathy case of Joubert Syndrome with compound heterozygous mutations in *TA3*. This presents the $Ta3^{fl/fl;NesCre}$ mutant mice as a valuable model system to study a rare but clinically relevant condition.

Abbreviations

(4-IPBA)	4-iodophenylboronic acid
(4OHT)	4-hydroxytamoxifen
(4V)	fourth ventricle
(ACIII)	adenylyl cyclase III
(Arl13b)	ADP-ribosylation factor-like protein 13b
(BCA)	bicinchoninic acid
(BMP)	bone morphogenetic protein
(bp)	base pairs
(BrdU)	bromodeoxyuridine
(BSA)	bovine serum albumin
(Cb)	cerebellum
(CC)	corpus callosum
(cDNA)	complementary DNA
(Cep)	centrosomal protein
(CPu)	caudate putamen
(Ctip2)	COUP-TF1 interacting protein 2
(Cux1)	homeobox protein cut-like 1
(Cx)	cortex
(DABCO)	1,4-Diazobicyclo-(2,2,2)-octane
(DAPI)	4',6-Diamidino-2-Phenylindole
(DAPT)	N-(N-(3,5-Difluorophenacetyl-L-alanly))-S-phenylglycine-t-Butyl Ester
(DEPC)	Diethylpyrocarbonate
(DG)	dentate gyrus
(DMEM)	Dulbecco's Modified Eagle Medium
(DMEM/F-12)	Dulbecco's Modified Eagle Medium:Nutrient Mixture F-12 (1:1)
(DMSO)	dimethyl sulfoxide
(DNA)	deoxyribonucleic acid
(DSCP)	decussation of the superior cerebellar peduncles
(E18.5)	refers to embryonic stages (e.g. embryonic day 18.5 = E18.5)
(ECL)	enhanced chemiluminescent
(EDTA)	ethylenediaminetetraacetic acid
(EGL)	external granule layer
(Ent)	entorhinal cortex
(FGF)	fibroblast growth factor
(fl)	flox
(g/c)	guanine/cytosine
(GAPDH)	glyceraldehyde 3-phosphate dehydrogenase
(GCL)	granule cell layer
(gDNA)	genomic DNA
(GEF)	guanine nucleotide exchange factor
(GNP)	granule neuron precursor

(HC)	hippocampal commissure
(hEGF)	human epidermal growth factor
(hFGF)	human fibroblast growth factor
(HRP)	horseradish peroxidase
(IC)	internal capsule
(IFT)	intraflagellar transport
(IGL)	internal granule layer
(JS)	Joubert syndrome
(Ki67)	marker of proliferation MKi-67
(Kif3a)	kinesin family members 3a
(LAS)	Leica Application Suite
(LSD)	lateral septal nuclei (dorsal)
(LV)	lateral ventricle
(MCM2)	mini-chromosome maintenance protein 2
(mEGF)	mouse epidermal growth factor
(MKS)	Meckel-Gruber Syndrome
(ML)	molecular layer
(NCBI)	National Center for Biotechnology Information
(NeuN)	neuronal nuclei
(OCT)	Optimal Cutting Temperature
(P5)	postnatal stage 5
(PaS)	parasubiculum
(Pax6)	paired box protein 6
(PBS)	phosphate buffer saline
(PBST)	PBS + Tween-20 (0.1%, v/v)
(PC)	Purkinje cell
(PCL)	Purkinje cell layer
(PCM1)	pericentriolar material 1
(PCNA)	proliferating cell nuclear antigen
(PCR)	polymerase chain reaction
(Pen-Strep)	penicillin + steptomycin antibiotic
(PFA)	paraformaldehyde
(PH3)	phospho-histone-3
(PrS)	presubiculum
(PVDF)	polyvinylidene fluoride
(qPCR)	quantitative PCR
(R1)	rhombomere 1
(Rf)	relative mobility
(RGC)	radial glial cell
(RMS)	rostral migratory stream
(RNA)	ribonucleic acid
(ROI)	region of interest
(RQI)	RNA quality indicator score
(rRNA)	ribosomal RNA

(RT)	reverse transcriptase
(Satb2)	special AT-rich sequence-binding protein 2
(SDS)	sodium dodecyl sulphate
(SDS-PAGE)	sodium dodecyl sulphate polyacrylamide gel electrophoresis
(SGZ)	subgranular zone
(Shh)	sonic hedgehog
(SVZ)	subventricular zone
(Ta3)	talpid3
(TBE)	tris-Borate EDTA buffer
(Tbr1)	T-box brain protein 1
(TE)	tris-HCl EDTA buffer
(TEM)	transmission electron microscopy
(TEMED)	tetramethylethylenediamine
(Tris)	tris(hydroxymethyl)aminomethane
(wt)	wild type

Chapter 1 – Introduction

Talpid3 (Ta3) is an important centrosomal protein shown to be essential in the formation of primary cilia and motile cilia. Primary cilia are unique organelles able to transduce a variety of cellular signals and are especially important in brain development. Lack of cilia or loss of their function can result in a number of clinical conditions known collectively as 'ciliopathies'. In order to discuss the role of Ta3 in a meaningful context, here I review the current literature on centrosomal and cilia biology. This is followed by the role of primary cilia in signal transduction and their contribution to brain development.

1.1 The Structure and Formation of Primary Cilia

Primary cilia are highly conserved sensory organelles which protrude from the cell surface like an antenna. They are non-motile structures and have an axoneme made of microtubules. These microtubules are arranged in nine pairs to form a cylinder, named the "9+0" arrangement (Fig. 1.1a). Motile cilia are different and have "9+2" arrangement with an additional microtubule pair in the centre. The basal body is found at the base of primary cilia and it acts as a microtubule organising centre coordinating the movements of numerous proteins to and from the cilium (Fig 1.1a). Motor proteins facilitate this movement and enable primary cilia to act as dynamic structures and adapt in response to cellular changes. In addition, the primary cilium acts as a specialised compartment with a unique environment and the presence of transmembrane receptors allows it to transduce extracellular signals.

1.1.1 Key steps in cilia formation

Early reports described the occurrence of cilia throughout the cell cycle with the exception of mitosis (Dingeman, 1969, Fonte et al., 1971), suggesting they are actively assembled and disassembled in response to mitotic signals. The formation of primary cilia is complex. However, elegant transmission electron microscopy (TEM) studies first describing the sequence of events in detail have stood the test of time and the terminology is still used today (Sorokin, 1962). In recent years renewed interest in primary cilia has led to the

identification of numerous molecular components and we are beginning to unravel the molecular events required for their construction.

The starting point for the formation of primary cilia is the basal body. The centrosome forms the core of the basal body and it consists of a mother and a daughter centriole. In the formation of primary cilia the basal body matures and becomes surrounded by specialized proteins which attach directly to the centrioles or nearby as satellite structures. In the process of maturation the centrioles also move towards the edge of the cell and the mother centriole associates with the plasma membrane in a process known as 'docking'. Three major features acquired by the membrane-associated mother centriole are the rootlets, basal feet and transition fibres; the last of which act as connections to anchor the centriole and plasma membrane (Anderson, 1972) (Fig 1.1a). During the process of docking, whilst the basal body is at the edge of the cell but before it becomes fully associated with the plasma membrane, small vesicles originating from the Golgi apparatus are recruited to the distal tip of the mother centriole. These vesicles are said to 'dock' with the mother centriole and the vesicles fuse to form a cap known as the ciliary vesicle (Fig 1.1b). Microtubules begin to extend from the centriole and invaginate the vesicle into a mushroom shape, known as the ciliary bud. The microtubules continue to elongate forming a shaft and the lengthening vesicle thins to form the ciliary sheath. Eventually the ciliary sheath fuses with the plasma membrane allowing the primary cilium to extrude from the cell covered in the ciliary membrane (Sorokin, 1962) (Fig 1.1b). Cilia continue to elongate and become highly specialised with proteins trafficking along the microtubules and transmembrane proteins become embedded in the ciliary membrane.

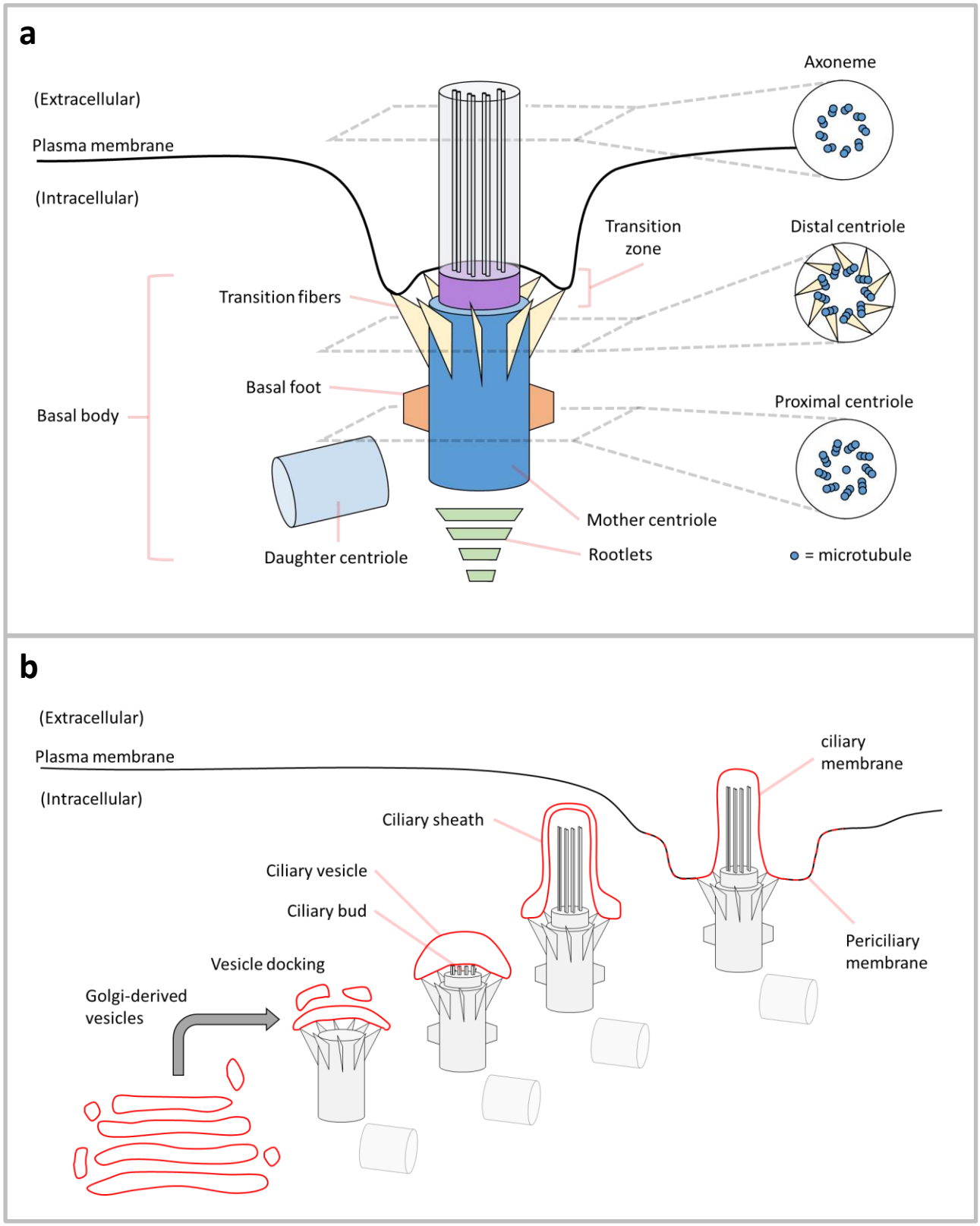

Figure 1.1 Structure and formation of primary cilia. a) Schematic of structural components of the primary cilia. Dashed grey lines indicate point of cross section indicated on right. Image adapted from (Bettencourt-Dias et al., 2005). b) Schematic illustration of primary cilia formation. Golgi-derived vesicles dock with distal appendages to form the ciliary vesicle and begin axonemal elongation. The ciliary sheath surrounding the growing axoneme fuses with the plasma membrane to form the primary cilium

1.1.2 The basal body and its maturation

Centrioles are short cylindrical structures and their core is formed from triplets of microtubules (Fig 1.1a). They contain γ-tubulin which is required for nucleation of repeat dimers of α- and β-tubulin which subsequently polymerise to form microtubules. γ-tubulin is also found in satellite structures surrounding the centrosome and acts to nucleate additional microtubules which extend throughout the cell. Motor proteins such as dynein and kinesin are able to transport cargo along microtubules enabling the basal body to function as a well-connected hub for vesicular protein trafficking.

Vesicles which are trafficked to the primary cilia first arrive at centriolar satellites where they associate with proteins such as pericentrin and pericentriolar material 1 (PCM1) (Dammermann and Merdes, 2002). Both pericentrin and PCM1 interact with a number of trafficking proteins and an interaction of significance is between PCM1 and Bardet-Biedl syndrome protein 4 (BBS4). BBS4 is part of a large protein family which form a multi-protein complex called the 'BBSome'. The BBSome is thought to coat vesicles destined for the primary cilium (Jin et al., 2010). Trafficking of ciliary vesicles requires the Rab GTPase, Rab8, and its guanine nucleotide exchange factor (GEF) Rabin8 (Nachury et al., 2007, Yoshimura et al., 2007). Together the BBSome and Rab proteins help define the membrane identity and enable the correct trafficking of ciliary vesicles; they are therefore essential components in cilia formation.

As part of their trafficking role, both Rab8a and Rabin8 have been shown to interact with a number of basal body proteins; two of note are the centrosomal protein of 164 kDa (Cep164) and Cep290 (Schmidt et al., 2012, Tsang et al., 2008). Cep164 has been shown by immuno-electron microscopy to localise as a ring around the distal tip of the mother centriole (Graser et al., 2007). It is thought to have a role in the docking of vesicles and their membrane attachment, working in cooperation with other proteins such as Cep83/CCDC41 (Joo et al., 2013), sodium channel and clatherin linker 1 (SCLT1), Fas binding factor 1 (FBF1) (Tanos et al., 2013) and Cep89/CCDC123 (Tanos et al., 2013, Sillibourne et al., 2011). In addition to this, Cep164 has a dual role in the formation of the ciliary bud due to its ability to recruit tau tubulin kinase 2 (TTBK2) to the distal centriole (Cajanek and Nigg, 2014).

TTBK2 has been proposed as a key initiator for microtubule growth by removing the inhibitory capping protein, CP110 (Goetz et al., 2012). Precocious microtubule elongation is prevented by the presence of CP110, which is recruited by the protein Cep97 (Spektor et al., 2007). Their localisation is facilitated by the protein Kif24 which is a kinesin motor and also has the ability to depolymerase centriolar-specific microtubules (Kobayashi et al., 2014). Another protein which interacts with the CP110 capping protein but has a role promoting cilia growth is Cep290 (Tsang et al., 2008).

Cep290 is present at centriolar satellites where it binds PCM-1 (Kim et al., 2008), Rab8a and has been shown to be essential for their centrosomal localisation (Tsang et al., 2008). Cep290 is also present at the distal centriole and, in addition to CP110, it binds the coiled-coil and C2 domains-containing protein 2A (CC2D2A) (Gorden et al., 2008) and nephrocystin-5 (NPHP5) (Schafer et al., 2009). Studies in *Chlamydomonas* have suggested that Cep290 acts as a gatekeeper present in the transition zone; regulating protein entry into the cilia axoneme (Craige et al., 2010, Betleja and Cole, 2010). Furthermore, recent data from Drivas et al (2013) demonstrates that the N- and C-terminal of Cep290 can bind the plasma membrane and microtubules respectively suggesting both a structural and regulatory role in the transition zone. Cep290 is able to interact with numerous binding partners and mutations can often exhibit pleiotropic effects. For this reason, Cep290 is a causative allele in many of the clinical conditions with disrupted primary cilia (Waters and Beales, 2011). The basal body is a complex structure with many interacting proteins, all of which are important for cilia formation and function. A summary of important centrosomal proteins relevant to this project are listed in Table 1.1.

Table 1.1 Summary of key centrosomal proteins

Ta3 interacting proteins are highlighted in bold.

Name (s)	Location	Binding partners	Known functions	References
PCM1	Pericentriolar matrix	Cep290, Disc1, BBS-4,	- Pericentriolar scaffold - Recruitment of centriolar proteins - Microtubule organisation	(Kamiya et al., 2008, Dammermann and Merdes, 2002, Kim et al., 2008)
Pericentrin	Pericentriolar matrix	γ-tubulin, Pericentrin, Protein Kinase A,	- Pericentriolar scaffold - Nucleate microtubules	(Doxsey et al., 1994)
Rab8	Pericentriolar matrix	Cep164, Cep290, **Ta3**	- GTPase required for vesicle trafficking to primary cilia	(Nachury et al., 2007)
Rabin8	Pericentriolar matrix	Cep164, Cep290, **Ta3**	- Guanine nucleotide exchange factor required to activate Rab8 - Required for vesicle trafficking to primary cilia	(Nachury et al., 2007)
Cep164	Distal centriole (mother), nuclear foci	TTBK2, Rabin8, CCDC92, Sclt1	- Recruitment of Ttbk2, Rab8, Rabin8 to centrosome - Function in the DNA damage response pathway	(Graser et al., 2007, Cajanek and Nigg, 2014, Schmidt et al., 2012, Chaki et al., 2012, Sillibourne et al., 2011)
TTBK2	Distal centriole (mother)	Cep164	- Initiator of cilia growth - Remove Cp110 - Phosphorylate and stabilise Cep164	(Goetz et al., 2012)
Cep83 (Ccdc41)	Distal centriole (mother), Golgi-complex	IFT20	- Recruitment of Cep164, Cep89, Sclt1, Ift120 to centrosome - Vesicle docking and membrane attachment	(Joo et al., 2013, Tanos et al., 2013)
Sclt1	Distal centriole (mother)	Fbf1, Cep164	- Recruitment of distal appendages Fbf1 and Cep164 - Docking of cilia vesicles and cilia formation	(Tanos et al., 2013)
Cep89 (Cep123, Ccdc123)	Distal centriole (mother)		- Docking of cilia vesicles and cilia formation	(Tanos et al., 2013, Sillibourne et al., 2011)
Fbf1	Distal centriole (mother)	Sclt1	- Docking of cilia vesicles and cilia formation	(Tanos et al., 2013)
Cp110 (Centriolin)	Distal/proximal centrioles	Cep97, Centrin, Calmodulin, Cep290, Cep76,	- Caps distal centrioles, supressing elongation and ciliogenesis	(Spektor et al., 2007, Chen et al., 2002, Tsang et al., 2008, Kobayashi

		Kif24, **Ta3**	- Role in centrosome duplication	et al., 2014)
Cep97	Distal centriole	CP110, **Ta3**	- recruits Cp110 to distal centriole - required to prevent precocious ciliogenesis	(Spektor et al., 2007)
Cep290 (Nphp6)	Distal centriole, pericentriolar matrix	CP110, Rab8a, CC2D2A, NPHP5, PCM1, **Ta3**, plasma membrane, microtubules	- Essential for cilia formation - Structural role in transition zone tethering membrane and microtubules - Gatekeeper controlling entry/exit of proteins in/out of the cilium	(Tsang et al., 2008, Craige et al., 2010, Kim et al., 2008)
Sas-6	Procentriole	SAS-6, Cep135	- Procentriole formation - Homodimers form a wheel to contact microtubules of centriolar barrel	(Dammermann and Merdes, 2002, Leidel et al., 2005)
Cpap (Cenpj)	Procentriole	Cep120, Cep135	- Procentriole formation	(Lin et al., 2013)
Plk4	Procentriole	Cep152	- Procentriole formation	(Habedanck et al., 2005, Bettencourt-Dias et al., 2005)
Cep120 (Ccdc100)	Procentrioles	Cep120, Cep290, Cep164, Ninein, **Ta3,** Microtubules,	- Centriole elongation - Role in Interkinetic nuclear migration	(Lin et al., 2013, Xie et al., 2007)
C2CD3 (Talpid2)	Procentrioles, pericentriolar matrix	OFD1	- Centriole elongation - Recruitment of TTBK2 - Distal appendage assembly	(Hoover et al., 2008, Thauvin-Robinet et al., 2014, Ye et al., 2014)
Talpid3	Distal centrioles (mother and daughter)	Cp110, Cep97, Kif24, Cep290, PCM1, Cep120, Rab8	- Docking of cilia vesicles to centrioles and cilia formation -Regulate level of Cep120 at daughter centriole	(Kobayashi et al., 2014, Wu et al., 2014, Bangs et al., 2011, Yin et al., 2009)

1.1.3 Motor proteins of the axoneme

The movement of proteins along microtubules is essential for the formation of primary cilia. Not only does it direct proteins to the basal body but also traffics them to the tip of the growing axoneme. Movement along the axoneme occurs by a process known as intraflagellar transport (IFT). This trafficking is also required to maintain the cilium as a specialised microenvironment and facilitate its role transducing extracellular signals. A summary of IFT components is shown in Figure 1.2.

Microtubules are polar structures and grow or shorten by the addition or removal of tubulin monomers at the 'plus end'. Anterograde transport towards the plus end of microtubules is facilitated by Kinesin-II motors which include kinesin family members 3a and 3b (Kif3a, Kif3b) and Kinesin associated protein 3 (KAP3) (Fig 1.2). IFT proteins form a complex with these motors called the 'IFT-B' particle and include IFT88, IFT172 and IFT20. Conversely, retrograde transport towards the minus end of microtubules is controlled by Dynein-II motors composed of the subunits dynein cytoplasmic 2 heavy chain 1 (DYNC2H1), dynein cytoplasmic 2 light intermediate chain (DYNC2LI1) and IFT proteins including IFT122 and IFT140 (Goetz and Anderson, 2010).

The tip of primary cilia, where these two mechanisms interact, also contains Kinesin-IV family proteins Kif7 and Kif27 (Fig 1.2) (He et al., 2014, Nozawa et al., 2013). All of these IFT proteins are important for growth and function of primary cilia. Loss of IFT function can result in altered structure and size of primary cilia for example; loss of Kif7 results in elongated cilia and faster depolymerisation under nocodazole treatment suggesting a role limiting growth and stabilising microtubules (He et al., 2014). Many IFT components, such as IFT88 of Kif3, are essential for formation of primary cilia and also motile cilia (Pazour et al., 2000, Takeda et al., 1999).

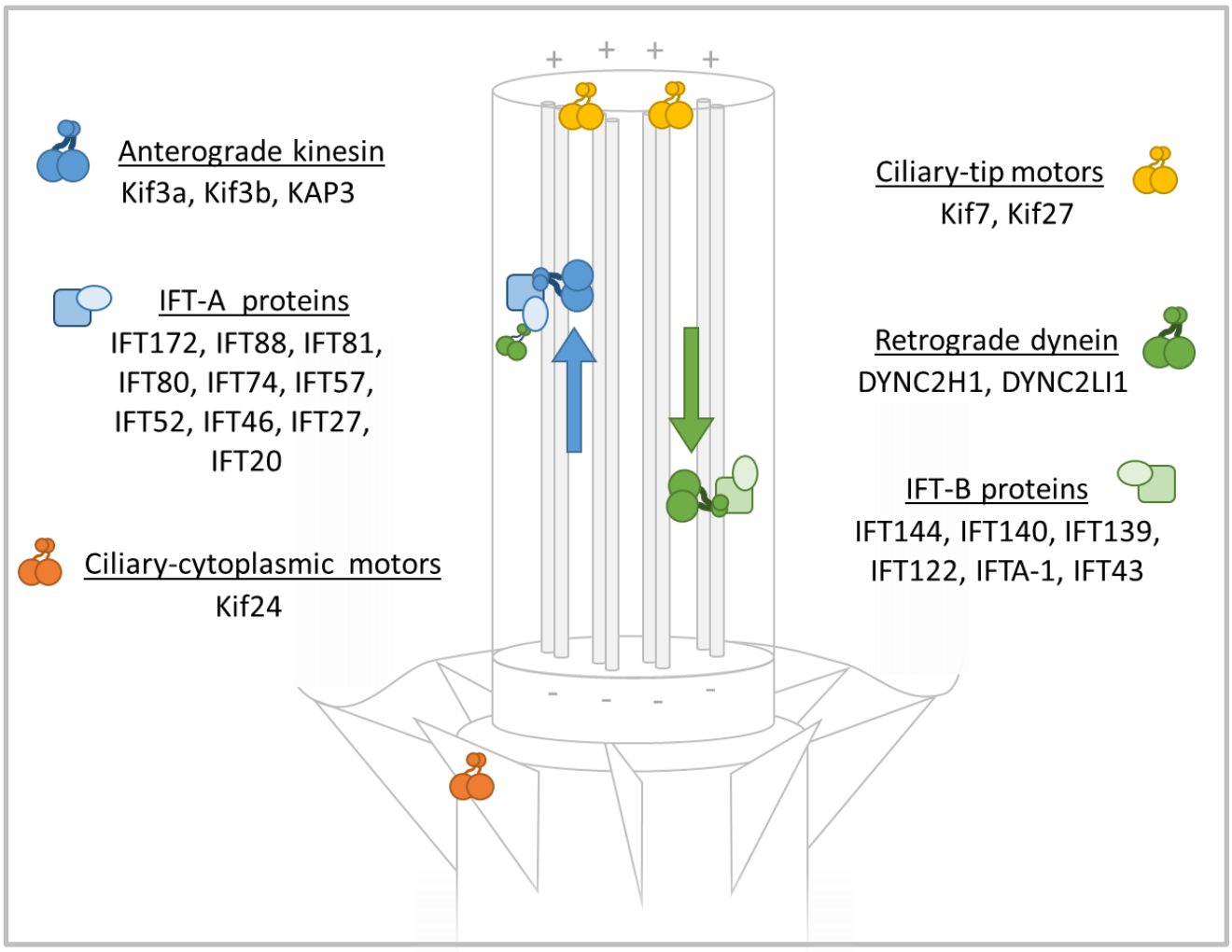

Figure 1.2 Intraflagellar transport proteins
Anterograde kinesin motors move towards the plus end and comprise of Kif3a, Kif3b and KAP3; these work alongside IFT-B proteins. Retrograde dynein motors move towards the minus end and comprise DYNCH2 and DYNC2LI1; these work alongside IFT-A proteins. Motors found at the ciliary tip include Kif7 and Kif27. Kif24 is required for the correct localisation of CP110. Image adapted from (Goetz and Anderson, 2010).

1.1.4 Cilia-independent functions of the centrosome

The centrosome forms the major microtubule organising centre in the cell (Rieder et al., 2001). In addition to their role in primary cilia, centrioles have a key function in the segregation of chromosomes during mitosis. Centrosomes begin to duplicate during the S-phase of the cell cycle when procentrioles form at the proximal end of both mother and daughter centrioles. In the G2-phase the procentrioles elongate, mature and during mitosis they migrate to polar ends of the cell. Here, the centrosomes act to nucleate and organise microtubules known as the mitotic spindles. They extend into the centre of the cell, attach to chromosomes and act to segregate them in the process of mitosis. Newly formed daughter cells each retain one of the centrosomes following cytokinesis. Only upon completion of mitosis and cytokinesis are the centrosomes free to mature into the basal body and form primary cilia; a process in actively cycling cells which can often be short-lived. Due to their sequential nature these processes are under tight regulation with centrosomal proteins functioning throughout the cell cycle.

The key steps in centriole biogenesis were elegantly described by Kleylein-Sohn et al (2007). Using systematic knockdown and immunoelectron microscopy they describe the sequence of events in the biogenesis of centrioles. Polo-like kinase 4 (Plk4) is first activated and localises at the presumptive procentriole. This is followed by recruitment of spindle assembly abnormal protein 6 (SAS-6), centrosomal protein 4.1-associated protein (CPAP), Cep135 and γ tubulin. Finally CP110 forms a cap on the distal procentriole tip, regulating the addition of α/β-tubulin to the elongating microtubules. The microtubules then become stabilised through polyglutamylation. Another protein shown to be present at procentrioles is C2 calcium-dependent domain containing protein 3 (C2CD3/Talpid2) (Thauvin-Robinet et al., 2014). Here it is thought to have role in centriole elongation and loss or disruption of this protein prevents further maturation having knock-on defects in basal body formation and ciliogenesis (Hoover et al., 2008). C2CD3 has also been shown to bind Oral-facial-digital syndrome 1 protein (OFD1) and the two partners thought to have antagonistic roles in regulating centriole length.

Cep120/Ccdc100 is another protein which is important for centriole elongation and it binds to microtubules and CPAP (Lin et al., 2013). The abundance of Cep120 protein increases throughout S- and G2-phase of the cell cycle but is dramatically reduced after

mitosis. A yeast two-hybrid screen predicted interactions of Cep120 with Cep290, Cep164, Ninein and transforming acidic coiled-coil (TACC) proteins (Xie et al., 2007). Interestingly, Xie and colleagues demonstrated that neuron precursors have particularly high levels of Cep120. They suggested that its interaction with TACC proteins has an important role in interkinetic nuclear migration (IKNM).

The process of IKNM is a phenomenon observed in neuroepithelia and is an oscillatory process where nuclei translocate in a basal-to-apical direction as cells prepare to undergo mitosis. A model proposed by Spear and Erickson (2012) suggests that prior to mitosis, motor proteins drive the nuclear movement along microtubules organised at the centrosome. At this stage, the centrosome is anchored at the apical membrane in its capacity as a basal body of the primary cilium. Once the nucleus has migrated, changes in cellular and nuclear shape occur through modifications in the actin cytoskeleton and at the G2- to M-phase transition of the cell cycle the cilium is deconstructed. This allows the centrioles to migrate, form the spindle poles and separate the chromosomes. This process neatly connects the primary cilium-dependent and independent roles of the centrosome and illustrates its importance throughout the cell cycle.

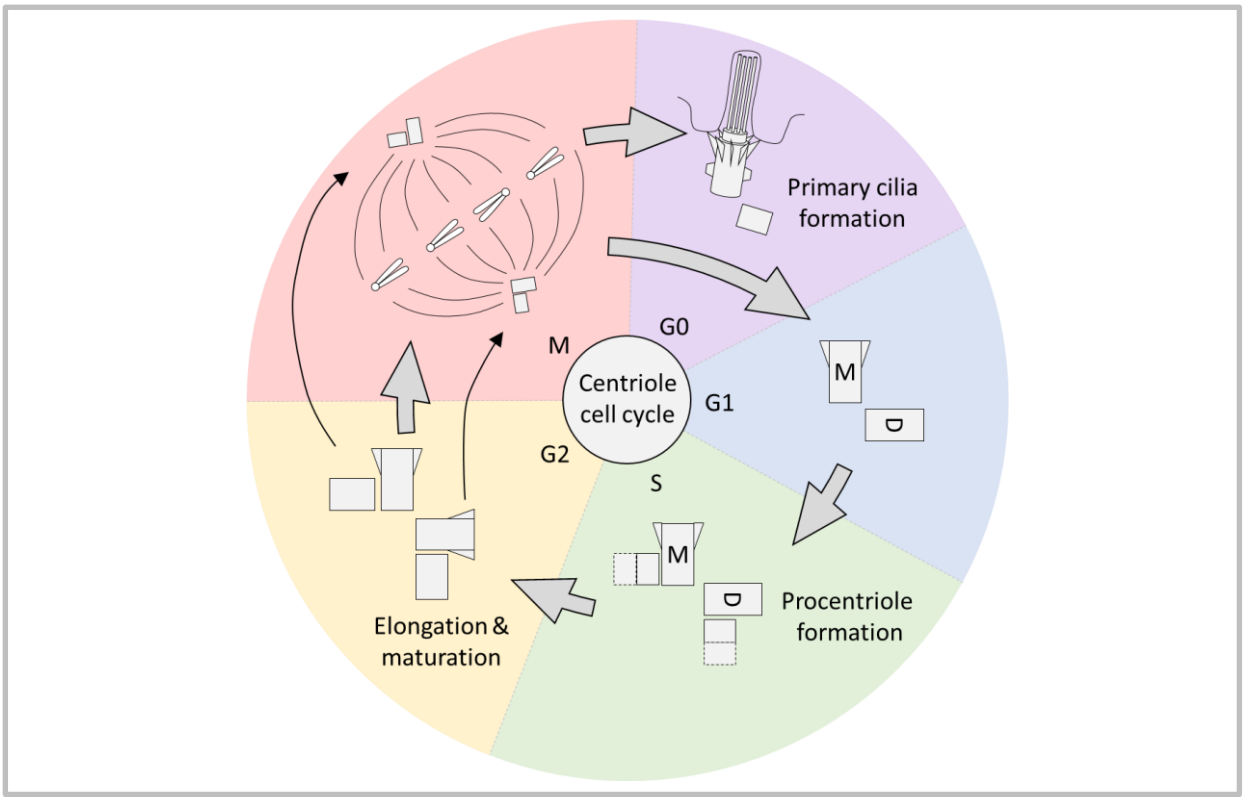

Figure 1.3 The centrosome cell cycle.
During S phase both mother and daughter centriole form procentrioles. During G2 the procentrioles elongate and mature and upon transition into Mitosis separate to form the spindle poles and separate chromosomes. In G0/G1 the centrioles are able to mature, form the basal body and form a primary cilium. Abbreviations: M, mother, D, daughter. Image adapted from (Nigg, 2002).

1.2 Talpid3

Given the complex range of centrosomal activities, identifying and understanding new proteins is essential to furthering our knowledge of centrosomal and primary cilia biology. One protein whose function is beginning to be unravelled is Ta3. It is essential for the formation of primary cilia (Yin et al., 2009) and has been shown to interact with a number of key basal body proteins (Kobayashi et al., 2014, Wu et al., 2014). This places Ta3 as an important protein with further investigation required to better understand its function.

1.2.1 Introduction to Talpid3

Ta3 is a centrosomal protein that was first identified through a lethal defect in a flock of chickens with reduced hatchability. Prominent features of the affected mutants were spade-shaped limbs likened to that of a mole (Talpa) (Fig 1.4a). The causative allele was named in sequence with similarly described mutants; *talpid*^{1} (Cole, 1942) and *talpid*^{2} (Abbott et al., 1960).

The *talpid*^{3} mutant chick has a distinct pleiotropic phenotype with midline facial defects, cyclopia (Ede and Kelly, 1964a), shortened limbs displaying polydactyly and a lack of cartilage-bone formation (Ede and Kelly, 1964b) (Fig 1.4a,b). Chick and mice with disruption of *Ta3* also have defects in the dorso-ventral specification of the neural tube (Davey et al., 2006, Bangs et al., 2011) (Fig 1.4c). Nearly all of these phenotypes have been attributed to defects in the Hedgehog (Hh) signalling pathway (Lewis et al., 1999) and the causative locus identified as *KIAA0586* (Davey et al., 2006). In mutant chicks the *Ta3* sequence was shown to have an insertional mutation resulting in a premature stop codon nine residues later and a truncated protein of 366aa compared to the wild type 1524aa (Davey et al., 2006). Ultrastructural studies in the neural tube later demonstrated that the truncated protein results in a loss of primary cilia. The basal body appeared to mature and migrate towards the apical membrane but failed to dock or properly orientate itself (Yin et al., 2009). This was confirmed in the mouse where loss of functional Ta3 was also shown to prevent docking of the basal body with the apical membrane resulting in a loss of primary cilia (Bangs et al., 2011). More specifically, detailed studies using cultured human cells have

suggested that the docking process is interrupted at the point where small intracellular vesicles dock with the distal tip of the mother centriole (Kobayashi et al., 2014). Although some vesicles were seen to attach at the mother centriole their fusion to form the capping ciliary vesicle was absent. This prevented further growth of the ciliary vesicle or attachment with the plasma membrane resulting in a failure of cilia formation. Although this most recent study used siRNA and achieved 70-90% knockdown of Ta3 protein it provided an excellent indication to the exact point at which Ta3 acts in cilia formation.

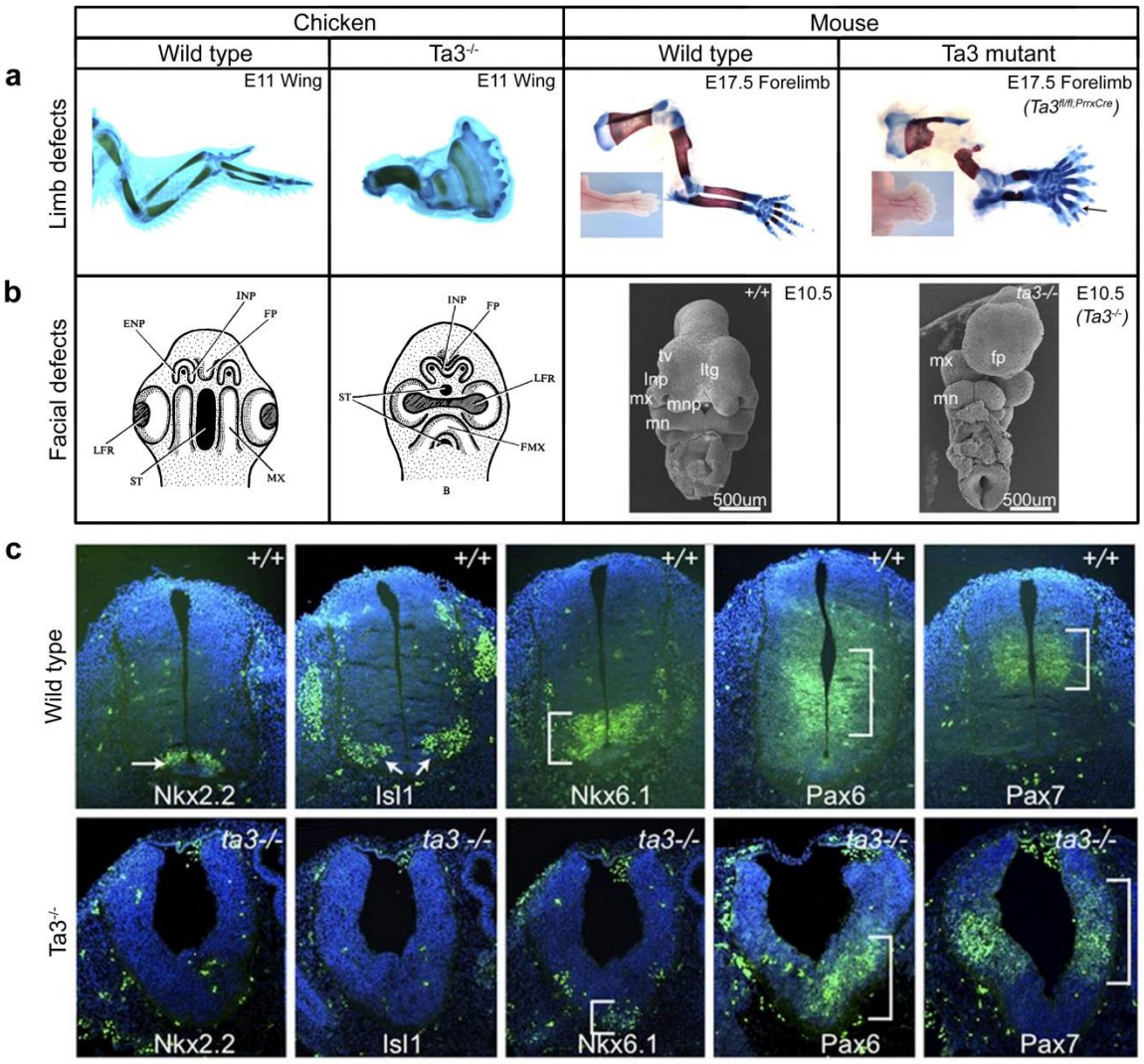

Figure 1.4 Phenotypes following loss of *Ta3* in chick and mouse

(a) Chicken and mouse *Ta3*$^{flfl;Prrx}$ mutants exhibit polydactyly. Images taken from (Bangs et al., 2011). Chicken wings (E11) of wildtype and *Ta3* mutant stained with alcian blue. Mouse forelimbs (E17.5) of wildtype and limb-specific conditional *Ta3* mutant stained with alcian blue and alizarin red. (b) Chicken and mouse constitutive *Ta3* mutants exhibit midline facial defects. Chicken images taken from (Ede and Kelly, 1964a) and mouse images taken from (Bangs et al., 2011). Chicken: Schematic illustration of early chicken embryo. Mutants exhibit cyclopia and fusion of structures across the midline. ENP, external nasal process; FMX, fused maxillary processes; FP, frontal process; INP, internal nasal process; LFR, lens-forming region; MX, maxillary process; ST, stomodaeum. Mouse: Scanning electron micrograph of E10.5 embryos. Mutants exhibit of fusion of lateral and medial nasal processes creating a frontal process across the midline. fp, frontal process; ltg, lamina terminalis groove; lnp, lateral nasal process; mn, mandibular process; mx, maxillary process; mnp, medial nasal process; np, nasal pit; tv, telencephalic vesicle. (c) E10.5 *Ta3* mutant mice show defective dorso-ventral specification in the neural tube. Images taken from (Bangs et al., 2011). Immunohistochemistry of neural transcription factors, Nkx2.2, Isket1, Nkx6.1, Pax6 and Pax6.

1.2.2 Molecular role of Talpid3

A limited number of attempts have recently tried to identify binding partners of Ta3. In a screen looking for components binding the capping protein, CP110, Kobayashi and colleagues (2014) identified Ta3 as a prominent binding partner. Immunoprecipitation experiments also demonstrated weaker interactions of Ta3 with Cep97, Kif24 and Cep290. In the same study, tandem mass spectrometry of material immunoprecipitated with FLAG-tagged Ta3 identified PCM1 as an additional binding partner and further immunoprecipitation studies showed an interaction with Rab8. The group highlight a role of these Ta3-interacting components with protein trafficking and vesicle attachment to the basal body. They demonstrate that loss of Ta3 results in an accumulation of centriolar satellite proteins either as a cause or consequence of a failure in cilia formation. Despite the large number of binding proteins identified it remains unclear which of the interactions are direct with Ta3 or as a result of multi-protein complexes present at the centriole.

Another study using a yeast two-hybrid system with Ta3 as bait identified Cep120 as an interacting partner (Wu et al., 2014). They show that Ta3 is found mainly at the mother centriole where counterintuitively they suggest it has a role limiting the level of Cep120 which is found predominantly at the daughter centriole. They highlight the importance of this regulation and emphasise the role of Cep120 in procentriole formation. Given the interaction of Ta3 with CP110, this could suggest an earlier role of Ta3 in centriole maturation, which in turn could have a knock on effect on vesicle docking and cilia formation. The centriolar proteins interacting with Ta3 are highlighted in bold in table 1.1.

Given the importance of the centrosome as the microtubule organising centre it is important to consider cilia-independent roles of Ta3 in cellular function. In the neural tube of chick mutants, analysis of the cytoskeleton showed defects in the apical distribution of F-actin (Yin et al., 2009). Culture of mutant limb-bud cells also showed increased actin at the ruffled membrane and many actin-rich filopodia extending from cells. In addition, in both chick and mouse loss of *Ta3* resulted in a reduced number of stress fibres and focal adhesions with cells migrating slower and with less directionality (Yin et al., 2009, Bangs et al., 2011). Regrowth of microtubules following nocodazol treatment was also slower in mutant cells. Despite these defects, the process of cell division in *Ta3* mutants appears relatively unaffected. Spindles form and separate chromosomes effectively and in cycling

embryonic stem cells there is little effect on the cell cycle (Ferguson and Subramanian, Unpublished). This raises the intriguing question of what cilia-independent roles Ta3 is required for. It is yet to be determined whether the effects on cytoskeleton and cell migration are a primary defect due to loss of Ta3 or whether they are secondary to a loss of primary cilia.

1.2.3 Molecular organisation of Talpid3 and its transcripts

The *Ta3* gene is conserved across vertebrate organisms with its importance demonstrated in chickens (Davey et al., 2006), mice (Bangs et al., 2011), zebrafish (Ben et al., 2011) and human cells (Kobayashi et al., 2014). Initial genetic mapping studies by Davey and colleagues (2006) demonstrated that the gene order surrounding the *Ta3* locus is also conserved in vertebrates. The chicken *Ta3* gene is located on chromosome 5 and is encoded by 30 exons to produce a single transcript (*TALPID3-201*) of 4931 bases in length (1524aa). In mouse, the *Ta3* gene is located on chromosome 12 in cytoband C1 (*MGI: 2700049A03Rik*). Similar to chickens, the mouse *Ta3* is encoded by 30 exons with the longest transcript (*2700049A03Rik-001*) produced being 5763 bases in length (1520aa). An alternative transcript is also produced lacking exons 28 and 29 (*2700049A03Rik-201*). In addition, a third C-terminal transcript is predicted (*2700049A03Rik-002*) which is thought to begin from exon 16, lack exons 28 and 29 producing a possible product of 2173 bases in length (656aa), however this is yet to be confirmed experimentally. The three mouse *Ta3* transcripts are illustrated in Figure 1.5. Human *TA3*, in comparison, has more alternate transcripts but the largest (*KIAA0586-001*) produces a protein with a very similar structure to the mouse and chicken.

The *KIAA0586-001* human transcript is designated as the canonical *TA3* product; it is distributed across 32 exons (31 coding) and creates a transcript of 8233 bases in length (1533aa). There are also other transcripts which include additional exons present between the canonical exons 5-6 and 31-32. Similar to mouse there is also a predicted C-terminal *TA3* product (*KIAA0586-013*) but in contrast it is much smaller with an expected length of only 814 bases (208aa). To date, there has been no study into the significance of the mouse or

human *Ta3* transcripts. A summary of chicken, mouse and human transcripts are listed in table 1.2.

Despite efforts to produce recombinant protein the three-dimensional structure of Ta3 is yet to be determined. There are no predicted functional domains and little is known about the structure (Davey et al., 2006). The Ta3 protein is known to have coiled-coil regions with predicted regions of disorder and low complexity (Fig 1.5). In particular, one coiled-coil region is found in a highly conserved sequence between 498-585aa (Yin et al., 2009). It is found in exons 11 and 12 and has been shown to be an essential region for the proper Ta3 function (Yin et al., 2009, Bangs et al., 2011). Analysis of tagged constructs demonstrate that only full length protein is able to functionally rescue mutant cells but the coiled-coil domain alone is sufficient for centrosomal localisation (Yin et al., 2009, Kobayashi et al., 2014). Domain constructs have also demonstrated the coiled-coil region is required for association of Ta3 with Cep120 (Wu et al., 2014).

Table 1.2 *Talpid3* transcripts in Chicken, Mouse and Human

Information taken from Ensembl database (Cunningham et al., 2015). Abbreviations, bp, base pairs, aa, amino acids. *Italics* indicate predicted protein coding transcripts. For human TA3, KIAA0586001 is the canonical transcript and (asterisk*) indicates additional exons.

Species	Transcript name	Transcript ID	length (bp)	length (aa)	Exons
Chicken	KIAA0586-201	ENSGALT00000037343	4931	1523	1-30
Mouse	2700049A03Rik-001	ENSMUST00000149564	5763	1520	1-30
	2700049A03Rik-201	ENSMUST00000045907	5499	1432	1-27, 30
	2700049A03Rik-002	*ENSMUST00000129376*	*2173*	*656*	*16-27, 30*
Human	KIAA0586-001	ENST00000619416	8233	1533	1-32
	KIAA0586-201	ENST00000556134	5912	1504	1-33 (6*)
	KIAA0586-202	ENST00000619722	5597	1463	1,3-32
	KIAA0586-004	ENST00000423743	5339	1504	1,3-33 (6*)
	KIAA0586-003	ENST00000354386	5226	1644	1-34 (6*, 32*)
	KIAA0586-002	ENST00000261244	4807	1472	2-13, 15-32
	KIAA0586-010	*ENST00000555833*	*846*	*234*	*1,3-8*
	KIAA0586-013	*ENST00000555397*	*814*	*208*	*26, 28-30, 32*
	KIAA0586-008	*ENST00000554463*	*582*	*132*	*1,3-7*

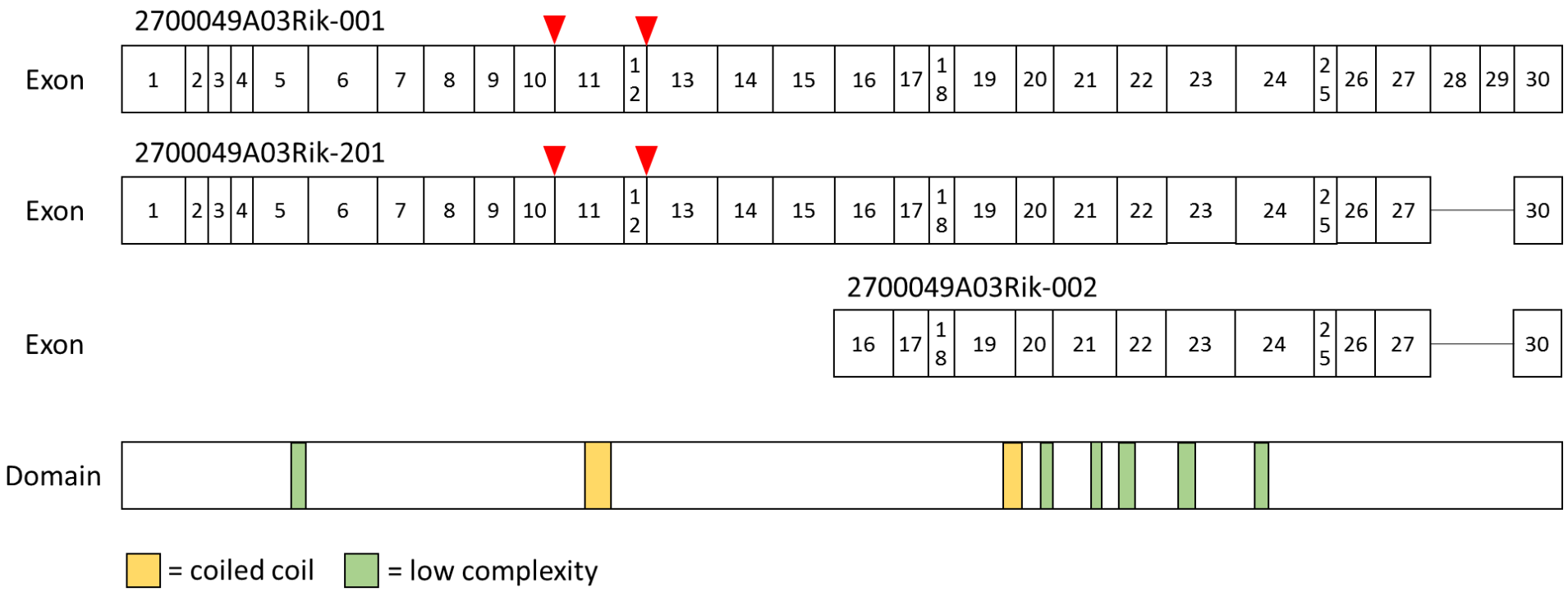

Figure 1.5 The domain structure of mouse Talpid3. Full length talpid3 has 30 exons with a smaller splice variant of 28 exons and one with alternative start site of 13 exons. The domain structure has two coiled-coil regions (yellow) and multiple regions of low complexity (green). Red arrowed indicate the forward-facing LoxP sites which are present in the introns between Exons 10-11 and 12-13. Genomic information taken from Ensembl genome browser (Cunningham et al., 2015)

1.2.4 Sub-cellular localisation of Talpid3

In chick embryonic fibroblasts, studies using Ta3-specific antibodies and tagged constructs have demonstrated its localisation to the centrosome throughout the cell cycle except during mitosis (Yin et al., 2009). During both anaphase and telophase it was found to have a diffuse distribution. This was also shown in human retinal pigment epithelial cells (RPE1) where Ta3 localised at the basal body of primary cilia and at both mother and daughter centrioles in G1. Interestingly it could be observed in all four centrioles in G2 following their duplication prior to mitosis (Kobayashi et al., 2014). In the same study, the group used structured illumination microscopy and suggested that Ta3 forms a ring-shape at the extreme distal tip of centrosomes and localised very closely with CP110 and Cep164. A recent study has further suggested that the level of Ta3 is higher at the mother centrioles however this has not been described in other publications and the quality of the data presented suggested the difference between mother and daughter may only be marginal (Wu et al., 2014).

1.2.5 Generation of conditional *Talpid3* mutant mouse

In 2011 a conditional mouse model utilising the 'Cre-LoxP' system was generated by Bangs and colleagues to target the function of *Ta3*. The Cre-LoxP system is a versatile strategy routinely employed to disrupt gene function. It was discovered in a P1 bacteriophage where two 34bp sequences known as a *LoxP* sites are recognised by the Cre-recombinase enzyme which is able to recombine the DNA (Sternberg et al., 1981, Sauer and Henderson, 1988). Depending on the orientation of *LoxP* sites the flanked sequence can be inverted, moved or deleted and is a beautifully simple two-component system used to modify DNA sequence *in vivo* (Rossant and Nagy, 1995).

The *Ta3* conditional mutant mouse was designed to have forward-facing *LoxP* sites in the intronic regions between exons 10-11 and 12-13 ($Ta3^{fl/fl}$) (Bangs et al., 2011). When crossed with a mouse expressing the Cre enzyme, recombination occurred to effectively remove exons 11 and 12 which is the region containing the conserved coiled-coil domain (Figure 1.5). The group crossed the $Ta3^{fl/fl}$ mice with a ubiquitous *Cre* deleter strain (*Gt(ROSA)26Sortm16 Cre*). This generated $Ta3^{fl/wt\ Gt(ROSA)26Sortm16Cre}$ mice with heterozygous

loss of *Ta3* function (*Ta3*$^{+/-}$). Further intercrosses were able to generate homozygous mutant embryos with complete disruption of *Ta3* (*Ta3*$^{-/-}$). They demonstrated that the coiled-coil region was required for the formation of primary cilia and effective signalling in the hedgehog (Hh) pathway. Embryonic *Ta3*$^{-/-}$ mice only develop to E9.5 on an inbred BL6 background and E10.5 on an outbred CD1 background where they exhibit vascular defects and midline facial deformities.

The vascular defects at E10.5 included accumulation of fluid around the heart known as pericardial oedema and significant haemorrhaging of vessels (Bangs et al., 2011). In sectioned tissue the heart also appeared enlarged. In addition, *Ta3*$^{-/-}$ mutant mice showed aberrant looping of the heart with randomisation of looping direction which indicated defects in left/right axis specification. The defect in left/right axis specification was demonstrated further by aberrant expression of *Nodal* around the node and lateral plate mesoderm at E8.0 and is consistent with the known roles of primary cilia in the developing mammalian node. The vascular defects seen in *Ta3*$^{-/-}$ mutant mice are similar to those described in the *talpid*^{3} mutant chick (Davey et al., 2007) however the looping defects are not with *talpid*^{3} mutant chick embryos showing normal left/right axis specification (Bangs et al., 2011). These differences in left/right axis specification are likely to be due to evolutionary divergent mechanisms of breaking bilateral symmetry with chickens having a cilia independent mechanism (Stephen et al., 2013).

Ta3$^{-/-}$ mutant mice also demonstrated disrupted dorso-ventral identities in the early neural tube consistent with the role of Hh signalling defining these structures (Fig 1.5c) (Bangs et al., 2011). The group then went on to investigate the role of Ta3 in the developing limb by crossing with the limb-specific *Prrx-Cre* deleter strain (Fig 1.5a). Thanks to the versatility of the *Cre-LoxP* system there is great potential to cross *Ta3*$^{fl/fl}$ mice with other Cre deleter strains to avoid the embryonic lethality and investigate the function of Ta3 in other organ systems; it is this approach which forms the experimental basis for the current study.

1.3 Primary cilia and their role in signal transduction

The highly specialised role of primary cilia is attributed to the axoneme and its ability to act as a distinct cellular compartment. The cilial micro-environment is maintained as a result of the tight physical association of the distal centrosome to the membrane at the transition zone. EM microscopy suggests the space between these transition fibres is too small to allow the passage of vesicles (Anderson, 1972, Sorokin, 1962) and it is proposed to act as a diffusion barrier helping to regulate the contents of the axoneme (Spencer et al., 1988). Proteins localised on the plasma membrane are also regulated in their ability to move to the primary cilia membrane or are actively trafficked there. Many of the membrane anchored or transmembrane proteins facilitate the function of primary cilia to transduce extracellular signals.

1.3.1 The hedgehog pathway is transduced through the primary cilium

The Hh signalling pathway is able to influence a range of cellular activity including cell fate, tissue patterning, migration, proliferation and survival. The Hh pathway is one of the best studied intercellular signalling pathways and was originally identified in a screen looking at mutations affecting the *Drosophila* body plan (Nusslein-Volhard and Weischaus, 1980). In *Drosophila* the pathway forms a relatively simple system where a single ligand (Hh) is able to activate receptors found at the plasma membrane which then influence intracellular effectors and transduce the signal to elicit a cellular response. In mammals, this pathway has evolved in to a highly specialised system with multiple ligands which activate receptors found at the primary cilium. The involvement of the primary cilium was first discovered in mutant mice with disrupted IFT components which developed defects attributed to loss of signalling (Huangfu et al., 2003, Liu et al., 2005).

The generally accepted model of Hh signalling in mammals is summarised in figure 1.6. In unstimulated cells, the inhibitory transmembrane receptor, Patched1 (Ptc1), localises at the base of the cilium. Here it has a repressive effect on the seven-pass transmembrane protein Smoothened (Smo) which is found in vesicles in the cytoplasm (Rohatgi et al., 2007). In this state, members of the glioma-associated oncogene (Gli) family are bound to Suppressor of Fused (SuFu) which is thought to inhibit their nuclear translocation (Ding et

al., 1999). In addition, some Gli proteins are proteolytically processed into short repressor forms (GliR) which then translocate to the nucleus where they directly repress transcription of Hh-target genes (Wang et al., 2000). This proteolytic processing is initiated by the activity of protein kinase A (PKA) which acts to target it for proteosomal degradation (Wang et al., 2000). PKA has been shown to localise at the basal body (Barzi et al., 2010) or slightly proximal to the basal body where it has a key role promoting the formation of cleaved GliR molecules and limiting action of full length active Gli (GliA) (Tuson et al., 2011). The Gli-SuFu complex is trafficked through the ciliary axoneme but it has been suggested that PKA activity on Gli occurs at the basal body after its exit from the cilium (Tuson et al., 2011). In the unstimulated state, the kinesin Kif7 has also been shown to localise at the basal body where it is thought to form a complex with Gli proteins and promote the formation of GliR and limit their accumulation in the axoneme (Liem et al., 2009).

Upon stimulation of the pathway, Sonic hedgehog (Shh), Indian hedgehog or Desert hedgehog ligands bind to Ptc1 receptors which subsequently move away from the cilium. Activation of Ptc1 then releases the repression on Smo which accumulates in the cilia axoneme (Corbit et al., 2005, Rohatgi et al., 2007). Kif7 also translocates into the cilia axoneme and promotes the accumulation of SuFu and Gli in the cilia tip (Goetz and Anderson, 2010, Haycraft et al., 2005). Active Smo in the cilium acts to inhibit SuFu allowing the full length Gli proteins (GliA) to translocate to the nucleus and activate gene transcription (Tukachinsky et al., 2010).

The Gli protein family is comprised of three members. Gli1 only has an activator domain and acts as an obligate activator of Hh targets (Dai et al., 1999) whereas Gli2 and Gli3 have activator and repressor domains. Although Gli2 and Gli3 are capable of acting in either form, they exhibit different preferences with Gli2 predominantly acting as an activator (Gli2A) and Gli3 as a repressor (Gli3R) (Sasaki et al., 1999, Dai et al., 1999, Pan et al., 2006). The activation and proteolytic processing of Gli2 and Gli3 has been shown to occur at the cilium (Liu et al., 2005, Haycraft et al., 2005, Kim et al., 2009) and this means that primary cilia mutants often exhibit complex phenotypes with both gain and loss of Hh function (Davey et al., 2006). Target genes include cell cycle regulators such as *N-Myc* and *CyclinD* (Kenney et al., 2003) in addition to feedback loops upregulating expression of *Gli1* (Marigo et al., 1996b, Goodrich et al., 1996), and *Ptc1* (Marigo et al., 1996a, Lee et al., 1997).

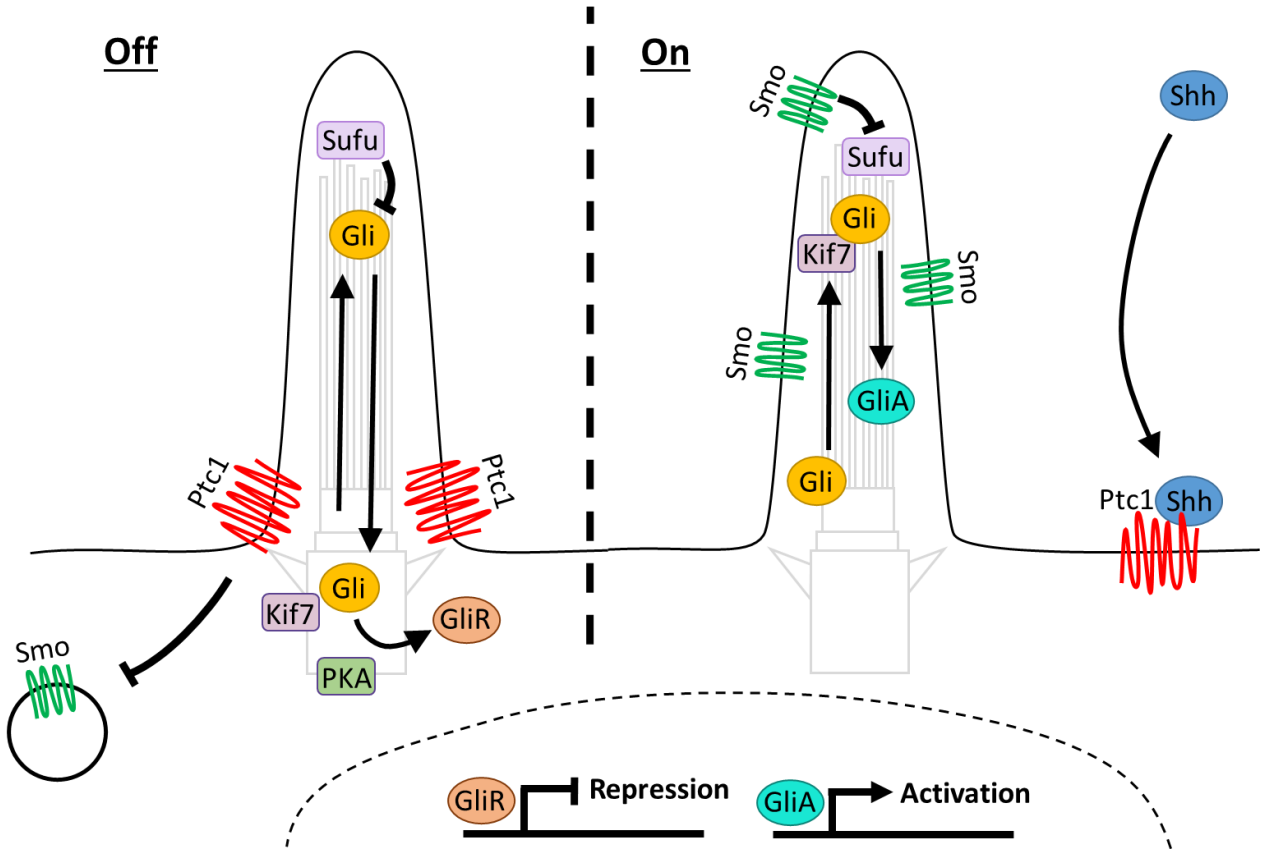

Figure 1.6 Major components of the Hedgehog signalling pathway

In the 'Off' state Ptc1 is found at the base of primary cilia and has a repressive effect on Smo, where it is found in cytoplasmic vesicles. Sufu acts as an inhibitor, preventing the nuclear translocation of Gli. Some Gli protein is also proteolytically processed into short repressor forms (GliR) to repress Hh target gene transcription. Protein kinase A (PKA) found at the basal body is required to target Gli for proteolytic processing. Kif7 forms a complex with Gli to prevent its accumulation in the cilia axoneme. In the 'On' state Hh ligand (Shh, Ihh or Dhh) can bind to Ptc1 to release the repressive effect on Smo. This allows Smo, Kif7, Gli and Sufu to accumulate in the primary cilia. Smo inhibits the action of SuFu and active Gli is able to translocate to the nucleus to activate Hh target gene transcription. Image adapted from Goetz and Anderson 2010.

1.3.2 Other signalling pathways are transduced through the primary cilium

Primary cilia have also been implicated in the regulation of many other signalling pathways. Cilia have been suggested to influence the Wnt signalling pathway and the balance between canonical and non-canonical signalling (Lancaster et al., 2011, Simons et al., 2005). However, this role is controversial and the significance of cilia in Wnt signalling has yet to be demonstrated *in vivo* (Ocbina et al., 2009). Furthermore, the non-canonical planar cell polarity pathway (PCP), which orientates cells with apical-basal polarity, has been shown to require primary cilia in epithelia (Jones et al., 2008).

Several tyrosine kinase receptors and their downstream effectors have been shown to localise at primary cilia. Epidermal growth factor (EGF) has been shown to influence the signalling of cilial protein Polycystin2 (Ma et al., 2005) and EGF-receptor has been shown to localise at primary cilia in the subventricular zone (SVZ) (Danilov et al., 2009) and airway smooth muscle cells (Wu et al., 2009). Insulin-like growth factor-1 receptor (IGF-1R) localises at the basal body during adipocyte differentiation with loss of IFT components preventing the IGF signalling response (Zhu et al., 2009). In fibroblasts, Platelet derived growth factor receptor α (PDGF- α) has been shown to be regulated through the primary cilia (Schneider et al., 2005) and the angiopoietin receptors, Tie-1 and Tie-2, have also been found on motile cilia in the oviduct (Teilmann and Christensen, 2005). Conversely, fibroblast growth factor (FGF) signalling has been suggested to have a role regulating the length and function of primary cilia in a range of epithelial tissues (Neugebauer et al., 2010). Other signalling receptors including those for notch pathway (Ezratty et al., 2011), serotonin (Brailov et al., 2000) and somatostatin (Handel et al., 1999) have also been detected in the membrane of primary cilia. Importantly, with the exception of Hh signalling, very few studies have demonstrated the functional significance of other signalling pathways in primary cilia mutants *in vivo*.

Primary cilia are also able to transduce other types of signal which are independent of diffusible signalling molecules. For example, in the kidney they have a role converting mechanosensory signals into calcium fluxes through the Polycystin proteins (Nauli et al., 2003, Pazour et al., 2002). In retinal cells the highly specialised cilia contain the transmembrane protein rhodopsin, which is responsive to light (Takemoto and Cunnick,

1990). This demonstrates that primary cilia can have distinct cellular roles based on the cell-type in which they are present.

1.3.3 Other cellular roles of primary cilia

There are a number of cellular processes which are inherently linked with primary cilia but distinct from their direct signalling roles. Components of the autophagy pathway have been shown to localise at the basal body. Both formation of primary cilia and autophagy share some common IFT machinery and signal transduction has been shown to directly induce autophagy (Pampliega et al., 2013). Conversely, autophagy has also been shown to promote the growth of primary cilia suggesting a mechanistic role in their formation (Tang et al., 2013). Components of primary cilia have also been linked with the endocytic pathway. Disruption of ADP-ribosylation factor-like protein 13b (Arl13b), a GTPase found in primary cilia, caused defects in both endocytic recycling and trafficking to late endosomes and lysosomes (Barral et al., 2012).

Migration of many cells is also regulated through the primary cilium, albeit mainly as a consequence of signal transduction. In fibroblasts, migration is guided by PDGF signalling, and as a result, primary cilia mutants show defects in wound healing response and fibroblast chemotaxis both *in vivo* and *in vitro* (Schneider et al., 2010). Patients with human ciliary dyskinesia have also been shown to have reduced migration of blood neutrophils (Koh et al., 2003). Furthermore, a non-canonical role for Shh has been demonstrated where a cilia-independent role of Smo is thought to control migration through transcription-independent mechanisms (Bijlsma et al., 2012). The authors of this study demonstrate that the disruption of primary cilia leads to an increased level of chemotaxis which they propose was due to the balance between ciliary and non-ciliary Smo activation.

1.4 The role of primary cilia in brain development

Considering the range of pathways thought to be regulated through primary cilia, a complex process such as brain development is thought to require them at a range of stages. The most significant roles of primary cilia in brain development have been discovered through study of neural development in primary cilia mutants. To place their role in a meaningful context it is first important to outline the key steps in brain development.

1.4.1 Key steps in brain development

The entire central nervous system develops from the neural tube. In the mouse this structure is formed around embryonic day 8 (E8.0) when ectoderm undergoes neural induction to form a tube of multipotent neuroepithelial cells. Early markers include the intermediate filament nestin and the transcription factor sox1. These stem cells are capable of self-renewal and able to produce the majority of cell types in the brain including neurons, astrocytes and glia. From E10.5 these cells lose their epithelial character, begin expressing glial markers and extend radially through the tube in an apico-basal orientation. They continue expressing nestin in addition to markers such as glial fibrillary acidic protein (GFAP). These cells are known as radial glial cells (RGCs) and they are restricted neural progenitors which are still capable of self-renewal and still able to produce neurons, astrocytes and glia which populate the growing tube. The earliest neurons are formed from E10.5 in a process known as neurogenesis. RGCs undergo mitosis at the apical surface of the ventricular zone and either symmetric or asymmetric divisions act to form neurons, neuroblasts, intermediate precursors or expand the RGC population. Intermediate precursors, unlike the RGCs, migrate basally and undergo mitoses away from the ventricular surface to populate the growing tube.

At the earliest stage of brain development (~E8.0) the neural tube is already acquiring regional identity. Signals including Wnt, FGF and Retinoic acid (RA) induce a posterior fate in the neural tube (Rallu et al., 2002). The anterior head region is formed through inhibition of these signals by antagonists such as Cerberus and dickkopf which are produced by the underlying anterior visceral endoderm (AVE) (Fig 1.7a). At this early stage the brain can be divided into the forebrain (prosencephalon), midbrain (mesencephalon) and hindbrain (rhombencephalon). Dorsal-ventral specification begins in the neural tube

where Sonic hedgehog (Shh) is expressed in the notochord and ventral neural tube and members of the bone morphogenetic protein (BMP) family are expressed dorsally (Fig 1.7b). These opposing morphogen gradients determine cell fate and cause the expression of different neural transcription factors across the dorso-ventral axis (Fig 1.4c) (Ribes and Briscoe, 2009). Further regional identity is provided from E8.0 by distinct organising centres including the anterior neural ridge (ANR), zona limitans intrathalamica (ZLI) and isthmic organiser (IsO) which produce fibroblast growth factors (FGF), Shh and Wnt/Fgf8 respectively (Wurst and Bally-Cuif, 2001) (Fig 1.7b).

The mature structures of the adult brain can be neatly grouped based on their embryonic origin (Lein et al., 2007) (Fig 1.7d). The forebrain becomes divided further into the telencephalon and diencephalon and the hindbrain becomes divided into the metencephalon and myencephalon. One of the largest and most obvious adult brain structures is the cerebrum which is derived from the telencephalon. The dorsal cerebrum, also known as the pallium, develops into the cerebral cortex and the hippocampus whereas the ventral cerebrum forms the olfactory bulbs and the cerebral nuclei, also named the basal ganglia. The diencephalon forms the thalamus and hypothalamus whereas the mesencephalon develops into the midbrain; including structures such as the superior and inferior colliculi. The hindbrain develops from the rhombencephalon and includes the pons, medulla and cerebellum. More specifically, the cerebellum originates from rhombomere 1 (R1) (Wingate and Hatten, 1999). From E10.5 the boundary between R1 and the mesencephalon, known as the isthmic organiser (IsO), exhibits and a complex gene regulatory network involving Wnt and FGF8 to specify the cerebellar primordia (Sato et al., 2001, Chi et al., 2003). Shh is also thought to influence this by potentiating the FGF8 signal in addition to regulating the dorso-ventral fate and cell survival (Blaess et al., 2006). Despite folding into a specialised and highly complex structure, the brain retains its tubular origin in the form of fluid filled ventricles. Cerebrospinal fluid (CSF) fills the ventricles and is produced by the choroid plexus (Johanson et al., 2008).

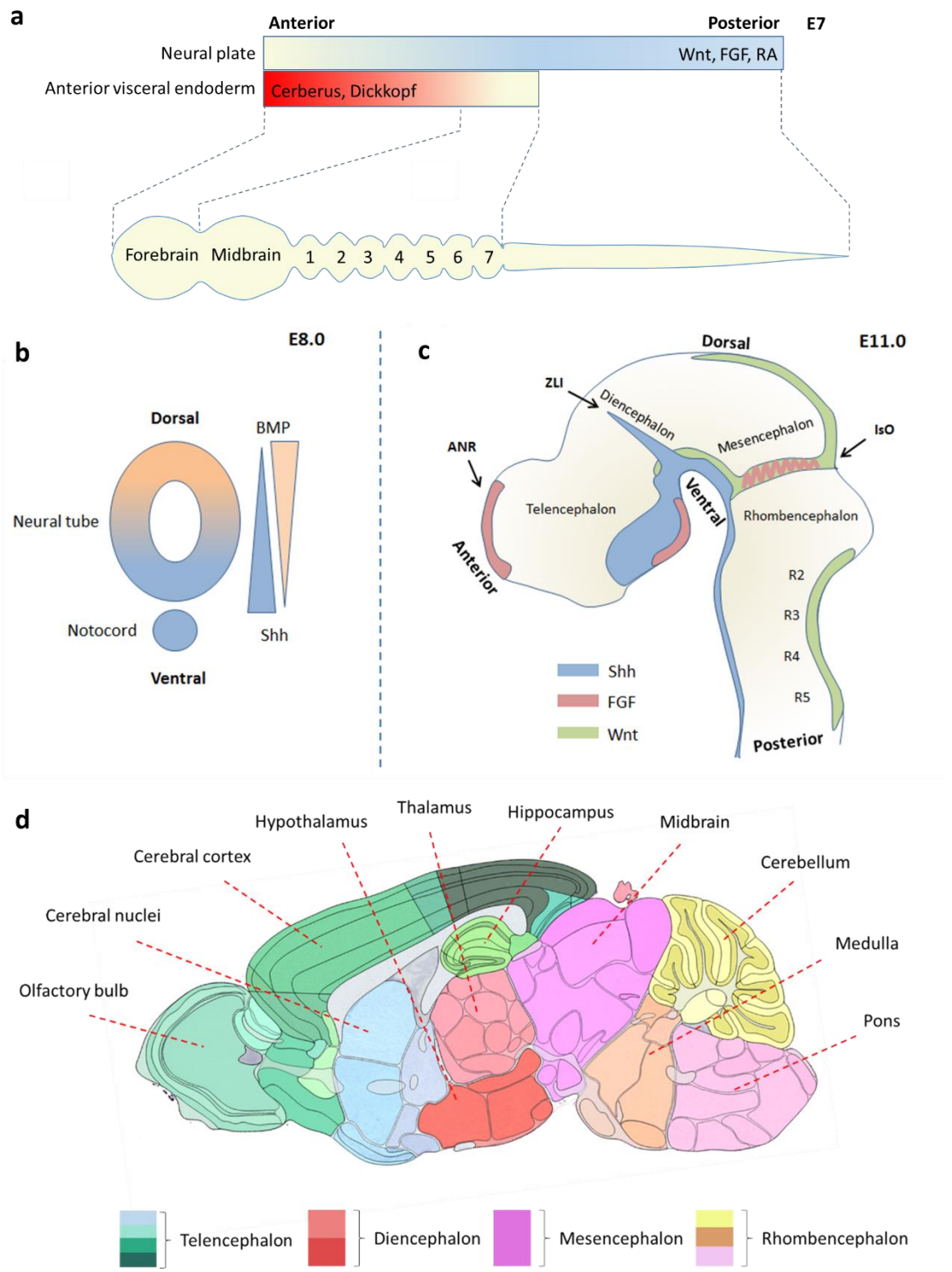

Figure 1.7 Early patterning in the developing brain

a) Anterior-posterior identity of the neural tube is established through posteriorising signals including Wnt, FGF and RA. The brain region is specified by blocking these signals with antagonists such as Cerberus and Dickkofp which are produced by the underlying AVE. Numbers indicate rhombomeres. Image adapted from (Rallu et al., 2002). (b) Dorsal-ventral patterning of the neural tube is determined through opposing gradients of ventral Shh and dorsal BMPs. (c) Regional identity is provided by distinct organising centres including the anterior neural ridge (ANR), zona limitans intrathalamica (ZLI) and isthmic organiser (IsO). These produce FGF, Shh and Wnt/Fgf8 respectively. Image taken from (Wurst and Bally-Cuif, 2001). (d) Major regions in the adult brain. Olfactory bulb, cerebral nuclei, cerebral cortex and hippocampus derive from the telencephalon. Thalamus and hypothalamus derive from the diencephalon. Midbrain structures derive from the mesencephalon. The cerebellum, medulla and pons derive from the rhombencephalon. Image taken from Allen Brain Atlas [Internet]. Available from: www.brain-map.org.

The cellular complexity seen in the developing brain is increased further due to the migration of neurons. Many neurons also leave an axonal trail when they migrate, allowing increased connections between regions. Migrating neurons follow three generalised phases; first they extend a leading process to identify attractive or repulsive cues. The nucleus then moves in a process known as 'nucleokinesis' and the trailing process is retracted (Nadarajah and Parnavelas, 2002). Neurons can attach to a range of substrates when navigating the brain. One common mechanism utilises the underlying scaffold of RGC fibres which act as a guide to their final destination. This type of glial-guided migration usually occurs through layered structures such as the cortex, hippocampus and cerebellum (Purves et al., 2001).

After all of the broad regional specifications haven taken place, the brain continues to grow and diversify due to the proliferation of neural progenitors. A relevant example is the cerebellum which undergoes a high level of proliferation from E17.5 and continues several weeks after birth. Here, Shh acts as a mitogen to drive proliferation of the granule neuron precursors (GNPs) which mature into granule neurons; the most numerous cell type in the adult brain (Dahmane and Altaba, 1999). After the first few weeks of birth and throughout life the number of cycling progenitors decreases however, two neurogenic regions persist into adulthood (Ming and Song, 2011). RGCs present in the SVZ of the lateral ventricles produce neuroblasts which migrate along the rostral migratory stream (RMS) to the olfactory bulb (Doetsch et al., 1999). The second niche is in the dentate gyrus of the hippocampus. Here, RGCs from the subgranular zone (SGZ) produce neuroblasts which populate the neighbouring granule cell layer (GCL) (Altman and Das, 1965). Progenitors in both the SVZ of the lateral ventricles and the SGZ of the hippocampus have also been identified in humans (Sanai et al., 2004, Eriksson et al., 1998). These neurogenic niches can be very complex and are regulated by a number of signals. In particular, the hippocampal progenitors are regulated by factors including Shh (Lai et al., 2003) and Wnts (Lie et al., 2005). The progenitors are also responsive to infusion of other factors such as Brain Derived Neurotrophic Factor (BDNF) (Benraiss et al., 2001), its receptor tropomyosin receptor Kinase B (TrkB) (Li et al., 2008) or FGF (Rai et al., 2007).

1.4.2 Brain development in constitutive cilia mutants

Due to the importance of cilia in multiple organ systems, many mouse mutants with constitutive loss of primary cilia display embryonic lethality between E9.5-E12.5. These include anterograde motors: IFT88 (Willaredt et al., 2008), IFT172 (Gorivodsky et al., 2009), Kif3a (Kinesin family member 3A) (Huangfu et al., 2003), and basal body proteins: Fantom (Ftm) (Besse et al., 2011), Oral-Facial-Digital syndrome-1 (Ofd1) (Ferrante et al., 2006), Meckel Syndrome-1 (MKS1) (Weatherbee et al., 2009) and Ta3 (Bangs et al., 2011). All of these mutants show defects in dorsal-ventral patterning of the neural tube (Fig 1.4c) which is attributed to disruption of Shh signal transduction. As this step underpins the early regional specification of the developing brain, the study of later roles of primary cilia requires conditional mutagenesis to bypass both the early lethality and early patterning defects.

1.4.3 Later roles of primary cilia in brain development

The predominant neural phenotype observed in conditional primary cilia mutants occurring after the early patterning steps is one of reduced proliferation and are commonly attributed to defective Shh signal transduction. Widespread loss of Kif3a or IFT88 in the second half of gestation resulted in reduced proliferation of cerebellar granule neurons (Spassky et al., 2008, Chizhikov et al., 2007). Similarly, loss of Kif3a or basal body protein Stumpy also caused reduced proliferation in the SGZ of the hippocampus (Han et al., 2008, Breunig et al., 2008). Surprisingly, and in direct contrast to other primary cilia mutants, conditional loss of Kif3a has been shown to result in overgrowth of the cortex due to increased cell cycle kinetics (Wilson et al., 2012). This demonstrates that the phenotypes of primary cilia mutants are not all equal. Further investigation of phenotypes following the loss of novel cilia components, such as Ta3, will be important in understanding their function.

Another common observation in cilia mutants is the development of hydrocephaly. There are several factors which may cause this including loss of motile cilia normally found on the ependymal layer, this affects cerebrospinal fluid (CSF) flow and subsequent closure of the cerebral aqueduct resulting in an accumulation of fluid in the ventricles (Ibanez-Tallon et al., 2004, Banizs et al., 2005, Tissir et al., 2010). CSF production by the choroid plexus is also

thought to be affected in primary cilia mutants (Banizs et al., 2005). A recent study suggested that the PDGFα-dependent regulation of a subpopulation of ventricular progenitors is also a causative factor in cilia-dependent hydrocephaly (Carter et al., 2012).

A fascinating study by Higginbotham and colleagues ablated primary cilia component Arl13b in a range of time points. They demonstrated that loss of cilia prior to establishment of the initial RGC layer resulted in a complete reversal of the apico-basal polarity resulting in the brain forming in an inverted fashion (Higginbotham et al., 2013). Loss at later stages did not recapitulate this phenotype and no other studies have described such a striking defect suggesting that the timing and severity of cilia disruption is critical to the developmental phenotype.

An alternative approach used to investigate neuronal primary cilia in two recent studies used overexpression of proteins usually found at the primary cilium to disrupt their function (Guadiana et al., 2013, Massinen et al., 2011). Microinjection and electroporation into embryonic brain with constructs encoding tagged serotonin receptor (5HT6) or somatostatin receptor 3 (SSTR3) caused a lengthening of primary cilia and displacement of other cilia components resulting in a loss of cilia function (Guadiana et al., 2013). The authors described defects in the dendritic arborisation of pyramidal neurons and show the effect can be rescued by overexpression of the components which were displaced. In a similar study overexpression of tagged doublecortin domain containing 2 (DCDC2) in neuronal cultures demonstrated a primary cilia localisation and also resulted in cilia elongation (Massinen et al., 2011). They further described an increase in basal Hh target gene transcription and PDGFα which, when studied in *C.elegans* also lead to an aberrant neuronal morphology. Although overexpression of primary cilia components is likely to cause disruption through complex competitive interactions it still suggests an interesting role of cilia in neuronal morphology and dendrite organisation. In support of this, further electroporation studies using a dominant negative *Kif3a* construct demonstrated that hippocampal primary cilia were required for refinement of dendrites and synapse formation in new-born neurons. They revealed that loss of cilia resulted in an increase in canonical Wnt signalling and rescue of this was able to restore normal dendrite formation (Kumamoto et al., 2012).

In addition to neuronal morphology, primary cilia have been implicated in neuronal migration. As mentioned earlier the formation of the radial glial scaffold appears to have a dependence on the cilium and therefore glial-guided migration can be affected as a secondary consequence of primary cilia defects (Higginbotham et al., 2013). An alternative study has demonstrated that tangential migration of interneurons in cortical development, a process which is regulated by guidance cues rather than a glial scaffold, is also dependent on cilia (Higginbotham et al., 2012). The authors demonstrated that the distance migrated by GABAergic interneurons is reduced in cortices with ablated Arl13b. They suggest that a range of guidance cue receptors, in addition to serotonin, are localised at the cilium which include: BDNF, Glial derived neurotrophic factor receptor (GFRα-1), Stromal cell-derived factor-1 receptors (CXCR4, CXCR7), Neuregulin-1 receptor (ErbB4), Slit receptors (Robo 1, Robo 2) and Hepatocyte growth factor receptor (MET). Although the presented images of protein localisation aren't especially convincing, they suggest that the Arl13b mutant presented an altered frequency of receptors along the cilia. They further present interesting time lapse data of migrating neurons. They show the cilium located near the apical tip and as the neuron pauses the cilia length and dynamics significantly increase, almost as if reaffirming the migration cues before continuing migration. In the mutant this process of migrating and pausing is disrupted which the group propose is responsible for reduced migratory distance however when they remove cilia at a later time point this defect is not observed. This once more highlights the time-dependent phenotype observed in conditional primary cilia mutants.

1.4.4 Disruption primary cilia causes human ciliopathies

Although their occurrence is rare, there are a number of human conditions in which cilia are disrupted; these are collectively termed 'ciliopathies'. The syndromes often include a number of organ systems such as the brain, limbs, kidneys and eyes but many have clinical manifestations unique to the defective cilia component. The more common conditions are Nephronophthisis (NPHP), Joubert Syndrome (JS), Meckel-Gruber syndrome (MKS), Bardet-Biedl Syndrome, Senior Løken syndrome (SLS) and Leber's Congenital amaurosis (LCA) (Waters and Beales, 2011). For a table showing the variety of phenotypic symptoms see table 1.2. To complicate the disease classifications, many of the proteins were identified and

named as causative agents of specific conditions but have later been found to cause multiple syndromes for example; Meckel-Gruber syndrome protein 1 (MKS1) is able to cause both Meckel-Gruber Syndrome (MKS) and Joubert Syndrome (JS). Cep290 is one of the most well studied proteins causing human ciliopathies. It is found in nearly all of the known conditions with over 100 causative mutations identified (Coppieters et al., 2010).

Neural defects of human ciliopathies often include hydrocephaly and hypoplasia or aplasia of the cerebellar vermis. In JS a thickening of the cerebellar peduncles and narrowing of the midbrain tegmentum causes a distinct shape evident in axial MRI scans known as the 'Molar Tooth Sign' (Patel and Barkovich, 2002). As the cerebellum is chiefly responsible for motor coordination, ataxia is a common symptom associated with this malformation. In MKS a common neural tube defect is the failure of the neural tube to close properly causing a bulge or protrusion of the occipital lobe, known as occipital meningo-encephlocele (Paetau et al., 1985). Cortical defects seen in JS also include supernumerary small folds known as polymicrogyria and thin corpus callosum (Dixon-Salazar et al., 2004). Another phenotype commonly described in ciliopathies is mental retardation which although is a more generalised term again emphasises a role for cilia in neural development.

Table 1.3 Summary of the Human ciliopathies. Both the causative genes and the broad phenotypic defects are listed. Table adapted from (Gerdes et al., 2009, Waters and Beales, 2011) with additional information from (Ye et al., 2014, Baala et al., 2007).

Condition	Leber's Congenital amaurosis (LCA)	Senior Løken syndrome (SLS)	Nephronophthisis (NPHP)	Meckel-Gruber syndrome (MKS)	Bardet-Biedl Syndrome (BBS)	Joubert Syndrome (JBTS)	Oral Facial Digital syndrome (Ofd)
Causative genes:	*CEP290, RPGRIPL1*	*CEP290, NPHP1, NPHP3, NPHP4 NPHP5, INVS*	*CEP290, NPHP1, NPHP3, NPHP4, NPHP5, INVS, GLIS2, NEK8, TMEM67, RPGRIPL1, XNPEP3*	*CEP290, NPHP3, TMEM67, RPGRIPL1, BBS-2,-4,-6, MKS1, MKS2, MKS3, TMEM216*	*CEP290, TMEM67, BBS1-12, 15, MKS1,*	*CEP290, NPHP1, AHI1, TMEM67, RPGRIPL1, ARL13b, TMEM216, INPP5E, MKS3,*	*CEP290, TMEM216, OFD1, C2CD3/TALPID2*
Phenotype							
Cerebellar hypoplasia			✓		✓	✓	✓
Occipital encephalocele				✓			
Hepatic disease		✓	✓	✓	✓	✓	
Renal disease		✓	✓	✓	✓	✓	✓
Mental retardation	✓		✓		✓	✓	✓
Obesity					✓	✓	
Polydactyly				✓	✓	✓	✓
Retinopathy	✓	✓	✓		✓	✓	✓
Situs inversus		✓	✓	✓	✓	✓	
Skeletal dysplasia				✓			
Cleft palate				✓			✓

1.4.5 Disruption of centrosomes causes Microcephaly

In contrast to many of the ciliopathy symptoms, defects in the centrosome are also capable of causing clinical human conditions with surprising difference in phenotype. Autosomal recessive microcephaly (MCPH) is characterised by reduced brain size of more than three standard deviations of which the cerebral cortex is disproportionately small (Mochida and Walsh 2001). Nine causative genes have been implicated of which five are centrosomal (*CPAP*, *CEP152*, *CEP135*, *STIL* and *CDK5RAP2*) and two are found at mitotic spindle poles (*WDR62* and *ASPM*) (Chavali et al., 2014).

The primary cause of MCPH is a result of reduced proliferation of neural progenitors during development. Knockdown of related genes have been shown to result in altered cleavage plane and a switch from symmetric to asymmetric cell divisions, i.e. a reduction in equal divisions, which would normally propagate the progenitor population, and an increase in unequal division to produce neurons which is a shift eventually acting to deplete the progenitor pool (Fish et al., 2006, Gruber et al., 2011). Another cause of reduced proliferation seen in MCPH is defective mitosis, increased cell cycle exit and apoptosis (Lizarraga et al., 2010). A study in zebrafish looking at a range of MCPH proteins demonstrated a delay in prometaphase and abnormal centrosome maturation and duplication (Novorol et al., 2013). Mitotic delay is commonly reported in MCPH and these interruptions are able to trigger premature cell cycle exit of proliferating cells, even if mitosis eventually progresses normally (Uetake and Sluder, 2010). Whilst there appears to be a range of causes of MCPH the common factor is the regulation of centrosome, whether it be duplication, maturation or its ability to complete mitosis.

1.4.6 Other clinical conditions associated with primary cilia

Centrosomal proteins have also been associated with other human conditions. *Disrupted in Schizophrenia 1* (*DISC1*) is one of few genes whose disruption contributes to familial forms of Schizophrenia (Millar et al., 2000). This is a complex condition where symptoms include hallucinations, delusions, social withdrawal and cognitive dysfunction. Interestingly DISC1 has been shown to localise at the centrosome, bind microtubules and displays a punctate perinuclear pattern (Morris et al., 2003). More recently DISC1 has been

shown to interact with both PCM1 and BBS4 with disruption of any of the three resulting in defective migration, with simultaneous reduction of both BBS4 and Disc1 having a more severe effect (Kamiya et al., 2008). Furthermore the study identified a candidate mutation in *PCM1* as a risk factor in Schizophrenia.

An additional candidate gene *Abelson Helper Integration Site 1 (AHI1)* which is generally considered a causative element of Joubert syndrome has also been identified as a risk locus for Schizophrenia (Amann-Zalcenstein et al., 2007, Ingason et al., 2007). In the same region, single nucleotide polymorphisms in *AHI1* were also identified in patients with Autism Spectrum Disorders (ASD) which correlated with many patients with JBST also exhibiting ASD (Alvarez Retuerto et al., 2008).

1.5 Project aims and objectives

Primary cilia and centrosomes are required for a range of cellular functions and are essential for correct mammalian development, especially in a complex structure such as the central nervous system (CNS). The regulation and formation of primary cilia and centrosomes is still under intense investigation and we are beginning to gain an understanding of the essential molecular components. Ta3 is a basal body protein shown to be essential for formation of primary cilia (Yin et al., 2009). Recent data has also demonstrated its interaction with important centrosomal proteins including Cep290, Cp110, Cep97, Cep120 and Rab8 (Kobayashi et al., 2014, Wu et al., 2014).

The aims of this project are to explore the roles of Ta3, and primary cilia in the developing brain. Thanks to the versatility of the Cre-LoxP system, it will utilise the recently described *Ta3*$^{fl/fl}$ mouse (Bangs et al., 2011) to conditionally target the function of *Ta3* in a spatially and temporally defined way. A *Cre*-deleter strain expressing the Cre recombinase enzyme under the control of a *nestin* promoter/enhancer will be used to target recombination of *Ta3* in the developing CNS.

The *nestin Cre*-deleter (*NesCre*) is a very common strain used to cause conditional deletion in the developing nervous system from around E10.5 onwards. It was generated over 15 years ago and there are a number of resources demonstrating its recombination in the developing brain (Tronche et al., 1999, Heffner et al., 2012, Liang et al., 2012). The *NesCre* strain is a well-recognised neural deleter and due to its high usage in numerous other studies, it will allow the best possible comparison between similar conditional mutants which may help to better elucidate the roles of Ta3. The commercial availability of the deleter and its long standing use make it both a practical and useful approach to study the role of Ta3 in the developing brain. Currently there is limited information on the neural role of Ta3 beyond mid-gestation and we expect mice to have a notable and informative phenotype in the developing and adult brain. Work will primarily focus on characterising the phenotype of this conditional mouse mutant.

Initially, gross morphological and histological differences in developing brain structures will be assessed and notable phenotypes will provide areas of focus for further study. Full characterisation will involve immunohistochemistry to assess proliferation,

migration and differentiation of neuronal subtypes. Additional molecular approaches and *in vitro* cell culture will try to examine the cellular phenotype and attempt to address the underlying mechanisms. Given the clinical significance of primary cilia and centrosomal function, this study aims to contribute to better understanding the roles of Ta3 in the context of neural development.

Chapter 2 – Methods

Analytical grade chemical were obtained from Sigma-Aldrich, UK or Fisher Scientific, UK. All solutions were made with MilliQ ultrapure water and sterilised by autoclaving. Recipes and solutions used are listed in appendix 1.

2.1 Mice colony management and experiments

2.1.1 Mouse strains

Mice carrying the floxed *Ta3* allele (*Ta3*$^{fl/fl}$) were generated as described previously (Bangs et al., 2011) and were maintained as a homozygous line (fl/fl) on an inbred Bl6 background. The Cre deleter mouse strains (1) *B6.Cg-Tg(Nes-Cre)1kln/J* (*NesCre*) (Tronche et al., 1999) and (2) *B6.Cg-Tg(Ubc-cre.EsR1)1Ejb/J* (UbcCreER^{T2}) (Ruzankina et al., 2007) were obtained from The Jackson Laboratory and maintained as hemizygous lines on inbred Bl6 backgrounds.

2.1.2 Mouse colony management

Mice were maintained on a twelve hour light/dark cycle with access to food and water *ad libitum*. All procedures were approved by University of Bath Ethical Review and were conducted in accordance with UK Home Office guidelines and the UK Animals (Scientific Procedures) Act, 1986.

2.1.2 Breeding to generate experimental mice

Ta3 mice were bred to NesCre mice to produce stud males of genotype *Ta3*$^{fl/wt;NesCre}$, these were maintained by keeping males from experimental crosses between males (*Ta3*$^{fl/wt;NesCre}$) and females (*Ta3*$^{fl/fl}$). Ta3 mice were bred to UbcCre mice to produce stud males of genotype *Ta3*$^{fl/fl;UbcCre}$, these were maintained through breeding between males (*Ta3*$^{fl/fl;UbcCre}$) and females (*Ta3*$^{fl/fl}$).

2.1.3 Genotyping

Isolation of DNA: For genotyping purposes, tail biopsies and ear punches were taken from postnatal mice at weaning. Tissues were digested overnight at 54°C in lysis buffer (200

µl, appendix 1.1) containing Proteinase K (50 µg/ml). Digested lysates were extracted with an equal volume of buffered phenol (pH7.4):chloroform:isoamyl alcohol (25:24:1), and centrifuged (5 min at 16060 x g). The upper aqueous phase was removed to a fresh tube, and DNA precipitated by the addition of cold absolute ethanol (2.5 volumes) followed by incubated on ice (15 min). The precipitated DNA was centrifuged (15 min at 16060 x g), the supernatant was removed and DNA pellet washed with 70% ethanol (1 ml, v/v). DNA was centrifuged (15 min at 16060 x g), 70% ethanol removed and pellet was briefly air dried. The DNA precipitate was dissolved in TE buffer (50 µl, appendix 1.2). The genomic DNA quality and yield was assessed by electrophoresis on an agarose gel (0.8% w/v, described in section 2.1.4) buffered with TBE (appendix 1.3).

Polymerase chain reaction (PCR): Genotyping of mouse strains was carried out by PCR using GoTaq® Flexi DNA Polymerase (Promega, UK), according to manufacturer's instructions. Table 2.1 shows primer sequences used for PCR. For each primer pair a master-mix was created, divided equally between reaction tubes and DNA sample added. Final reaction volume was 30 µl; see table 2.2 for reaction components and table 2.3 for cycling conditions. PCR products were run, together with low molecular weight ladder, on agarose gel (1.5% w/v, described in section 2.1.4) buffered with TBE.

Table 2.1 List of mouse genotyping primers

Name	Sequence	Product	Reference
Talpid3 (flox)	FP-5' TGCCATGCAGGGATCATAGC 3' RP-5' GCTAGTACATTGCTGCAAGC 3'	470bp (fl), 351bp (wt)	(Bangs et al., 2011)
Talpid3 (deleted)	FP-5' TGCCATGCAGGGATCATAGC 3' FP-5' GAGCACACTGGAGGAAAGC 3'	273bp	(Bangs et al., 2011)
Cre	FP-5' CATTACCGGTCGATGCAACGAGTGATGAG 3' RP-5' GAGTGAACGAACCTGGTCGAAATCAGTGCG 3'	408bp	Subramanian Lab

Table 2.2 Components and concentrations for PCR reactions

Component	Concentration
GoTaq Flexi Buffer	1 X
MgCl2	1.5 mM
dNTP	0.2 mM (each base)
Forward primer	1 µM
Reverse primer	1 µM
GoTaq Polymerase	1.25 U
Betaine (optional)	1 M
DMSO (optional)	1-5% (v/v)
Water	-
DNA Template	<0.5 µg

Table 2.3 Cycling conditions for PCR reactions

Step		Temperature	Duration	Cycles
1	Denaturation (initial)	95 °C	3:00	1
2	Denaturation	95 °C	0:30	35
	Annealing	55 °C	0:30	
	Extension	72 °C	1:00	
3	Extension (final)	72 °C	5:00	1
	End	4 °C	∞	

2.1.4 Agarose gel electrophoresis

PCR products were analysed by gel electrophoresis. Agarose (0.8-1.5% w/v) was melted in TBE using a microwave. Once cooled, ethidium bromide was added (0.5 µg/ml) and solution poured into a gel casting mould. Once set, gels were placed in electrophoresis tank filled with TBE and samples loaded into wells. PCR products created using GoTaq® Flexi DNA polymerase contained blue and yellow dyes ready-to-load, other DNA samples were mixed with DNA loading buffer (appendix 1.4). Gels were electrophoresed at fixed voltage (5 V/cm).

2.1.5 Recording mice behaviour

Movement and behaviour of mutant and wild type mice was recorded using a Nikon D3100 camera with tripod over an open cage. Bedding was temporarily removed during filming and behaviour recorded (1-5 min). Periods of representative behaviour were selected and appropriate labels added using Windows Movie Maker Live software.

2.2 Histology and Histochemistry

2.2.1 Gelatin subbed slides

Microscopic slides were subbed to improve adherence of sections. Briefly, new slides were soaked in Ethanol:HCl (1:1, HCl 10.17 M) overnight, thoroughly washed with tap water (10-15 changes) followed by soaking in deionised water (2 x 30 min). Slides were subbed by dipping three times in gelatin-chromium alum solution (Appendix 1.5) and allowed to dry. Subbed slides were wrapped in aluminium foil and baked at 200°C (2-3 hours).

2.2.2 Dissection and processing of tissues

Brains were dissected from postnatal mice euthanised by intraperitoneal injection of sodium pentobarbitone solution (200 mg/kg) (Euthatal; Merial Animal Health Ltd, UK). Dissected brains were rinsed in ice cold phosphate buffered saline (PBS), where necessary they were bisected in sagittal or coronal orientation before fixing in ice cold paraformaldehyde (PFA, 4% w/v in PBS) or methanol:acetic acid (3:1). Tissues were fixed overnight at 4°C.

PFA fixed brains were either embedded in wax or frozen in OCT. For wax embedding, PFA fixed brains were washed in PBS (1 hour), dehydrated through increasing

ethanol series (1 hour each in 30%, 50%, 70%, 80%, 90%, 95%, 100% v/v), followed by isopropanol (1 hour) and cleared in toluene (2 x 30 min). Methanol:acetic acid fixed tissues were washed in 70% ethanol and dehydrated and cleared as described above. Cleared brains were infiltrated with molten paraffin-wax at 58°C (Fibrowax™, VWR International, Leuven) (2 x 12-24 hours). Brains were orientated in paraffin-wax filled moulds, allowed to set and blocks stored at 4°C until sectioned.

PFA fixed brains for cryosectioning were washed in PBS (1 hour), transferred to sucrose solution (30% w/v in PBS with azide 0.05% w/v) and allowed to sink at 4°C (approximately 1 – 4 days). Brains were transferred to a 1:1 solution of sucrose:OCT™ (Optimal Cutting Temperature Compound, VWR, UK) at 4°C (30 min). Tissues were placed in moulds containing OCT™ and frozen on a metal plate cooled on dry ice. Once frozen, tissue blocks were stored at -80°C until sectioned.

2.2.3 Sectioning of tissues

Paraffin sections (10 µm) were cut using a microtome (Leica Jung RM2035). Sections were floated on warm water (40 °C), mounted on subbed slides, dried overnight (40 °C) and stored at 4°C. Frozen OCT embedded brains were cryosectioned (20 µm) using a cryostat (Leica CM1850). Sections were pressed onto cold subbed slides and slowly warmed to room temperature. Sections were dried at room temperature (30 – 60 min) and stored at -20°C.

2.2.4 Hematoxylin and eosin Staining

Sections of paraffin embedded brains were dewaxed in Histoclear™ (National Diagnostics, Yorkshire) or Xylene (2 x 5 min) and rehydrated through decreasing ethanol series (2 x 3 min: 100%, 1 x 3 min: 95%, 75%, 50%, 30% v/v) with a final wash in water. They were immersed in Mayer's Hematoxylin (5 min), rinsed in water (2 x 2 min), and treated with ammonia water (0.0005% v/v, 30 sec) to develop the blue colour. Slides were washed in water (2 x 2min), dehydrated through increasing ethanol series (2 min x 30%, 50%, 70%) and counterstained in Eosin-Y (1% w/v in 70% ethanol, 2 min). They were quickly rinsed in an ethanol series (3 sec: 70%, 90%, 2 x 2 min: 100%), cleared in Histoclear™ or Xylene (2 x 5 min) and coverslips were mounted with DePeX™ mounting medium (Gurr; VWR International, Leuven). Frozen OCT embedded sections were allowed to warm to room temperature, washed with PBS (5 min), water (5 min) and stained as described above.

2.2.5 Silver Staining

Silver staining was performed using Garvey's alternative method (Garvey et al., 1999). Sections of paraffin embedded brains were dewaxed in Histoclear™ or Xylene (2 x 5 min) and rehydrated through decreasing ethanol series (2 x 3 min: 100%, 1 x 3 min: 95%, 75%, 50%, 30% v/v) with a final wash in water. Sections were then sensitised in silver nitrate solution (0.1% w/v silver nitrate, 0.0025% w/v citric acid) at 65°C (5 min). They were quickly dehydrated through increasing ethanol series (1 x 3 sec: water, 95%, 100%) and held in gum mastic solution (2.5% w/v in ethanol, 5 min). Slides were placed in freshly prepared developing solution (appendix 1.33) at 65°C and desired staining intensity was determined empirically (4-8 min). Reaction was stopped in water, slides dehydrated through increasing ethanol series (1 x 3 min: 30%, 50%, 75%, 95%, 2 x 3 min: 100%), cleared in Histoclear™ (2 x 5 min) and coverslips were mounted with DePeX™.

2.2.6 Immunohistochemistry

Sections of paraffin embedded brains were dewaxed in Histoclear™ or Xylene (2 x 5 min). Slides were rehydrated through decreasing ethanol series (2 x 5 min: 100%, 3 min: 95%, 75%, 50%, 30%), washed in water (5 min) and PBS (5 min). Frozen embedded sections were warmed to room temperature and washed in PBS (5 min) to remove OCT. If required, antigen retrieval was carried out by placing sections in antigen retrieval solution (appendix 1.6) and microwaved until boiling. Once buffer was boiling, paraffin embedded sections were microwaved (20 min), after which they were allowed to cool (20 min). In the case of frozen embedded sections, once buffer was boiling both slides and buffer were transferred to a boiling water bath (20 min), after which they were allowed to cool (20 min). After antigen retrieval, slides were washed in PBS (5 min).

Slides were briefly dried, sections circumscribed with ImmEdge PAP pen (Vector laboratories Ltd., UK) and incubated in blocking buffer (50-100 µl, appendix 1.7) at room temperature (1 hour). Blocking buffer was removed and primary antibodies diluted in fresh blocking buffer were added to the sections (50-100 µl). Antibodies were incubated overnight at 4 °C, Table 2.4 lists the primary antibodies used. For dual labelling up to two primary antibodies were diluted in the same mixture. Slides were washed in PBS with Tween-20 0.1% (v/v) (PBST, 4 x 10 min). Appropriate secondary antibodies were used at a dilution of 1:1000 in blocking buffer, Table 2.5 lists secondary antibodies used. For dual

labelling up to two secondary antibodies were used in the same mixture. In all cases 4',6-Diamidino-2-Phenylindole (DAPI) was also added to secondary antibody mixture (1 µg/ml). Slides were washed in PBST (2 x 10 min) followed by PBS (2 x 10 min) and coverslips mounted with Mowiol (Polysciences Inc., Germany, appendix 1.8).

2.2.7 BrdU administration and detection

Bromodeoxyuridine (BrdU, 20 mg/mL in PBS) was administered to mice by intraperitoneal injection (100 mg/kg bodyweight) one hour prior to euthanasia. Brains were dissected, fixed in methanol:acetic acid and processed as described in section 2.2.2. Paraffin sections were cut as described in 2.2.3. Paraffin sections were dewaxed overnight in xylene and rehydrated as described in section 2.2.6. Sections were incubated in HCl (0.1 M) containing Pepsin (0.01% w/v) at room temperature (20 min). Slides were washed in PBS (2 x 10 min), slides briefly dried and sections circumscribed with PAP pen. BrdU incorporation was detected by immunohistochemistry using monoclonal antibody to BrdU, as described in section 2.2.6.

Table 2.4 List of primary antibodies used for immunohistochemistry

Target	Host	Dilution	Supplier	Code
Adenylyl cyclase III	rabbit	1:1000	Santa Cruz	C-20
Acetylated α-tubulin	mouse	1:1000	Sigma-Aldrich	T6793
Beta III tubulin	mouse	1:500	Chemicon	MAB1637
BLBP	rabbit	1:500	AbCam	Ab32423
BrdU	mouse	1:50	DSHB	G3G4
Calbindin d-28k	mouse	1:4000	Swant	300
Caspase-3 (active)	rabbit	1:2000	AbCam	Ab13847
Ctip	rat	1:500	AbCam	Ab18465
Cux1	rabbit	1:50	Santa Cruz	SC13024
Dcx	rabbit	1:200	Cell signal	460 4S
GABA	rabbit	1:500	Sigma-Aldrich	A2052
GAD65/67	rabbit	1:500	Millipore	Ab1517
gamma-tubulin	rabbit	1:1000	Sigma-Aldrich	T5192
GFAP	mouse	1:400	Sigma-Aldrich	G3893
GFAP	rabbit	1:100	Invitrogen	180063
Gli1	rabbit	1:500	Cell Signal	V812
Ki67	rabbit	1:100	Millipore	Ab9260
MCM2	goat	1:100	Santa Cruz	SC9839
Nestin	mouse	1:50	DSHB	Rat401
NeuN	mouse	1:1000	Millipore	Mab377
Neurofilament	mouse	1:5	DSHB	2H3
Parvalbumin	rabbit	1:2000	Swant	PV25
Pax6	rabbit	1:500	Covance	PRB-278P

PCNA	mouse	1:4000	Cell signalling	2586
Pericentrin	rabbit	1:2000	AbCam	ab4448
Phosphohistone 3	rabbit	1:1600	Cell Signal	3377
Reelin	mouse	1:1000	DSHB	5RA
Satb2	rabbit	1:100	AbCam	Ab51502
Sox2	rabbit	1:500	Millipore	Ab5603
Tbr1	rabbit	1:500	AbCam	Ab31940
Tbr2	rabbit	1:500	AbCam	Ab23345
TGN46	rabbit	1:500	AbCam	Ab16052
VGlut1	guinea pig	1:6000	Millipore	Ab5905

Table 2.5 List of secondary antibodies used for immunohistochemistry. All secondary antibodies were used at 1:1000 dilution. † and * indicate the most commonly used dual labelling pairs.

Fluorophore name	Specificity	Molecular Probes® cat #
Alexa Fluor 488*	Goat anti-Mouse	A-11001
Alexa Fluor 488†	Goat anti-Rabbit	A-11034
Alexa Fluor 488	Goat anti-Guinea Pig	A-11073
Alexa Fluor 488	Donkey anti-Goat	A-11055
Alexa Fluor 594*	Goat anti-Rabbit	A-11012
Alexa Fluor 594	Donkey anti-Goat	A-11058
Alexa Fluor 568†	Goat anti-Mouse	A-11004
Alexa Fluor 568	Rabbit anti-Mouse	A-11061
Alexa Fluor 488	Goat anti-Rat	A-11006

2.3 Image acquisition and analysis

2.3.1 Brightfield and fluorescence microscopy

Brightfield images were acquired with DMRB microscope using Leica DFC490 camera and Leica Application Suite (LAS) software. Low power brightfield images were obtained with Leica WILD MZ8 stereomicroscope using Leica DFC490 camera. Fluorescence images were acquired with DM5500B microscope equipped with motorised stage and Leica DFC360FX camera. Depending on the tissue thickness or specific stain either single images or Z-stacks were acquired using LAS software. For Z-stacks only, LAS 3D-deconvolution algorithm was applied to reduce out-of-focus light. Following deconvolution, either a single plane of focus was selected or Z-stacks were merged to create a maximum intensity 3D projection. Comparisons were always made between images acquired and processed in exactly the same way.

2.3.2 Image processing

Fiji imaging software was used to measure length, area, angle and cell counts (Schindelin et al., 2012). Data were subsequently exported to Microsoft Excel or Minitab17 for further analysis. Fiji software was also used to 'stitch' large composite pictures from overlapping fluorescence images. Sequential images of equal exposure were taken in a grid across the region of interest with adjacent images having a small overlap. Software aligned identical overlapping regions to stitch images together. Brightfield and fluorescence images were processed using Adobe Photoshop software to adjust brightness. Adjustments were always applied to whole images and equally between comparable images.

2.3.3 Statistical analysis

Statistical analysis was completed using Minitab17 software. Results were tested for normal distribution using Anderson Darling test and scores with $P > 0.05$ were deemed normal. The Bonett's test, a modified version of Lavard's test, and was used to determine variance of the mean and scores with $P > 0.05$ were deemed to have equal variance. Normal data with equal variance were analysed using parametric tests; typically a Students T test was used for comparison of means. Data that did not have either a normal distribution or equal variance were transformed to improve the distribution. If transformation was successful, parametric analyses were completed on transformed data however if data still

violated these assumptions non-parametric analyses were completed; typically a Mann-Whitney U test was used for comparison of median values.

2.3.4 Quantification of primary cilia

The number of cells with primary cilia were identified by immunolabelling for adenylyl cyclase III (ACIII), as described in section 2.2.6. Nuclear DAPI label was used to quantify the total number of cells and the number of cells with a primary cilium expressed as a percentage. In the cerebellum, for the external granule layer (EGL) a region of interest (ROI) spanning 25 µm in length and covering the whole EGL cross-section was selected. For the internal granule layer (IGL) a 25 µm square ROI was drawn at the IGL/molecular layer (ML) boundary. In the hippocampus; a ROI of 50 µm width was selected spanning a cross-section of both granule cell layer (GCL) and sub granular zone (SGZ). ROIs utilised the full tissue thickness imaging a Z-stack of 20 µm depth. ROIs were selected from three slides per mouse and used to calculate an average value. Average values from three mice were then used to make comparisons (n=3). Data were normal with equal variance and a T-test was used to show significance between means.

2.3.5 Cerebellar proliferation analysis

Proliferation in the EGL was quantified by selecting a ROI spanning 200 µm length from each cardinal lobe and counting the total number of DAPI+, BrdU+ and PH3+ cells. Ages P10/P15 had sparse number of PH3+ cells and so a larger ROI was used encompassing the entire crown; the distance was measured and number of cells per 200 µm calculated. ROIs were selected from three slides per mouse and used to calculate an average value. Average values from three mice were used to make comparisons (n=3). Data were normally distributed with equal variance so a T-test was used to show statistical significance.

Proliferation and cell density in the IGL was quantified by selecting a 50 µm square ROI and the total number of DAPI+, BrdU+ and PH3+ cells counted. Data were normally distributed with equal variance so a T-test was used to show statistical significance.

2.3.6 Cerebellar length measurements

EGL thickness was quantified by taking five equally spaced width measurements per cardinal lobe. Measurements were selected from three slides per mouse and used to

calculate an average value. Average values from three mice were used to make comparisons (n=3). Data were normally distributed with equal variance so a T-test was used to show statistical significance.

2.3.7 Cerebellar apoptosis quantification

The number of Caspase-3 positive cells in the EGL and IGL was estimated by counting the total number of immunostained cells within each cardinal lobe per slide. The number of positive cells per 10000 μm^2 was calculated for comparison. Measurements were selected from three slides per mouse and used to calculate an average value. Average values from three mice were used to make comparisons (n=3). Data from the EGL and IGL were normally distributed with equal variance so a T-test was used to show significance between mean values.

2.3.8 Cerebellar nuclear analysis

Nuclear area and orientation was quantified from DAPI labelled sections using ROIs spanning 50 µm length from EGL for each cardinal lobe. All ROIs were rotated to adjust the EGL to a horizontal orientation and all discernible nuclei traced using the FIJI imaging software. Orientation was calculated using 'fit ellipse' function which draws an ellipse of best fit and calculates the major angle in the range 0-180°. All angles greater than 90° were 'mirrored' within a 0-90° range using the following equation: $\sqrt{(x-180)^2}$. Angles were grouped into nine equal bins (10° per bin) and the number of cells in each bin expressed as the percentage of total cells measured. Measurements were taken from one ROI for P5/P10 mice and two ROIs from P15 for each lobe per slide.

For nuclear area comparisons, measurements were selected from three slides per mouse and used to calculate an average value. Average values from three mice were used to make comparisons (n=3). Data were normally distributed with equal variance so a T-test was used to show significance between mean values.

2.3.9 Analysis of cerebellar Purkinje cells

The total number of Purkinje cells was quantified from cerebella immunohistochemically labelled for calbindin-d28k. Before counting, multiple microscope

images were stitched as described in 2.3.2 to visualise the entire cerebellar cross-section. The total cerebellar area was measured for each slide and used to calculate Purkinje cell density. Purkinje cells counted from three slides per mouse and used to calculate an average value. Average values from three mice were used to make comparisons (n=3). Data were normally distributed with equal variance so a T-test was used to show significance between mean values.

Primary dendrite length was calculated from confocal images acquired using a Zeiss LSM510 META confocal microscope. Measurements of twenty six cells taken from two-four slides from one mouse for control and mutant. Cells were selected at random from the crown region of anterodorsal, central and posterior lobes. Data were normally distributed with equal variance and presented using bar chart. As only one mouse was used for analysis statistical tests were not completed.

2.3.10 Analysis of cerebellar glial morphology

Representative glial outlines were obtained using FIJI imaging software. Images labelled immunohistochemically for GFAP were converted to 8-bit grey scale. Brightness and contrast were adjusted to clearly display glial outlines and images pseudocoloured to provide contrast.

2.3.11 Hippocampal thickness analysis

GCL or SGZ thickness was quantified by taking five equidistant measurements for each section and an average thickness obtained. Three sections from each mouse were used to calculate an average and three mice were used form comparisons (n = 3). Data were normal with an equal variance so a T-test was used to compare mean values.

2.3.12 Hippocampal cell type analysis

Hippocampal cell type analysis and proliferation was quantified from sections colabelled for Paired box protein (Pax-6) and Neuronal nuclei (NeuN) or mini-chromosome maintenance protein 2 (MCM2) and marker of proliferation MKI67 (Ki67). The total number of labelled cells was counted in the GCL or SGZ and the area measured. The number of cells per 50000 μm^2 was calculated for comparison. Data were acquired from three slides per mouse and used to calculate an average. Average values from three mice were used for

comparisons (n=3). All other data were normal with equal variance and was compared using a T-test.

The proportion of Ki67 and MCM2 cells was compared by expressing the number of single- and double-labelled cells as a percentage of total labelled cells for each section quantified. Data were acquired from three slides per mouse and used to calculate an average. Average values from three mice were used for comparisons (n=3). Percentages were normal with equal distribution and T-test was used to compare mean values. Ki67-positive cells with GFAP-positive fibres were identified using high magnification images of individual cells through a 20 µm z-stack. The number of single- and double-positive cells were quantified and the total number of labelled cells pooled to calculate the final percentage. Due to the low number of cells, statistical tests were not completed.

2.3.13 Hippocampal quantification of misplaced neurons

NeuN-positive neurons positioned outside of the dentate gyrus were identified by drawing a line to determine the outer boundary of the GCL. A ROI was selected encompassing the entire length of the GCL and extending 50 µm into the ML. The number of NeuN-positive cells were quantified and expressed as number of cells per 1000 µm. Data were acquired from three slides per mouse and used to calculate an average. Average values from three mice were used for comparisons (n=3). Data were normally distributed with equal variance and a students T-test was used to compare means.

2.4 RNA analysis and qPCR

2.4.1 Preparation of RNase-free glassware and solutions

RNase-free glassware, equipment and solutions were used for all experiments involving RNA. Glass beakers, measuring cylinders, petri dishes and dissecting tools were baked at 200°C (2-3 hours) to destroy RNase enzymes. MilliQ-water, PBS, and EDTA, were treated with diethylpyrocarbonate (DEPC, 0.1% v/v), mixed well and left overnight. Glass bottles were rinsed with DEPC-treated MilliQ water and also left overnight. DEPC-treated solutions and glassware were autoclaved to inactivate DEPC. Solutions containing chemicals sensitive to DEPC (TE, TBE) were made using baked glassware, DEPC-treated water, DEPC-treated EDTA and autoclaved. RNase-free 70% ethanol was made using DEPC-treated water. Where DEPC-treatment or baking was not possible and all surfaces, electrophoresis tanks

and gloves were treated with RNase ERASE (MP Biomedicals, UK) and rinsed with DEPC-treated water.

2.4.2 Isolation of total RNA from tissue

Mice were euthanised as described in section 2.2.2 and brains dissected and rinsed in DEPC-treated PBS. Tissues were quickly minced with scalpel blade, placed in pre-weighed tube (1.5 ml), weighed and 1 ml Trizol (Invitrogen, UK) added per 100 mg wet tissue weight; typical values ranged from 10-100 mg. Tubes were vortexed, frozen using liquid nitrogen and stored at -80°. Samples were thawed and homogenised by passing several times through P1000 pipette, followed by five freeze-thaw cycles using liquid nitrogen and 37°C water bath. Samples were passed through P200 pipette with additional freeze thaw cycles until smooth. To remove insoluble material, Trizol was centrifuged (16060 x g for 10 min) at 4°C and supernatant transferred to new tube. Chloroform was added (1/5th Trizol volume), shaken vigorously (15 sec) and allowed to rest (3 min). Phases were separated by centrifugation (16060 x g for 15 min) at 4°C and the upper aqueous phase transferred to a fresh tube. Glycogen was added to a final concentration of 0.05-1 µg/µl, mixed well and RNA precipitated with isopropanol (5/6th volumes of recovered upper aqueous phase, approx. 50% original Trizol volume). Samples were incubated at room temperature (10 min) and precipitated RNA was centrifuged (16060 x g for 10 min) at 4°C. Supernatant was removed, precipitated RNA was washed with 70% ethanol (1 ml) and centrifuged (16060 x g for 10 min) at 4°C. Precipitated RNA was briefly dried and dissolved in DEPC-treated water (typically 50-200 µl). Concentration and purity was assessed using Nanodrop spectrophotometer (Fisher, UK). Ratios of 260/280 nm and 260/230 nm were used to assess RNA purity; values of >1.8 were deemed acceptable.

2.4.3 RNA quality assessment: agarose gel analysis

Quality of RNA was assessed by running 100-500 ng on RNase-free agarose gel (1.5%). Gels were made as described in 2.1.4 using RNase-free TBE, dedicated RNase-free agarose powder and omitting ethidium bromide. Gel tanks were treated with RNase ERASE and washed with DEPC-treated water. RNA samples were mixed with sample denaturing buffer (10 µl, appendix 1.9), heated to 65°C (5 min) and cooled on ice (2 min). Denatured

samples were then mixed with RNase-free DNA loading buffer (2 µl) and loaded into wells. To assess RNA degradation 28S and 18S ribosomal RNA (rRNA) bands were observed. RNA samples of high quality had sharp bands with little smearing and a 28S:18S ratio of approximately 2:1.

2.4.4 Removal of genomic DNA (gDNA) from RNA samples

High quality RNA samples were treated with DNA-*free* Kit (Ambion, UK) to remove any remaining gDNA. Reactions contained RNA (10 µg), DNase I buffer and rDNase I (2 U) in a total reaction volume of 50 µl. Samples were incubated at 37°C (30 min) and the reaction halted by adding DNase inactivation reagent (0.2 volumes) and incubating at room temperature (2 min). Samples were centrifuged (16060 x g for 2 min) and supernatant transferred to fresh tube. Nanodrop and agarose gel analysis, as described in sections 2.4.2 and 2.4.3, were repeated to confirm RNA concentration and quality.

2.4.5 RNA quality assessment: Experion analysis

Quality of selected RNA samples was also analysed using Experion RNA StdSens Analysis Kit (BioRad, UK). RNA samples were prepared and analysis chips primed according to manufacturer's instructions. RNA ladder, followed by samples were loaded into the chip and run through the machine with the Experion software generating an electropherogram. Software compared the 28S and 18S ribosomal peaks in addition to degraded material to generate an RNA quality indicator (RQI) score; acceptable samples had values greater than eight.

2.4.6 Complementary DNA (cDNA) synthesis

cDNA was synthesised using high quality RNA and the RevertAid H Minus Reverse Transcriptase Kit (Thermo Scientific, UK). Duplicate reactions were set up with one omitting reverse transcriptase enzyme as control (RT-). RNA (2 µg) was mixed with Oligo-dT primers (0.5 µg) and water added to final volume of 12 µl (RT+) or 13 µl (RT-). Primers were annealed by heating to 65° (5 min) and cooled on ice (5 min). A master mix sufficient for all reactions was made and 7 µl added to all RT- reactions. Reverse transcriptase enzyme was added to the remaining master mix and 8 µl added to remaining RT+ reactions making a final reaction volume of 20 µl. Reaction mix had final concentration of buffer (1 X), RiboLock

RNase inhibitor (20 U), dNTP mix (1 mM) and RT+ contained RevertAid H Minus Reverse Transcriptase (200 U). Reactions were incubated at 42°C (60 min) followed by inactivation at 70°C (5 min). A working stock of cDNA was diluted using DEPC-treated water (10 ng/µl) and divided into small aliquots; both original reaction and working aliquots were stored at -20°C.

2.4.7 Design of quantitative real-time PCR experiments

Quantitative real-time PCR (qPCR) was completed using iQ-SYBR Green Supermix (BioRad, UK) with 10 ng of template cDNA per reaction. To ensure equal cDNA comparisons, reactions were created by mixing sufficient iQ-SYBR Green Supermix, cDNA and water for all genes to be analysed. Mixes were divided, primers added (200 nM final concentration) and further subdivided into three technical replicates on PCR plates. Reactions had a final volume of 20 µl. RT- controls were run with GAPDH primers to demonstrate no contaminating gDNA was present. All other primers were intron spanning and did not require use of RT- controls. See table 2.6 for qPCR primer sequences and table 2.7 for qPCR cycling conditions. Expression levels were quantified relative to GAPDH and comparisons were made between three or four control and mutant mice (n=3 or n=4). Students T-test was used to compare mean expression values between control and mutant mice.

2.4.8 Primer design and qPCR efficiency

Most primer sequences were taken from previously published studies. All primers used for qPCR were tested at a range of known template dilutions and used to estimate PCR efficiency before carrying out qPCR analysis. Only reactions with efficiencies between 90-110% were used. Melt curves were also analysed to ensure amplification of single DNA product and this was confirmed by separating sample on an agarose gel (1.5%) as described in section 2.1.4.

Table 2.6 List of primers used for qPCR

Name	Sequence	Product	Reference
GAPDH:	FP- 5'CCTTCCGTGTTCCTACCCCCAATG 3'	155bp	(Yusa et al., 2009)
	RP- 5' GGAGACAACCTGGTCCTCAGTGTA 3'		
Gli1:	FP-5' TTCGTGTGCCATTGGGGAGG 3'	440bp	(Maye et al., 2000)
	RP-5' CTTGGGCTCCACTGTGGAGA 3'		
Gli2:	FP- 5' TTCGTGTGCCGCTGGCAGGC 3'	425bp	(Maye et al., 2000)
	RP- 5' TTGAGCAGTGGAGCACGGAC 3'		
Gli3:	FP-5'TTCGTGTGCCGCTGGCTTGA 3'	444bp	(Maye et al., 2000)
	RP-5' TGAATGGCTGCCGGAATCTC 3'		
Ptc1:	FP-5' GGTCACACGAACAATGGGTCT3'	682b	(Maye et al., 2000)
	RP- 5'CACATTCCACGTCCTGTAGC 3'		
Smo:	FP-5' TGGGATCCAGTGCCAGAACCCGCT 3'	562bp	(Maye et al., 2000)
	RP-5' ACGGTACCGATAGTTCTTGTAGCC 3'		
Axin2:	FP-5' GCGACGCACTGACCGACGAT 3'	196bp	(Lorenz et al., 2011)
	RP-5' GCAGCAGGTTCCACAGGCGT 3'		
Wnt3a:	FP-5'CAAGCACAACAATGAAGCAGGC 3'	199bp	(Kemp et al., 2005)
	RP-5'TCGGGACTCACGGTGTTTCTC 3'		
Wnt7a:	FP-5'CGACTGTGGCTGCGACAAG 3'	200bp	(Kemp et al., 2005)
	RP-5'CTTCATGTTCTCCTCCAGGATCTTC 3'		
Delta-like1:	FP-5' GGTTGCTCTGTGTTCTGCCG 3'	142bp	(Trombly et al., 2009)
	RP-5'GTTGGTCATCACACCCTGGC 3'		
Delta-like3:	FP-5'CTGGACCTTGTGATGGGAACC 3'	112bp	(Trombly et al., 2009)
	RP-5'CTCACCTCACATCGAAGCCC 3'		
Hes1:	FP-5'GAGCACAGAAAGTCATCAAAGCC 3'	133bp	(Trombly et al., 2009)

	RP-5’TCTCTAGCTTGGAATGCCGG 3'		
Hes5:	FP-5’GAGATGCTCAGTCCCAAGGAG 3'	203bp	(Trombly et al., 2009)
	RP-5’GCGAAGGCTTTGCTGTGTTT 3'		
Notch1:	FP-5’CGTGGATTCATCTGTAGGTGC 3'	134bp	(Trombly et al., 2009)
	RP-5’CATAGGCAGGTGGGACTACG 3'		
Notch2:	FP-5’ GCTGTCAATAATGTGGAGGCG 3'	125bp	(Trombly et al., 2009)
	RP-5’ TTGGCCGCTTCATAACTTCC 3'		

Table 2.7 Cycling conditions for qPCR

Step		Temperature	Duration	Cycles
1	Collect well factors	95 °C	2:30	1
	Denaturation (initial)	95 °C	0:30	
2	Denaturation	95 °C	0:10	40
	Annealing	60 °C	0:30	
	Extension (fluorescence acquisition)	72 °C	0:30	
3	Extension (final)	72 °C	5:00	1
	Melt curve analysis	55-98°C	-	
	End	4 °C	∞	

2.4.9 Identification of *TA3* mutations in human ciliopathies

Samples of gDNA from human patients with ciliopathy conditions were provided by Dr Andrea H Németh (Nuffield Department of Clinical Neurosciences, University of Oxford). Primers were designed to human *TA3* to cover complete exons and extend approximately 150 bp into intronic regions. Primers were designed using Primer-BLAST (NCBI) to have a melting temperature of 60°C and G/C content as close as possible to 50%. Primer sequences are listed in Table 2.8. Primer sequences were design by the author but all PCR reactions, purification and sequence analysis was completed by project student Fay Stafford under the supervision of the author.

PCR reactions were completed using Expand High Fidelity PCR system (Roche, UK) using cycling conditions described in Table 2.3. PCR products were treated with Exonuclease I (EXO) (Fermentas) and shrimp alkaline phosphatase (SAP) (Promega). A reaction containing PCR mixture (10 µl), Exonuclease I (1 µl, 20U) and Alkaline phosphatase (2 µl, 2U) was incubated at 37 °C for 15 min. Reactions were inactivated by heating at 85 °C for 15 min.

Products were purified using Qiaquick columns (Qiagen). Briefly, PB buffer was added to PCR product at a ratio of 5:1, this was then transferred to Qiaquick column and centrifuged (16060 x g for 1 min). Flow-through was discarded, 0.75 ml PE buffer added to column and centrifuged (16060 x g for 1 min). Flow-through was discarded, column was centrifuged once more (16060 x g for 1 min) and any remaining flow-through removed. DNA was eluted by adding 50 µl EB buffer (10 mM TrisHCl, pH 8.5) to the column. It was allowed to stand (1 min) and column centrifuged (16060 x g for 1 min). Eluted DNA was transferred to a new tube and small sample (1 µl) resolved on agarose gel (1.2%) as described in Section 2.1.4. Concentration of DNA was determined using a Nanodrop and diluted to 2 ng/µl. Sequencing reactions were completed by Eurofins Genomics Ltd using the same primer sequences used for PCR reactions and BigDye terminator cycle sequencing kit with an ABI3100 automated sequencer (Applied Biosystems). Chromatograms were analysed for frameshifts and sequences were aligned using Clustal W (EMBL-EBI). Frameshifted sequences were translated using the ExPasy Translate Tool.

Table 2.8 Primers used for sequencing of human Talpid3 exons 1-12 of Rik-001 and exon 6 of Rik003, using Joubert Syndrome patient genomic DNA. Primers were designed to span each exon of Rik-001 and exon 6 of Rik003 and approximately 100-200bp of flanking intron on either side. Table indicates the primer pairs used, the exon these correspond to, primer sequences, melting temperature (Tm) and amplicon size. *Italic text* indicates an additional primer pair used to amplify exon 6 of the longer Talpid3 transcript: Rik-003.

Primer	Exon (in Rik-001)	Template Strand	Tm (°C)	Amplicon Size (bp)
hTa3Ex1_565nt_F	ENSE00002500400	CCCTTAGACGCCGATTCGTT	59.4	565
hTa3Ex1_565nt_R		GTATCTCCAGAACGCCCGAG	61.4	
hTa3Ex2_457nt_F	ENSE00003723337	AGCTTTGTGGATGTTCGACATTT	57.1	457
hTa3Ex2_457nt_R		CGGGAAACAGGGTCAGTTTT	57.3	
hTa3Ex3_287nt_F	ENSE00003691021	AATTGTCTTTCCAACTTCTGCGT	57.1	287
hTa3Ex3_287nt_R		ACAAGGCATGCTGCTAATCAAAC	58.9	
hTa3Ex4_662nt_F	ENSE00003504620	CCTCCCAGAACACAGTAGTCAC	62.1	662
hTa3Ex4_662nt_R		ACCATTGCAAACCTTATTCTGGATT	59.8	
hTa3Ex5_338nt_F	ENSE00003557894	GATCGTGGAATGCTATGGCTG	59.8	338
hTa3Ex5_338nt_R		TGTCTAGCACCATGAGAAATGCT	58.9	
hTa3Ex6_432nt_F	ENSE00003515380	ACCAAATGACCTTGTTTGATAGGTG	59.7	432
hTa3Ex6_432nt_R		TGAGAGCAACTACAATGTTCCT	56.5	
hTa3Ex7_551nt_F	ENS00003642505	AGACATTTAGTGGGTAAAGGCTC	58.9	551
hTa3Ex7_551nt_R		AGTTACCCGCATTACAGGAGAA	58.4	
hTa3Ex8_408nt_F	ENSE00003620803	GGCATCACTGCTGCTACTACA	59.8	408
hTa3Ex8_408nt_R		TGCTCAGGAAATATGTTTTCAGCTT	58.1	
hTa3Ex9_448nt_F	ENSE00003665131	TGGGGTGAAGTTATTTCTCTACACT	59.7	448
hTa3Ex9_448nt_R		GCTTGATTTTCCCAGCAAGGG	59.8	
hTa3Ex10_376nt_F	ENSE00003645941	AGAAGCTAACTTAGGCCAGAATACA	59.7	376
hTa3Ex10_367nt_R		AAGGGGGAAGATATATTAGCATCAA	58.1	
hTa3Ex11_482nt_F	ENSE00003525938	GTCTCTTGTGATTTTCTGTGTTTCA	58.1	482
hTa3Ex11_482nt_R		TCACTTGGTGAAGGCCTCTG	59.4	
hTa3Ex12_561nt_R	ENSE00003473799	TGCCTGGCCCACATTAGTAT	57.3	561
hTa3Ex12_561nt_R		AAGTTCCACATCTTCAAAGTCAAT	55.9	
hTa3Rik3Ex6_429F	*ENSE00001430787*	*GTCACAAAGTGTACATCAATAGTGC*	*59.7*	*429*
hTa3Rik3Ex6_429R		*TCAGACAAGCTGCTGTGGTT*	*57.3*	

2.5 Western blot

2.5.1 Whole cell protein lysate preparation

Mice were euthanized as described in section 2.2.2 and brains dissected and rinsed in PBS. Brains were quickly minced with scalpel blade, placed in pre-weighed tube (1.5 ml), weighed and 1 ml sample lysis buffer (appendix 1.10) added per 100 mg wet tissue weight; typical values ranged from 10-100 mg. Tubes were vortexed, frozen using liquid nitrogen and stored at -80°. Brains were thawed and homogenised through 21G to 30G needles. Insoluble material was removed by centrifuging (16060 x g for 5 min), supernatant was divided into small aliquots and frozen at -80°C.

2.5.2 Estimation of protein concentration

Total protein concentrations were estimated using BCA Protein Assay Kit (Pierce, UK). A range of known bovine serum albumin (BSA) standards were made using lysis buffer (2000 µg/ml, 1500 µg/ml, 1000 µg/ml, 750 µg/ml, 500 µg/ml, 250 µg/ml, 125 µg/ml, 25 µg/ml). Aliquots of sample protein extract were thawed and diluted in lysis buffer (1:5, 1:25). Working reagent was made according to manufacturer's instructions and 200 µl added to 96-well microplate followed by 10 µl of lysis buffer, BSA-standard or sample. All reactions were completed in triplicate wells and plates incubated at 37°C (30 min) to allow colour development. Optical density (562 nm) was measured and used to calculate BSA-standard curve; this was used to estimate sample total protein concentration.

2.5.3 Polyacrylamide gel electrophoresis

Sodium dodecyl sulphate polyacrylamide gel electrophoresis (SDS-PAGE) was used to separate protein extracts. Tris-glycine polyacrylamide gels were cast using BioRad Mini Protean 3 gel apparatus to a thickness of 0.75 mm. Resolving gel (7%) and stacking gel (5%) compositions are listed in appendix 1.11 and 1.12 respectively. Samples were prepared by mixing protein lysate (20 µg) with protein loading dye (appendix 1.13) and denatured at 100°C (5 min). Gels were placed in running buffer (appendix 1.14), samples and unstained PageRuler protein ladder (Thermo, UK) were loaded into wells. A fixed voltage (8 V/cm) was applied until dye front entered the resolving gel at which point, voltage was increased (15 V/cm) until bromophenol blue reached bottom of the gel.

2.5.4 Transfer

Proteins were transferred to membranes using the wet transfer method. Gels were removed from glass plates, washed with MilliQ-water (1 min) and moved to transfer buffer (15 min, appendix 1.15). PVDF membranes (40 µM pore size) were soaked in methanol (1 min) followed by transfer buffer until use. Transfer cassettes were constructed with gel and membrane sandwiched between blotting paper and foam pads. Cassettes were transferred to a Hoefer TE22 tank (Hoefer, UK) and filled with transfer buffer. A fixed voltage (50 V) was applied for 1-2 hours with cooling solution set at 20°C. Following transfer, membranes were washed with MilliQ-water (1 min) and stained with Ponceau Red (5 min, appendix 1.16) to assess transfer efficiency. Membranes were destained by rinsing in water (5-10 min). Gels were also stained with coomassie blue (3 hours, appendix 1.17) and destained (2-3 hours, appendix 1.18) to check transfer efficiency.

2.5.5 Antigen detection

Protein ladder stained with ponceau red was cut away from membrane and permanently stained with amido black stain (5-10 min, appendix 1.19) followed by destain (2-3 hour, appendix 1.18). Remaining membrane was placed in blocking buffer (1 hour, appendix 1.20). Primary antibodies were diluted in blocking buffer and incubated with membrane overnight at 4°C. Table 2.9 lists the antibodies used for Western blot. Membranes were washed in PBST (4 x 10 min) and incubated with HRP-conjugated secondary antibody at room temperature (1 hour). Membranes used to detect loading control were not stained with primary antibody and instead stained with GAPDH HRP-conjugated antibody at room temperature (1 hour). Membranes were washed in PBST (2 x 10 min) and PBS (2 x 10 min) followed by addition of enhanced chemiluminescent (ECL) reagent (Haan and Behrmann, 2007) (appendix 1.21).

Amido black-stained protein ladders were re-aligned with the immunolabelled membrane. Brightfield and chemiluminescence images were taken using a Fusion-SL imaging system (Vilber Lourmat, Germany). Molecular weights were estimated by measuring the total gel length and distance migrated by both protein ladder and samples. A standard curve was created by plotting Log protein ladder size (Daltons) against their relative mobility (Rf). The size of detected proteins was then estimated according to their Rf values and comparison with the standard curve.

Table 2.9 List of antibodies and dilutions used for Western blot

Target	Host	Dilution	Supplier	Code
Gli2	Rabbit	1:1000	AbCam	Ab26056
Gli3	Rabbit	1:500	SantaCruz	H280
GAPDH-HRP	Mouse	1:10000	AbCam	Ab9494
rabbit-HRP	Mouse	1:7500	AbCam	Ab6721

2.6 Cell culture

2.6.1 Isolation of hippocampal cells for neurosphere culture

Five day old pups were generated by breeding stud males of genotype *Ta3*$^{fl/fl;UbcCre}$ to females of genotype *Ta3*$^{fl/fl}$. Mice were culled by cervical dislocation and doused with 70% ethanol. Brains were removed using sterile surgical tools and placed in a bacteriological petri dish (Sterilin, UK) containing DMEM/F-12 media (Life Technologies, UK).

For hippocampal cultures; brains were cut into coronal slices, transferred to DMEM/F12 media and dorsal hippocampi were removed using sterile forceps and dissecting microscope. Hippocampi were transferred through three petri dishes containing dissection solution (2 ml, appendix 1.22) and incubated in digestion solution (2 ml, appendix 1.23) at 37°C (15 min). For whole brain cultures; brains were removed, transferred through three petri dishes containing dissection solution and placed in digestion solution. Here they were finely minced using iris scissors and allowed to incubate at 37°C (15 min).

Cells were titurated into a single cell suspension using P1000 pipette and diluted with DMEM/F-12 containing Serum (1% v/v, 6 ml) to quench remaining papain. Cell clumps were removed by passing through sieve (40 µM). Cells were transferred into a Falcon tube (15 mL) and centrifuged (840 x g for 8 min). Supernatant was removed and cells washed with DMEM/F-12 (6 mL). The cell suspension was centrifuged (840 x g for 8 min) and supernatant removed. Cells were resuspended in neurosphere culture medium (appendix 1.24) and plated in bacteriological petri dishes (10,000 cell/cm^2, Sterilin, UK). Hippocampal

cultures were typically resuspended in 2 ml culture medium and transferred into a single 3 cm bacteriological petri dish. Cells were incubated for seven days at 37°C with 5% CO_2.

The genotype of cultured cells was determined by taking from spare tissue following dissection. Tissue was treated as described in section 2.1.3 and PCR used to identify genotype. Experiments described in this project used data acquired from three *Ta3*$^{fl/fl;UbcCre}$ hippocampal neurosphere lines isolated from three different mice (referred to as # 1, 2, 3). Control hippocampal neurosphere cells of *Ta3*$^{fl/fl}$ were taken from a single line.

2.6.2 Passaging of cultured neurospheres.

Neurospheres were passaged by pH-disassociation every seven days and single cells resuspended in fresh culture media. Neurospheres were collected in a Falcon tube (15 mL), centrifuged (270 x g for 3 min) and supernatant removed. PBS (5 mL) was added to the petri dish to collect remaining neurospheres and transferred to the Falcon tube to wash the neurosphere pellet. Neurospheres were centrifuged again (270 x g for 3 min), supernatant removed and resuspended in DMEM/F-12 (200 µl). Neurospheres were transferred to round bottom cryovial tube (Nunc, UK) and alkaline DMEM/F-12 (200 µl, see appendix 1.25) was added. Two minutes after addition, neurospheres were titurated with P1000 pipette (approx. 20 times). Three minutes later (5 min after addition of alkaline DMEM/F-12) cells were titurated to single cell suspension (approx. 20 times). Two minutes later (7 min after addition of alkaline DMEM/F-12) cell suspension was neutralised with acid DMEM/F-12 (200 µl, appendix 1.26). Cells were titurated once more (approx. 5 times) and transferred through sieve (40 µM) into Falcon tube (50 ml). Cryovial was washed with DMEM/F-12 (1.4 mL) and added to tube. A small sample (50 µl) was mixed at a ratio of 1:1 with trypan blue and cell count performed using haemocytometer. When splitting multiple dishes of the same neurosphere line this method was scaled up accordingly. Cells were resuspended using culture media and plated in bacteriological petri dishes (5000 cell per cm^2, typically a 1:10 split).

2.6.3 Freezing and storage of cells

Cells were frozen by following the pH disassociation method described in section 2.5.2 and following cell count, cells were centrifuged (270 x g for 5 min). Supernatant was removed and cells were resuspended in cryostorage media (1 x 10^6 cells/ml, appendix 1.27).

Aliquots (900µl, 9 x 10^5 cells) were transferred to each cryovial tube, placed in an insulated polystyrene container and frozen at -80 °C.

Frozen cells were revived by thawing in a 37 °C water bath and transferred to a Falcon tube (15 ml). DMEM/F12 (10 ml) was used to wash the empty cryovial and added to 15 ml tube. Cells were centrifuged (270 x g for 5 min) and supernatant removed. Cells were resuspended in culture media and plated in bacteriological petri dishes (5000 cell/cm^2). Typically, one vial was sufficient for three 10 cm^2 dishes.

2.6.4 Tamoxifen administration to cell cultures

All induction experiments carried out *Ta3*$^{fl/fl}$ cells were between passage 3-6 and those on *Ta3*$^{fl/fl;UbcCre}$ were at passage 5. 4-hydroxytamoxifen (4-OHT) was dissolved in ethanol (1 mM) and stored at -20 °C. Prior to administration 4-OHT was diluted in culture media to make a working stock (100 µM). Cells were treated by addition of working stock into bacteriological dishes or 96-well tissue cultures plates (final concentration 1 µm) followed by gentle mixing. For all experiments described in the project tamoxifen was administered shortly after neurosphere disassociation followed by an additional dose after three days of growth. Exposure to light was minimised for all stocks and treated cultures.

2.6.5 HotSHOT cell lysis to assess recombination of *Ta3*

Neurosphere DNA was prepared for PCR using HotSHOT cell lysis (Truett et al., 2000). For each cell line either with or without tamoxifen administration, neurospheres samples (100 µl) were taken from two independent seven day cultures and transferred to 1.5 ml tube. Neurospheres were centrifuged (16060 x g for 10 min), supernatant removed and cell pellets frozen at -20°C until further use.

Cell pellets were allow to thaw and alkaline lysis reagent was added (30 µl, appendix 1.29). Tubes were placed in 95 °C water bath (30 min) and then transferred onto ice (2 min). Neutralisation reagent (30 µl, appendix 1.30) was added to cell lysates, mixed gently and samples stored on ice. PCRs were set up immediately as described in section 2.1.3 using 1 µl cell lysate and 50 µl final reaction volume. PCR products (20 µl) were separated on agarose gel (1.5%) as described in section 2.1.4. Remaining cell lysates were stored frozen at -20 °C.

2.6.6 Colony forming efficiency and colony size comparison

Colony forming efficiency and size was quantified from cells plated at clonal density (5000 cell/cm^2) in a 96-well tissue culture plate. For each cell line twelve wells were used to acquire data. Three *Tα3*$^{fl/fl;UbcCre}$ cell lines (#1, 2, 3) were used to compare the effect of tamoxifen administration. For each cell line the same dilution of cells was split between control and experimental wells using a multichannel pipette (55 µl containing 1600 cells). This was followed by addition of media alone or media supplemented with tamoxifen (final well volume 100 µl). Further administration of media with or without tamoxifen was repeated after three days (final well volume 150 µl). Comparisons were only made between the same cell line plated using the same starting dilution. Control cells of genotype *Tα3*$^{fl/fl}$ were also compared with and without tamoxifen administration. For colony size only, seven-day neurospheres cultured from petri dishes either with or without administration of tamoxifen were disassociated into single cells as described in 2.5.2. After disassociation they were plated in 96-well tissue culture plate as described above without any further administration of tamoxifen. These are referred to as 'passage +1'.

To measure colony size a single image was acquired from the centre of each of the twelve wells using Leica DMIL microscope equipped with Leica EC3 camera. The area of every visible colony was measured using Fiji imaging software and all measurements from 12 wells pooled. Colony areas did not have a normal distribution and transformation was unable to normalise the data. Median values were compared using a Mann-Whitney U test.

To measure colony forming efficiency images of whole wells were taken using Leica WILD MZ8 stereomicroscope equipped with DFC490 camera. The total number of neurospheres (>30 µm) were quantified for each well using Fiji imaging software. The neurosphere forming efficiency per well was calculated by dividing the total number of colonies by the number of cells inputted (1600) and multiplying by 100 to acquire a percentage. Colony forming efficiency was calculated for each well and 12 wells used to compare for each cell line. Data were normally distributed with equal variance and a students T-test was used to compare mean values.

2.6.7 BrdU administration and detection in neurospheres

BrdU was administered to neurospheres two hours prior to fixation. BrdU was first dissolved in DMSO (100 mM) and stored at -20 °C. Prior to administration, BrdU was diluted in culture media to make a working stock (10 mM). Cells were treated by addition of working stock into bacteriological dishes (final concentration 100 µm) followed by gentle mixing. After two hours, neurospheres were transferred to a Falcon tube (15ml), centrifuged (270 x g for 2 min) and supernatant removed. Neurospheres were washed with PBS (10 ml), centrifuged (270 x g for 2 min) and supernatant removed. Neurospheres were fixed with ice-cold methanol:acetic acid (3:1, >5 ml) and kept on ice (30 min). Neurospheres were allowed to settle, supernatant removed and neurospheres washed with 70% ethanol (10 ml). Neurospheres were allowed to settle, supernatant removed, washed again with 70% ethanol and stored at 4 °C.

BrdU incorporation was identified by whole mount immunohistochemistry. For transfer of all solutions, neurospheres were first allowed to settle and liquid carefully removed using a Pasteur pipette. Ethanol was removed from fixed neurospheres and PBS added (10 ml). PBS was removed, fresh PBS added (0.5 ml) and neurospheres transferred to a smaller 2ml tube. Any remaining neurospheres were collected by washing the empty 15ml tube with PBS (0.5 ml) and adding to the 2 ml tube. Supernatant was removed and neurospheres washed with fresh PBS (2ml). After 5 min PBS was removed, HCl added (1 ml, 2 M) and tubes were incubated at room temperature with occasional mixing (20 min). Supernatant was removed and neurospheres were quickly washed three times with PBS (2 ml). Supernatant was removed, fresh PBS added and mixed on a rotator (10 min). Supernatant was removed, PBT-block added (1 ml, appendix 1.28) and tubes were incubated at room temperature (1 hr). Supernatant was removed, monoclonal antibodies to BrdU (see table 2.4) diluted in PBT-block were added (200 µl) and tubes were placed on rocking platform at 4°C overnight. Neurospheres were washed four times with PBST and placed on a rotating mixer (4 x 30 min). Supernatant was removed, PBT-block containing secondary antibody (see table 2.5) and DAPI (1 µg/ml) were added (200 µl) and tubes were placed on a rocking platform at 4°C overnight. All subsequent steps were covered with foil to minimise exposure to light. Neurospheres were washed four times with PBST and placed on rotating mixer (4 x 30 min). Supernatant was removed and glycerol diluted in PBS (25%) added. After neurospheres had sunk (~1 hour) solution was changed to an increasing

glycerol series (~1 hour x 50%, 75%, 90%). The final glycerol stock contained DABCO (2.5% w/v) to limit photobleaching.

Labelled neurospheres were placed on a microscope slide in small drop of 90% glycerol and a coverslip gently placed on top. Whole mount images of intact neurospheres were acquired first. For quantification of BrdU incorporation, coverslips were tapped to squash neurospheres into a monolayer prior to image acquisition. Twelve neurospheres were quantified per cell line (n=12). For each neurosphere one image containing ~400 cells was taken and the total number of BrdU-positive nuclei was quantified and expressed as a percentage of total cell number, determined by DAPI-positive nuclei. Data were normally distributed with equal variance and a students T-test was used to compare mean values.

2.6.8 Acid washing coverslips

Coverslips were cut with a diamond pen into 0.5 cm squares. They were washed overnight in HCl (500 ml, 2 M), followed by ten washes of tap water. Coverslips were washed overnight in MilliQ water and separated on clean tissue paper. Once dry, coverslips were transferred into a glass petri dish and baked at 200 °C (2-3 hours). Prior to use, coverslips were transferred into single wells of 24-well tissue culture plate using sterile forceps.

2.6.9 Matrigel coating

Matrigel (BD Biosciences, UK) was diluted in ice cold DMEM (1:2) and stored at -20 °C. All dilutions were completed using pipettes chilled at 4 °C. Prior to use, Matrigel was thawed in the fridge and diluted (1:14) in ice cold DMEM/F12. Diluted Matrigel was added to each well of 24-well plate or on coverslips in 24-well plate (200 µl per well). Plates were chilled at 4 °C prior to addition of Matrigel. Coated plates were allowed to incubate at room temperature (2 hour) and stored for up to 2 day in an air-tight container at 4°C. DMEM supernatant was aspirated prior to use.

2.6.10 Neurosphere migration assay

Neurospheres of similar size were selected from seven-day cultures and transferred to a small Petri dish containing DMEM/F12 media using P20 Gilson Pipette. Single neurospheres were then transferred to single wells of a 24-well tissue culture dish coated in

matrigel (as described in section 2.5.9) and containing differentiation media (1 ml, appendix 1.31). Wells were imaged after two, twenty four, forty eight and seventy two hours using Leica DMIL microscope equipped with Leica EC3 camera. The total neurosphere area was measured from images taken after two hours using Fiji imaging software. The total area of the leading edge of radially migrating cells was also measured from images taken after twenty four, forty eight hours and seventy two hours. For each cell line 12 neurospheres were used to make comparisons and results pooled between cell lines (n=36). Data did not have an equal variance and could not be equalised by transformations so a Mann-Whitney test was used to show significance between median values.

2.6.11 Single cell differentiation

Neurospheres were disassociated using the pH method described in 2.5.2. Cells were resuspended in attachment media (200000 cell/ml, appendix 1.32) and 500 µl added per well of matrigel-coated coverslips in 24-well plate (50000 cell/cm^2). After two hours, media was aspirated and replaced with differentiation media (500 µl, appendix 1.31). After three days, media was aspirated and replaced with fresh differentiation media (500 µl). After six days, media was aspirated and cells washed with PBS (500 µl). PBS was aspirated and cells fixed on ice (30 min) with ice cold PFA (500 µl) or ice cold methanol:acetic acid (3:1, 500 µl). PFA-fixed cells were washed with PBS (2 x 10 min) and stored in PBS with sodium azide (0.05%, w/v) at 4 °C. Methanol:acetic acid fixed cells were washed in 70% ethanol (2 x 10 min) and stored in 70% ethanol at 4 °C.

2.6.12 Immunohistochemistry of cultured cells

Fixed cells on coverslips were transferred into a fresh 24-well culture plate containing PBS (10 min). PBS was aspirated and PBT-block was added (500 µl, appendix 1.28). Cells were allowed to block at room temperature (1 hour), block was aspirated and primary antibodies (see table 2.4) diluted in PBT-block were added (100 µl). Primary antibodies were allowed to incubate overnight at 4 °C. Primary antibodies were removed and PBST added (500 µl) to wash coverslips (10 min). PBST was aspirated and the wash repeated a further three times. PBST was aspirated and appropriate secondary antibodies (see table 2.5) and DAPI diluted in PBT-block were added (100 µl). Coverslips were incubated at room temperature (1 hour) after which secondary antibodies were removed.

PBST was added (500 µl) to wash coverslips (10 min), PBST was aspirated and wash repeated once more. PBS was then added (500 µl, 10 min), PBS was aspirated and wash repeated once more. A small drop of Mowiol (~20 µl, appendix 1.8) was placed on a microscope slide and coverslips were mounted with cells facing down. Once dry, coverslips were sealed with nail varnish and imaged as described in section 2.3.1.

2.6.13 Identification of F-actin using Phalloidin

F-actin was identified by following the initial steps of 2.5.12. After the first PBT-block Phalloidin conjugated to fluorescence Alexa Fluor® 488 Phalloidin (Life Technologies, UK) was diluted 5 µl per 200 µl of PBS with BSA (1% w,v) according to manufacturer's instructions. DAPI was also added to the Phalloidin-488 solution, added to coverslips and incubated at room temperature (30 min). Coverslips were washed with PBS (4 x 10 min) and mounted with mowiol as described in section 2.5.12.

2.6.14 Quantification of ciliated cells

Coverslips labelled for adenylyl cyclase III and acetylated α-tubulin were used to identify primary cilia. Two coverslips from each cell line were stained and four random ROIs were imaged from each coverslip. For each ROI the number of ciliated cells was quantified and expressed as a percentage of total cell number. Values were pooled between cell lines and used for comparison between conditions (n = 24). Data were normally distributed with equal variance and a students T-test was used to compare mean values.

2.6.15 Quantification of cell fate choice

Coverslips labelled for Nestin and GFAP were used to identify different cell types. One coverslip from each cell line was stained and four random ROIs imaged from each coverslip. For each ROI the number of single- and double-positive cells was quantified and expressed as a percentage of total cell number. Values were pooled between cell lines and used for comparison between conditions (n = 12). Data were normally distributed with equal variance and a students T-test was used to compare mean values.

2.6.16 Neurosphere migration directional analysis

Following neurosphere migration assay described in section 2.5.10 plates were fixed after seventy two hours on ice using cold PFA (500 µl). PFA-fixed cells were washed with PBS (2 x 10 min) and stored in PBS with sodium azide (0.05%, w/v) at 4°C. Cells were immunolabelled using the method described in 2.5.12 and primary antibody to TGN46 (table 2.4). After secondary antibody had been removed and cells washed with PBST and PBS, glycerol diluted in PBS (25%) was added (30 min). This was repeated with increasing glycerol concentration (50%, 75%, 90%) with final glycerol containing DABCO (2.5% w/v) to limit photobleaching. Wells were imaged using and EVOS® Cell Imaging System (Life Technologies, UK).

To quantify cell direction, ROIs (250 µm wide, 320 µm high) were selected on the left and right side of the leading edge of migrating cells. Left-ROIs were rotated 180° so the leading edge faced towards the right. For each cell visible in the ROI the direction was determined by the position of TGN staining relative to the nucleus. Cells orientated radially outwards (right) had a value of 0°, cells perpendicular to this had values of 90° (down) and -90° (up) and cells facing radially inward had values of 180° or -180° (left). Left and Right ROIs were taken from 4 neurospheres from each cell line and cell orientations pooled between conditions. Frequency histogram was used to show the number of cells in 30° bins spanning from -180° to 180°.

Chapter 3 – Gross phenotype of *Ta3*$^{fl/fl;NesCre}$ mice

3.1 Introduction

Primary cilia have distinct roles in brain development and they have varying importance depending on strict temporal boundaries. As a result, the phenotype of conditional cilia mutants will depend almost entirely on the time of disruption and the population of cells which are affected. One of the most common and widely available Cre-deleter strains used to cause genetic recombination in the developing CNS is the NesCre strain developed by Tronche and colleagues (1999). It is the only NesCre strain commercially available from The Jackson Laboratory which has a simple *nestin* promoter and enhancer driving the expression of a functional Cre. Others *nestin* lines are available but these often contain more complex constructs such as tamoxifen inducible fusion proteins.

The NesCre mouse was generated by oocyte injection of a construct in which the Cre recombinase is driven by the promoter and CNS-specific enhancer of the rat *nestin* gene. The Cre expression has been investigated using β-galactosidase reporter mice and the original authors describe its activity in the embryonic CNS from E11.5 (Tronche et al., 1999). Images from the database of the Cre Repository, made available by The Jackson Laboratory, also present β-galactosidase images with Cre activity from E10.5 in the developing brain (Heffner et al., 2012). They further show its complete coverage in early postnatal and adult CNS with scattered expression also present in the kidney, lung, pancreas and testis.

To date there are a limited number of studies looking at the disruption of primary cilia in neural tissues from mid-gestation onwards. To our knowledge only one basal body protein, Stumpy, has been targeted using the NesCre transgene (Town et al., 2008). Here we describe the gross phenotype of mice with conditional deletion of *Ta3* generated by intercrossing with the NesCre deleter strain. We present the gross morphological features of mutant mice and show that defects are most evident perinatally. Mice show ataxia, severe hydrocephaly and postnatal lethality. Striking phenotypes in brain regions, such as the cerebellum, cortex and hippocampus are identified and will be the focus of subsequent chapters. Finally we show that ependymal cells lack both primary and motile cilia as a consequence of *Ta3* loss.

3.2 Results

3.2.1 Generation of experimental mice

Stud males of genotype *Ta3*$^{fl/wt;NesCre}$ were first generated by crossing *Ta3* mice homozygous for the floxed allele (*Ta3*$^{fl/fl}$) with those carrying the *NesCre* transgene. Experimental mice were then acquired by breeding stud males to *Ta3*$^{fl/fl}$ females (fig 3.1a). Expression of Cre is known to cause robust recombination of *Ta3* resulting in loss of the conserved coiled-coil region in exons eleven and twelve (fig 3.1b). *Ta3* mice were genotyped using PCR to amplifying the region of genomic DNA spanning the first LoxP site as described previously (Bangs et al., 2011) (Fig 3.1c). Amplification of the *wildtype* allele produced a product of 351 bases whereas amplification of the *floxed* allele produced a product of 470 bases. Similarly, the presence of NesCre transgene was identified using PCR to amplify a product of 408 bases (Fig 3.1c).

Our first observation was that mice heterozygous for the *floxed* allele and carrying the *NesCre* transgene (*Ta3*$^{fl/wt;NesCre}$) showed no overt phenotype. Mice exhibited a physical appearance indistinguishable from control littermates with normal behaviour, motor coordination and life span. For this reason, analysis was focused on experimental mice homozygous for the *floxed* allele and carrying the *NesCre* transgene (*Ta3*$^{flfl;NesCre}$); from here onwards these are referred to as '*Ta3* mutant mice'. All comparisons have been made between control littermates homozygous for the *floxed* allele (*Ta3*^{flfl}); from here referred to as 'control mice'.

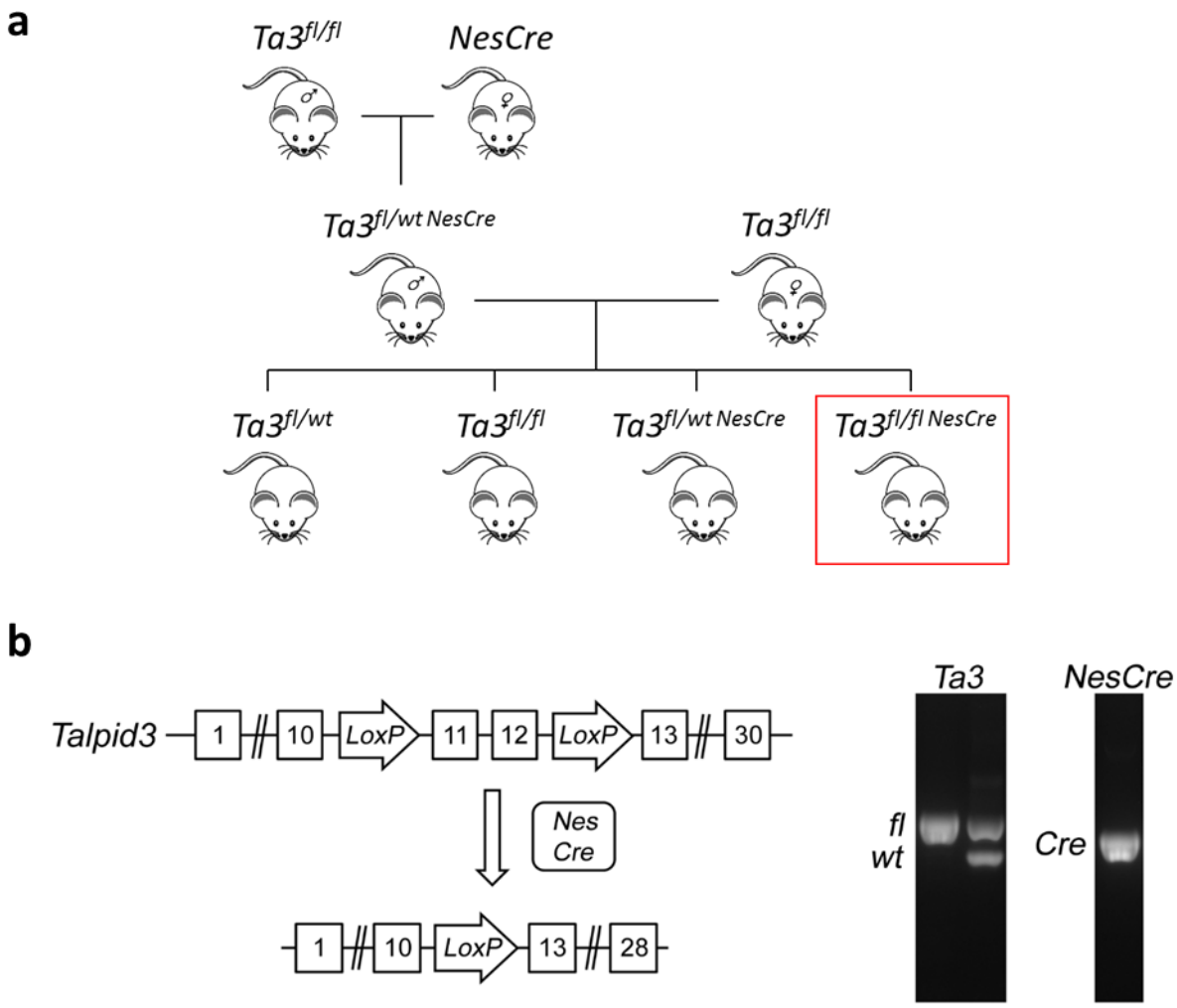

Figure 3.1 Breeding strategy used to generate experimental mice.
(a) Diagram indicating steps taken to generate mutant mice. First, mice homozygous for the floxed allele (Ta3$^{fl/fl}$) were crossed to *NesCre* deleter strain. Stud males (*Ta3*$^{fl/wt;NesCre}$) were then bred to homozygous Ta3 females (*Ta3*$^{fl/fl}$). Experimental mice should occur at frequency of 25% (*Ta3*$^{fl/fl;NesCre}$) as indicated by red box. (b) Diagram indicating Ta3 recombination in the presence of Cre recombinase. (c) Representative PCR products used to identify mouse genotypes.

3.2.2 Preliminary analysis of E14.5 *Ta3* mutant embryo has a modest phenotype

In initial studies embryonic stages were analysed using timed pregnancies. It was observed that the frequency of mutant mice collected at E14.5 was much lower than the 25% expected (4%, 1 from 23 embryos). To identify whether this was due to embryonic lethality, younger embryos were taken but the low frequency was consistent in stages obtained at E13.5 (0%, 0 from 27 embryos), E12.5 (14%, 2 from 14 embryos) and E10.5 (0%, 0 from 8 embryos), see table 3.1. During the course of the project, new data were made available demonstrating that insertion of the *NesCre* transgene was on chromosome 12 cytoband D1 (Valentine, 2010). This chromosome also includes the *Ta3* loci located on the adjacent region 12C1 (MGI: 2700049A03Rik). We suspected that the reduced frequency of experimental embryos was due to both alleles being on the same chromosome with linkage between $Ta3^{wt}$ and *NesCre* transgene (see appendix 2.0 for diagram). This resulted in a translocation event required to generate the mutant $Ta3^{fl/fl;NesCre}$ mice. Despite efforts to generate a stud male with *NesCre* transgene linked with $Ta3^{fl}$ allele the frequency of $Ta3^{fl/fl;NesCre}$ remained low throughout the project.

Although limited embryonic material was available, preliminary analysis of the single E14.5 mutant embryo was completed by staining with hematoxylin and eosin to identify tissue morphology, and silver stain to identify neuronal tracts (Fig. 3.2a-d). At this stage, the gross structure of both control and mutant embryos was very similar with little difference observed at comparable axial levels. The neocortex appeared to have a similar thickness and density between control and mutant (Fig. 3.2a,b). The developing cerebellum and choroid plexus also had comparable shape and size (Fig. 3.2c,d). Adjacent to the cerebellar primordia, the posterior edge of the mutant mid-brain appeared thicker but this was likely to be an artefact of the slightly oblique tissue orientation (Fig 3.2d – asterisk). One possible difference observed in the mutant embryo was a thinning or constriction of the superior colliculus but further embryos would be required to support this finding (Fig 3.2d – arrow). Other than these two observations, the mutant embryo appeared to develop relatively normally compared to control. Whilst embryonic stages were being obtained, postnatal stages were also being collected and showed a striking phenotype. Given the modest phenotype seen at E14.5, focus shifted to investigation of the postnatal mice.

Table 3.1 *Ta3*$^{fl/fl;NesCre}$ embryos have a lower than expected occurrence. Table shows embryonic mice collected and genotyped. *Ta3*$^{fl/fl;NesCre}$ mice were expected to constitute 25% of all litters. A limited number of embryos were not genotyped to completion (range indicated by hyphenated numbers). Abbreviation, E = embryonic.

Age	Number of embryos	Number of litters	Genotype frequency of retrieved embryos/mice			
			Ta3$^{fl/fl}$	*Ta3*$^{fl/wt}$	*Ta3*$^{fl/wt;NesCre}$	***Ta3***$^{fl/fl;NesCre}$ **(%)**
E10.5	8	1	4	0	4	0 (0%)
E12.5	14	3	5	2-7	0-5	2 (14%)
E13.5	27	3	3-7	3-7	17	0 (0%)
E14.5	23	3	11	1	10	1 (4%)
Total	**72**	**10**	**23-27**	**6-15**	**31-36**	**3 (4%)**

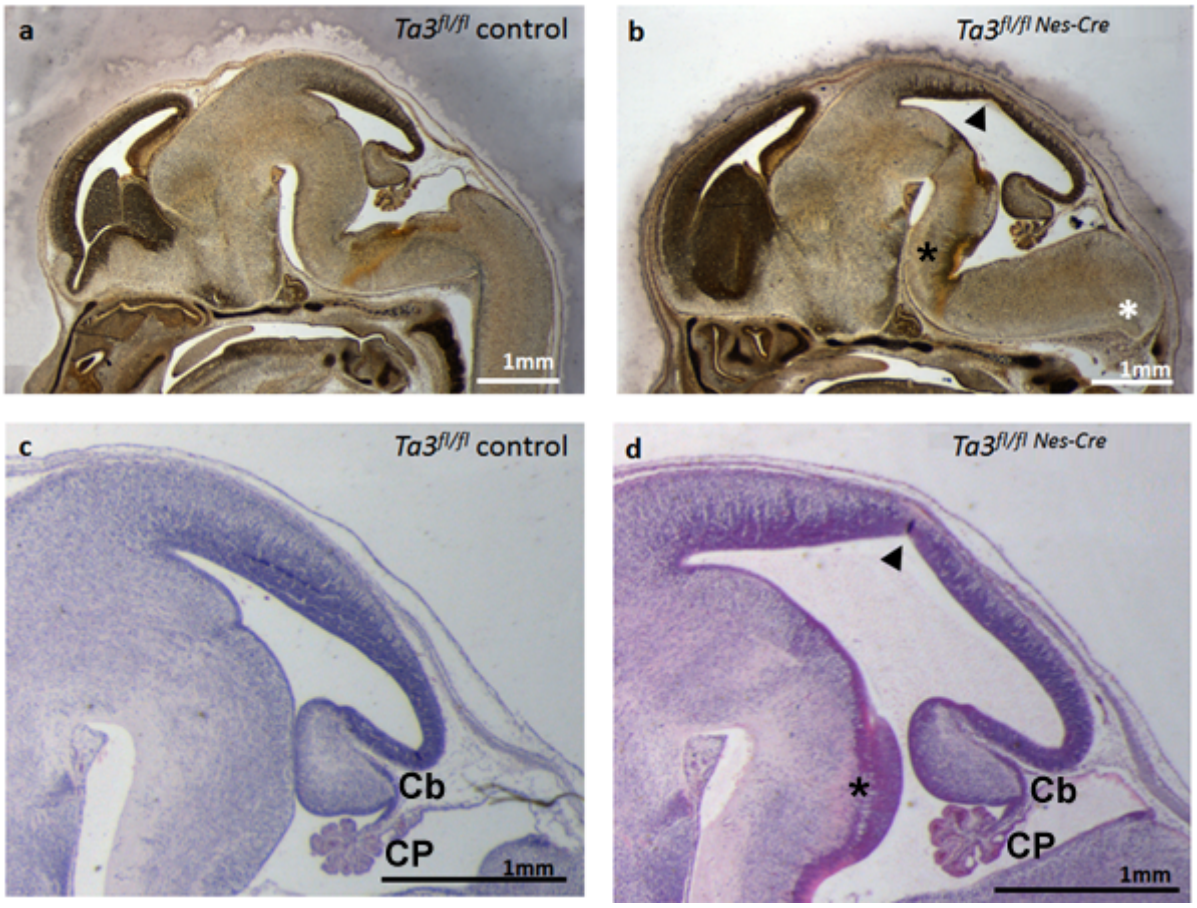

Figure 3.2 Embryonic *Ta3* mutant mice have modest phenotype.
One mutant mouse was collected at E14.5 and examined as a preliminary analysis. Silver stain to show neuronal tracts (a) control and (b) mutant. Hematoxylin and eosin stain for control (c) and mutant (d). Mutant embryo has similar gross organisation. Developing cerebellum (Cb) and choroid plexus (CP) have similar shape a size. Arrow indicates possible defect in superior colliculus. Asterisk (white) indicates lack of spinal cord cross section and asterisk (black) indicates thickened mid-brain edge; both are likely to be caused by slightly oblique tissue sections. Scale bars, 1mm (a-d).

3.2.3 Postnatal *Ta3* mutant mice are smaller with hydrocephaly

At birth all mutant pups examined (37/37 pups) were visually indistinguishable from their control littermates but by P15 they were smaller with a pronounced domed head (16/16 mice) (Fig. 3.3a). P10 mutant mice presented with mild ataxia which was evident in their wide gait and inability to maintain balance (19/19 mice). This progressed rapidly and by P15 the ataxia was very severe with mice showing difficulty standing and moving around the cage (Movie 3.1 – please see attached CD). Despite this, mutants were often found in the nest and occasionally showed purposeful movement to avoid open spaces. Mutant mice were still able to suckle and showed grooming behaviour with their forelimbs (Movie 3.1). Macroscopic examination of the P15 *Ta3* mutant brain revealed hydrocephaly which was first detectable at P5 and progressed in severity between P5 and P15, forcing the superior and inferior colliculi into a more posterior position (Fig. 3.3b-d). The P15 *Ta3* mutant brain also exhibited cerebella that were strikingly hypoplastic, with a very pronounced reduction in the vermis and at this postnatal stage there was a three-fold reduction in cerebellar mass (Fig. 3.3b-d).

Histochemical analysis of three P15 mice in the sagittal axis identified a compression and thinning of the *Ta3* mutant cortex with an obvious loss of structural integrity in the underlying corpus callosum (Fig 3.3d). The fragility of this structure often resulted in a detachment of the ventricular ependymal layer and the cortex also appeared to have subtle differences in the laminar structure. The olfactory bulbs were smaller and very delicate during dissection with fluid accumulation in the central region. Given the extent of the cerebellar and cortical phenotypes, these will be investigated in further detail in chapters 4 and 5.

Movie 3.1 *Ta3* mutant mice exhibit severe ataxia but maintain grooming behaviour (Please see attached CD)

(a) 'Ataxia' - P15 $Ta3^{fl/fl}$ and $Ta3^{fl/fl;NesCre}$ littermates moving around a cage. The $Ta3^{flfl;NesCre}$ mouse attempts purposeful movement but is unable to coordinate limbs or maintain balance. b) 'Grooming' - P15 $Ta3^{fl/fl;NesCre}$ mouse displays limited motor control but maintains its ability to feed and groom.

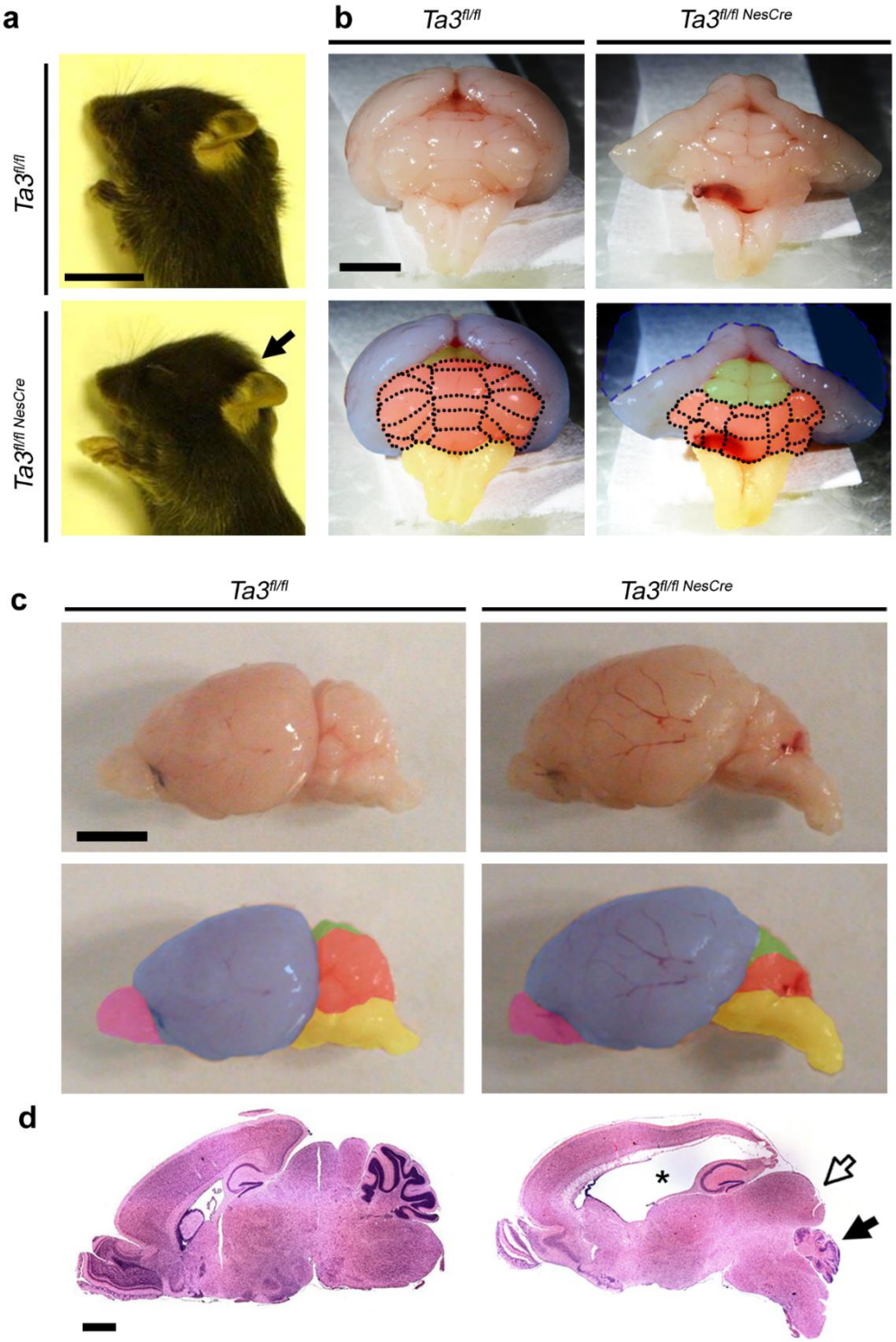

Figure 3.3 Postnatal *Ta3* mutant mice exhibit hydrocephaly and hypoplasia of the cerebellum. (a) P15 *Ta3*$^{fl/fl;NesCre}$ mice are smaller with domed head (arrow) (b) Posterior view of P15 brain, *Ta3*$^{fl/fl;NesCre}$ have hydrocephaly and hypoplasia of the cerebellum, the *Ta3*$^{fl/fl;NesCre}$ cerebrum appears slightly collapsed due to severe hydrocephaly indicated by the dashed blue line. (c, d) lateral view of P15 whole mount brains and sagittal sections stained with H&E. Left panel *Ta3*$^{fl/fl}$ and right panel *Ta3*$^{fl/fl;NesCre}$ mice. Note the severe hydrocephaly (asterisk), posterior shift in colliculi (white arrow) and hypoplasia of cerebellum (black arrow) in (d). Coloured regions indicate main brain structures; cerebellum (red), cerebrum (blue), colliculi (green), hindbrain (yellow), olfactory bulb (magenta). Scale bars, 10 mm (a), 3 mm (b,c - whole mount) and 2 mm (d- H&E sections)

3.2.4 P15 *Ta3* mutant mice have structural defects with altered neural tracts

The gross phenotype of P15 mutant brain was investigated further by immunohistochemically labelling serial horizontal sections taken from two mice with an antibody to neurofilament (165 kDa) to identify mature axonal tracts. One of the striking observations at this stage was a disruption in the axial position of regional structures, making direct comparisons more complicated. This was caused by the extent of hydrocephaly both shifting and compressing structures. Despite this, it was still possible to identify a number of key landmarks in the mutant brain for comparison with controls.

When looking at the ventricular system, it was clearly evident the lateral ventricles were most affected by CSF accumulation causing a ballooning of the cortex and detachment from the caudate putamen (CPu) (Fig 3.4a-c). The caudate putamen also appeared smaller with a lower density of axonal bundles (Fig 3.4c). At its base the internal capsule (IC), a dense band of motor and sensory neurons which travel to and from the cortex, also appeared narrow and constricted in the mutant. Looking at more posterior structures, the midbrain appeared thinner across the medio-lateral axis and the dentate gyri appeared squashed and more elliptical; this hippocampal phenotype will also be discussed in further detail in chapter 6. The mutant cerebellum was clearly underdeveloped and much thinner in the anterior-posterior axis but surprisingly displayed a comparable width across the medio-lateral axis (Fig 3.4a,b).

Cerebellar hypoplasia, ataxia and hydrocephaly are common features of human ciliopathies. One condition with a distinct phenotype in the posterior brain is JS. This disorder exhibits disruption of the cerebellar peduncles visible in axial MRI as the Molar Tooth Sign. Although this shape was not evident in mutant mice, they did show defects in the cerebellar peduncles, the major connections between the cerebellum and brain stem. On closer inspection of the midbrain, the decussation of the superior cerebellar peduncles (dscp), the point at which these tracts cross the midline, appeared abnormal with thickened tracts which were more compact (Fig 3.4 d).

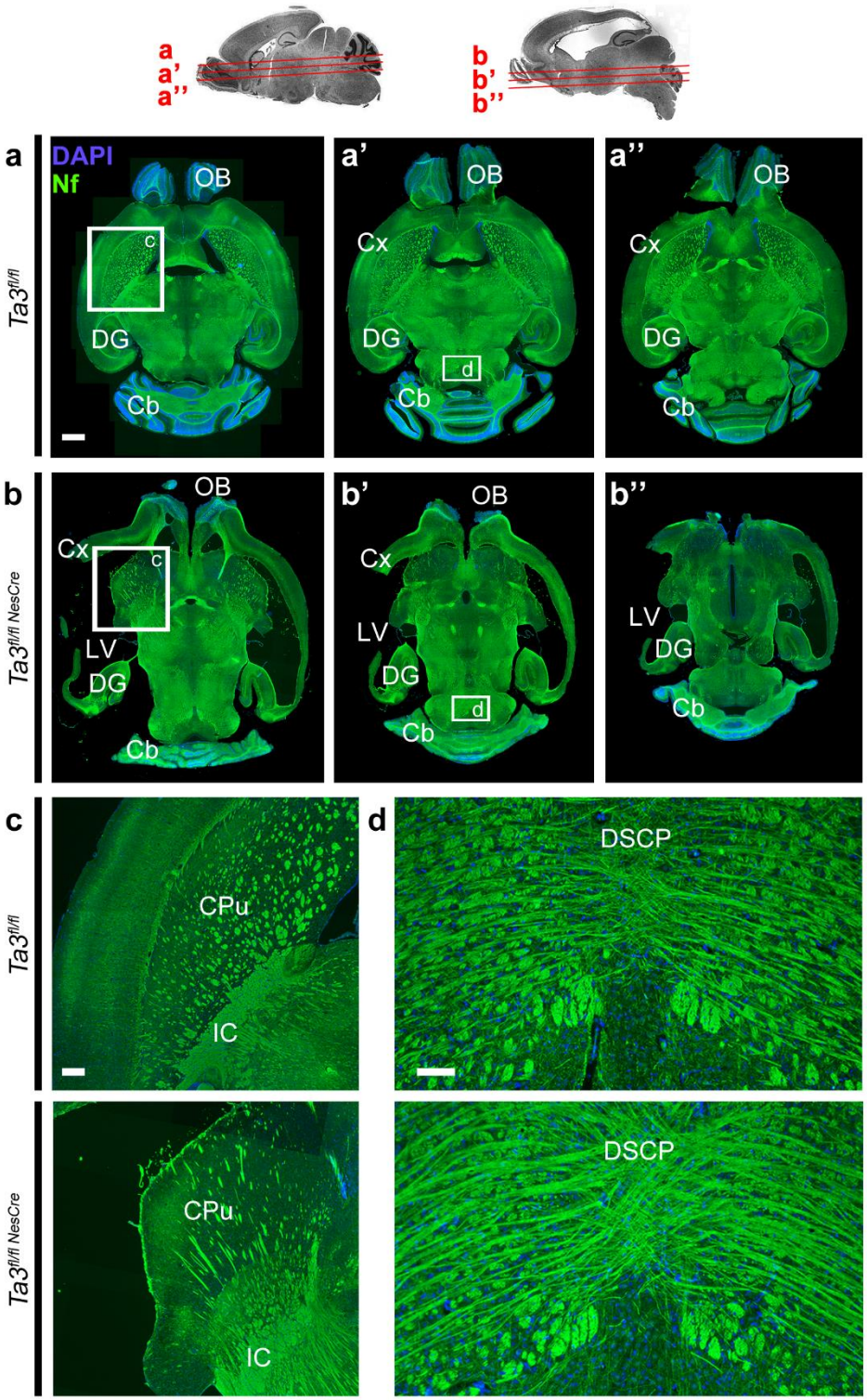

Figure3.4 Postnatal *Ta3* mutant mice exhibit gross structural defects in the mid- and hind-brain and abnormal decussation of the scps. P15 Serial horizontal sections stained for neurofilament. (a, b) different dorso-ventral positions as indicated on sagittal cross-section. Midbrain of the *Ta3*$^{fl/fl;NesCre}$ mice appears thinner and elongated and hydrocephaly of the lateral ventricles is clearly evident. (c) Higher magnification of boxed area. The caudate putamen is smaller with fewer neuronal bundles and is detached from the cortex. (d) Higher magnification of boxed area. The decussation of cerebellar peduncles appears disrupted with thickened tracts. Scale bars, 1 mm (a, b), 250 µm (c), 100 µm (d). Abbreviations: Cb, Cerebellum; Cx, Cortex; CPu, Caudate Putamen; DSCP, decussation of the superior cerebellar peduncles; DG, dentate gyrus; IC, internal capsule; LV, lateral ventricle. Brain structures were identified using the Mouse Brain Library C57BL/6J horizontal atlas (Rosen G.D. et al The Mouse Brain Library @ www.mbl.org.).

3.2.5 P5 *Ta3* mutant mice have posterior defects independent of hydrocephaly

Hydrocephaly is a clear factor contributing to the gross structural defects seen at P15. Serial horizontal sections were also analysed from two P5 mice. At this age, mutant mice are hard to visually identify from control littermates both by comparison of head shape or size and primitive motor coordination. The extent of hydrocephaly is also less severe allowing the identification of phenotypes caused by cellular defects rather than secondary to the enlarged ventricles.

P5 sections were labelled with neurofilament to compare gross neuronal architecture (Fig 3.5a,b). The caudate putamen, in contrast to P15, showed a comparable size and distribution of axonal bundles between control and mutant (Fig 3.5c). Although it still showed detachment from the cortex the extent was far less severe and only evident in limited sections in the middle of the dorso-ventral axis (Fig 3.5b). Similar to P15, the mutant internal capsule remained constricted. As noted previously, fluid accumulated in the olfactory bulbs resulting in a loss of tissue integrity in the central region (Fig 3.5bi,d). In the anterior midline, the corpus callosum was much thinner in the mutant (Fig 3.5e). This region had also become detached from the underlying dorsal lateral septal nuclei (LSD) resulting in its rounding in shape and shift in orientation. Posterior to this, the hippocampal commissure was more compact and exhibited a loss of connectivity and tissue integrity with the underlying tissues. Despite this, the mutant hippocampal commissure appeared similar in thickness and length to control, stretching across the medio-lateral aspect (fig 3.5e). As many of these anterior regions are closely associated with the lateral ventricles it is likely that they are a secondary result of the early hydrocephaly seen in the lateral ventricle.

The posterior region of the P5 mutant brain was far less affected by fluid accumulation. It showed little difference in the size of the fourth ventricle (4V) and the compressive effect was markedly less obvious than that seen at P15 (fig 3.5f,g). Despite this, early defects seen in the posterior region were still evident. The mutant P5 cerebellum was much thinner than control with a reduction in the size of folds but it maintained a comparable width across the medio-lateral axis (fig 3.5g). Analysis of the cerebellar peduncles showed a similar organisation between the control and mutant and, unlike P15, the decussation of the superior cerebellar peduncles were very comparable. However, in

regions more posterior to this, the peduncles seemed to have a lower density of tracts connecting the cerebellum and midbrain (fig 3.5f).

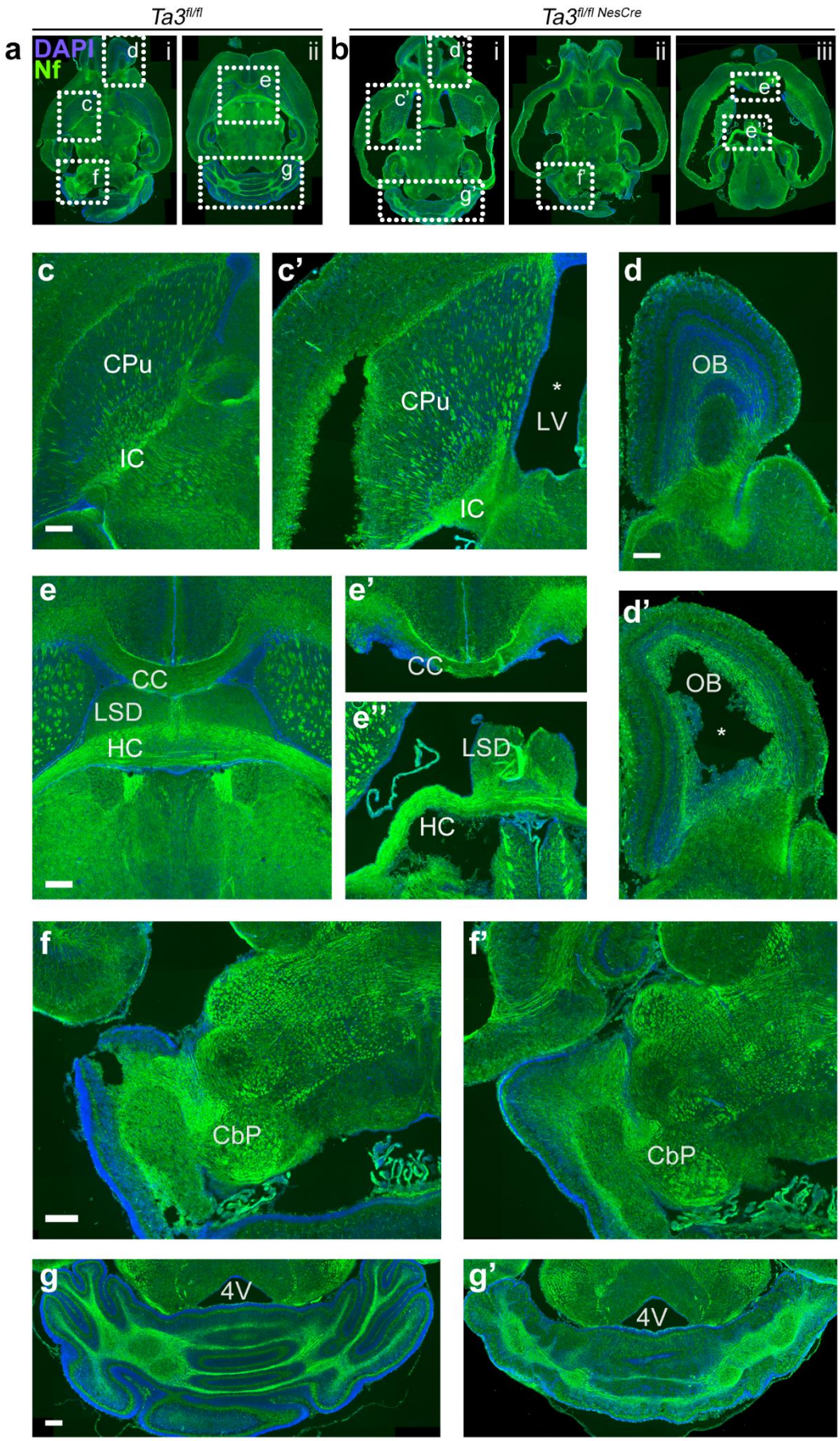
Ta3fl/fl
Ta3fl/fl NesCre
a
DAPI
Nf
d
i
ii
e
c
g
f
b
d'
i
ii
iii
c'
e'
e''
g'
f
c
CPu
IC
c'
CPu
*
LV
IC
d
OB
e
CC
LSD
HC
e'
CC
e''
LSD
HC
d'
OB
*
f
CbP
f'
CbP
g
4V
g'
4V

Figure 3.5 P5 *Ta3* mutant mice exhibit posterior phenotypes independent of hydrocephaly. P5 serial horizontal sections stained for neurofilament. (a, b) different axial positions from a ventral (i) to dorsal (ii/iii) position. Boxed regions indicate higher magnification images (c-g). Images identified with prime symbol (') indicate mutant sections. Control (c) and mutant (c') caudate putamen are comparable in size but the internal capsule is narrow and more constricted. Control (d) and mutant (d') olfactory bulbs, mutants exhibit fluid accumulation and loss of tissue integrity. Control (e) and mutant (e', e'') midline structures, mutants have a thinner corpus callosum, detached and disorientated lateral septal nuclei with loss of integrity under the hippocampal commissure. Posterior regions of the P5 cerebellum are less affected by hydrocephaly. Control (f) and mutant (f') cerebellar peduncles have comparable organisation, but mutant has a lower density of neural tracts. Control (g) and mutant (g') cerebellum, mutant is thinner with smaller folds. Scale bars; 1mm (a, b), 250 µm (c-g). Abbreviations: CbP, Cerebellar peduncle; CC, corpus callosum; CPu, Caudate Putamen; IC, internal capsule; HC, hippocampal commissure; LSD, lateral septal nuclei (distal); LV, lateral ventricle; OB, olfactory bulb; 4V, fourth ventricle. Brain structures were identified using the Mouse Brain Library C57BL/6J horizontal

3.2.6 *Ta3* Mutant mice lack ependymal motile and primary cilia

Hydrocephaly is likely to have an influential role in many of the gross structural defects exhibited in mutant mice. To assess the consequence of Ta3 loss and establish a cause of the hydrocephaly, cilia were identified in the ependymal zone lining the lateral ventricles from three control and three mutant P15 mice. Cilia-like structures emanating from the control ependymal tissue could be detected in high power images of sections stained with hematoxylin and eosin (Fig. 3.6a). In contrast, these structures were absent in mutant ependyma. Detection of cilia in this way is scarcely reported due to the lack of specificity. For this reason, adenylyl cyclase III (ACIII) and acetylated α-tubulin (AcTub) were also labelled to identify primary cilia and motile ependymal cilia respectively (Fig. 3.6b). Control ependyma clearly had numerous acetylated α-tubulin cilia extending from the ependymal layer into the ventricle (Fig 3.6b). adenylyl cyclase III-positive primary cilia were also seen projecting from cells in the ependymal layer, however there were fewer and they did not appear to project directly into the ventricle (Fig 3.6b). In stark contrast, the mutant ependymal layer showed nearly complete loss of both motile cilia and primary cilia in this region. This is consistent with the hematoxylin and eosin staining and confirms recombination of *Ta3* in this tissue was sufficient to cause loss of cilia.

Primary cilia were also identified by adenylyl cyclase III labelling in three control and three mutant mice aged E18.5, long before the development of hydrocephaly (Fig 3.7 a). In control ependymal, primary cilia could clearly be detected despite being much smaller length. Mutant ependymal, once more, showed near complete loss of primary cilia at this stage confirming recombination of *Tα3* even before birth.

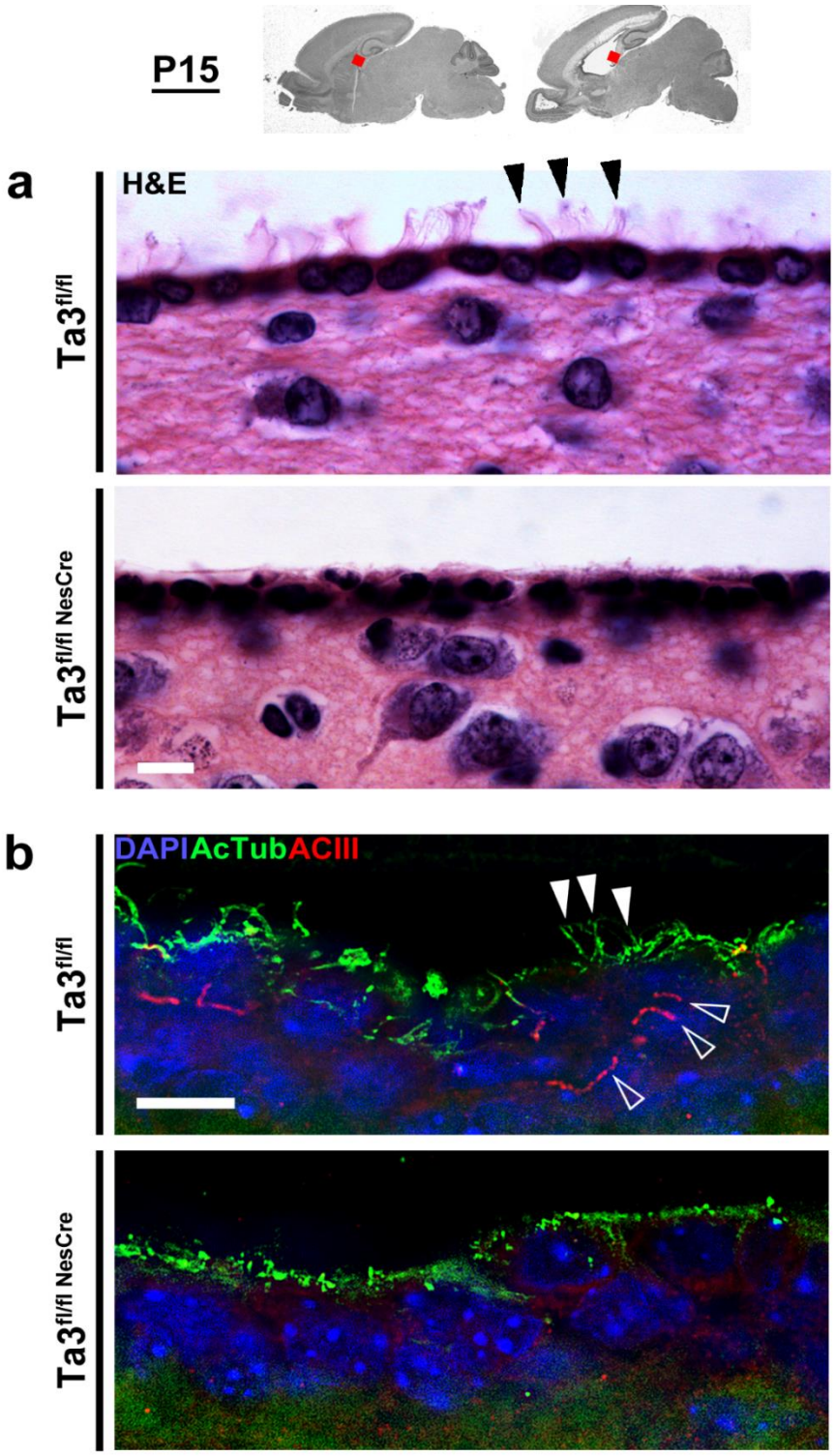

Figure 3.6 P15 *Ta3* mutant mice lack motile and primary cilia in the ependymal layer
Top row, images of sagittal P15 sections with red box indicating region of higher magnification. (a) P15 sagittal section stained with hematoxylin and eosin. In control, cilia-like projections can be seen projecting into the ventricle. These are absent in mutant ependymal. (b) P15 sagittal section with motile cilia (filled arrow) identified with acetylated α-tubulin (green) and primary cilia (hollow arrow) identified with adenylyl cyclase III (red). Mutant show a loss of both ciliary types. Scale bars; 10 µm (a, b)

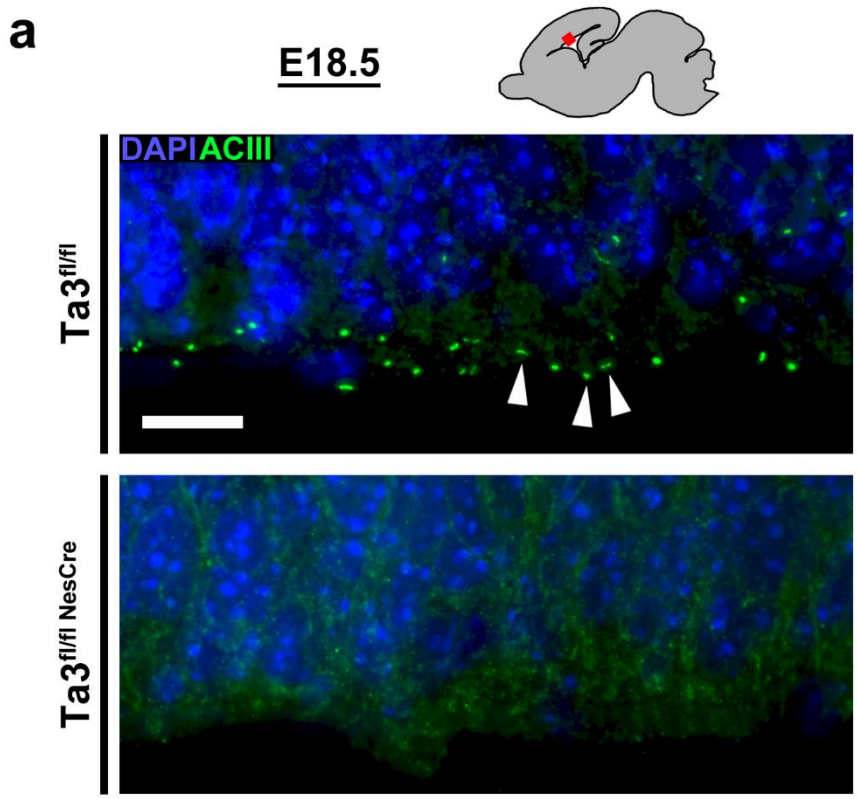

Figure 3.7 E18.5 *Ta3* mutant mice lack ependymal and primary cilia.
Top row, drawing of sagittal E18.5 section with red box indicating region of higher magnification. (a) E18.5 sagittal section with primary cilia (arrow) identified with adenylyl cyclase III (green). Mutant show nearly complete loss of primary cilia. Scale bars; 10 µm (a)

3.3 Discussion

Ta3 mice were crossed with the *NesCre* deleter strain in order to study the consequence of *Ta3* disruption specific to the developing nervous system. Analysis of a single E14.5 embryo suggested that there was little difference in the gross structural organisation. However, by P15 postnatal mice exhibited a striking phenotype with ataxia, hydrocephaly and hypoplasia of the cerebellum. Closer analysis of neural tracts attributed many of the anterior defects to enlargement of the lateral ventricles however by looking at younger P5 stages, when the hydrocephaly was less severe, defects in the posterior brain were identified which are likely to be independent cellular defects. Distinct phenotypes in the cerebellum, cortex and hippocampus were also identified and these phenotypes will be described in detail in chapters 4, 5 and 6.

The use of the *NesCre* deleter line is a practical tool for studying gene function in the developing CNS and is a well characterised, commercially available strain. Although difficulties were faced with the *NesCre* transgene and *Ta3* being on the same chromosome, acquisition of mutant mice was still possible to enable the study to progress. Disruption of *Ta3* in mice has previously been shown cause loss of primary cilia (Bangs et al., 2011). In chickens, disruption of *Ta3* has specifically been shown to cause loss of both motile cilia and primary cilia lining the ventricles (Stephen et al., 2013). Here we have demonstrated that mutant mice also show a striking loss of both motile and primary cilia using markers acetylated tubulin and adenylyl cyclase III respectively.

The detection of primary cilia is limited to a select group of immunohistochemical markers to show their presence. Often the most convincing detection of cilia is achieved by co-immunostaining for both basal body and axonemal markers simultaneously. A common combination using this approach, and one that is used routinely in the Subramanian laboratory, is detection of acetylated α-tubulin and γ-tubulin which recognises the stabilized tubulin molecules of the ciliary axoneme and the specialised centriolar components respectively. One limitation of using acetylated α-tubulin as an axonemal marker is that it is also present in stabilised microtubules elsewhere in the cell. Often in many tissues or *in vitro* this does not pose a problem as cilia are easily detectable by their shape projecting away from the cell body. However, in general we found detection of cilia in this way difficult

in brain tissue which may, in part, be due to the prominence of acetylated microtubules in both the axonal and dendritic cytoskeleton of neurons (Morales and Fifkova, 1991). One exception of this was the use of acetylated α-tubulin to effectively detect motile cilia projecting into the ventricle. Another limitation of using acetylated α-tubulin is that it does not differentiate between motile and primary cilia. In this study, detection of adenylyl cyclase III was used to specifically label primary cilia. This is a well-known marker shown in several studies to specifically label the cilia axoneme (Bishop et al., 2007, Arellano et al., 2012). Alternative cilia markers such as Arl13b (Caspary et al., 2007) are also available but, like adenylyl cyclase III, all of the best markers available derive from rabbit polyclonal sources. Similarly the same is found with many basal body markers meaning that throughout this project a suitable pair of antibodies to colabel both axoneme and basal body simultaneously was not possible. Despite this, the distinct shape, size, position and frequency of structures labelled by the adenylyl cyalse III enabled us to confidently determine the presence or absence of primary cilia.

The *Ta3*$^{fl/fl;NesCre}$ brain exhibited a striking loss of cilia however this was incomplete as a small number of cells still possessed a cilium. This incomplete loss of cilia is further demonstrated in subsequent chapters and may be due to a number of reasons. Although possible, it is unlikely that cilia are present in cells which have undergone recombination because Ta3 function has been shown to be essential for cilia formation (Bangs et al., 2011, Kobayashi et al., 2014). This suggests incomplete loss of cilia may be due to incomplete recombination in the brain. Firstly, cilia may still be present in the mutant brain on cells of a non-neural lineage, which do not express *nestin*. These would include the blood vessel endothelial cells and blood cells that extend throughout the brain, although these form distinct tube-like structures and were often easily differentiated from neural tissue. Another class of cell which may still have cilia present are microglia which have been suggested to constitute between 5-12% of brain cells in mice and between 0.5%-16.6% in brain cells in humans depending on the region (Block et al., 2007, Lawson et al., 1990, Mittelbronn et al., 2001). Importantly, despite being present throughout the brain, these cells originate from a macrophage lineage and are unlikely to undergo recombination (Prinz and Priller, 2014). Secondly it has been suggested that the *NesCre* delter exhibits mosaicism in its pattern of recombination (Corrales et al., 2006). This suggests that cells which express *nestin* as they progress through the neural progenitor stage somehow avoid recombination in the *NesCre*

strain. The reason for this is unclear but it is possible that it may be due to the design of the construct used.

One caveat of the *NesCre* line is that it actually uses a rat *nestin* promoter. This was likely to be used in the initial design due to the previous detailed characterisation of the rat *nestin* promoter region (Zimmerman et al., 1994). A consequence of this is, in mouse, the *NesCre* strain is reported to cause recombination in the CNS from E10.5 or E11.5 whereas the endogenous mouse *nestin* gene is expressed in the neuroepithelial tube from E8.0 (as discussed in section 1.4.1). A further limitation of the *NesCre* strain is that a recent study has suggested that the VZ and SVZ, where early embryonic neural stem cells reside, may not even undergo recombination by E12.5 or E14.5 (Liang et al., 2012). The group argue that recombination is only sufficient in these progenitor regions at perinatal stages. This data seems contradictory to other published reports (Tronche et al., 1999, Heffner et al., 2012) but could explain why a total loss of cilia was not observed. It could also suggest why a more conspicuous phenotype wasn't observed in embryonic stages at E14.5.

Considering these limitations of the *NesCre* line there are other deleters available. One such example is an alternative *nestin-Cre* deleter strain which is described to have recombination from E8.0 *(Nes8Cre) (Peterson et al., 2002)*. Whilst this may follow the endogenous expression of *nestin* more accurately*,* the disadvantage with a strain like this is that it is harder to acquire and infrequently used preventing detailed comparison between similar mutants. Despite the difficulties faced with the *NesCre* deleter used in this study it still represents one of the best starting points to study the conditional deletion of *Ta3* in the developing nervous system. It is widely used in the research community making it easily available, numerous other mutants have used the strain allowing useful comparisons and there are a number of studies which, although not always in agreement, have demonstrated its level of recombination during development (Tronche et al., 1999, Heffner et al., 2012, Liang et al., 2012).

In this study the *NesCre* strain was shown to cause a high level of recombination demonstrated by the striking loss of cilia and the striking neural phenotype. With this in mind, it is important to compare the gross phenotype of the mutant brain with both cilial mutants and those affecting signalling pathways known to act through the cilium. To our knowledge one other basal body protein, Stumpy, has been investigated in mice using the *NesCre* deleter (Breunig et al., 2008, Town et al., 2008). The Stumpy protein has been shown

to be essential for cilia formation with its loss resulting in an absence of cilia and those that are present display a malformed 'stumpy-like' appearance (Town et al., 2008). Apart from this, relatively little is known about the molecular roles of the Stumpy protein. Similar to *Ta3* mutants, *Stumpy* mutant mice (*Stumpy*$^{fl/fl;NesCre}$) exhibit a negligible phenotype during embryonic stages. Postnatally the mice develop hydrocephaly which is described as 'prominent' from P12 onwards. The group presents data showing stenosis between the third and fourth ventricles, loss of motile cilia lining the ependyma and disrupted flow of CSF as contributing factors. In an alternative study looking at a common mutation in Bardet-Biedl syndrome protein 1 (*Bbs1*$^{M390R/M390R}$), mice also have disruption of cilia and develop hydrocephaly (Carter et al., 2012). They suggest a mechanism, in contrast to the *Stumpy*$^{fl/fl;NesCre}$ mice, where defective PDGF signalling in a distinct subset of progenitors lining the ventricles results in a low proliferation and survival which leads to the development of hydrocephaly. Whilst the study doesn't address the exact mechanism of how the disrupted progenitors results fluid accumulation, they show compelling evidence of a correlation between the two. Hydrocephaly has also been reported in other cilia mutants: *Kif3a*$^{fl/fl;hGFAPCre}$ (Han et al., 2008) and *IFT88*$^{fl/-;NesCre}$ (Chizhikov et al., 2007) however the mechanisms were not investigated. The first of these studies utilises the *GFAP-Cre* deleter line which is another commonly used strain (Schüller et al., 2008). It is one of several GFAP strains that causes widespread recombination in the majority of the brain including neurons, astrocytes and glia from approximately E10.5 as RGC progenitors begin to express GFAP. In many ways the *GFAP-Cre* is similar to the *NesCre* deleter causing widespread recombination in the brain from midgestation.

Analysis of *Shh* mutant mice driven by the *NesCre* deleter, *Smo*$^{fl/-;NesCre}$ and *Gli2*$^{fl/fl;NesCre}$, also exhibit hardly any embryonic phenotype (Machold et al., 2003, Blaess et al., 2006). In contrast to *Ta3* mutants, *Smo*$^{fl/-;NesCre}$ postnatal mice are described as having enlarged ventricles rather than hydrocephaly (Machold et al., 2003) which presumably represents a less severe phenotype. Interestingly, in the extra-toes mutant (*Gli3*$^{xt/+}$) heterozygous loss of Gli3, a molecule which predominantly acts as a repressor of Shh target genes, resulted in hydrocephaly (Johnson, 1967). Furthermore, hydrocephaly has been shown in mutants with loss of Wnt1 (Thomas and Capecchi, 1990) and downstream Wnt effector Dishevelled (Ohata et al., 2014), although the latter has a much less severe phenotype.

From these data it is clear that cilia, both motile and primary, have an important role regulating CSF in the postnatal brain. It is also evident that deregulation of Shh or Wnt signalling pathways, which are known to act through primary cilia, are also an important influence. Although this project hasn't focused on Ta3 induced hydrocephaly there are several mechanisms which are likely to contribute to its occurrence: (i) loss of motile cilia in the ependyma resulting in inadequate movement of CSF, (ii) disrupted signalling (PDGF, Shh, Wnt) affecting the proliferation and survival of responsive cells, (iii) it is also possible that dysregulation of choroid plexus cells, those responsible for producing the CSF, may be deregulated.

Another observation in *Ta3* mutant mice is a loss of tissue integrity in the centre of the olfactory bulb. Upon dissection this appeared to be the result of fluid accumulation which could be due to excess fluid from the nearby ventricles. Abnormal olfactory bulb development has also been described in *Stumpy*$^{fl/fl;NesCre}$ mice (Breunig et al., 2008, Town et al., 2008). Interestingly a more severe phenotype is observed with constitutive loss of basal body protein Rpgrip1L/Fantom (*Ftm*$^{-/-}$) (Besse et al., 2011); here embryonic stages have ectopic olfactory progenitors which fail to expand perinatally resulting in complete loss of the olfactory bulbs. Agenesis is also observed with disruption of the retrograde cilial motor Tetratricopeptide Repeat Domain 21B (Ttc21b/IFT139) (Stottmann et al., 2009). In contrast to many primary cilia mutants, loss of retrograde motors has been reported to cause an increased level of Shh signalling. In this study, Stottman et al were able to partially rescue olfactory bulb formation by creating a double mutant with complete loss of Tct21b and heterozygous loss of the Shh allele. This demonstrated that the correct level of cilial Shh transduction is important in the formation of the olfactory bulbs. The involvement of Shh signalling is further demonstrated in *Smo*$^{fl/-;NesCre}$ and *Gli2*$^{fl/fl;NesCre}$ mutant mice which were described as having abnormal olfactory bulb formation. Constitutive loss of Wnt2a has also been shown to cause a slight but significant reduction in the length of the olfactory bulbs (Tsukiyama and Yamaguchi, 2012).

Whilst the olfactory phenotype observed in *Ta3* mutant mice could be due to misregulation of cilia-associated Shh or Wnt signalling pathways, the hydrocephaly is also likely to contribute to the observed fragility. CSF is known to be closely associated with the lymphatic vessels and olfactory nerves (Johnston et al., 2004). Therefore, it is possible that excess fluid from the ventricles could accumulate and cause damage in the developing

bulbs. In *Ta3* mutant mice it is probable that the loss of cilia contribute to the olfactory bulb defects in two way; through misregulated signal transduction, with Shh being a likely candidate, and a secondary effect of the hydrocephaly cannot be ruled out.

Many of the anterior defects seen in postnatal *Ta3* mutant mice, such as the disruption of the caudate putamen and internal capsule, are closely associated with the lateral ventricles making it difficult to distinguish phenotypes which are not a secondary result of hydrocephaly. In contrast, many of the posterior defects such as hypoplasia of the cerebellum and abnormal cerebellar peduncles are likely to be independent phenotypes. This idea is supported by the study of *Stumpy*$^{fl/fl;NesCre}$ mice which also show cerebellar defects (Breunig et al., 2008). In an interesting approach, the group compares mutant mice to control mice with idiopathic hydrocephaly of equal severity, in addition to making comparisons with wild type siblings. They identified distinct differences between the two groups but importantly did not show posterior defects in mice with hydrocephaly. In support of this, an alternative study looking at mouse axonemal dynein heavy chain (Mdnah5), a cilia protein only found in ependymal motile cilia, showed that mutant mice lacking Mdnah5 function develop hydrocephaly but also appear to have almost normal development of the hindbrain and cerebellum (Ibanez-Tallon et al., 2004). This demonstrates that it is possible for the cerebellum to develop normally in the presence of hydrocephaly, suggesting that the hypoplasia and disruption of the peduncles is an independent feature. The cerebellar phenotype is discussed further in chapter 4.

Ta3 is a cilial protein and defects in Ta3 are not currently known to cause any clinical condition. The phenotype of *Ta3* mutant mice presented here reflects a number of neural defects which are characteristic of human ciliopathies. In particular, JS exhibits a number of similar features including ataxia, hypoplasia of the cerebellar vermis with thickening and elongation of the cerebellar peduncles (Maria et al., 1999). Numerous genes have been linked as causative alleles of JS including Cep290 (Valente et al., 2006), which is known to interact with Ta3 (Kobayashi et al., 2014). This raises the possibility that Ta3 represents a causative allele of human ciliopathies. This idea is explored further in chapter 5.

Chapter 4 – Cerebellar phenotype of *Ta3*$^{fl/fl;NesCre}$ mice

4.1 Introduction

The cerebellum is a brain structure which modifies and coordinates motor signals and undergoes the majority of its growth postnatally as animals learn to move. In the mature cerebellum, Purkinje cells (PC) and their elaborate dendritic abor are the main targets of excitatory input (Apps and Garwicz, 2005). They form a monolayer, also known as the Purkinje cell layer (PCL), where their cell soma marks the outer boundary of the inner granule layer (IGL) and they extend an extensive dendritic tree into the overlying molecular layer (ML). Mossy fibres are one of two inputs into the cerebellum. They originate from subcerebral nuclei and synapse with granule neurons present in the IGL. Granule neurons continue the circuit by extending axons into the ML where they birfurcate into parallel fibres and then make excitatory synapses with the dendritic spines of Purkinje cells. The second input arises from the inferior olivary nucleus and their climbing fibres make direct contact with the Purkinje cell dendrites. In addition to these two excitatory influences on Purkinje cells, there are a host of inhibitory interneurons including Golgi cells which modulate granule output in addition to stellate- and basket cells which modulate the Purkinje output. Purkinje cells form the main output of the cerebellum forming inhibitory synapses with deep cerebellar nuclei (Wang and Zoghbi, 2001). A simplified diagram of the adult cerebellar circuitry is illustrated in Fig 4.1a.

The cerebellar primordia develop at the boundary of the mid- and hindbrain and require Fgf8 and Wnt1 signals from the Isthmic organiser (Wurst and Bally-Cuif, 2001) (Illustrated in Chapter 1, Fig 1.7c). From approximately E13.5 Purkinje, basket, Golgi, and stellate neurons are born in the ventricular region of the neural tube and migrate radially to form the early cerebellum (Wang and Zoghbi, 2001). Granule neuron progenitors (GNPs) originate from the rhombic lip which is a transient structure found between the neural tube and the roof plate of the fourth ventricle. GNPs migrate to form a cell layer around the cerebellar primordia known as the external granule layer (EGL). Around the time of birth GNPs present in the EGL undergo a massive proliferation. Postmitotic granule neurons first migrate tangentially and extend a trail of parallel fibres (Komuro et al., 2001). They then shift in direction and migrate inwards using Bergmann glia as a radial scaffold to reach their final resting place the IGL (Xu et al., 2013). Postnatally the structure of both Purkinje cells

and Bergmann glia mature into a complex network present in the ML. This process is largely complete by P15-20. Cerebellar development is illustrated in Fig 4.1b.

Sonic Hedgehog (Shh) is a key morphogen in cerebellar development; produced by Purkinje cells from E17.5 it drives GNP proliferation and differentiation of Bergmann glia (Dahmane and Altaba, 1999, Lewis et al., 2004, Wallace, 1999, Wechsler-Reya and Scott, 1999). In addition to its early function in the isthmic organiser, Wnt signalling also has a postnatal role regulating the proliferation and differentiation of GNPS (Lorenz et al., 2011). Notch and BMPs also influence the balance between proliferation and differentiation of cells in the postnatal cerebellum (Roussel and Hatten, 2011).

In mice, the ablation of genes involved in cilia formation (Chizhikov et al., 2007, Spassky et al., 2008) leads to cerebellar hypoplasia and ataxia with defective Shh signalling and impaired proliferation of GNPs. In human ciliopathies with loss of primary cilia including Joubert Syndrome (JS) and Meckel-Gruber Syndrome (MKS), the reduction in GNP proliferation is also linked to defects in Shh signalling (Aguilar et al., 2012). Here we present the cerebellar phenotype of $Ta3^{fl/fl;NesCre}$ mice and describe the defects in detail. Mice have defective proliferation of GNPs resulting in hypoplasia and reduced foliation. Granule neurons also show defective migration with ectopic granule neurons in the ML. Organisation of both Purkinje cells and Bergmann are severely disrupted. We demonstrate that mice have significant loss of primary cilia and reduction in Shh response. Together with data presented in Chapter 3 the phenotype of *Ta3* mutant mice show great similarity with neural defects present in human ciliopathies. Finally, we identify a human case of JS which has mutations in the TA3 gene suggesting the *Ta3* mutant mouse could act as a model to study the rare but clinically significant syndrome.

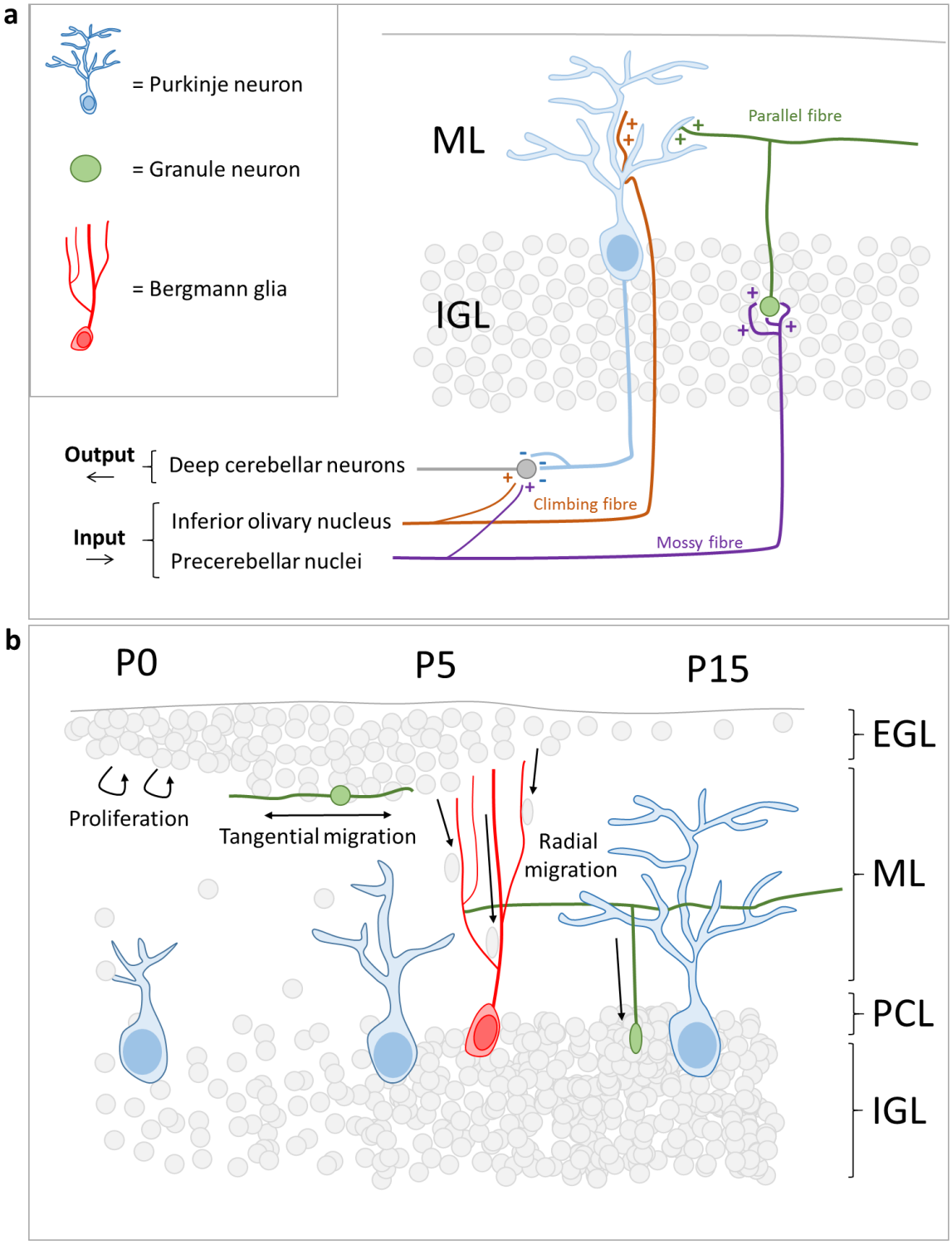

Figure 4.1 The adult cerebellar circuitry and cerebellar development

(a) A simplified illustration of the cerebellar circuitry. Purkinje cells are the main targets of excitatory input from the precerebellar nuclei and inferior olivary nucleus arriving via granule neurons and climbing fibres respectively. (b) The majority of cerebellar development occurs after birth. Shh produced by Purkinje cells acts to stimulate proliferation of granule progenitors present in the EGL. Granule neurons migrate tangentially laying down parallel fibre axons. They continue to migrate inwards along Bergmann glia forming a dense IGL. Abbreviations; EGL, external granule layer, IGL, internal granule layer, ML, molecular layer, PCL, Purkinje cell layer. (a) adapted from (Apps and Garwicz 2005).

4.2 Results

4.2.1 *Ta3* mutant cerebella are smaller with reduced foliation and fewer granule neurons

Macroscopic examination of the brains of P15 *Ta3* mutant mice was presented in Chapter 3 (section 3.2.3). Observation of the hindbrain revealed that the mutant cerebella were strikingly hypoplastic with a very pronounced reduction in the vermis.

The 5 cardinal lobes of the cerebellum (anterobasal, antero-dorsal, central, posterior, inferior) and the 4 principal fissures arise first during development and these subsequently lengthen and bifurcate into lobules and sublobules (Sillitoe and Joyner, 2007; Wang and Zoghbi, 2001). Since the *Ta3* mutant mice had a hypoplastic cerebellum, we analysed the cerebellar histology throughout postnatal development to compare the effects on foliation (Fig 4.2). For each age group (E18.5, P0, P5, P10, P15) at least three mutant brains and three control brains were analysed in the sagittal orientation. In contrast to the normal developmental sequence of the cardinal lobes and fissure formation seen in control mice, the *Ta3* mutant cerebella showed a dramatic loss of foliation which was most severe in lateral regions. Medial regions showed the longest folds/deepest fissures, this region also had the most consistent phenotype between mutant mice. For this reason, all further comparisons were made using medial regions (Fig 4.2a-d).

The formation of the cardinal lobes in *Ta3* mutant cerebella was retarded and this was first evident in the E18.5 cerebella in which the fissures were barely visible (Fig 4.2a). There was no significant increase in the size or foliation in the *Ta3* mutant cerebella between days 5-15 (Fig 4.2e,f). At P15, only the 5 cardinal lobes were present in the *Ta3* mutant cerebellum and the fissures remained shallow (Fig 4.2d) suggesting a defect in proliferation and growth. The cross sectional area of the vermis was significantly reduced in the *Ta3* mutant cerebella (Fig 4.2e). Closer analysis of stained sections showed that mutants had a disruption of the laminar organisation. The PCL was disorganised and the boundary between the IGL and ML was poorly defined (Fig 4.2h,i). In addition, the ML and the IGL were highly disorganized and the integrity of the layers was lost in P15 *Ta3* mutant cerebella (Fig 4.2d).

The most striking feature of the cellular histology in the *Ta3* mutant cerebellum was the thin EGL at P5 with the average between the five mutant lobes having a 49% reduction in mean thickness compared to control. This coincided with mutants having a reduction in

the number of granule cells present in the EGL with an average reduction of 36% in the mutant compared to control (Fig 4.3a-c). This reduction in size and cell number was evident in all of the cardinal lobes at P5 and P10. However, by P15 the control EGL had become depleted of cells consistent with their proliferation and migration into the IGL. Mutants also showed a depletion of cells at P15 but not to the same extent as control, resulting in a slightly wider mutant EGL however this was not statistically significant (Fig 4.3b).

GNPs in the GCL proliferate and eventually migrate to their final position to the IGL. A loss of granule neuron density was also evident in mutant IGL with mutants showing an average reduction of 27% compared to control at P5 (Fig 4.3d). This difference in IGL density became more apparent at P10 and P15 as the control IGL became densely populated with granule neurons, however due to this high density cells were difficult to quantify.

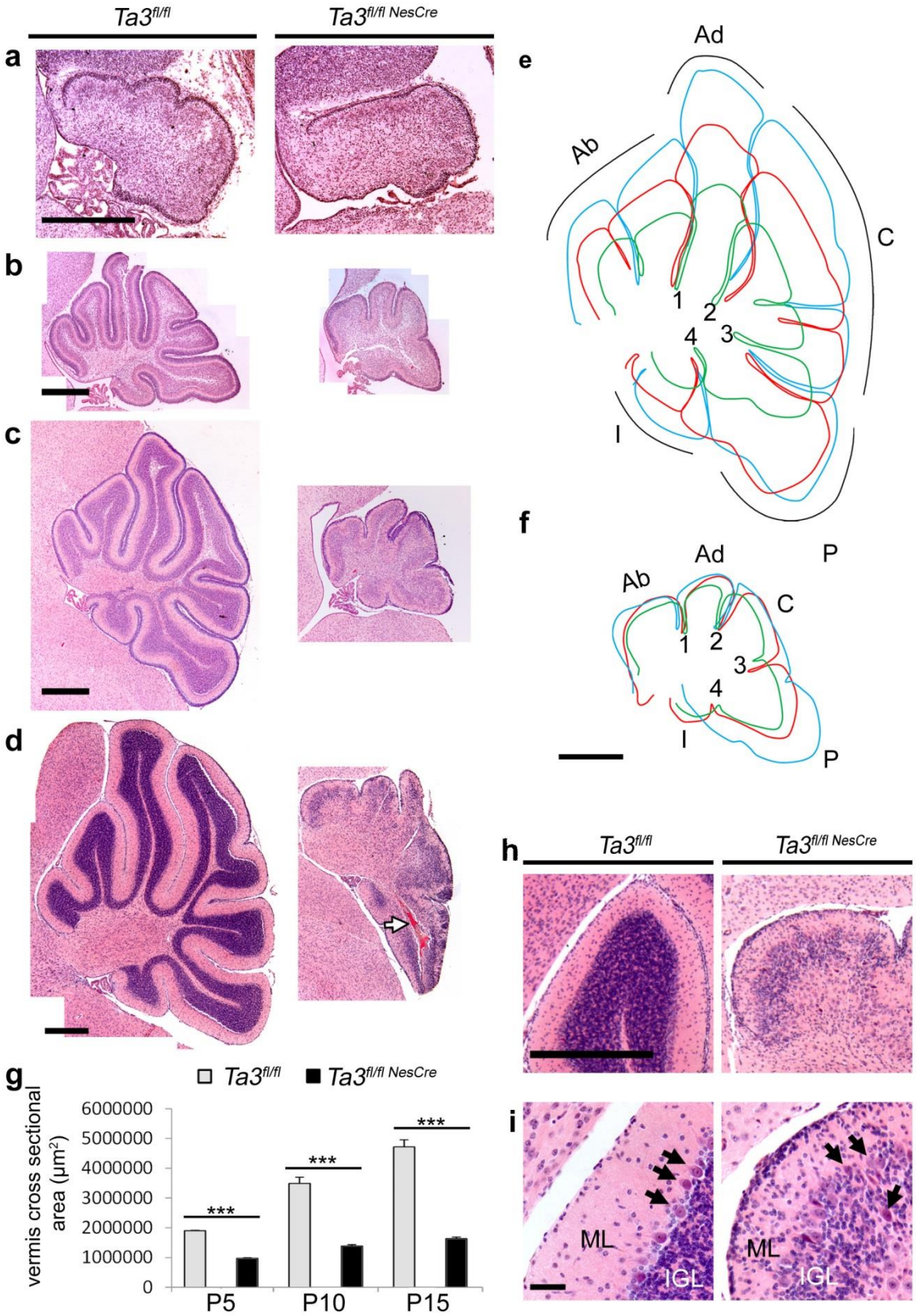

Figure 4.2 Postnatal *Ta3* mutant cerebella have reduced growth, loss of granule neurons and a disorganized PCL. *Ta3* mutant cerebella at (a) E18, (b) P5, (c) P10, and (d) P15 have reduced foliation and are smaller in size. P15 mutant mice develop hematoma in the posterior cerebellar lobe (white arrow). (e) Control cerebella show consistent growth between P5 (green), P10 (red) and P15 (blue). (f) Mutant cerebella show little growth and only exhibit the four principle fissures (1-4) and five cardinal lobes. Ab-anterobasal; Ad-anterodorsal; C-central; P-Posterior; I-inferior. (g) Vermis sagittal cross-sectional area is significantly reduced in the mutant cerebella when compared to the control cerebella and (h,i) reduced granule neuron density in the IGL and a disorganized PCL with ectopic PCs in the IGL (Fig. 2i; black arrows), some PCs appear pycnotic. Mutant ML also shows clusters of cells at P15 which are absent in the control ML. Scale bars, 500 µm (a-e,f,h), 50 µm (i). Error bars: (g) s.e.m (n = 3), *** P≤0.001, (two tailed Students-t test)

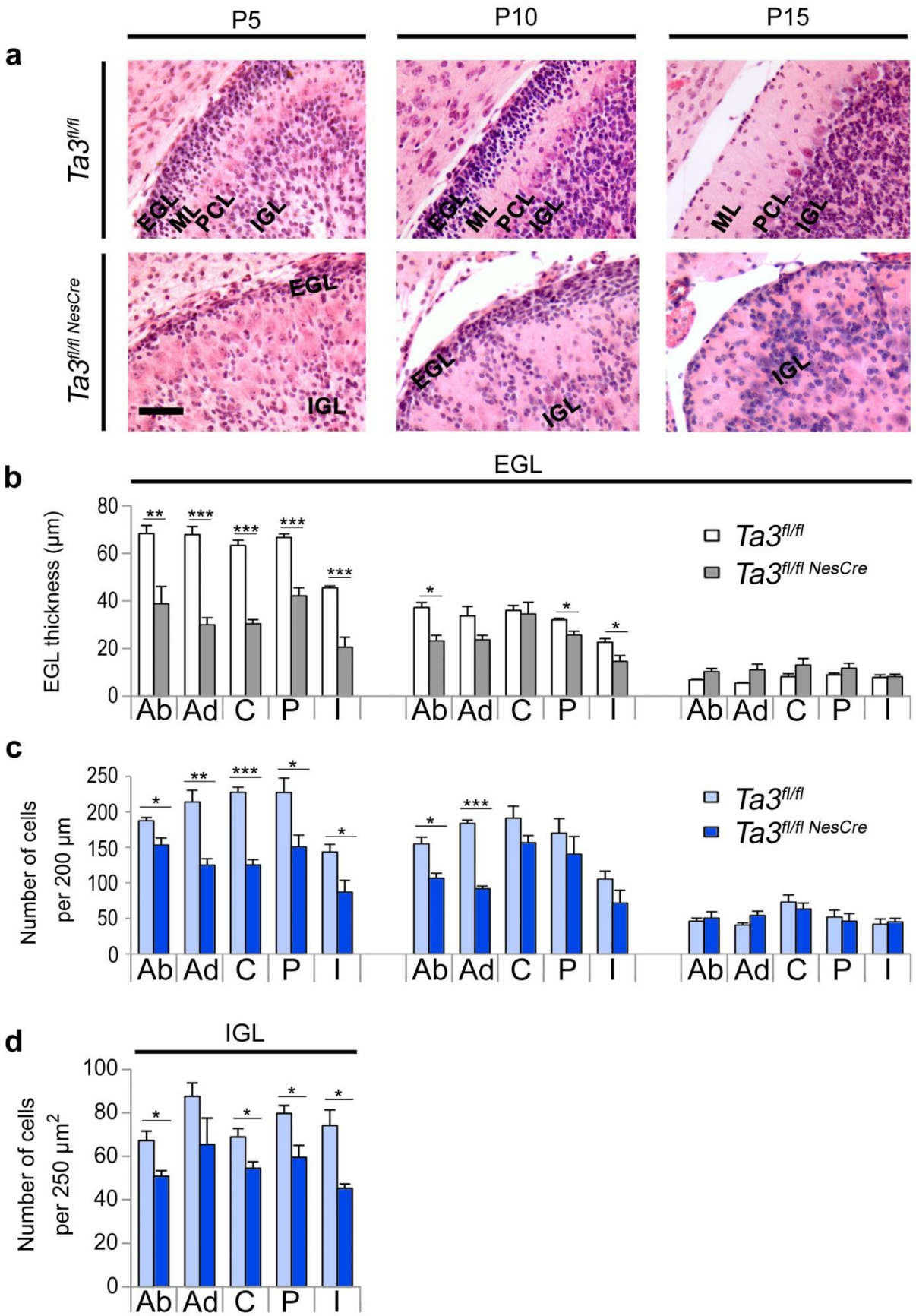

Figure 4.3 *Ta3* mutant EGL is thinner with reduced cell density.

(a,b) In P5 and P10 *Ta3* mutant cerebella the EGL is considerably thinner in comparison to control. (c) P5 and P10 *Ta3* mutant cerebella have a reduced number of cells in the EGL. (d) P5 *Ta3* mutant cerebella have a lower total cell density in the IGL. Ab-anterobasal; Ad-anterodorsal; C-central; EGL-external granule layer; I-Inferior; IGL-internal granule layer; P-posterior. Error bars: (b, c,d) s.e.m (n = 3), *** P≤0.001, ** P≤0.01, * P<0.05 (two tailed Students-t test).

4.2.2 *Ta3* mutant mice lack primary cilia

Previously it was demonstrated that loss of *Ta3* causes a reduction of primary cilia in mutant mice (section 3.2.6). To confirm that the cerebellar defects we observed were also due to loss of primary cilia, we analysed the cerebella of *Ta3* mutant mice by immunostaining for adenylyl cyclase III (ACIII), a protein shown to localise at primary cilia in neurons and glial cells (Bishop et al., 2007).

Quantification of ACIII positive structures from three control and three mutant mice demonstrated that in P5 cerebella of control mice the majority of cells in the EGL possessed a primary cilium (Fig 4.4a). In contrast, cerebella of *Ta3* mutant mice, showed fine dots staining positive for ACIII but importantly these did not resemble primary cilia (Fig 4.4a). We quantified the percentage of ciliated cells and found that 64.4% of cells in the control EGL were ciliated while in the mutant only 18.7% appeared to have a cilium (Fig 4.4b). Noticeably, control cells at the IGL/ML boundary had very long cilia. We quantified the number of cilia in a 25µm square ROI in the IGL starting from the IGL boundary. In control IGL we detected cilia on 60.9% of cells however *Ta3* mutant mice, cilia were present on only 8% of cells (Fig 4.4c,d). The small percentage of cells possessing primary cilia in the *Ta3* mutant EGL and IGL could be due the mosaic expression of the *NesCre* transgene which could leave a few cells with the intact Ta3 protein.

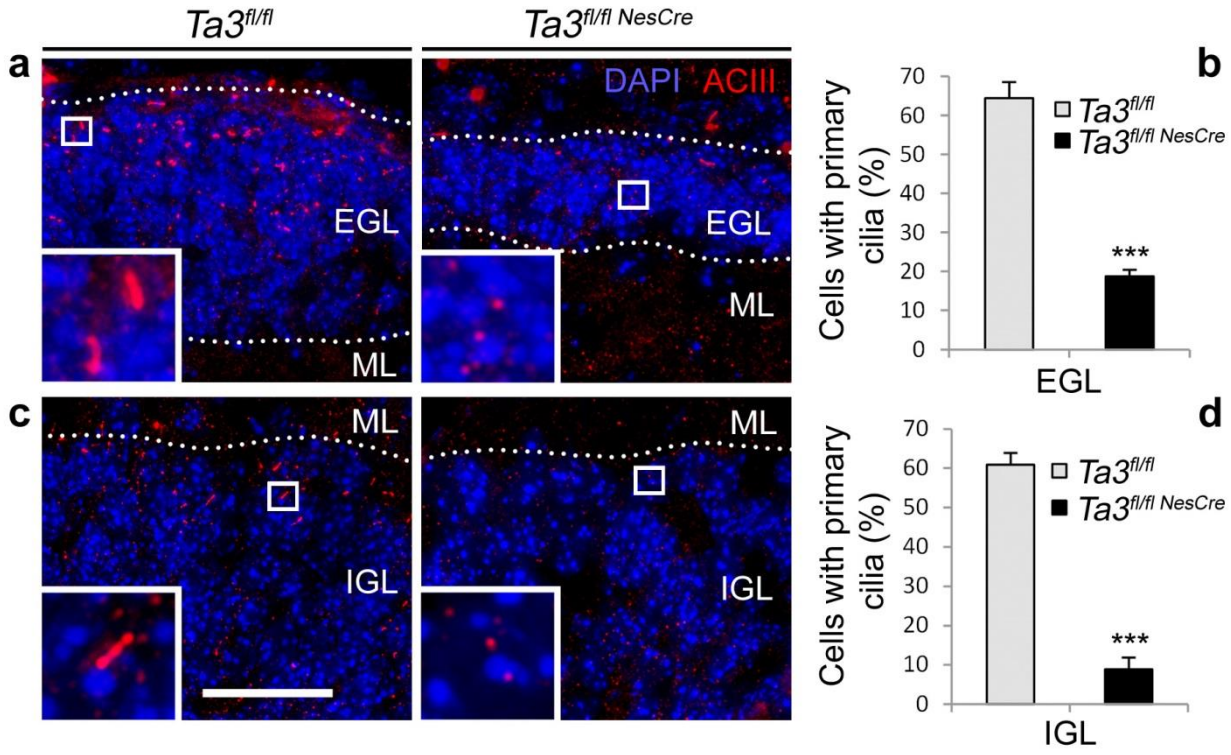

Figure 4.4 *Ta3* mutant mice lack primary cilia in the cerebellum

P5 $Ta3^{fl/fl;NesCre}$ cerebella have a significantly fewer adenylyl cyclase III-positive primary cilia in (a) EGL and (c) IGL. Inset in both (a) and (c) – higher magnification of boxed area showing a well formed cilium; (b & d) quantification of cilia in the EGL and in the outer IGL, using a ROI 25 X 25 µm square at the IGL/ML boundary inclusive of the PCL. Dotted lines indicate EGL and IGL boundaries. EGL-external granule layer; ML-molecular layer; IGL- internal granule layer. Error bars (b,d), s.e.m. (n=3). *** P<0.001 (two tailed Student's t test). Scale bars, 25 µm (a,c).

4.2.3 Loss of *Ta3* causes reduced proliferation and increased apoptosis in GNPs

The immature cerebellum begins it massive growth and organisation from E18.5 onwards. To better understand why mutants exhibited a thinner EGL and smaller number of granule neurons we first identified the early progenitors and investigated their proliferation at this early stage. Cells were immunolabelled for the mitotic marker phospho-histone3 (PH3) and proliferating cell nuclear antigen (PCNA) and the number of proliferating cells in the each of the emerging cardinal lobes was quantified (Fig 4.5b,c). The detection of PCNA often labels a greater number of cells compared to PH3 due to it being present in a longer proportion of the cell cycle (S-phase vs M-phase) and the protein also having a relatively long half life (~20 hours) (Bravo and Macdonald-Bravo, 1987). For these reasons, it can often act as a as a more sensitive quantification of the level of proliferating cells.

The number of PH3 or PCNA cells were quantified from three control and three mutant mice either throughout the EGL region or in the central region of IGL (indicated by white line on Fig 4.5). In the mutant EGL, there was a significant reduction in the number of PH3-positive cells in the anterobasal region but the trend continued in all of the remaining regions. There was also a significant reduction in the number of mutant PCNA-positive cells in all regions (Fig 4.5c). In contrast, the reduction in proliferating cells was much less evident in mutant IGL with fewer regions showing a significant difference. Despite this, nearly all mutant IGL regions still showed a trend of decreased proliferation (Fig 4.5d).

A considerable reduction in the number of granule cells and EGL thickness was observed in the postnatal cerebella of *Ta3* mutant mice. To assess whether the proliferative defect persisted in postnatal stages, the thymidine analogue, Bromo-deoxyuridine (BrdU) was administered to three control and mutant mice aged P5, P10 and P15 one hour prior to sacrifice. Immunohistochemistry for BrdU and PH3 identified cycling cells in S-phase or mitosis respectively (Fig 4.6a). In P5 mutant mice there was a significant reduction in the number of proliferating BrdU-positive cells in three of the lobes and PH3-positive cells in two of the lobes yet all of the remaining lobes still followed the same trend (Fig 4.6b,c). This trend continued until P10, but to a lesser extent with one of the regions showing significant differences in the number of BrdU-positive cells and two showing significant differences in PH3-positive cells. By P15 the rate of proliferation reduced considerably in both control and mutant cerebella such that the differences in proliferation observed earlier were not obvious (Fig 4.6b,c). Analysis of proliferation in the P5 mutant IGL showed only a moderate

reduction in proliferation, consistent with the observation at E18.5. Although only the posterior lobe showed a significant reduction, the remaining lobes still followed the trend (Fig 4.6d).

To assess whether the loss of cell density was due to a combination of reduced proliferation and increased levels of apoptosis we also labelled cells for cleaved caspase-3 in three control and three mutant mice (Fig 4.7a,b). Quantification of caspase-3 positive cells in the P5 EGL revealed that mutants had a small but a significant increase at the 5% level in the number of apoptotic cells per unit area (Fig 4.7c). Interestingly this was not the case in the IGL, where mutants were not significantly different to control. In the ML numbers were too low to draw any meaningful conclusions (Fig 4.7c). This demonstrates that postnatal mice exhibit a lower density of granule neurons both in the EGL and IGL due to reduced proliferation and increased apoptosis.

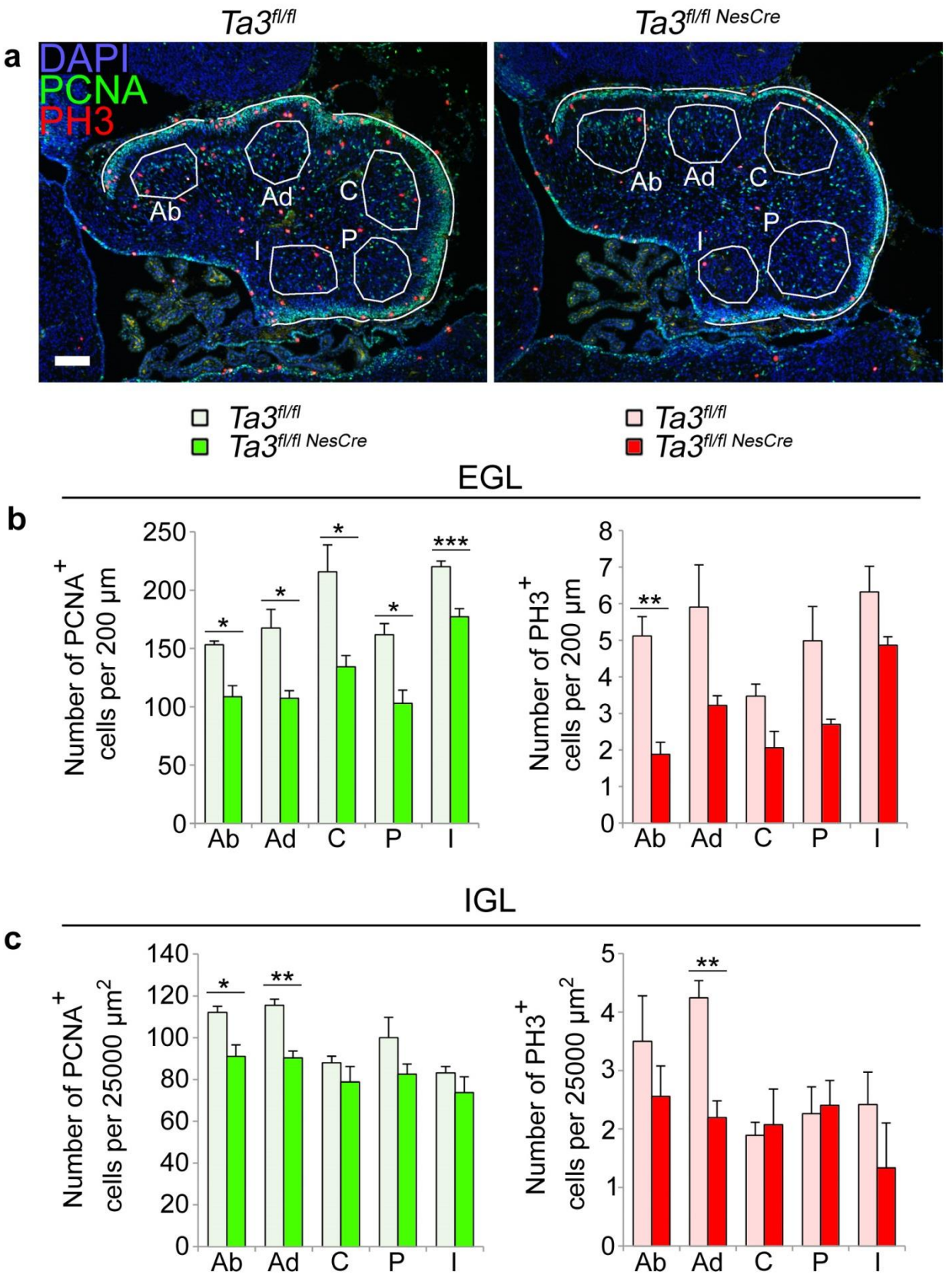

Figure 4.5 E18 *Ta3* mutant cerebella have reduced progenitors and proliferation.

(a) E18 mutant cerebella have fewer Pax6-positive progenitors and thinner EGL. (b) E18 mutant cerebella have reduced number of PCNA-positive and PH3-positive proliferating cells. (c) Significant reduction of proliferation in all regions of the EGL in mutant cerebella and (d) marginal reduction of proliferation in some regions of IGL in mutant cerebella. Ab-anterobasal; Ad-anterodorsal; C-central; EGL-external granule layer; I-Inferior; IGL-internal granule layer; P-posterior; PCNA-proliferating cell nuclear antigen; PH3-phosphohistone-3. Error bars; (b,c) s.e.m (n = 3), NSD = no significant difference, *** P≤0.001, ** P≤0.01, * P<0.05 (one tailed Students-t test); Scale bar. 50 um (a), 100 um (b).

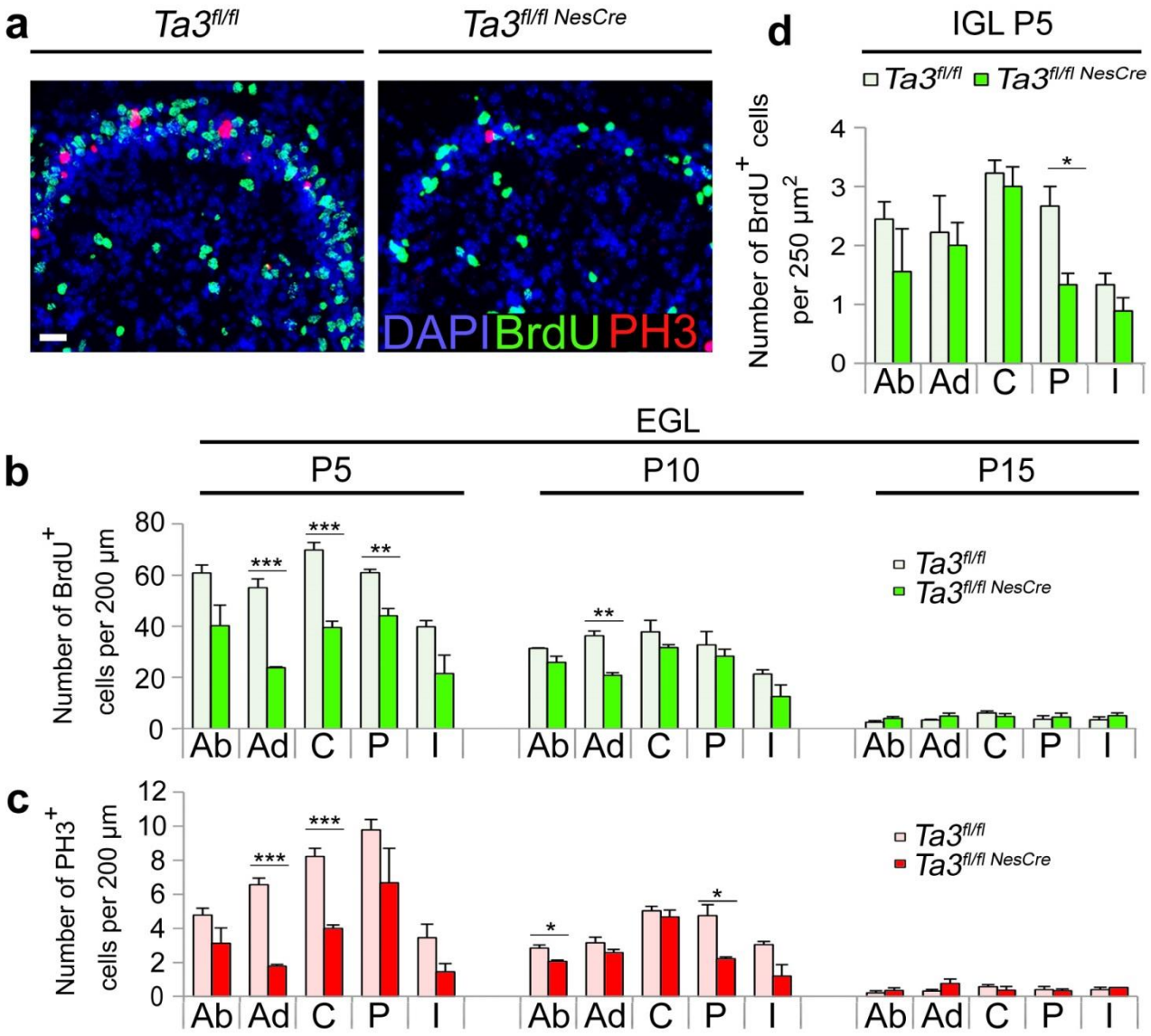

Figure 4.6 *Ta3* mutant EGL has reduced proliferation.

(a) P5 Anterodorsal fold of cerebella showing $BrdU^+$ and $PH3^+$ cells. (b) Mutant P5 and P10 cerebella have a reduction in the number of BrdU-positive cells in the EGL. (c) Mutant P5 and P10 cerebella also have a lower number of $PH3^+$ cells in the EGL. (d) Mutant cerebella show a reduction in the number of $BrdU^+$ cells in the IGL. Ab-anterobasal; Ad- anterodorsal; BrdU-Bromodeoxyuridine; C-central; EGL-external granule layer; I- Inferior; IGL-internal granule layer; P-posterior; PH3-phosphohistone-3. Error bars; (b-d) s.e.m (n = 3), *** P≤0.001, ** P≤0.01, * P<0.05 (two tailed Students-t test). Scale bar- 50 µm (a).

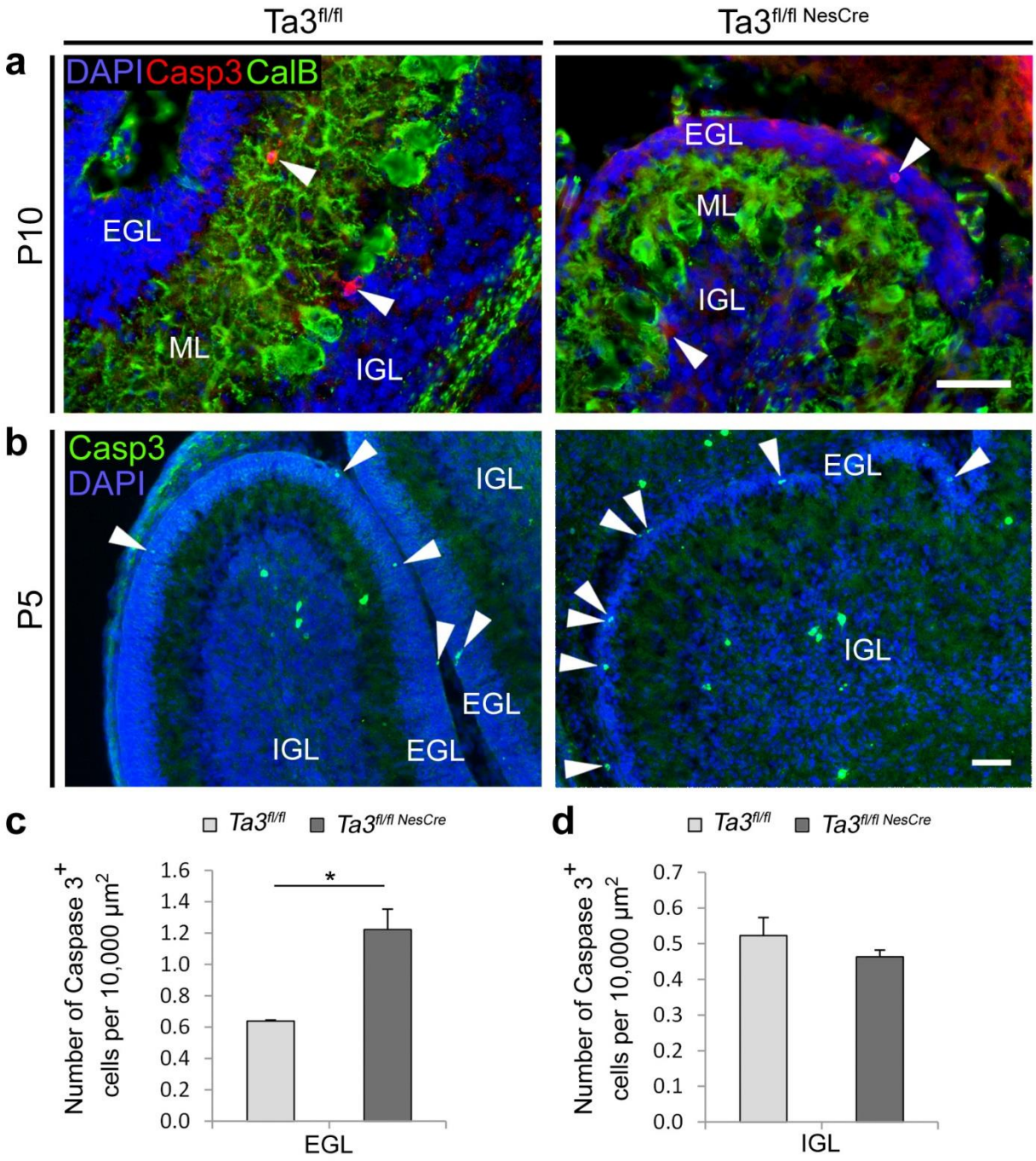

Figure 4.7 P5 *Ta3* mutant EGL has increased apoptosis

(a) P10 cerebella immunohistochemically labelled for Cleaved caspase-3 (red) and calbindin d-28k (green). Purkinje cells do not undergo apoptosis in control or mutant cerebella. Arrows indicate Caspase-positive cells. (b) P5 cerebella labelled for cleaved caspase 3. Quantification of apoptotic cells in EGL (c) and IGL (d). Mutants show a significant increase in apoptosis in the EGL. Arrows show apoptotic cells in the EGL. Error bars; (c, d) s.e.m (n = 3), * $P<0.05$ (two tailed Students-t test). Scale bar- 50 µm (a, b).

4.2.4 *Ta3* Mutant cerebella have misoriented GNPs and misplaced mature neurons

In addition to the reduced proliferation and increased apoptosis in the mutant EGL, we also observed that the cells appeared more elliptical and were tangentially orientated in the mutant cerebellum. As nuclear morphology is a good indicator of cell shape we analysed and quantified the nuclear orientation and nuclear area of cells in the EGL in sections from three mutant and three control mice. In the P5 control EGL, nuclei tended to orientate in a radial direction and this shifted to a tangential orientation in the granule cell depleted EGL by P15 (Fig 4.8a,b). In the mutant cerebellum however, the P5 EGL cells were already predominantly tangentially orientated and remained as such until P15. Measurement of nuclear area also showed that in the control EGL the nuclei were more compact with a smaller mean area (Fig 4.8c). Interestingly, the misorientation of the mutant nuclei correlated with an increased number of tangentially orientated glial fibres in the EGL. Double labelling for the GNP marker Pax6 and glial fibrillary acidic protein (GFAP) at P10 clearly showed parallel glial fibres extending radially through the control EGL (Fig 4.9a). However, the mutant GFAP-positive fibres exhibited a more aberrant organisation with more tangential fibres. In mutant EGL these tangential glial fibres were often found next to the tangentially orientated Pax6 positive GNPs suggesting a causative link (Fig 4.9a).

As granule cells become postmitotic they first migrate tangentially then radially towards to IGL. In mutant mice the boundaries of the ML appeared less defined with a significantly increased number of ectopic cells. To identify these cells we double stained for Pax6 and the mature neuron marker NeuN. In control cerebella, granule cell progenitors in the EGL and migrating cells in the ML strongly express Pax6 and the cells of the IGL are negative for Pax6 (Fig 4.9b). Immature cells of the EGL and ML have very low levels of NeuN and this expression becomes stronger as they mature in the IGL in control mice. In mutant cerebella, however, we see a number of cells strongly expressing NeuN in the ML with barely detectable expression of Pax6 indicating that they are mature granule neurons. These cells are present as clusters but they are heterogeneous in the level of Pax6 and NeuN they express (Fig 4.9b). It is likely that these ectopic NeuN positive cells have undergone premature maturation in the ML before reaching the IGL due to defective migration.

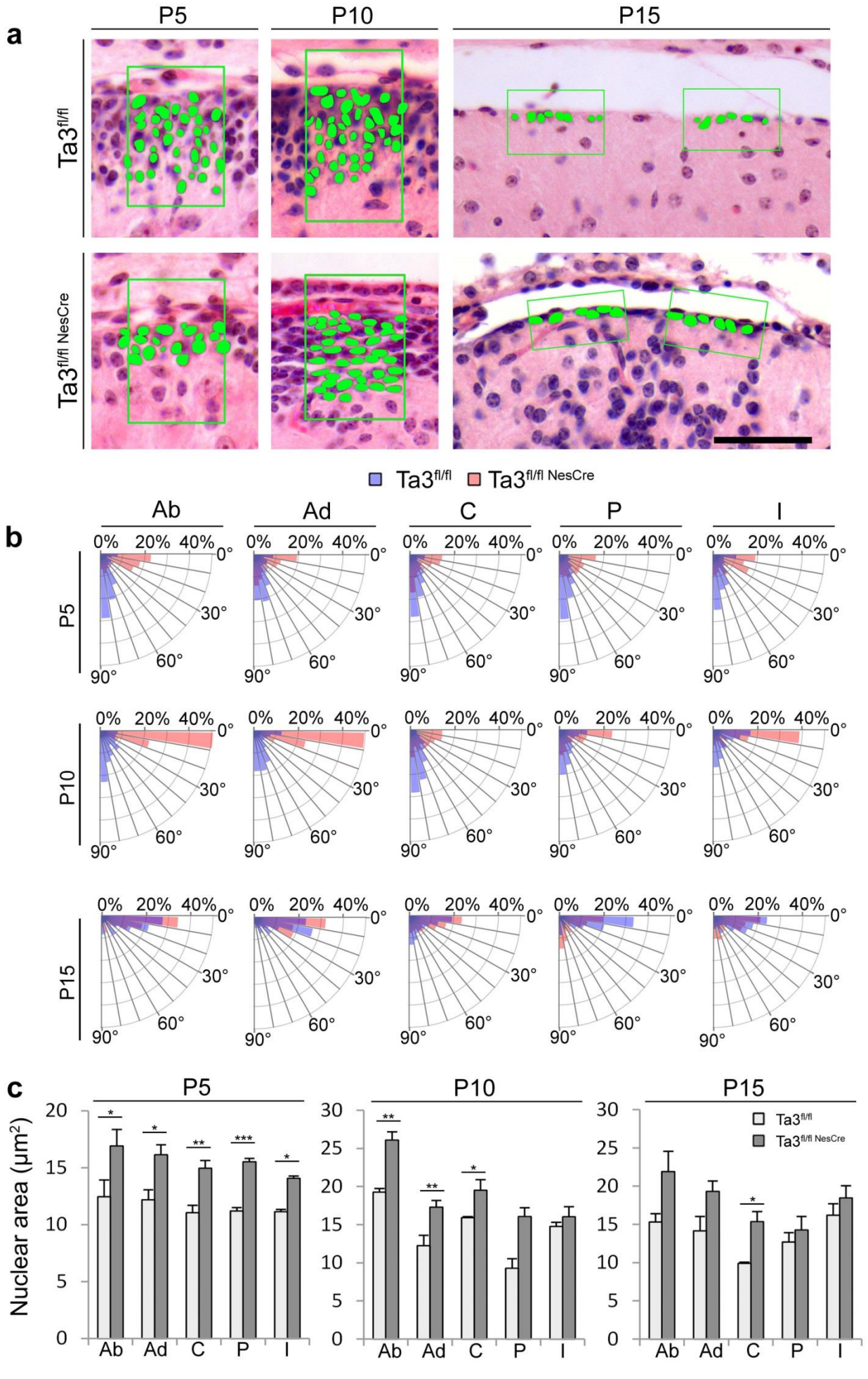
a
P5
P10
P15
Ta3fl/fl
Ta3fl/fl NesCre
Ta3fl/fl
Ta3fl/fl NesCre
b
Ab
Ad
C
P
I
P5
P10
P15
0%
20%
40%
0°
30°
60°
90°
c
P5
P10
P15
Nuclear area (µm2)
Ta3fl/fl
Ta3fl/fl NesCre
Ab
Ad
C
P
I

Figure 4.8 *Ta3* mutant GNP nuclei have tangential alignment and larger size

(a) Representative images of P5, P10, P15 cerebella showing EGL of the anterobasal fold. Boxed nuclei filled in green illustrate sample used for nuclear analysis. (b) Radial plot showing frequency of nuclear orientation. P5 and P10 mutants have a higher frequency of tangentially aligned nuclei. Control (Blue bars), Mutant (Red bars). Angle of bar indicates orientation grouped within 10° bins (0° = parallel with EGL, 90° = perpendicular to EGL). Length of bar indicates percentage frequency. (c) Box plots showing median nuclear area of P5, P10, P15 EGL. Mutant EGL nuclei have a higher median nuclear area. Error bars; (c) s.e.m (n = 3), *** $P < 0.001$, ** $P < 0.01$, * $P<0.05$ (two tailed Students-t test). Scale bar- 50 µm (a).

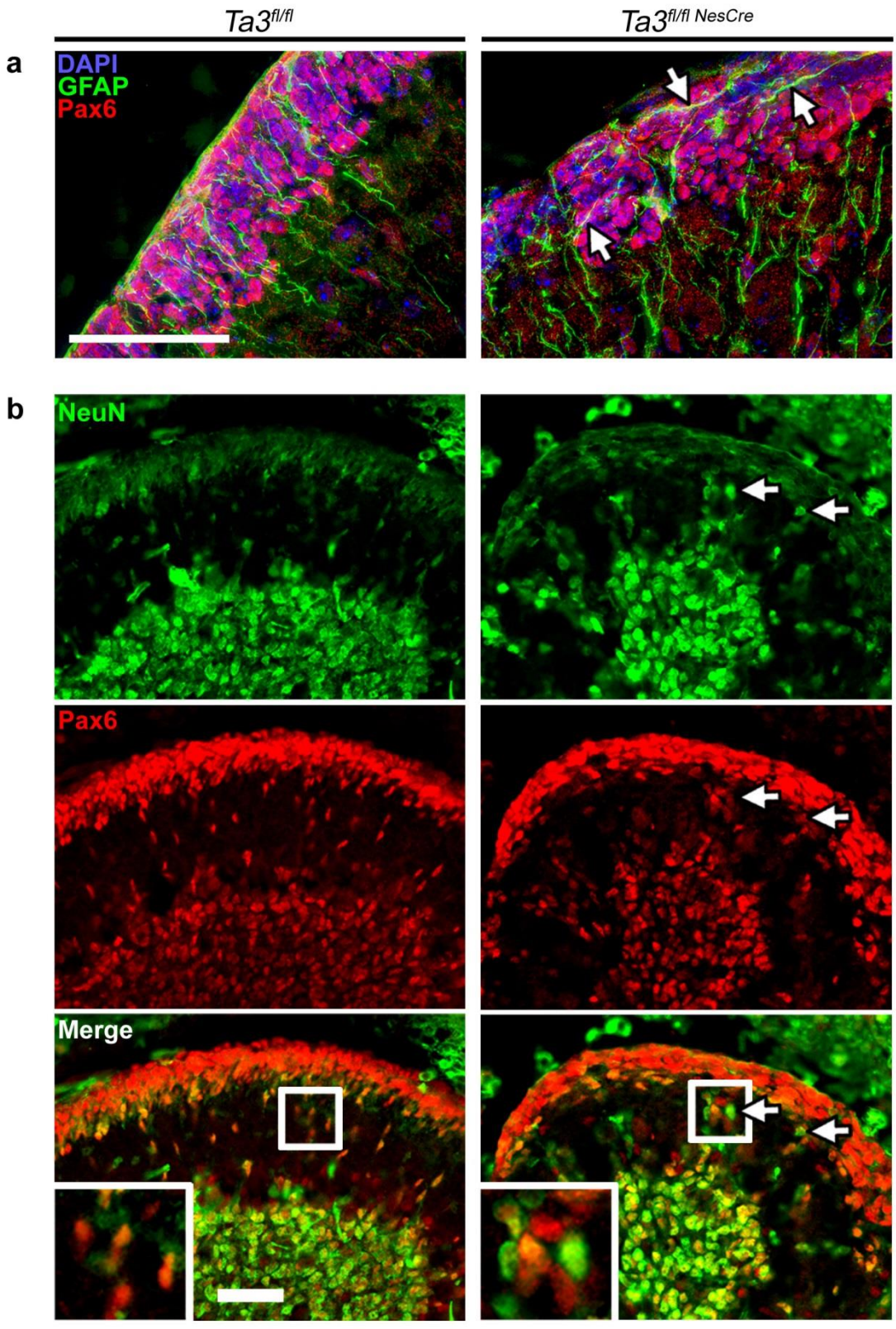

Figure 4.9 *Ta3* mutant cerebella have tangential glial scaffold and misplaced progenitors

(a) P10 mutant EGL has increased number of tangential GFAP fibres (green, white arrows) which correlates with misorientated Pax6 cells (red). (b) P10 cerebella immunohistochemically labelled for NeuN (green) and Pax6 (red). Arrows indicate ectopic $NeuN^{+}$ cells in the molecular layer. Boxed region indicates enlarged area showing ectopic NeuN+ cells in the molecular layer. Scale bars, 50µm (a,b)

4.2.5 Glial scaffold and axonal defects in *Tα3* mutant mice

Bergmann glia form the scaffold on which the granule neurons migrate to the IGL. To further assess the morphology of the glial scaffold, we stained sections of the cerebellum for GFAP at P5, 10 and 15. In control cerebella the glial scaffold consisted of parallel well organized fibres which increased in density by P15 (Fig 4.10a). In mutant cerebella, there was a reduction in the number of Bergmann glia and a concomitant loss in the density of glial fibres extending through the ML (Fig 4.10a). The glial scaffold in the mutant cerebella was not only less dense but it was also disorganized. The glial fibres were more tangentially orientated instead of having a radial and parallel organization seen in the control cerebellum (Fig 4.10a,b). The difference between the control and mutant glial scaffold became increasingly apparent across the time series as, in control, glial became better organised whereas the mutant organisation appeared to worsen (Fig 4.10c).

Bergmann glia were further identified by labelling their radial fibres for intermediate filament nestin and their cell soma with glial marker BLBP (Fig 4.11a). In P5 control, the positioning of the cell soma followed the boundary between the IGL and ML whereas in mutant despite many being present at the IGL/ML boundary, numerous cell bodies were mislocalised throughout the ML (Fig 4.11a). By P15 the mislocalised Bergmann glia were more apparent consistent with the increasing disorganisation (Fig 4.11b).

To further characterize the organisation of the ML we stained for the 165kDa neurofilament to identify axonal tracts. At P5 the organization appeared similar between control and mutant with a punctate distribution throughout the ML (Fig 4.12a). Long axons originating towards the central nuclei were also visible and extended radially through the IGL however there was a greater density of axons in *Tα3* mutant cerebella (Fig 4.12a). By P10 the ML in the control cerebellum had well-developed distinct axonal tracts which extended in both tangential and radial orientations and was more prominent in the basal half of the ML (Fig 4.12b). In contrast, in the *Tα3* mutant cerebellum, the tracts extended predominantly in the radial axis (Fig 4.12b). This phenotype became more prominent by P15 with the majority of axons in control having tangential organisation whereas, in the mutant, axons were radial with a disorderly appearance (Fig 4.12c).

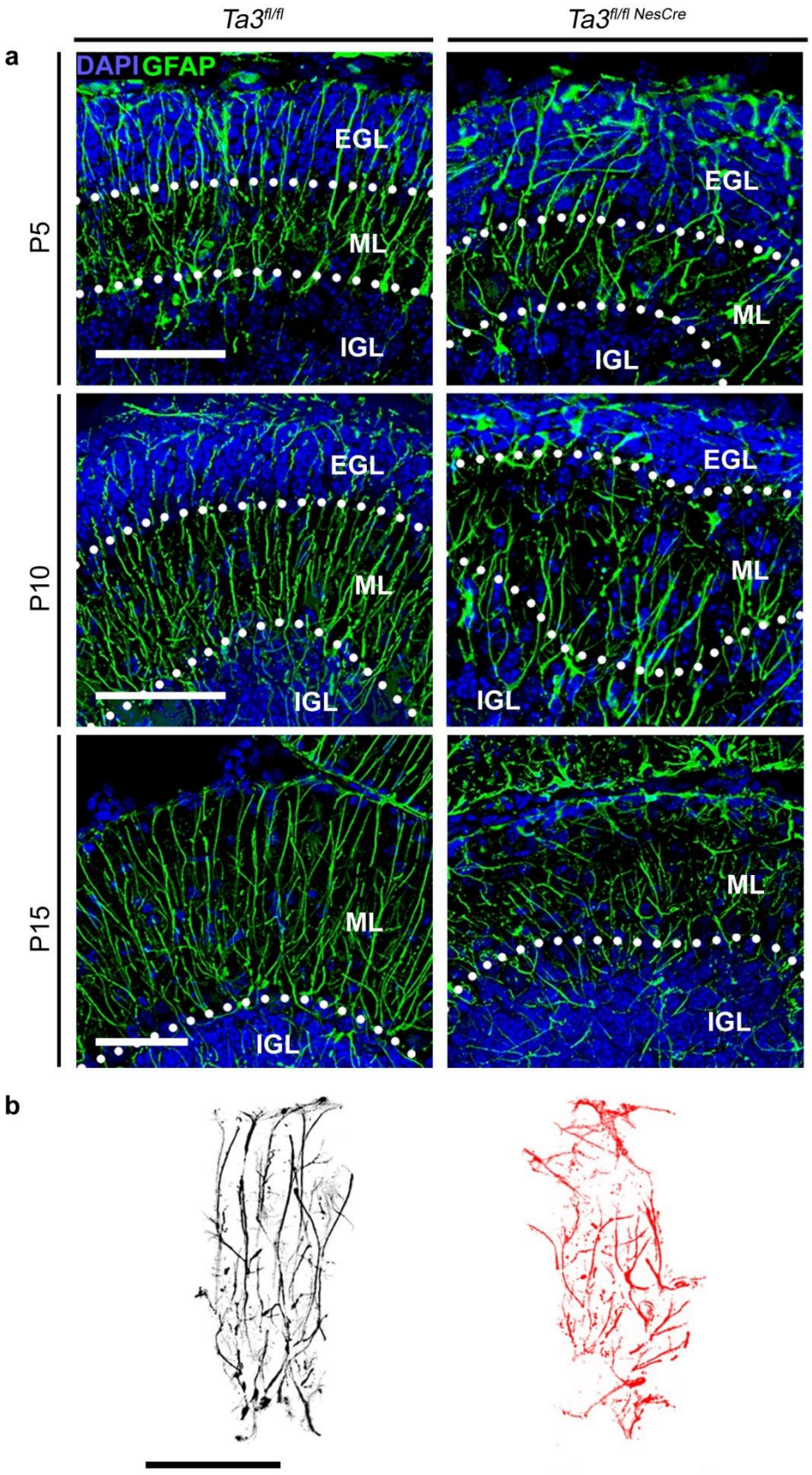

Figure 4.10 *Ta3* mutant glial scaffold is malformed

(a) P5, P10, P15 cerebella labelled for GFAP (green). Mutants have fewer Bergmann glia with those present having fewer radially aligned branches. (b) Representative outline of P15 glial fibres labelled for GFAP. Scale bars, 50µm (a,b)

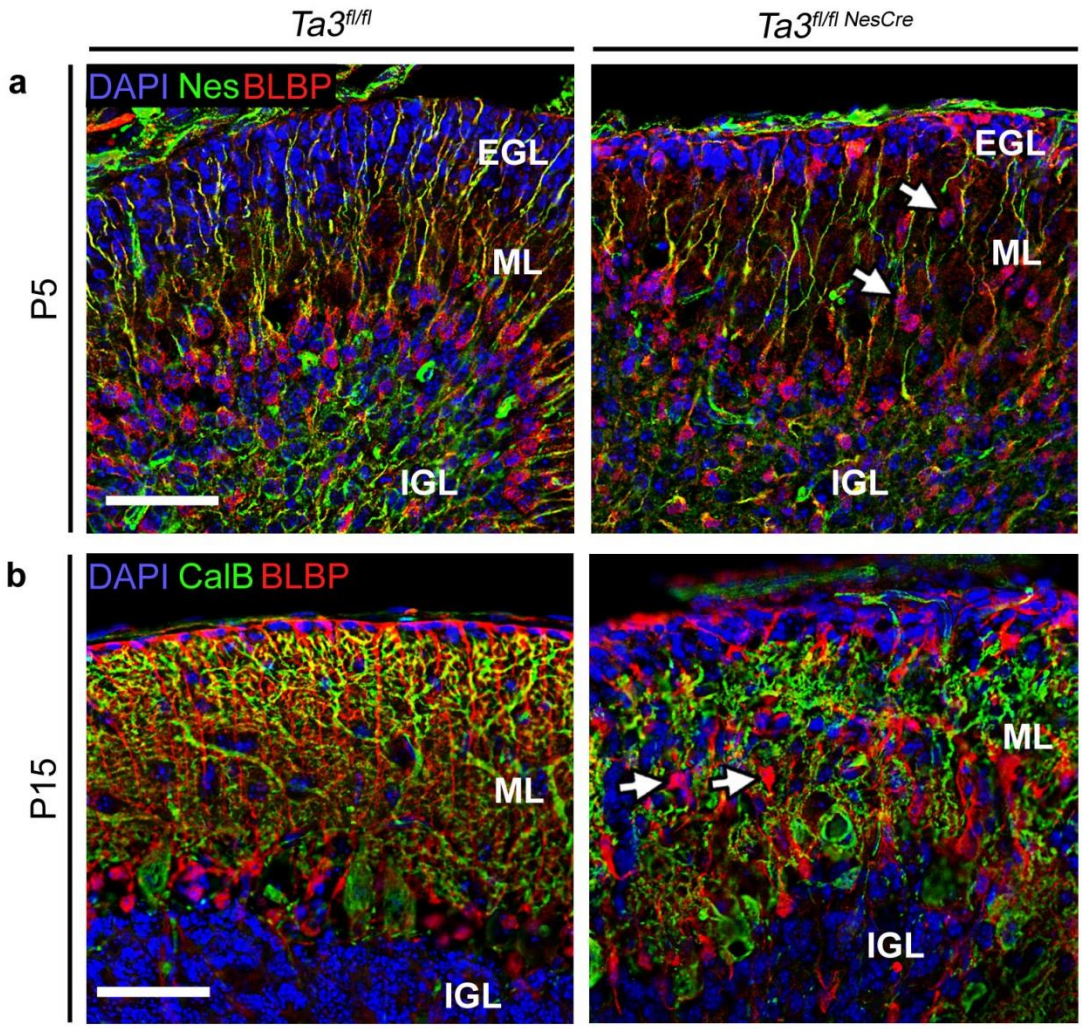

Figure 4.11 *Ta3* mutant Bergman glia are misplaced

(a) P5 Bergmann glia labelled for Nestin (green) and Blbp (red). Mutants exhibit fewer radial fibres and misplaced Bergmann glia in the ML (white arrow). (b) P15 cerebella labelled for Calbindin d-28k (green) and Blbp (red). Mutants have mislocalised Bergmann glia (white arrow) with loss of end-feet in the EGL. Scale bars, 50 µm (b)

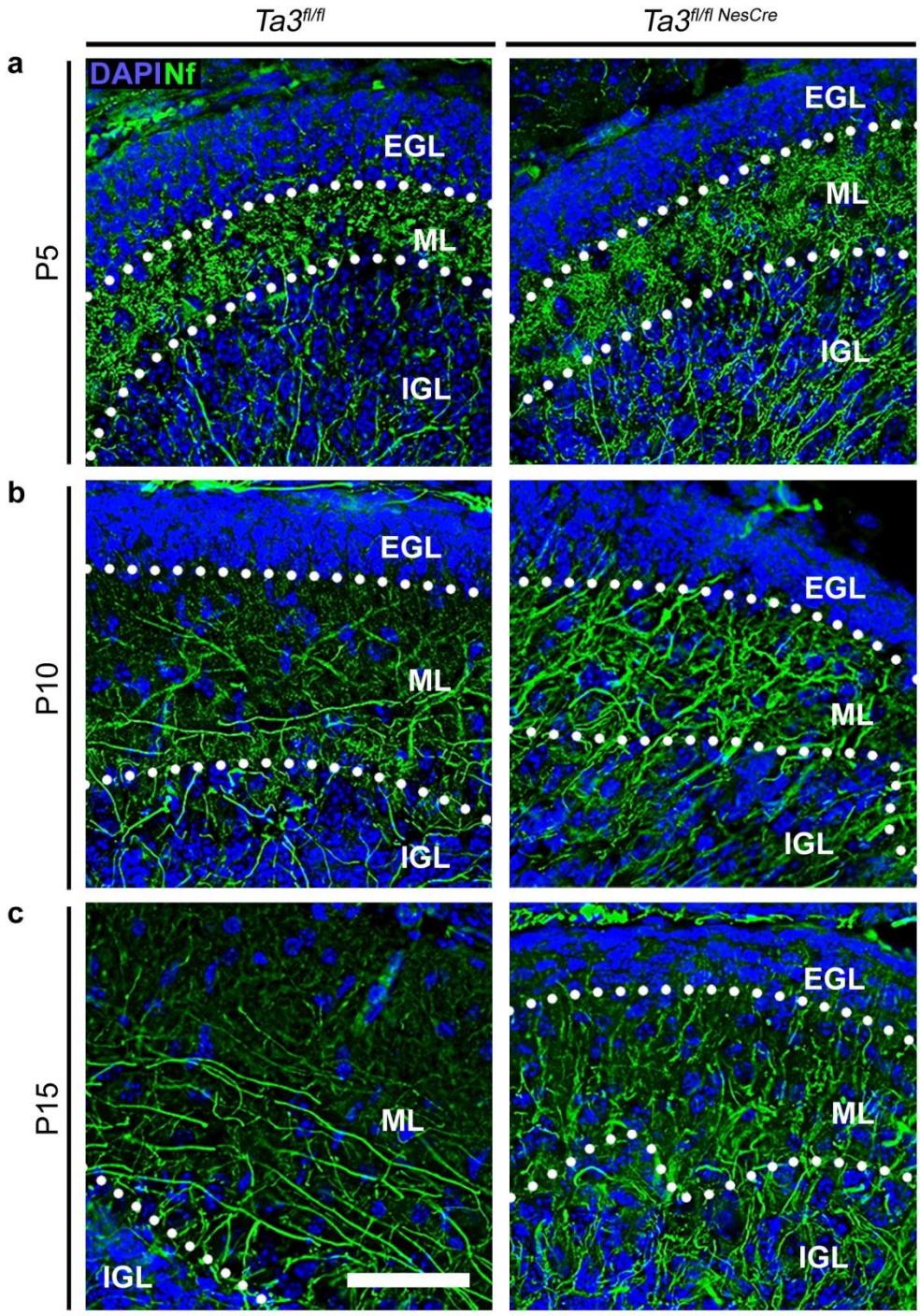

Figure 4.12 *Ta3* mutant cerebella have disorganised neurofilament distribution

P5, P10, P15 cerebella labelled for Neurofilament (green). (a) At P5 neurofilament has a similar punctate distribution in the molecular layer (ML) between control and mutant. (b) By P10 axons are clearly visible with mutants having a clear disorganisation and higher density. (c) By P15 parallel fibres are evident in control but these are not present in mutant which has disorganised radial fibres . Scale bars, 50µm (a-c)

4.2.6 The *Ta3* mutant Purkinje cell layer is disorganised with abnormal Purkinje cells

In control mouse cerebella, the Purkinje cells start expressing Shh when they integrate into the PCL and the secreted Shh acts as a potent mitogen leading to massive proliferation of the GNPs (Dahmane and Altaba, 1999). In H&E stained sections of the control cerebellum, the Purkinje cells formed a distinct monolayer surrounding the IGL (Fig 4.3a). However, we observed a disorganized PCL in the *Ta3* mutant cerebellum with heterotopic Purkinje cells (Fig 4.3a). In many JS/MKS cases also it has been observed that that the integrity of the PCL is lost and the cerebellum contains heterotopic Purkinje cells (Aguilar et al., 2012).

To investigate this further, we stained Purkinje cells with an antibody to Calbindin D-28k (Milosevic and Zecevic, 1998), a calcium binding protein. We found the *Ta3* mutant cerebella had a disorganized PCL with groups of Purkinje cells occurring at the base of the folds and in ectopic regions in the centre of the IGL as well in the ML (Fig 4.13a,b). Although the mutant cerebella were smaller than control, they had a surprisingly high density of Purkinje cells. Quantification of Purkinje cells from three P10 control and three mutant mice revealed that, per section, *Ta3* mutant cerebellum had a 24% reduction in the total number of Purkinje cells but a density approximately twice that of control (Fig 4.13c,d). Since there was an apparent loss of Purkinje cells in the *Ta3* mutant mice, we investigated if the reduction in Purkinje cell numbers was due to increased cell death. Immunohistochemical staining for the apoptotic marker cleaved-Caspase3 together with Calbindin D-28K did not detect any apoptotic Purkinje cells in control or mutant at P10 (Fig 4.7a).

The mutant Purkinje cells also displayed a disruption in their dendritic arborisation and exhibited a degree of asymmetry and disorganisation (Fig 4.13e). In addition, a small number of Purkinje cells appeared to be completely misorientated, extending processes in the wrong direction (Fig 4.13e) and this correlated with the loss of the discrete layering in the cerebellar cortex and the lack of post-natal growth of the cerebellum. In the control cerebellum, the Purkinje cells displayed a characteristic pattern of dendrites with a clear primary branch which bifurcated to eventually form the numerous spiny branches at the distal tips. Quantification of thirty Purkinje cells from a single control mouse and a single mutant mouse using confocal microscopy suggested that in mutant cerebella, the Purkinje cells had a shorter primary dendrite (Fig 4.13e,f,g,h) which branched into fine structures more similar to the spiny distal tips (Fig 4.13e,f,g,h). The Purkinje cells lacked thicker core

branches and instead thinner, more irregular dendrites extended radially. Due to the dendrite imaging analyses being completed on a single mouse, statistical analyses were not completed.

Interneurons such as the Golgi, basket and stellates cell are also located around the PCL. To identify the organisation of these cells we completed double immunohistochemistry for Calbindin D-28K and Parvalbumin; the latter is another calcium binding protein known to bind all of the above interneurons (Milosevic and Zecevic, 1998). Cells which were parvalbumin-positive but Calbindin-negative identified this population of interneurons. At E18.5 the staining of calbindin and parvalbumin appeared mutually exclusive; parvalbumin-positive interneurons were located more centrally in the cerebellum and had a similar number and distribution in control and mutant mice (Fig 4.14a). There was also a population of Parvalbumin-positive cells in the rostral section of EGL, this was also consistent between control and mutant cerebella and was not seen at later stages. This transient presence in the EGL is consistent with reported data in humans (Milosevic and Zecevic, 1998). At later stages interneurons were clearly visible through their lack of calbindin staining (Fig 4.14b,c). In mutant P5 cerebellum there appeared to be more interneurons present in the EGL compared to control (Fig 4.14b). However, by P15 the distribution of interneurons appeared surprisingly comparable between control and mutant (Fig 4.14c). Both had a scattering of cells predominantly in the ML and considering the disorganisation seen throughout the ML it was hard to observe a distinct difference between the control and mutant.

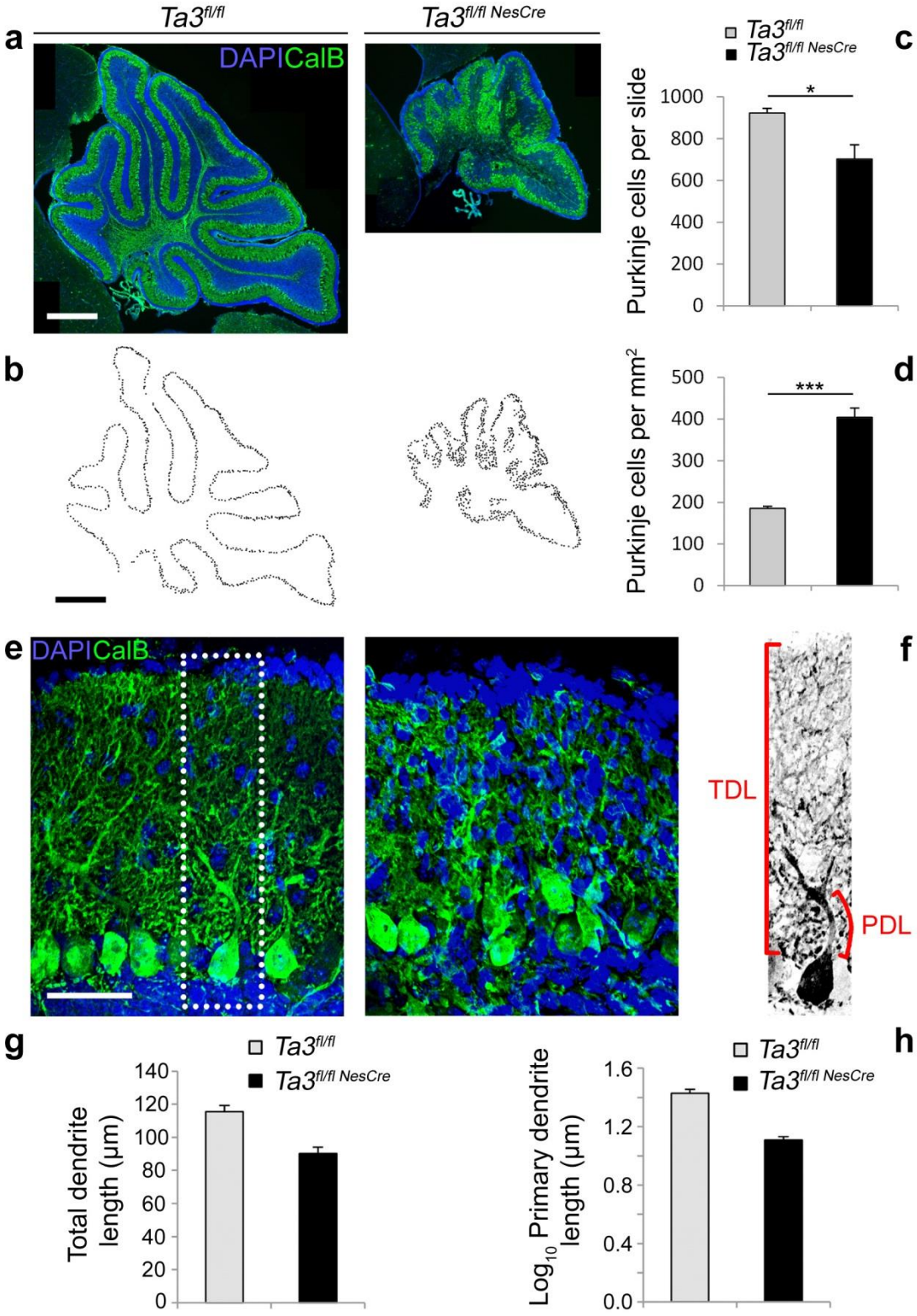

Figure 4.13. *Ta3* mutant cerebella have a disorganised PCL and PCs with a disrupted dendritic arborisation. Mutant and Control cerebella stained for Calbindin. (a) P10 mutant cerebella have disorganised and multi-layered PCL (b) black dots indicate trace of the PC bodies which give a clear picture of the extent of disorganization of the PCL and clusters of PCs at the base of the folds in mutant. (c) Mutant cerebella have a reduced number of Purkinje cells per section. (d) Mutant cerebella have a higher density of Purkinje cells. (e) P15 *Ta3* mutant Purkinje cells have a disorganised dendritic arborisation. Boxed region in (e) is of the trace image seen in (f) illustrating the total dendrite length and primary dendrite length. (g) Mutant Purkinje cells have a reduced total dendrite length and (h) lower primary dendrite length, data transformed (log10) to equalise sample variance. PCL- Purkinje cell layer; CalB- calbindin; PDL-primary dendrite length; TDL-total dendrite length. Error bars; (c,d) s.e.m. (n=3). *** P<0.001, * P<0.05 (two tailed Student's t test). (g,h) s.e.m. (data from 30 PCs from single mouse). Scale bar, 500 µm (a,b), 50 µm (e).

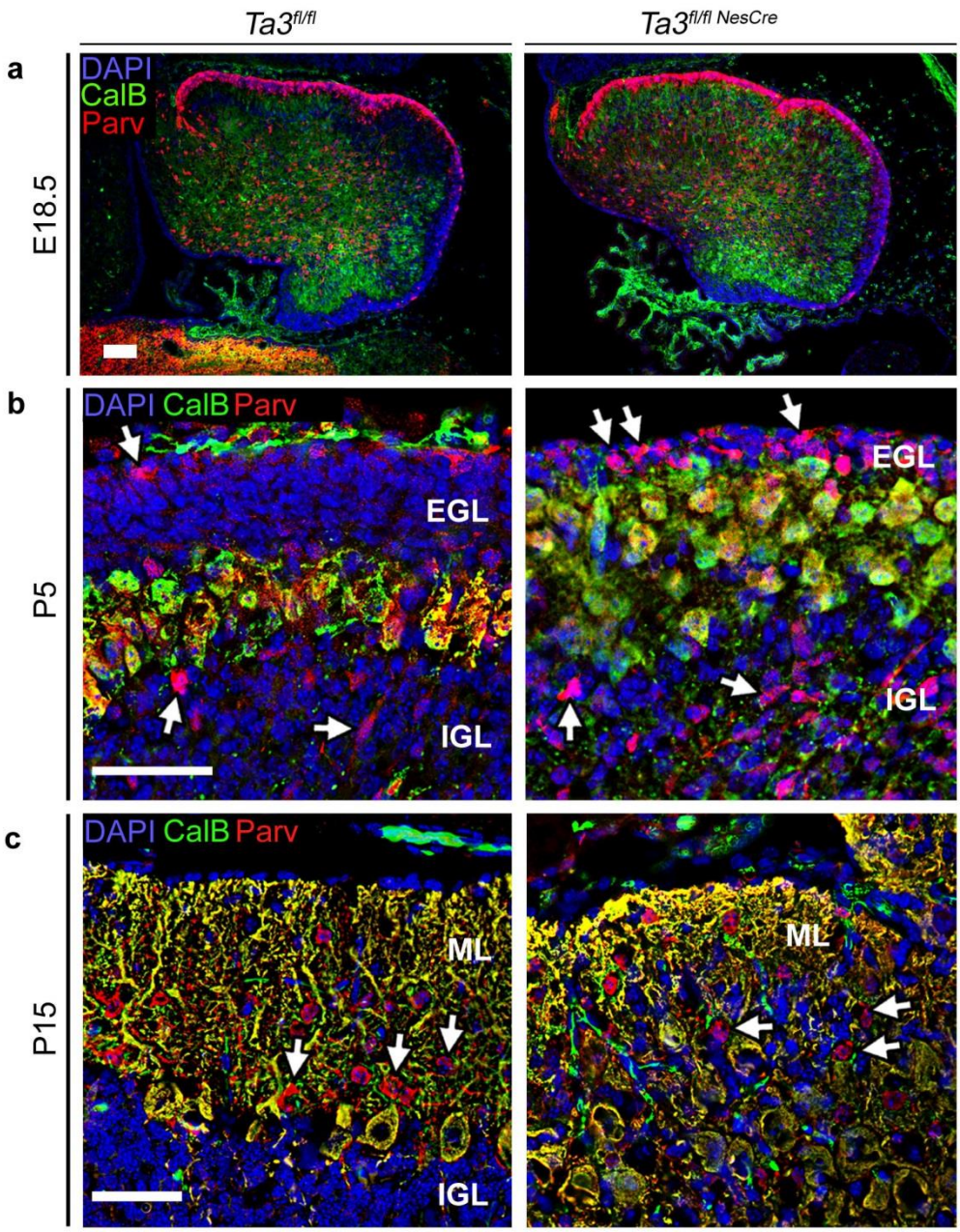

Figure 4.14 *Ta3* mutant interneurons have comparable distribution to control

(a) E18 cerebella labelled for Parvalbumin (red) and Calbindin (green). (b) P5 cerebella immunohistochemically labelled for Calbindin d-28k (green) and Parvalbumin (red). Region showing mutant with increased interneurons present in IGL and large cluster of Purkinje cells filling the ML. (c) P15 cerebella labelled for Calbindin d-28k (green) and Parvalbumin (red). Mutants exhibit a similar number of interneurons but they are misplaced. Arrows indicate Calbindin-negative Parvalbumin-positive interneurons. Scale bars, 100 µm (a), 50 µm (b,c)

4.2.7 Effects of *Ta3* loss on cerebellar circuits

Since aberrations were observed in both GNP proliferation as well as a disorganization of the ML and IGL, together with abnormal organization of the Purkinje cells and their dendrites, we investigated if there were defects in formation of cerebellar circuits. We visualized the different subsets of nerve terminals on the dendrites of Purkinje cells by immunostaining with antibodies directed against distinct nerve terminal associated proteins. Excitatory synapses formed by the climbing fibres and granule cell parallel fibres were labelled with antibodies against vesicular glutamate transporter 1 (VGluT1) (Fremeau et al., 2001). We labelled inhibitory terminals with antibodies against glutamic acid decarboxylase (GAD 65/67), the enzyme responsible for GABA synthesis which identifies presynaptic inhibitory terminals originating from stellate and basket interneurons. In both control and *Ta3* mutant Purkinje cells, GAD65/67 synapses were present throughout the dendritic arbor (Fig 4.15a,b). In the *Ta3* mutant cerebellum, the overall density and distribution of synapses was comparable to control which would reflect the relatively normal distribution of interneurons seen with parvalbumin staining.

In the control cerebellum, the excitatory synapses were clustered at the primary dendrites of the Purkinje cells. However, in the *Ta3* mutant cerebellum, this clustering was disrupted and staining for the synapses was seen throughout the dendritic arborisation extending into the entire ML (Fig 4.15c,d). These staining patterns suggest that the cerebellar circuitry is significantly disrupted in the *Ta3* mutant mice and this is not surprising given the abnormalities in the Purkinje cells and granule cells.

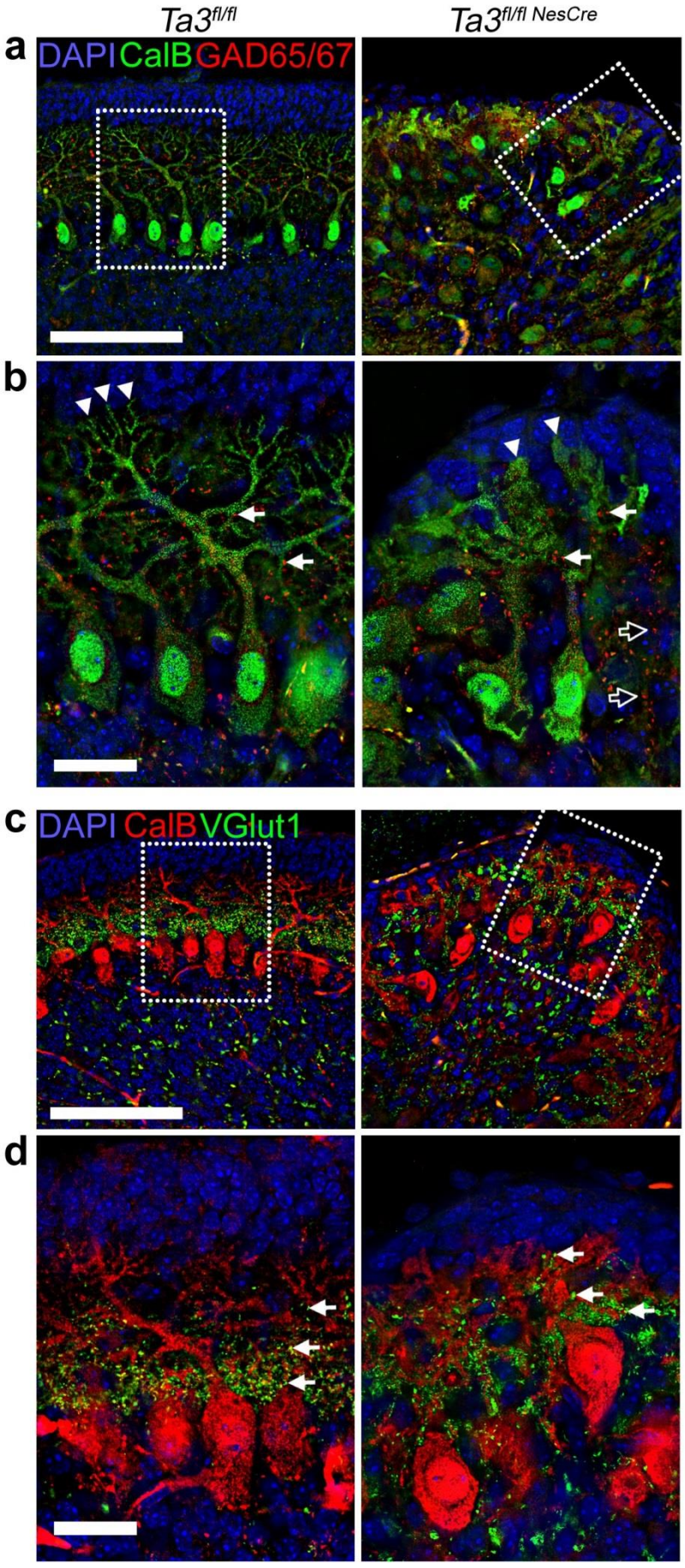

Figure 4.15 *Ta3* mutant PCs form inhibitory and excitatory synapses which are disorganized. (a-b) GAD65/67 synapses; P10 mutant PCs show GAD65/67 positive inhibitory synapses throughout the PC dendritic arborisation which are mostly normal. Box indicates (b) region of higher magnification. (c-d) VGlut1 synapses; P10 mutant PCs exhibit VGlut1 positive excitatory synapses which are abnormal. Staining in control cerebella is clustered at the primary dendrite region contacted by the parallel fibres from the granule cells, but in the mutant cerebella the excitatory synapses extend throughout the dendritic arborisation. Box indicates (d) region of higher magnification. CalB-calbindin; GAD-glutamic acid decarboxylase; VGlut1-vesicular glutamate transporter1. Scale bar, 100 µm (a,c), 25 µm (b,d). White arrow heads-dendritic spines; white arrows-indicate synapses; Outlined black arrows – indicate abnormally placed synapses.

4.2.8 Loss of *Ta3* predominantly affects Shh signalling

Primary cilia are known to be essential for Hedgehog signalling (Chizhikov et al., 2007, Spassky et al., 2008) and it has been shown by Aguilar et al that levels of *GLI 1* and *PTC 1* mRNA are significantly reduced in most cases of JS (Aguilar et al., 2012). We assessed the effects of loss of *Ta3* and cilia on Shh pathway components in the cerebella of P15 *Ta3* mutant mice and compared this with control animals. The levels of *Gli1*, *Gli3* and *Ptc1* mRNA were all significantly reduced in *Ta3* mutant mice (Fig 4.16a). The expression of *Gli1* and *Ptc1* are excellent indicators of Shh activity as their expression is known to be directly regulated by it.

In addition to the reduced mRNA levels of *Gli1* in mutant mice, immunostaining also showed a reduced level of Gli1 immunoreactivity and disorganised distribution (Fig 4.17a-c). In P15 control mice discrete puncta were observed around the PCL, consistent with previously described Lac-Z reporter expression (Corrales et al., 2006). In mutant mice there were fewer Gli1-positive cells which were harder to identify and more disorganised, consistent with the loss of *Gli1* mRNA expression and disruption in the PCL (Fig 4.17a-c).

The expression levels of components of the Notch signalling pathways (*Notch1, 2, Delta-like1, 3*) and Notch-responsive genes (*Hes1, Hes5*) were also investigated (Fig 4.16b). No significant differences were observed in any of the components (Fig 4.16b). The Wnt signalling pathway is suggested to have a role in cerebellar development. Since we see significant aberrations in cerebellar patterning, we analysed the expression of *Wnt3a* and the Wnt-responsive gene *Axin2* but found no significant change in expression (Fig 4.16c). However, we did see a considerable reduction in the expression of *Wnt7a* (Fig 4.16c).

To further assess the defect in Shh signalling, processing of both Gli2 and Gli3 proteins were analysed by Western blot (Fig 4.18a,b). Analysis of Gli2 protein detected two high molecular weight bands at 179kDa and 169kDa and a lower protein at 89kDa which correspond to Gli2A and Gli2R respectively. Mutant mice showed a consistent reduction in Gli2A bands and a slight reduction in Gli2R, consistent with the reduced mRNA expression (Fig 4.18a). The level of Gli2A appeared more affected than Gli2R showing a relative decrease in ratio of Gli2A:Gli2R, this indicated that the Gli processing could be affected.

Analysis of Gli3 protein showed similar results; in all control mice a faint band was observed at 185kDa and one at 93kDa corresponding to Gli3A and Gli3R respectively. A non-specific band was also seen at 142kDa which is consistent with previous studies using the

antibody (Yu et al., 2011). The level of Gli3A was low in mice of both genotypes, however, in the cerebella of mutant mice there was a noticeable increase in the level of Gli3R (Fig 4.18b). This resulted in a relative decrease in the ratio of Gli3A:Gli3R (Fig 4.16b). These analyses demonstrate the deregulation of Shh signal transduction consistent with the findings of Aguilar and colleagues in JS patients.

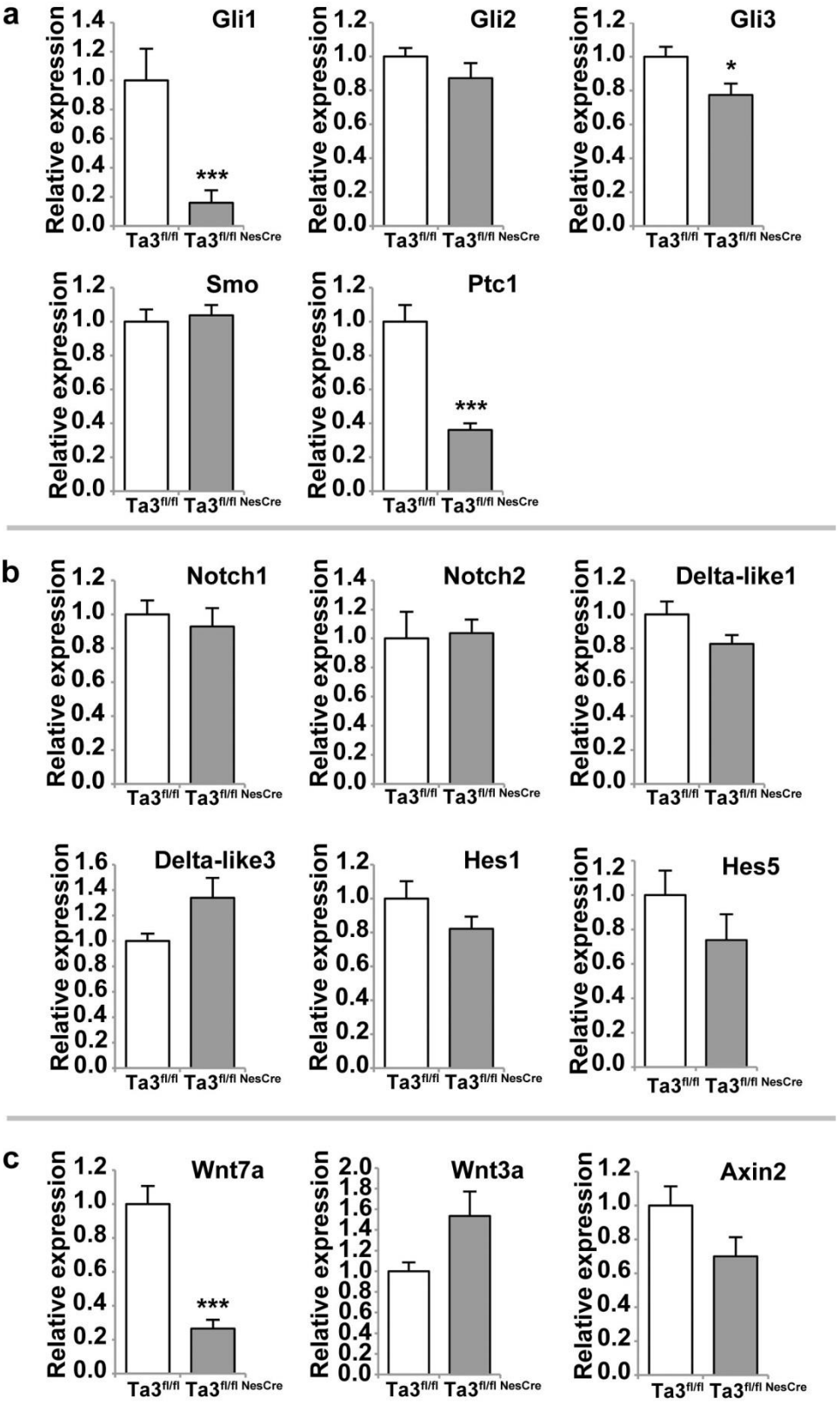

Figure 4.16 Sonic hedgehog and Wnt7a signalling are reduced in the *Ta3* mutant cerebella. qPCR of key (a) Shh, (b) Notch and (c) Wnt pathway components in the cerebella of control and mutant mice. (a) *Gli1, Gli2, Gli3, Ptc*, *Smo* relative mRNA expression. Mutants exhibit a significant reduction in expression of *Gli1, Gli3* and *Ptc1*. (b) *Notch1*, *Noch2*, *Delta-like1*, *Delta-like3*, *Hes1*, *Hes5* relative mRNA expression. (c) *Wnt7a*, *Wnt3a*, *Axin2* relative mRNA expression. Mutants exhibit a significant reduction in expression of *Wnt7a*. Expression levels were calculated relative to *Gapdh* expression. All data were acquired from 4 mice except mutant Hes5 and Wnt3a which was acquired from 3 mice. Error bars; (a-c) s.e.m. (n=4 or 3).

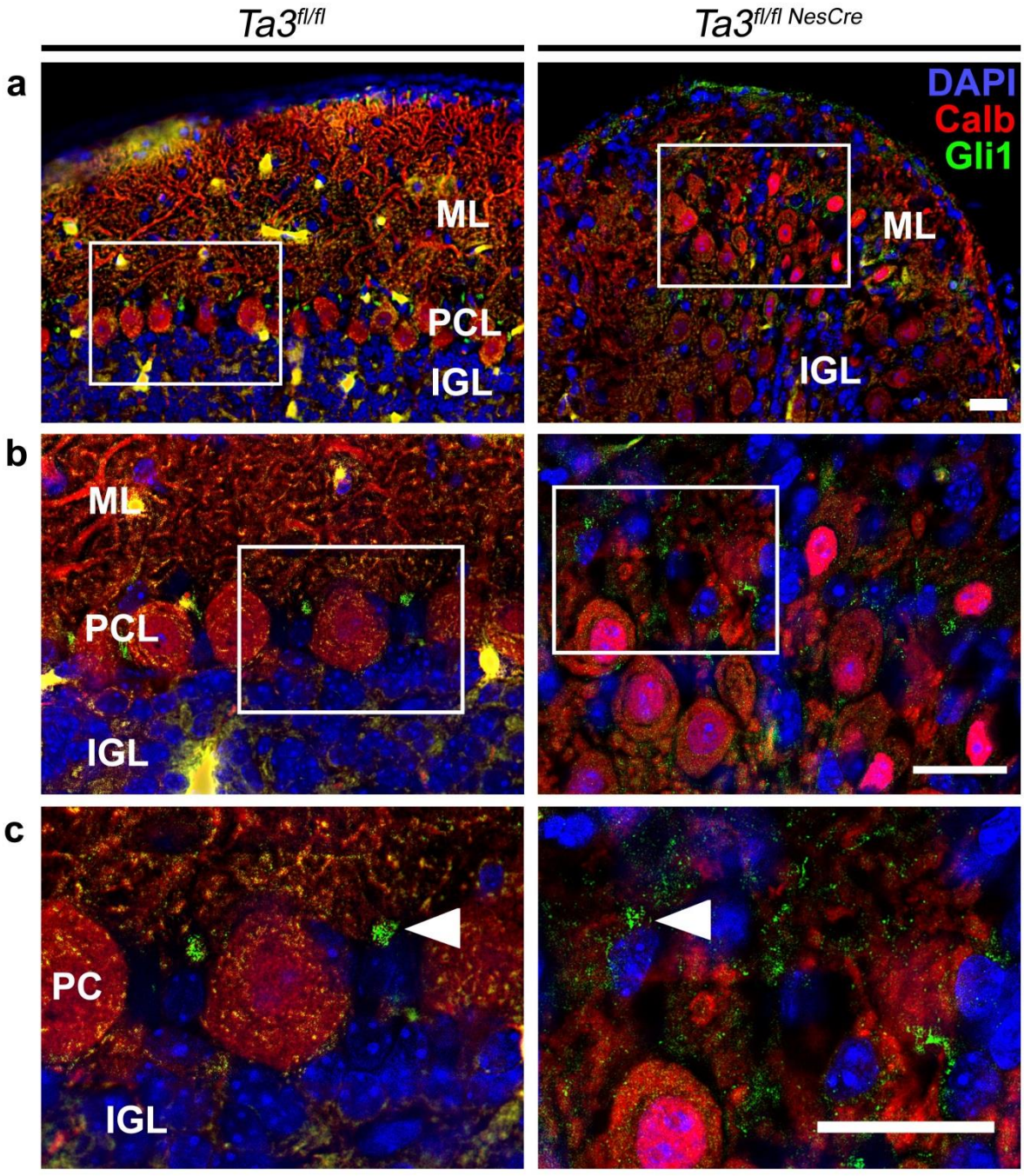

Figure 4.17 *Ta3* Mutant mice have reduced Gli1 expression.

P15 cerebella stained for Gli1 (green) and Calbindin (red). Ta3$^{fl/fl}$ mice show numerous Gli1 puncta in cells adjacent to Purkinje cells (indicated by white arrow). Mutant mice do have cells with Gli1 puncta but they are reduced in number and their distribution is disorganised consistent with the disrupted PCL. Boxed regions in (a) and (b) indicate regions of higher magnification shown in (b) and (c) respectively. Bright yellow fluorescence represents autofluorescence. Scale bars, 25 µm (a-c).

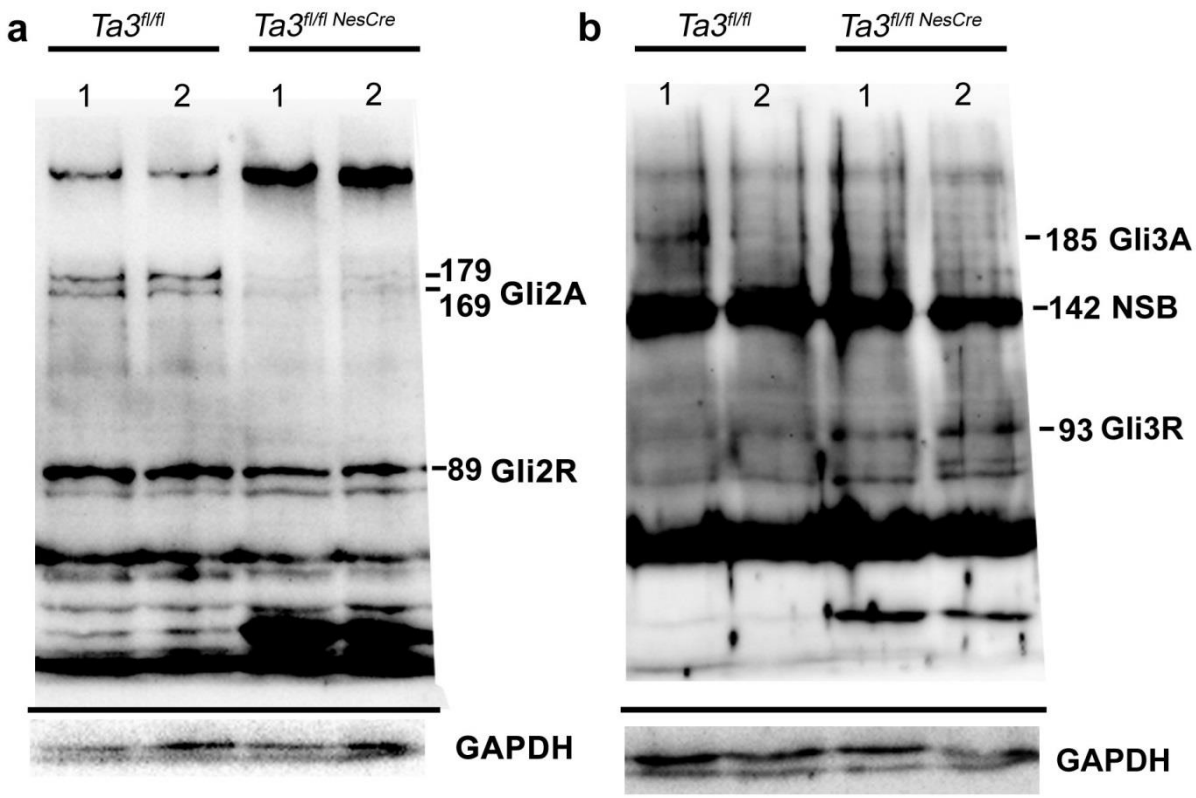

Figure 4.18 *Ta3* Mutant mice have defective Gli2 and Gli3 processing in the cerebellum.
Western blot using total protein extracted from P15 cerebella. Two mice were used for control and mutant (indicated by 1, 2). (a) Identification of mutant Gli2 shows a loss of two high molecular weight bands (179 and 169 kDa) corresponding to Gli2a. Mutants also show a slight reduction 89 kDa band thought to be Gli2R. (b) Identification of Gli3 shows a very faint band in one control sample (185 kDa) corresponding to Gli3a. This is barely detectable in the other control or mutant mice. Mutant mice show an increased in 93 kDa band corresponding to Gli3R. Non-specific band seen at 142kDa is consistent with previously published literature. Gapdh loading control is seen with fainter band below corresponding to migrating dye front.

4.2.9 A clinical case of Joubert syndrome with mutations in *TA3*

The results from this section were collected under the supervision of and using primers designed by the author. Experimental procedures and analysis were completed by the undergraduate project student Fay Stafford (University of Bath).

The phenotype of the *Ta3* mutant mice described throughout the project so far was found to be very reminiscent of the neural phenotypes present in human ciliopathies and in particular JS/MKS. Through clinical collaboration with Dr Andrea H Németh we were able to gain access to genetic material acquired from clinical cases of JS which had no identified genetic cause, so-called 'gene negative' cases. These cases had first been screened using targeted capture and next generation sequencing of all the 27 known known Joubert associated genes (Appendix 3, Supplementary table 3.1) but were unsuccessful in identifying a causative mutation.

To investigate whether defects in *TA3* may be a causative allele, primer pairs were designed to amplify products spanning the whole exon and approximately 150 bases into the flanking introns. Genomic DNA from four gene negative patients was then used as a template for high fidelity PCR reactions which were then analysed using Sanger sequencing. Initially, reactions amplifying the first 12 exons were completed and sequencing of the remaining exons is currently in progress.

Sequence analysis revealed that one patient had compound heterozygous mutations in *Ta3* (Fig 4.19a). This patient has several of the core clinical features of JS including ataxia, developmental delay and the molar tooth sign on axial brain MRI (Fig 4.19b, Table 4.1). One of the mutations we identified is a 1 bp deletion in exon 5 which creates a frameshift starting at codon Arg143 (Fig 4.19c). The new reading frame is predicted to result in a stop codon three positions downstream and since this mutation is located within the first third of the gene it is likely that this truncated transcript will be targeted for nonsense mediated decay. However, if the truncated transcripts are translated, the protein products of the major transcripts from the *TA3* locus will lack the coiled coil domains (aa182-223 and aa 467–501) as well as the region spanning aa 467 – 554 predicted to be required for centrosomal localization (UniProt, Appendix 3, Supplementary Fig 3.1). Some of these residues are contained within the conserved exon 12. Exons 11 and 12 are essential for the

function of Ta3 as seen from our conditional knockout mice as well as from earlier reports (Yin et al., 2009, Bangs et al., 2011).

The other identified mutation is a splice site substitution in intron 10 which affects the canonical 5' splice acceptor site of exon 11 (Fig 4.19d). The consequence of this change is predicted to be the skipping of the conserved exon 11. Sequencing of *TA3* exons 5 and 11 in the parents of the affected individual shows that they are heterozygotes with the father carrying the exon 5 frame shift mutation and the mother with 5'splice site variant affecting exon 11 (Fig 4.19e,f). This confirms that the heterozygous mutations in the JS subject are *in trans* and both alleles are affected.

Table 4.1 Summary of the clinical features of JS patient with mutations in *TA3*

Genetic features	
Consanguinity	-
Neurological features	
Hypotonia	+
Ataxia	+
Psychomotor delay	+
Intellectual disability	+
Breathing abnormalities	-
Seizures	-
Macrocephaly	Relative (Height 2-9th centile; Weight 25th Centile; OFC 75th centile)
Ophthalmic features	
Retinopathy	-
Coloboma	-
Oculomotor apraxia	+
Nystagmus	-
Other	Duanes syndrome (inability to abduct the eyes with retraction of eyeball); Hypermetropic astigmatism
Other clinical features	
Polydactyly	-
Renal	- no evidence of cysts
Hepatic	-
Obesity	-
Cranial MRI findings	
Molar Tooth Sign	+
Cerebellar vermis dysgenesis	-
Hypoplasia of brainstem	-

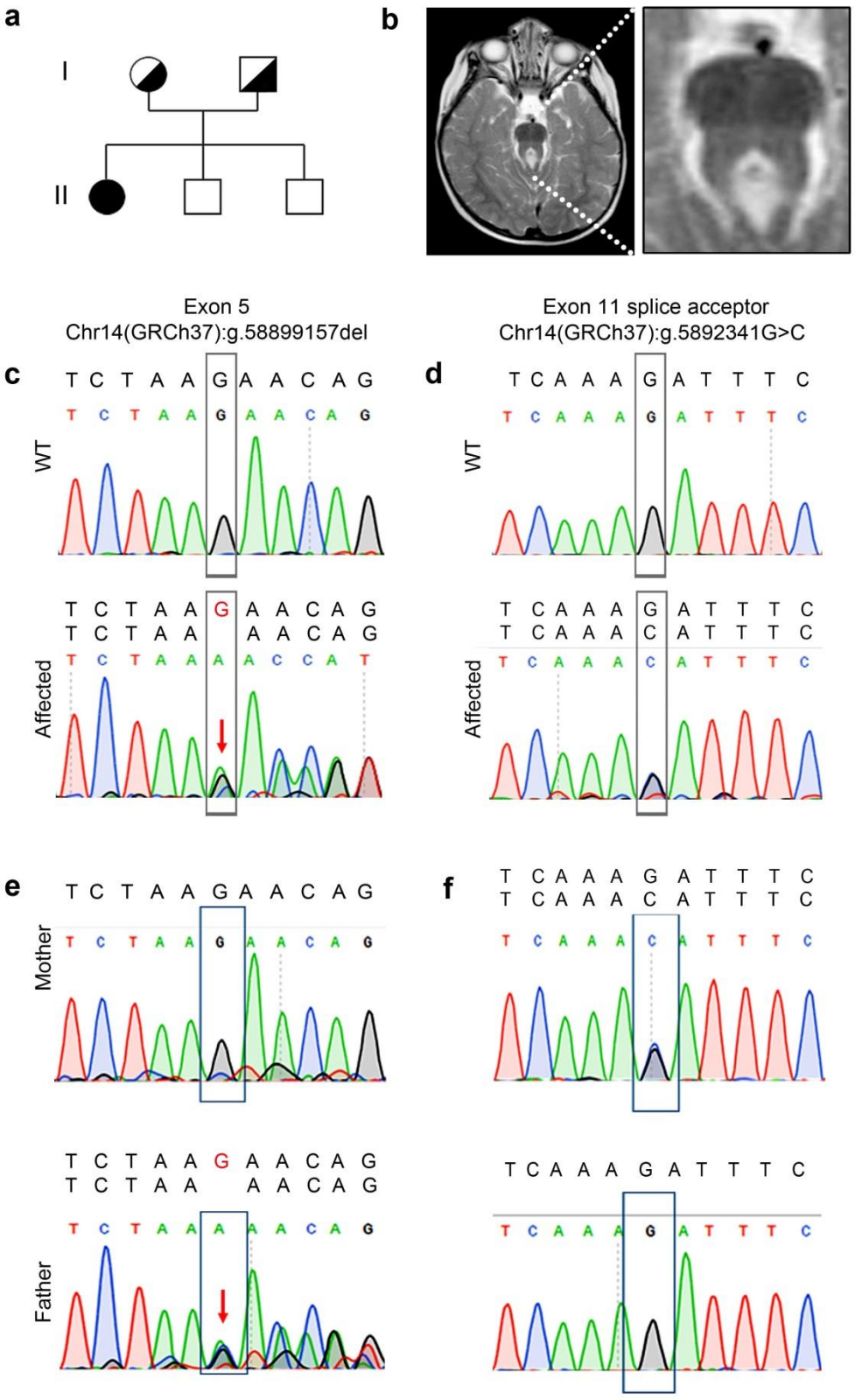

Figure 4.19 Mutations in *TALPID3* in Joubert syndrome

(Note: experiments, sequence analysis and figure preparation were supervised by the author but completed by undergraduate project student Fay Stafford). (a) Pedigree showing the parent carriers and one affected individual (b) Axial MRI of brain of affected individual showing the 'Molar Tooth Syndrome' (c) Sequence trace of control and affected exon 5 with the one bp deletion in the affected. Red arrow indicates the position of the frameshift mutation (d) Sequence trace of control and affected exon 11 and flanking intron 10 showing splice site mutation in intron 11 of affected (e) Sequence trace of exon 5 of parents showing the single base pair deletion. The red arrow shows the position of the frameshift mutation (f) Sequence trace of exon11 with flanking intron 10 of mother with splice site mutation in intron 10 but no mutation in exon 5.

4.3 Discussion

The cerebellar defect is one of the most striking developmental phenotypes of the *Ta3* mutant mice. They have a hypoplastic cerebellum with a loss of granule neurons resulting from their reduced proliferation and survival. The granule neurons also show altered orientation and defective, often incomplete, migration with mature neurons found in the ML. These migration defects coincide with an aberrant scaffold formed by the Bergmann glia. Purkinje cells also show a severely disrupted organisation with malformed dendrites which clearly caused misplacement of synaptic termini. The mechanistic cause was shown to be the result of loss of primary cilia and the Shh pathway was shown to be severely disrupted in mutant mice. Combined with data from Chapter 3, the *Ta3* mutant mice show phenotypes very similar to those present in clinical ciliopathies. Here, through collaboration with clinical investigators we demonstrate the presence of genetic mutations in *TA3* in a human case of JS.

Given that neurological defects are seen in human ciliopathies, until recently there have been only a small number of studies in mice looking at the role of primary cilia and cilia components in the cerebellum. The basal body component, *Stumpy*, has been shown to have gross cerebellar defects following conditional deletion using the *NesCre* deleter. The *Stumpy* mutant cerebellum appeared largely comparable to the *Ta3* mutant however the description of the phenotype was limited and focused mainly on the hippocampus (Breunig et al., 2008). Analysis of the Ta3-binding protein Cep120 has also been investigated following conditional loss in the CNS but again the level of detail describing the cerebellar phenotype was limited (Wu et al., 2014). Loss of Cep120 using the *NesCre* deleter ($Cep120^{fl/-;NesCre}$) resulted in hypoplasia caused by reduced proliferation. They showed no difference in apoptosis using the TUNEL assay which is in contrast to the *Ta3* mutant phenotype. Interestingly, Wu and colleagues also suggest that the defect is caused by loss of primary cilia in addition to a reduction in centriole duplication preventing normal cell division. This is in contrast to the *Ta3* mutant phenotype which has not been shown to affect centriole duplication or progression through the cell cycle (Yin et al., 2009, Bangs et al., 2011)(unpublished observations).

The IFT proteins Kif3a and IFT88 have been shown to be important for GNP proliferation, organisation of the PCL and correct development of the Bergmann glia (Spassky et al., 2008, Chizhikov et al., 2007). In conditional *Kif3a* mutants using the *human GFAP-Cre* deleter (*Kif3a*$^{fl/-;hGFAP}$), the proliferative defects were absent at E16.5 and began at E18.5 coinciding with the beginning of *Shh* expression in this region (Spassky et al., 2008). E16.5 *Ta3* mutant mice were not investigated in the current study. Unlike the postnatal stages, the E18.5 *Ta3* mutant cerebella were somewhat similar to control. Despite showing a thinner EGL with reduced proliferation and foliation, the mutant GNPs were still present in the correct location suggesting their migration from the rhombic lip was not dramatically affected. In addition, the EGL parvalbumin staining in the rostral folds was comparable between control and mutant. We believe that the E18.5 *Ta3* mutant phenotype represents the very early stages of the cerebellar defect, consistent with other primary cilia mutants.

Spassky and colleagues demonstrated that cultured granule neurons and brain slices with loss of *Kif3a* were unable to exhibit a proliferative response to ectopic Shh (Spassky et al., 2008). In the same study, conditional mutation of *Smo* (*Smo*$^{fl/fl;hGFAPCre}$) resulted in a more severe foliation phenotype than loss of *Kif3a* when using the same *hGFAP-Cre* deleter. The authors attribute the milder phenotype in the *Kif3a* mutants to a reduction in the level of Gli3R. This theory was supported by an earlier study showing that heterozygous loss of *Gli3* was able to partially rescue the cerebellar phenotype seen in *Smo* mutants (Blaess et al., 2006). Importantly, double-mutants with loss of *Kif3a* and *Smo* exhibited the milder foliation defect demonstrating that primary cilia are upstream of Smo when regulating Gli processing (Spassky et al., 2008).

The severity of the conditional *Smo* mutant described by Spassky and colleagues (*Smo*$^{fl/fl;hGFAPCre}$) also appeared more severe than the *Ta3* mutant cerebellum (Spassky et al., 2008). In studies targeting *Smo* using the same *NesCre* deleter (*Smo*$^{fl/fl;NesCre}$), E18.5 *Smo* mutant mice also appeared to have a more severe foliation defect compared to E18.5 *Ta3* mutant mice (Blaess et al., 2006). When trying to explain this defect the results seen in *Ta3* mutant mice do show defects in the processing of Gli2 and Gli3 however, in contrast to *Kif3a* mutants, an apparent increase in Gli3R is observed compared to control. This does not explain why *Ta3* mutants would exhibit a phenotype of reduced severity compared to *Smo* mutants, it is also in contrast to the *Kif3a* mutant cerebellum. One important consideration is that protein levels were analysed at P15 which is towards the latter stages of cerebellar

development and as such Gli protein levels were harder to detect. Analysis of P5 tissue would strengthen the current finding and provide a greater understanding of Gli processing in *Ta3* mutant cerebella.

At later postnatal stages *Ta3* mutant mice showed the greatest foliation in medial regions and severe defects in lateral regions; this effect was also illustrated in horizontal sections presented in Chapter 3 (Fig 3.4 & 3.5). In lateral regions of mutant cerebellum it was often difficult to accurately identify folds and the curvature of the brain made it difficult to demonstrate consistent cellular phenotypes. For this reason, analysis focused on the medial phenotype. Interestingly, postnatal stages of $Smo^{fl/fl;NesCre}$ mutant mice showed the same medio-lateral effect (Corrales et al., 2006). They went on to show that areas of higher foliation correlated with unexpected regions of *Gli1* expression indicating incomplete or leaky recombination caused by the *NesCre* deleter. This possibility may account for some of the ciliated cells still present in the *Ta3* mutant cerebellum. In the current study, it was planned to assess the level of recombination in *Ta3* mutant mice using a LacZ/eGFP reporter strain (Z/EG) (Novak et al., 2000), however due to unforeseen circumstances the line was unavailable for use. Despite the possible mosaicism in the *NesCre* deleter, medial sections still showed a striking loss of primary cilia and a notable phenotype. Due to this medio-lateral effect comparison between *Smo* and *Ta3* mutant mice at postnatal stages was approached with caution with both showing an approximately comparable levels of severity (Corrales et al., 2006). The studies describing conditional loss of $Smo^{fl/fl;NesCre}$ predominantly focused on the gross cerebellar phenotype and the extent of foliation but the histological details are not discussed (Corrales et al., 2006, Blaess et al., 2006).

Earlier loss of Gli2 from the cerebellar primordia using the *En1Cre* deleter strain ($Gli2^{fl/zfd;En1Cre}$) resulted in a phenotype reminiscent of *Ta3* mutant mice albeit much less severe (Corrales et al., 2006). *Gli2* mutant mice have a reduced number of granule neurons causing a multi-layered PCL and a modest reduction in their dendritic branching. Although the soma of the Bergmann glia were correctly placed their fibres were also misshapen. The gross organisation of *Gli2* mutant mice was still similar to control and a well-defined laminar structure was still present. These phenotypes clearly resemble elements of the *Ta3* mutant further suggesting the lack of Shh signalling is likely to be a dominant factor. Sadly double mutants with loss of both *Gli1* and *Gli2* were made but the histology was not described in detail (Corrales et al., 2006).

Many of the gross and histological phenotypes seen in *Ta3* mutant cerebella reflect the loss of Shh signalling in the cerebellum. Here we demonstrate that *Ta3* mutant mice lack primary cilia, which are well known to facilitate the transduction of the Hh pathway. We show that mice have an overall reduction in the Shh response, as demonstrated by a reduction in the *Gli1* and *Ptc1* mRNA expression. Furthermore the levels of GliA and GliR are not comparable to control suggesting defects in Gli processing. Interestingly, reduced Shh and hypoplasia of the cerebellum is also a described in human ciliopathies including JS syndrome (Aguilar et al., 2012). However, when trying to model the disease in mice, the disruption of known proteins found in JS such as Cep290 and Ahi (Delous et al., 2007, Dixon-Salazar et al., 2004, Ferland et al., 2004, Lee et al., 2012, Sheng et al., 2008) show no defect in GNP proliferation or effects on Shh pathway components. In this respect the GNP defects seen in our *Ta3* conditional mutant mice is similar to that seen in JS/MKS (Aguilar et al., 2012).

Other signalling pathways have also been suggested to localise at primary cilia and include Wnt, Planar Cell polarity and Notch pathways in addition to tyrosine kinase, serotonin and somatostatin receptors (Goetz and Anderson, 2010) however their exact cilial roles are poorly understood and often controversial. To try and address this we analysed the expression of members of the signalling pathways and also known target genes to assess the overall pathway activation. Despite the importance of Wnt in early cerebellar development we saw no significant difference in *axin2* expression levels, a well-known negative regulator of Wnt signalling which is upregulated on canonical pathway activation (Jho et al., 2002).

The role of primary cilia in Wnt signalling is still under debate but many studies that support an interaction between the two suggest that loss of primary cilia results in potentiated Wnt responsiveness (Corbit et al., 2005, Gerdes et al., 2009). The adenomatous polyposis coli (APC) protein is part of a complex which degrades β-catenin. Loss of APC or Ctnnb1 are both able to cause elevated canonical Wnt response and targeting them using the *Math1-Cre* caused a granule cell phenotype not unlike the *Ta3* mutant (Lorenz et al., 2011). *APC* mutant mice had a smaller cerebellum which was attributed to an increased level of differentiation at the expense of proliferation. Clusters of ectopic granule neurons were present in the ML and the PCL was also disrupted. In the *APC* mutant mice they

demonstrate an upregulation of *Axin2* mRNA expression at P7. In *Ta3* mutant cerebellum expression of *Axin2* mRNA was analysed at P15 and if anything a slight reduction was observed suggesting that canonical Wnt signalling was not affected. Given the similarities between the two phenotypes, further investigation at earlier developmental stages will prove interesting to see whether other signalling defects are present earlier in the *Ta3* mutant cerebellar development.

Interestingly, a reduction in Wnt7a expression was observed in mutant cerebella. This signalling molecule is implicated in granule cell development and has been shown to be expressed postnatally in the IGL (Lucas and Salinas, 1997). Through *in vitro* cultures, it has also been shown to be important for axonal spreading and branching. We speculate that the *Wnt7a* defect seen in the mutant cerebellum reflects the maturation and migration defects seen in the granule neurons. Whether it is a cause or effect of the *Ta3* mutant phenotype remains to be seen but a plausible explanation is that the loss of granule neurons results in a lower proportion of cells expressing *Wnt7a*. This hypothesis could be supported by assessing the expression of other granule cell specific genes such as *Math1* (BenArie et al., 1997). Better still, experiments utilising sorted cell populations would provide valuable data as to the regulation of signalling pathways in different cell types.

Cerebellar granule cells are an excellent cell type to study migration as they first migrate tangentially followed by radially into their final position in the IGL. One notable defect in the Ta3 mice was the altered orientation of EGL nuclei to a predominantly tangential direction. Live imaging studies have described how postmitotic cells in the deeper region of the EGL become bipolar and spindle shaped extending horizontal processes in the tangential direction (Komuro et al., 2001). They then round up, extending a third process into the ML and migrate in the radial orientation. This normal process of granule migration appears completely disrupted in the *Ta3* mutant cerebellum. At both P5 and P10 mutant granule neurons had a predominantly tangential orientation in the EGL. This correlated with greater incidence of tangentially orientated fibres from Bergman glia. Despite this, many mature granule neurons did still reach their final position in the IGL. The obvious loss of parallel fibres is also strikingly apparent in the *Ta3* mutant cerebellum. It is unclear whether the loss of parallel fibres is solely down to the reduction in granule cell number or whether their extension of tangential fibres is also affected. To better study the migration of granule

neurons *in vivo* birth dating studies using BrdU could be used to track their progress. The use of slice cultures would also allow live cell imaging to monitor their migrational behaviour.

The *Ta3* mutant cerebellum exhibited a disorganised and multi layered PCL which in *Ta3* control mice was present as a single monolayer. A similar multi-layered phenotype was described following conditional loss of *IFT88* and *Kif3a* using either *NesCre* or *hGFAP-Cre* deleter strains (Chizhikov et al., 2007). Importantly, use of the *hGFAP-Cre* line has previously been reported to lack excision in Purkinje cells (Zhuo et al., 2001), but the evidence presented for this is limited. The multi-layered Purkinje cell phenotype was seen in mutants using either *NesCre* or *hGFAP-Cre* strains and the authors argue that disruption of the Purkinje boundary is secondary to the granule cell deficit rather than the loss of primary cilia directly affecting the Purkinje cells.

The idea that Purkinje cell development can be disrupted by granule proliferation alone is supported by recent data describing the cerebellar phenotype following compound loss of *CyclinA1* and *CyclinA2* using the *NesCre* deleter (*CyclinA1*$^{-/-}$*::CyclinA2*$^{fl/fl;NesCre}$) (Otero et al., 2014). The mutation prevented cell cycle progression through G2 ultimately resulting in a loss of proliferation. The mutants have an understandable loss of EGL proliferation and foliation but this also resulted in lamination defects with aberrant Purkinje dendrites. Importantly they also target *CyclinA2* and *N-myc* using the *Math1-Cre* deleter, which is specific to granule neurons. In areas where recombination had occurred, defects in lamination and Purkinje dendrites were still evident. This strongly suggested that proliferation of granule neurons alone has a role regulating the correct laminar organisation and Purkinje cell maturation. This is concept is supported further in mice with constitutive loss of *CyclinD1* (Pogoriler et al., 2006) and *CyclinD2* (Huard et al., 1999). These mice show very mild phenotypes in comparison but differences were still observed in the Purkinje dendrite organisation and histogenesis.

The dependence of Purkinje cell position on granule neuron proliferation can perhaps be explained by the malformed boundary between the IGL and ML. It is also possible that their disrupted cell shape is due to aberrant migration of precursors through the ML. Synaptic contact with granule neurons has been shown to be a key mechanism regulating the dendritic maturation of Purkinje cells *in vitro* (Baptista et al., 1994). *Ta3*

mutant mice had a striking disorganisation of glutamatergic synapses but still relatively high numbers were evident. A contributing factor to the *Ta3* mutant Purkinje cell defects could be the disruption of synaptic contacts. It would be fascinating to better investigate the synaptic contacts made in the mutant cerebellum and assess whether their distribution or even their functional activity has an effect on the Purkinje cell formation. Further studies utilising electron microscopy and electrophysiology would be invaluable in assessing the synaptic contribution to the phenotype.

When considering the role of Ta3 in Purkinje cells, dysfunction of primary cilia has also been shown to result in disruption of dendrite outgrowth. In cell cultures mutant cortical neurons were shown to have smaller dendritic arbors which were much less complex than control (Guadiana et al., 2013). Loss of primary cilia *in vivo* has also been shown to affect dendritic outgrowth and synapse formation (Kumamoto et al., 2012). Furthermore primary cilia have been shown to share a number of structural similarities with dendritic spines (Nechipurenko et al., 2013) but the contribution of cilial proteins has yet to be investigated. Although the loss of granule proliferation in *Ta3* mutant cerebella is likely to contribute to the Purkinje cell phenotype, it is tempting to speculate that loss of primary cilia may also play a contributory role.

Further studies which utilise different cell specific *Cre* deleters will be important in dissecting the cellular requirement of primary cilia in the developing cerebellum. The ability to target *Ta3* in the primary cell types will help to separate the complex phenotype described here. In addition *in vitro* cell culture will play an important role in dissecting the molecular phenotype. In particular, it will be fascinating to study the behaviour of Purkinje cells, Bergmann glia and GNPs in culture and establish whether their malformation in the *Ta3* mutant cerebellum is context dependent or an intrinsic cellular defect.

Considering the description of *Ta3* mutant mice throughout chapters 3 and 4, mice exhibit a number of the neurological hallmarks of JS including ataxia, a hypoplastic cerebellum, reduced vermis and abnormal decussation of the scps. We identified a human JS patient with compound heterozygous mutations confirming that mutations in *TA3* do indeed cause JS. The two mutations appear very distinct; the frame shift in exon 5 causes a premature stop codon and is likely to result in nonsense mediated decay whereas the mutation in the splice site is likely to cause the skipping of exon 11. It is therefore possible

that the latter mutation could retain some functional activity of TA3. This would provide an explanation as to why the patient didn't exhibit other JS traits such as polydactyly.

Hypomorphic alleles for *CC2D2A* and *TMEM67* have been reported in cases of JS but often mutations with complete loss of function are found in MKS (Szymanska et al., 2014). Constitutive loss of *Ta3* in mice has previously been shown to cause embryonic lethality (Bangs et al., 2011). This supports the idea that some functional protein may remain in the compound heterozygous *TA3* mutations found in JS. It is possible that clinical conditions with complete disruption of *TA3* may result in a more severe MKS-like phenotype and embryonic lethality.

At this early stage it is not possible to assess how common *TA3* mutations are in human JS. However, personal communication (M. Hurles and D. Fitzpatrick) suggests that other patients with JS do also have mutations in *TA3*. Currently only the first 12 exons of *TA3* have been analysed in the four 'gene negative' samples. It cannot be ruled out that the remaining 3 candidates do not have mutations in the C-terminal of *TA3* or even within intronic regions. Analysis of the remaining exons in addition to larger patient cohorts is currently in progress.

In summary, we have investigated the cerebellar phenotype of *Ta3* mutant mice which exhibit a hypoplastic cerebellum with a disorganised structure. Mice show reduced proliferation of GNPs which have increased apoptosis and aberrant migration. In addition, both Bergmann glia and Purkinje cells show defects in cell morphology. Loss of *Ta3* was demonstrated to cause a reduction of primary cilia and a concomitant disruption of Shh signalling. Finally, in combination with data from chapter 3, *Ta3* mutant mice display a number of characteristics consistent with human ciliopathies. Here we identify a human case of JS with compound heterozygous mutations in *TA3*; this places the *Ta3* mutant mice as a useful model to better understand the clinical condition.

Chapter 5 – Cortical phenotype of *Ta3*$^{fl/fl;NesCre}$ mice

5.1 Introduction

The cortex is an important brain structure which receives sensory input, controls motor output and has complex roles in perception, memory, thought and consciousness. The structure is derived from the embryonic dorsal telencephalon and forms a thick shell surrounding the left and right halves of the cerebrum. In higher mammals the cortex becomes highly folded to increase the surface area and allow increased functional capacity. In mice the adult cortex is divided into broad regions along the anterior-posterior axis with the three major regions being the motor, sensory and visual cortex. It is also separated along the dorsal-ventral axis into six layers with layer I being the outermost superficial layer and layer VI being the deepest inner layer. Underlying the cortex is the corpus callosum, a dense band of fibres which connect the left and right hemispheres. These fibres become myelinated between P11-P45 and become the largest white-matter structure in the brain (Sturrock, 1980).

The staggering diversity and complexity of cortical neurons can be simplified into two major cell types; projection neurons and interneurons. Projection neurons, also called pyramidal neurons, are glutamatergic, excitatory neurons which originate in the dorsal half of the telencephalon. They are born in the ventricular zone (VZ) from where they migrate radially to more basal layers. In the adult cortex there is a great diversity in projection neuron subtypes which are found in different cortical layers and project axons to various brain regions.

The projection neurons in deep layers make connections with other regions of the brain termed corticofugal projections. These can be divided into two types; those found predominantly in layers VI make connections with the thalamus (corticothalamic projection neurons) and those found predominantly in layer V which make connections with the tectum, pons and spinal cord (collectively termed subcerebral projection neurons) (Molyneaux et al., 2007). In superficial layers II/III are projection neurons which make connections with the basal ganglia (intracerebral) or other cortical layers (cortico-cortical projection neurons). A key pathway connecting the left and right cortical hemispheres sees tracts extend radially inwards where they join the corpus callosum and form a prominent

commissure to cross the midline and then extend radially to the contralateral hemisphere (callosal projection neurons). Many of these projection neurons can be identified by expression of transcription factors. The predominant projection neuron position and key identifying transcription factors are listed in figure 5.1.

During the development of the cortex, projection neurons originate from radial glial cell (RGC) progenitors present in the VZ. These are multipotent progenitors capable of forming all cortical projection neuron subtypes. From E10.5 the RGCs divide asymmetrically to maintain the RGC pool and produce new neurons which form the preplate layer (Angevine and Sidman, 1961). New neurons then migrate into the middle of the preplate layer forming a new cortical plate layer and separating the preplate into the outer marginal zone and the inner subplate. Successive rounds of newborn neurons continue to migrate from the VZ to the outer edge of the cortical plate to form new cortical layers. This causes the cortical plate to form in an inside-out manner (Marin-Padilla, 1978, Angevine and Sidman, 1961).

The earliest born neurons populate the deepest cortical layers and comprise corticofugal neurons (Greig et al., 2013). Corticothalamic projection neurons peak in birth around E12.5 and subcortical projection neurons at E13.5. Later born neurons occupy the more superficial layers and the birth of callosal projections peaks around E15.5. As the production of projection neurons continues, instead of directly producing new neurons, the asymmetric divisions of RGCs switch to produce intermediate progenitors which migrate into the subventricular zone (SVZ). These act as transit amplifying cells and undergo symmetric divisions to produce neurons which migrate to upper cortical layers (Leone et al., 2008). A summary of cortical projection neurons and their formation is illustrated in figure 5.1 (Molyneaux et al., 2007).

One of the key signalling pathways regulating the fate of cortical neurons is FGF signalling. During embryogenesis a gradient is established from the rostral midline and involves FGF8, FGF15, FGF17. This morphogen gradient helps to establish opposing gradients of transcription factors across the rostro-caudal axis which further regionalise into columns with distinct activity (Sansom and Livesey, 2009). The patterning of the neocortex is also influenced by Wnt and BMP signalling from the dorsal midline; this influences both rostro-caudal and medio-lateral patterning and there is increasing evidence to suggest that Wnt signalling also has an important role in laminar specification (Chenn, 2008). BMP

signalling is thought to repress FGF8, which subsequently constrains Wnt expression and the three are thought to establish the different regional identities (Shimogori et al., 2004). FGF, Wnt and Shh are also known to have important roles driving the proliferation of neocortical progenitors (Zhou et al., 2006, Dahmane et al., 2001). In addition, Shh has been shown to have a role in ensuring the correct fate and layer specification in cortical neurons (Wang et al 2011).

The other major cell types in the cortex are cortical interneurons. These are predominantly GABAergic inhibitory neurons and provide intricate complexity to the cortex. They exhibit a distinctly different origin and are born in the ventral half of the telencephalon in the medial ganglionic eminence (MGE) and lateral ganglionic eminence (LGE). They first follow a tangential migration to the dorsal pallium and then migrate radially through the layers to their final cortical position (Anderson et al., 1997). The tangentially migrating neurons from the MGE peak in birth between E12.5-E16.5 and primarily move through the intermediate zone (Anderson et al., 2001). Those from the LGE peak in birth later between E14.5-E16.5 and move through the SVZ. Tangential migration of interneurons also occurs through the marginal zone and subplate (Lavdas et al., 1999, Polleux et al., 2002). By the first postnatal week, interneurons disperse radially through the cortex to their final resting position (Hevner et al., 2004).

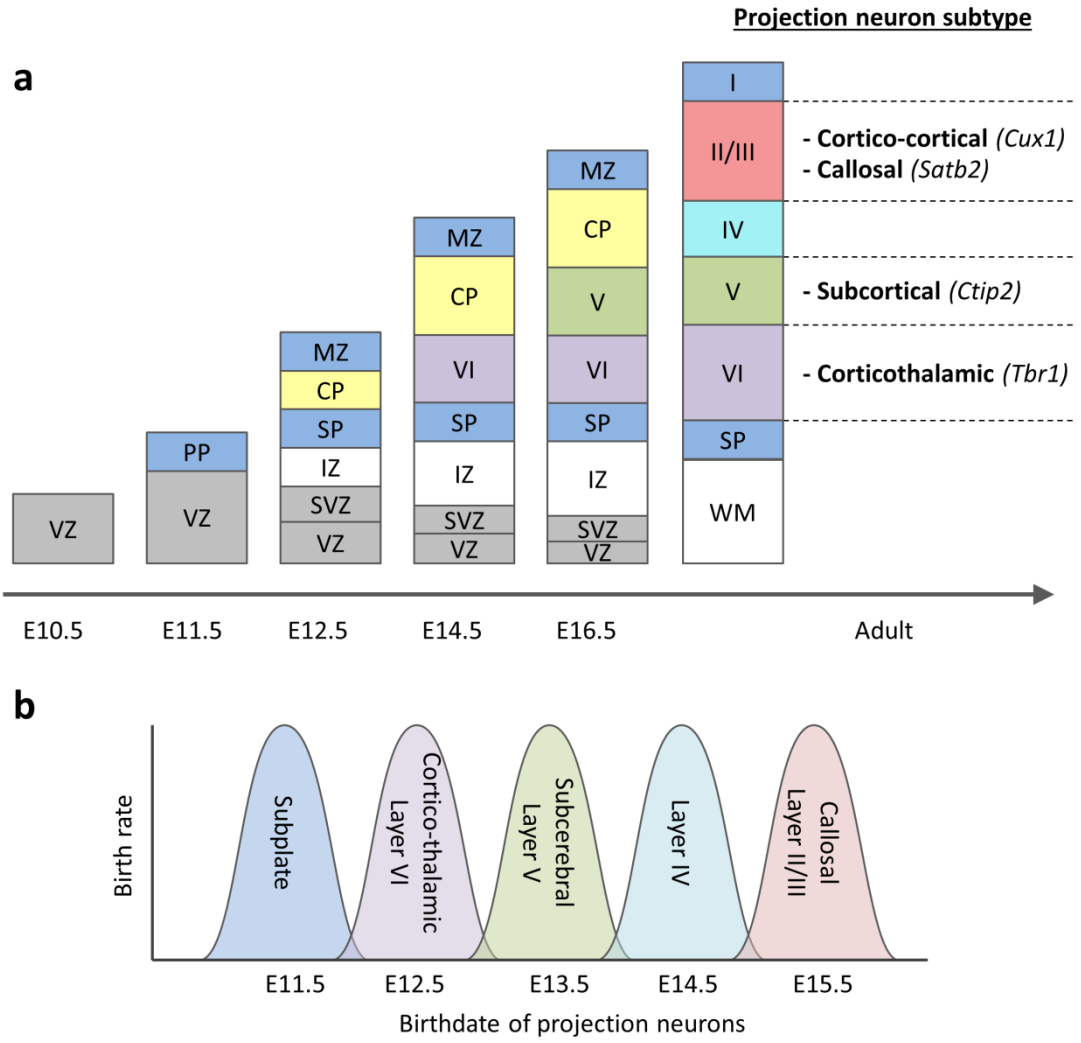

Figure 5.1 Summary of cortical layer development

(a) Stepwise formation of layers in the embryonic cortex. Preplate (PP) neurons are the first neurons produced. Cortical plate (CP) neurons divide the PP into the outer marginal zone (MZ) and inner subplate (SP). Corticothalamic neurons are the earliest born CP projection neurons and migrate to layer VI. These are followed by subcerebral neurons which migrate to layer V. Callosal projection neurons are the latest born and migrate to layers II/III. Cortical projection neurons can be identified by transcription factor expression (italic). (b) Projection neurons are produced throughout embryogenesis but peaks in neurogenesis occur in a sequential order. Simplified graph showing peaks in birthrates for projection neuron subtypes. SVZ, subventricular zone, VZ, ventricular zone, WM, white matter. Figure adapted from review by Molyneaux et al., 2007.

To date, relatively few studies have investigated the role of primary cilia in the later stages of cortical development. Mice with loss of primary cilia before E12.5 show severe dorso-ventral patterning defects (Besse et al., 2011, Bangs et al., 2011). Early disruption of primary cilia has also been shown to cause disruption of the tangentially migrating interneurons (Higginbotham et al., 2012, Baudoin et al., 2012). Mice with conditional loss of basal body component, *Stumpy*, describe a mild cortical phenotype with no notable defects (Breunig et al., 2008). In contrast, loss of ITF component, Kif3a, shows a dramatic increase in cortical size (Wilson et al., 2012). Considering the complexity of the developing cortex it is highly likely that primary cilia have a role in its development throughout development. Identifying the cortical phenotypes in $Ta3^{fl/fl;NesCre}$ mice will help to further our understanding into the role of primary cilia in later cortical development.

Here we present the cortical phenotypes of the $Ta3^{fl/fl;NesCre}$ mutant mice where, in early stages, they exhibit loss of cells in deep cortical layers. The phenotype increases in severity at postnatal stages with mice exhibiting a prominent loss of deep layer neurons which is distinct from compressive phenotypes resulting from the hydrocephaly. Cortices are further shown to have loss of primary cilia resulting in defective signalling through the Shh pathway.

5.2 Results

When assessing the *Ta3*$^{fl/fl;NesCre}$ phenotype major cortical defects were first identified in P15 mice. As described in Chapter 3, P15 mutants also exhibit hydrocephaly which progressed in severity in postnatal stages and was a confounding factor. For this reason, three key time points were selected to assess the cortical phenotype: E18.5 when there are no signs of hydrocephaly, P5 where there is moderate ventricular enlargement and P15 where hydrocephaly was the most severe. Three control and three mutant mice were analysed from each stage and together these results help to describe the progressive phenotype, elements of which are likely to be independent of the hydrocephaly.

5.2.1 E18.5 *Ta3* mutant mice show subtle defects in the deep cortical layers

Initial gross observations of E18.5 cortices saw no visible difference between control and mutant mice. In order to compare the cortical layers in greater detail a number of transcription factors and well-known layer markers were identified. Neural progenitors and mature neurons were first identified by expression of Pax6 and NeuN respectively. In controls, Pax6-positive cells formed a dense band in the VZ with interspersed cells in the intermediate zone (Fig 5.2a). The thickness of the VZ band showed slight variations due to the medio-lateral position but analysis of multiple sections suggested the VZ proliferative zone was equal between control and mutant. Mature NeuN-positive neurons in control were visible as a discrete band at the base of the cortical plate with an accumulation of mature neurons in the upper cortical plate (Fig 5.2a). In mutant sections, the band of NeuN-positive neurons at the base of the cortical plate appeared slightly more diffuse but otherwise a similar distribution was seen between control and mutant.

Outer layer pyramidal neurons can be identified by their expression of the transcription factor cut-like 1 (Cux1). It is expressed from their time of birth in the VZ/SVZ around E13-E17 until they reach their final position in layers II/III and to lesser extent in layer IV (Nieto et al., 2004). In control cortex Cux1-positive neurons were visible throughout the ventricular and intermediate zones and a band of brighter intensity was also seen in neurons which had already reached the developing layers II/III (Fig 5.2b). Special AT-rich sequence-binding protein 2 (Satb2) is a transcription factor expressed by Cux1-positive neurons but is also present in pyramidal neurons throughout layers II-VI (Britanova et al., 2005). It is required for the formation of callosal projections which connect left and right

sides of the cortex via the corpus callosum (Alcamo et al., 2008). Control Satb2 neurons showed a fairly even distribution throughout the cortical plate. Comparison between control and mutant showed little difference in the number or distribution of Cux1- or Satb2-positive neurons (Fig 5.2b). However, the boundary between the intermediate zone and the cortical plate, the subplate, did appear larger and more diffuse in the mutant cortex (Fig 5.2b).

Deep cortical layers can be identified by labelling for T-box brain 1 (Tbr1); this transcription factor is expressed in early born neurons from E10-E13 and labels cells in layer VI and also layer II/III (Bulfone et al., 1995, Hevner et al., 2001). These cells are predominantly glutamatergic corticothalamic neurons and, as the cortex forms in an inside-out fashion, are some of the oldest cortical neurons. Another deep layer marker which identifies neurons predominantly in layer V is the zinc-finger transcription factor Chicken ovalbumin upstream promoter transcription factor-interacting protein 2 (Ctip2) (Leid et al., 2004, Arlotta et al., 2005). The expression of Ctip2 is actually inhibited by Tbr1 which has a role determining the final destination of axonal projections (McKenna et al., 2011). Many Ctip2-positive neurons project axons to subcerebral locations such as the mid-, hindbrain and spinal cord and have been shown to be a key genetic determinant of corticospinal motor neuron differentiation (Arlotta et al., 2005). At E18.5 the presumptive deep layers VI and V were easily distinguished by the expression of Tbr1 and Ctip2 respectively. The number of Tbr1-positive cells was slightly reduced in mutant mice; this was most evident in the base of the cortical plate where a discrete band of Tbr1-positive labelling was present in control but reduced in mutant sections (Fig 5.2c). Although Ctip2 is strongest in presumptive layer V, fainter expression can also be seen in layer VI. Once more, the base of the mutant cortical plate appeared to have a reduced number of Ctip2-positive cells when compared to control (Fig 5.2d).

At E18.5 the proliferative zones in the cortex have a relatively high output compared to the later time points investigated, for this reason the progenitor population was analysed further. T-box brain 2 (Tbr2) is a transcription factor which labels intermediate progenitors present in the VZ and intermediate zone (Bulfone et al., 1999, Englund et al., 2005). Both control and mutant cortex showed a similar density of Tbr2-positive neurons in the VZ (Fig 5.2d). However, mutants had a reduced number of Tbr2-positive neurons in the intermediate zone and this was most notable at the boundary with the cortical plate. To further assess the progenitors in this region proliferating cells were identified by labelling

for PCNA and PH3 (Fig 5.3a). Interestingly, whilst the ventricular and subventricular zones appeared very similar between control and mutant, the intermediate zone appeared to exhibit a reduced level of proliferation in mutants however this reduction was not shown to be statistically significant (Fig 5.3b). Sections were also labelled for caspase-3 to assess the level of apoptosis but very few cells were positive in the cortex (~0-1 per slide) (data not shown). This was consistent between control and mutant suggesting little difference in apoptosis at this stage. These data demonstrate that *Ta3*$^{fl/fl;NesCre}$ mutants show mild layer disruption in the E18.5 cortex.

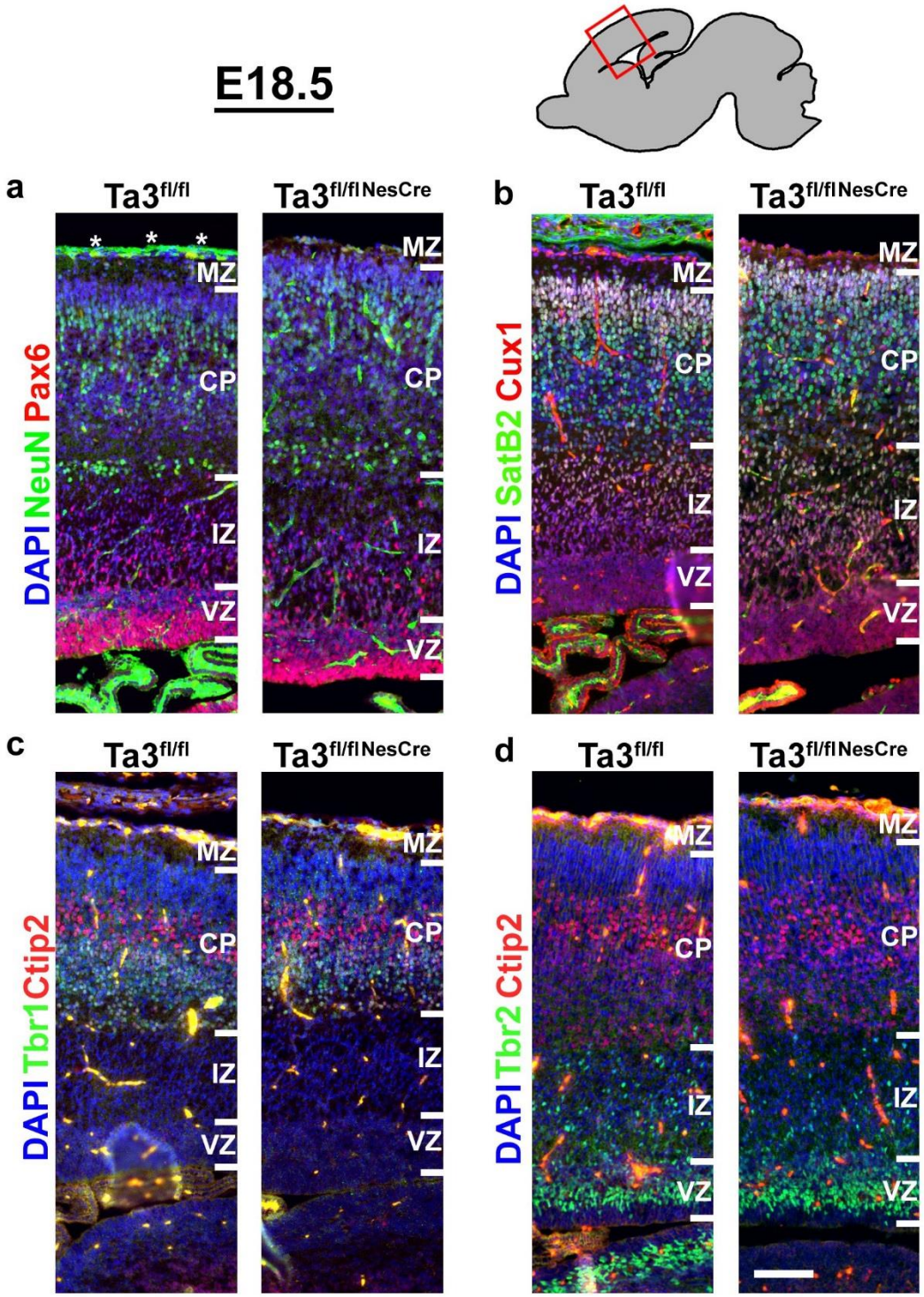

Figure 5.2 E18.5 *Ta3* mutant cortices have defects in the deep cortical plate

E18.5 sagittal sections showing cortical region indicated by red box. (a) Control and mutant have similar distribution of NeuN+ neurons (green) but the base of the mutant cortical plate appears more diffuse. Both control and mutant have comparable distribution of Pax6+ progenitors (red). (b) Control and mutant have a similar distribution of Satb2+ neurons (green) and Cux1 neurons (red) but a more diffuse appearance at the base of the cortical plate. (c) Mutants have a reduction in Tbr1+ neurons (green) at the base of the cortical plate. Above this layer, Ctip2+ neurons (red) have a comparable banding between control and mutant. (d) Deeper layer Ctip2+ neurons (red) are depleted at the base of the cortical plate. Mutants have a reduction of Tbr2+ neurons in the intermediate zone but normal numbers in the ventricular zone. Scale 100 µm (a-d). Asterisks (a) indicate folding of tissue causing increased fluorescence.

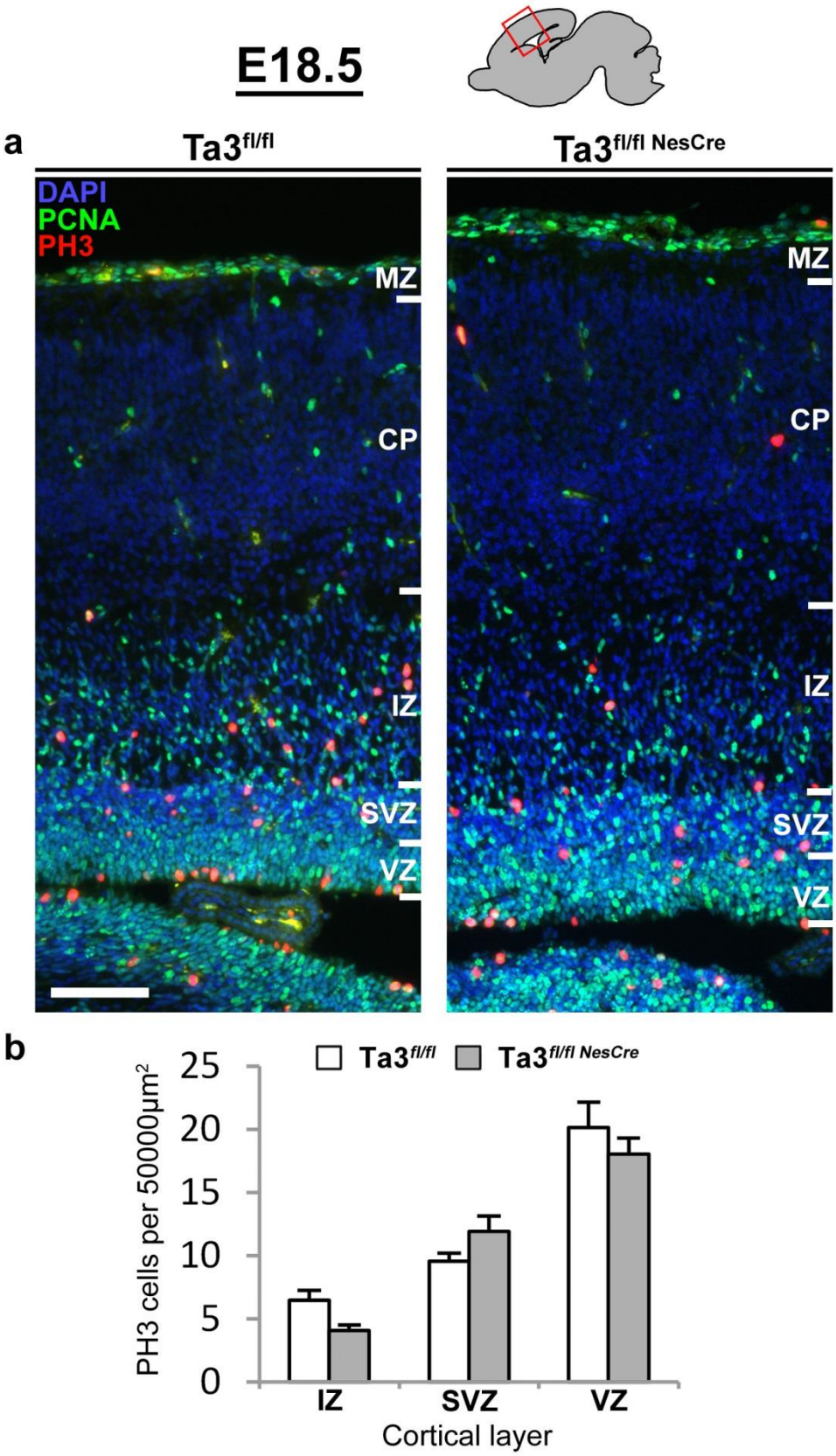

Figure 5.3 Analysis of proliferation in E18.5 *Ta3* mutant cortices

E18.5 sagittal sections showing cortical region indicated by red box. (a) Identification of PCNA+ (green) and PH3+ (red) progenitors. Mutants have a reduced number of PCNA+ and PH3+ cells in the intermediate zone. (b) quantification of PH3+ cells in the ventricular zone, subventricular zone and intermediate zone. Scale 100µm (a). Error bars: (b) s.e.m (n = 3)

5.2.2 P5 *Ta3* mutant mice have loss of deep layer neurons and a mild cortical compression

The cortical phenotype was also assessed in P5 mice, when the hydrocephaly had only a moderate severity (Fig 5.4a). Sections stained for hematoxylin and eosin showed a loss of integrity in the corpus callosum which often resulted in tearing or detachment from the cortical plate (Fig 5.4b). This defect, in addition to the hydrocephaly, made accurate comparison of the proliferative VZ problematic between control and mutant mice. The layering of the cortical plate, however, could still be meaningfully compared to assess the consequence of *Ta3* loss.

The mutant cortex showed significant thinning in posterior regions of the sensory and visual cortex due to hydrocephaly stretching the cortical wall; this was particularly evident at P15. For this reason the motor cortex in the anterior cortex was chosen for comparisons at both P5 and P15 (Fig 5.4a, Fig 5.7a). This region was the most comparable between control and mutant with arising defects more likely to be due to loss of primary cilia rather than a secondary consequence of hydrocephaly.

The superficial marker Cux1 showed a comparable thickness of layer II/III between control and mutants (Fig 5.4b). Mutant mice also exhibited the same approximate number and density of Cux1-positive cells compared to control, which was consistent with observations at E18.5. Analysis of Satb2 showed a comparable distribution of neurons between layers I-V however in layer VI the density of the neurons seemed increased and the thinner cortical size indicated the early signs of compression. In contrast to this relatively mild defect seen in the deep layer Satb2-positive neurons, mutant deep layer Tbr1-positive neurons showed a prominent reduction in layer VI (Fig 5.4c). Although Tbr1-positive neurons are the predominant neuron in layer VI, in adult brains they are also present in layers II/III. In control P5 cortex, Tbr1-positive neurons were seen in layers II/III in addition to layers V and VI which are presumably the result of incomplete migration at this developmental stage. Interestingly, in the mutant cortex the proportion of Tbr1-positive neurons which were migrating to superficial levels was unaffected and, if anything, appeared more prominent than control. The Tbr1-positive mutant neurons had migrated a similar distance compared to control neurons but, due to the thinner cortex, the relative distance migrated appeared further in comparison (Fig 5.7c).

Analysis of deep layer marker Ctip2 showed a similar distribution in the control and mutant cortices with small nuclei evident in deep layer VI and large projection neurons in

layer V (Fig 5.4d). However, mutant Ctip2-positive cells clearly showed a lower density of neurons in both layers which were most notable in layer VI. In comparison to the more subtle defects seen at E18.5, P5 mutant mice showed a striking loss of both Tbr1 and Ctip2 neurons in deep cortical layers.

Broad analysis of mature neurons with NeuN labelling also showed defects in deeper layers (Fig 5.4d,e). Mutants exhibited a dense band of large NeuN-positive cells in the deeper half of layer VI. Whilst a similar band was observed in control cortex, in mutants the band was thicker with a notable increase in fluorescence intensity. In control, above the dense NeuN-positive band in the middle of layer VI, numerous small neurons were present, however in mutants these neurons were either absent or had been obscured by the thickened NeuN band (Fig 5.4e). Importantly, the deep-layer NeuN defect described in mutants appears very different from the phenotype seen in the loss of Tbr1 and Ctip2 neurons. The thickened NeuN band seems most consistent with the Satb2 labelling and is likely to represent the early effects of ventricular compression.

Identification of the glial population by labelling for BLBP did not exhibit an obvious phenotype in mutant cortex. In both control and mutant the highest density of glia was evident between layers II-V and these were evenly spaced across the cortex (Fig 5.4e). P5 sections were also labelled for caspase3 to see whether any of the deep layer defects were due to elevated cell death. Similar to E18.5, P5 sections had a very low number of positive cells in both control and mutant with approximately 1-2 per section (data not shown). The distribution of caspase-positive cells did not show any consistent layer distribution making comparisons very difficult between control and mutant. This suggests that apoptosis at P5 is not a contributing factor to the mutant phenotype.

5.2.3 *Ta3* mutant mice have slight subplate defects

The data collected from the two time points demonstrated that the defects in E18.5 and P5 mutant mice were most evident in the deepest cortical layers. At E18.5 defects were also present in the intermediate zone. The boundary between intermediate zone and cortical plate is known as the subplate region. The orphan nuclear receptor Nr4a2 (Nurr1) is a recently described marker of subplate neurons born between E11.5-E12.5 (Arimatsu et al., 2003, Hoerder-Suabedissen et al., 2009). To further assess the specific subplate defects, Nurr1 was identified in E18.5 and P5 sections (Fig 5.5). At E18.5, control mice displayed a

narrow band of Nurr1 positive cells. Comparison with mutant mice showed a slight reduction in Nurr1 cells (Fig 5.5a). In P5 control, Nurr1 staining remained as a thin band marking the subplate with occasional cells present in layer VI. In comparison, mutant P5 cortices had a band of Nurr1 staining which was much narrower indicating a possible loss of subplate neurons (Fig 5.5b). Importantly, despite showing the mutant mice had defects evident in the subplate region they were not as prominent as those seen in deep cortical layers identified by Tbr1 and Ctip2, especially in P5 mice.

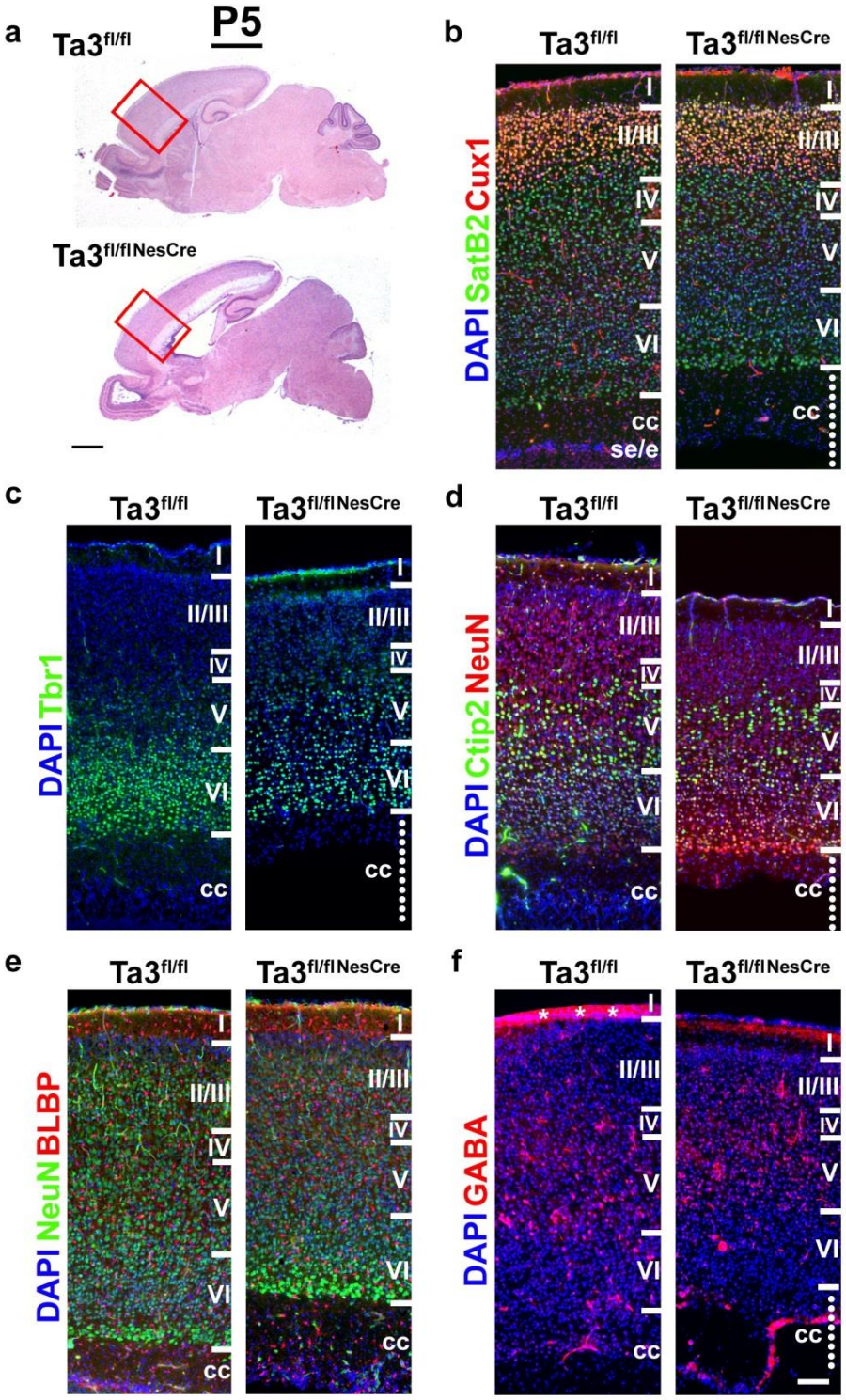

Figure 5.4 P5 *Ta3* mutant cortices have deep layer defects

(a) P5 sagittal sections stained with hematoxylin and eosin with red box indicating motor cortex selected for cortical analysis. (b) P5 control and mutant have a similar distribution of Cux1 neurons (red) in layers II/III and a mild compression of deep Satb2 neurons (green) in deep layer VI. (d) Mutants show a lower density of Tbr1+ neurons in deep layer VI and but the migrating population in layer V are more prominent. (e) Control and mutant show a similar distribution and density of mature NeuN+ neurons and BLBP+ glia. Mutants have a thickening of NeuN in lower half of Layer VI with loss of overlying cells with small nuclei. (f) Control and mutant show a similar distribution of GABAergic interneurons. Roman numeral indicate cortical layers. Dotted line indicates loss of integrity in the corpus callosum (cc). Scale 1mm (a), 100µm (b-f). Asterisks in (f) indicate folding of tissue section resulting in increased fluorescence.

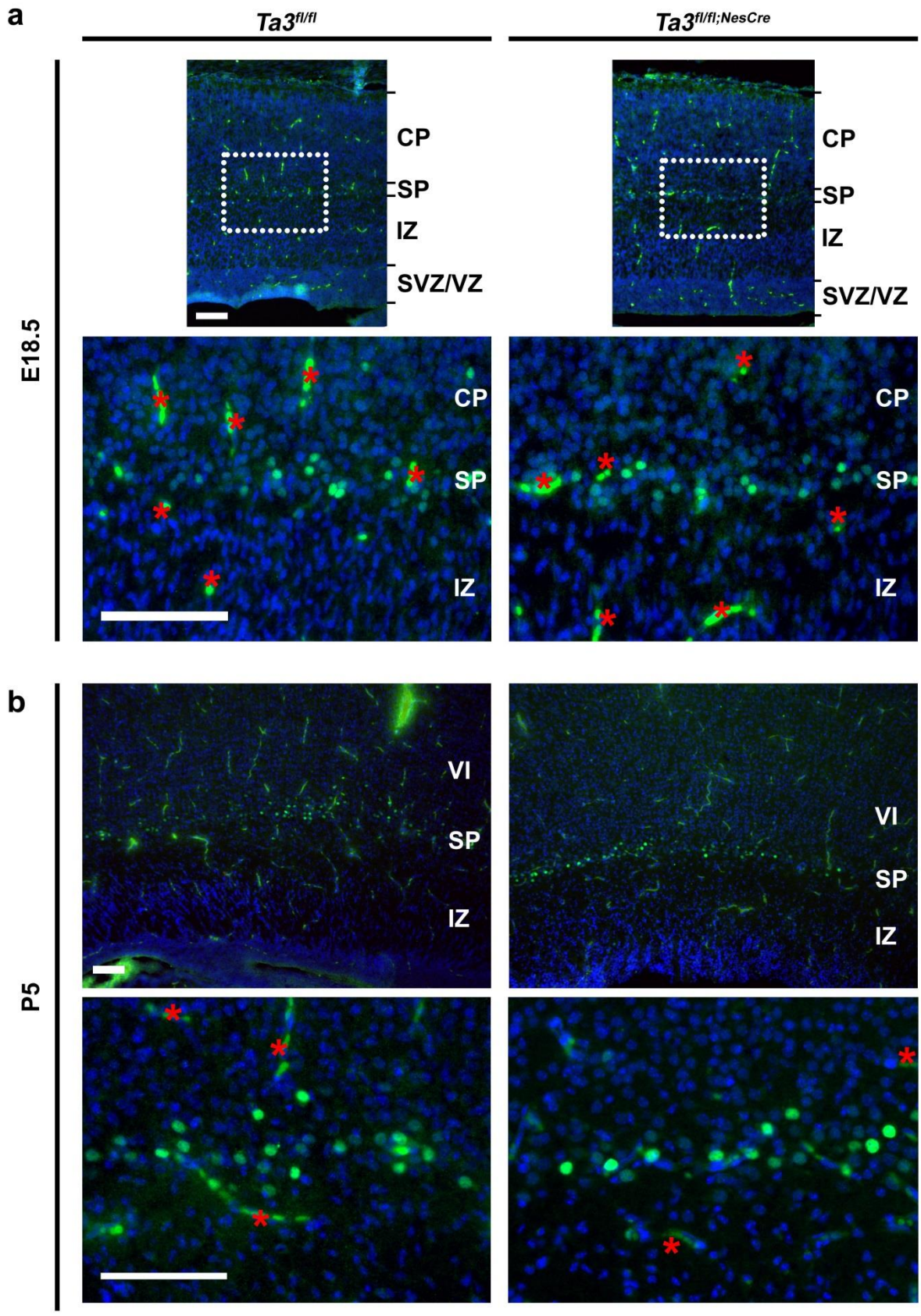

Figure 5.5 *Ta3* mutant cortices have reduction in Nurr1-positive subplate neurons

(a) E18.5 and (b) P5 cortices labelled with Nurr1 (green). Nurr1 clearly labels a neuronal population in the subplate zone. Mutant cortex has a slight reduction in Nurr1 cells at E18.5. By P5 the mutant subplate appears narrower compared to control with a small reduction in positive cells. Red asterisks indicates autofluorescence. Scale, 100 µm (a, b)

5.2.4 P5 *Ta3* mutant mice have no defects in interneuron placement

In addition to the cortical projection neurons, GABAergic interneurons are also present in the cortex and predominately make local circuits. Disruption of cilial component Arl13b has been shown to disrupt the migration of interneurons (Higginbotham et al., 2012). To test whether the $Ta3^{fl/fl;NesCre}$ mutant mice exhibited any interneuron phenotype, GABAergic interneurons were labelled at P5 (Fig 5.4f); this is approximately one day before interneuron migration is complete (Inamura et al., 2012). Little difference was seen between the distribution in control and mutant cortex. To confirm this, the number of GABAergic cells was quantified in the different cortical layers (Fig 5.6b). Due to the small size of layer IV and the ambiguity in determining the exact boundary, the number of neurons was quantified in grouped layers II/III, IV/V and VI. Despite a slight reduction in layer IV/V, no significant difference in the density of GABAergic interneurons was observed at this stage. Interestingly there was also no difference in the density of total cells, as determined by the quantification of nuclei in the different cortical layers (Fig 5.6a). This suggests that despite the mild compressive and stretching effects induced by the hydrocephaly in addition to the loss of deep cortical projection neurons, we were unable to detect a significant difference in number of cells per unit area (Fig 5.6a).

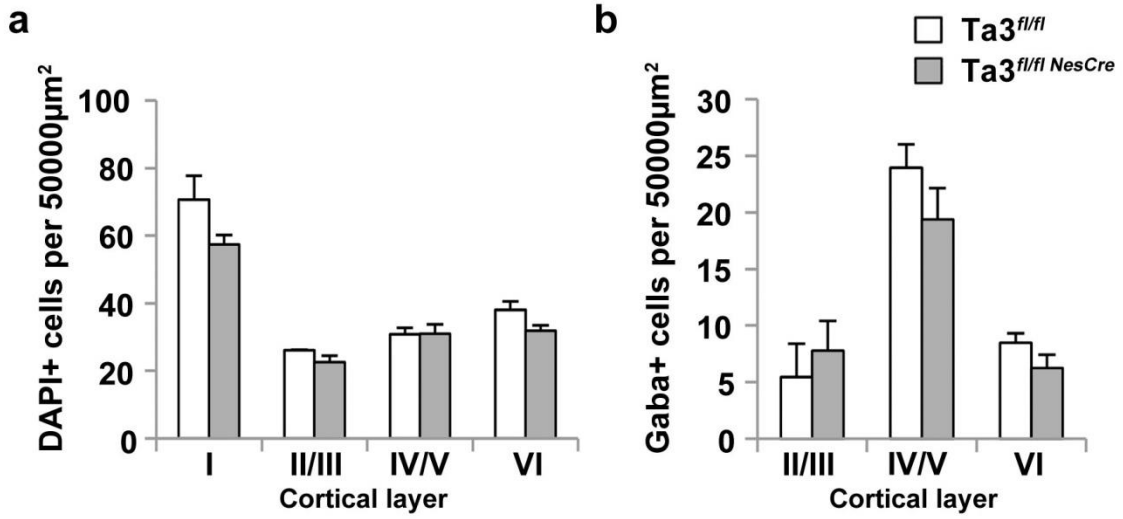

Figure 5.6 P5 *Ta3* mutant cortices show no difference in GABAergic interneuron placement
P5 motor cortex was selected and (a) total number of nuclei counted using DAPI stain and (b) total number of GABA+ neurons counted for each cortical layer. No significant difference was identified in any cortical layers. Due to the small size and ambiguity determining layer IV, this layer was pooled with layer V quantification. Error bars (a,b) s.e.m (n = 3)

5.2.5 P15 *Ta3* mutant mice have defects in deep cortical layers

P15 mice were the oldest stage investigated and mutants exhibited an increased severity of hydrocephaly. Staining for hematoxylin and eosin showed a compression of the mutant cortex and the loss of integrity seen in the corpus callosum was more pronounced than at P5 resulting in tearing and detachment from the cortex in the majority of sections. The upper half of deep layer VI also had a consistent band of faint eosin staining which was not evident in control (Fig 5.7a,b).

Comparison of superficial neurons using Cux1 showed that P15 mutants had a slightly thinner layer II/III. Although not quantified, the number and density of positive cells appeared similar between control and mutant (Fig 5.7c). This was also the case for Satb2-positive neurons where control and mutant had a comparable distribution of neurons between layers I-V however layer VI was severely affected and looked to be compressed (Fig 5.7c). Mutants had a dense band of Satb2-positive cells in the lower half of layer VI and a hazy band of reduced cell density lying above; this correlated with the faint eosin staining and is likely to be a direct effect of the ventricular expansion.

Tbr1 positive neurons were present in the P15 control layers VI and II/III. A small number were also still visible in layers IV and V, presumably because many were still migrating to their superficial positions as seen in P5 control. Comparison of P15 control and mutant seemed to show a loss of Tbr1-positive neurons compared to control (Fig 5.7d) and this appeared to be much more severe than that seen at earlier stages. Above this in layers V and IV, mutant cortex still had a comparable scattering of neurons migrating superficially. In layer II/III both control and mutant had a large band of Tbr1-positive neurons however in mutant cortex the neurons appeared to extend to the boundary with layer I, which was not evident in control. This defect was consistent with observations made at P5. In deep cortical layers the Ctip2-positive neurons looked to have a lower density of positive cells in the mutant layers V and VI (Fig 5.7e). Despite this apparent reduction, the distribution between control and mutant was similar with numerous small cells present in layer VI and projection neurons with large cell bodies in layer V (Fig 5.7e).

All mature neurons and glia were identified in the P15 cortex by staining for NeuN and BLBP respectively (Fig 5.7f). In P5 mice both control and mutant exhibit a thick band of NeuN in deep layer VI (Fig 5.4e). In the P15 control cortex this band had dispersed into a more distributed uniform staining in across layer VI (Fig 5.7e,f). In contrast, the bright NeuN band persisted in deeper half of mutant layer VI and also had a hazy band directly above it (Fig 5.7e,f). This effect was similar to the Satb2 distribution (Fig 5.7c) and the hazy eosin band described above (Fig 5.7a,b). In addition, in the mutant layer VI NeuN-band the neurons looked to be comparably larger in size compared to those seen in control. Despite the layering defects seen in the mutant neurons, the distribution of glial cells appeared relatively comparable between control and mutant (Fig 5.7f). The highest density of cells was evident between layers II-V and the cells were evenly spaced. This relatively unaffected glial phenotype was consistent with observations made at P5.

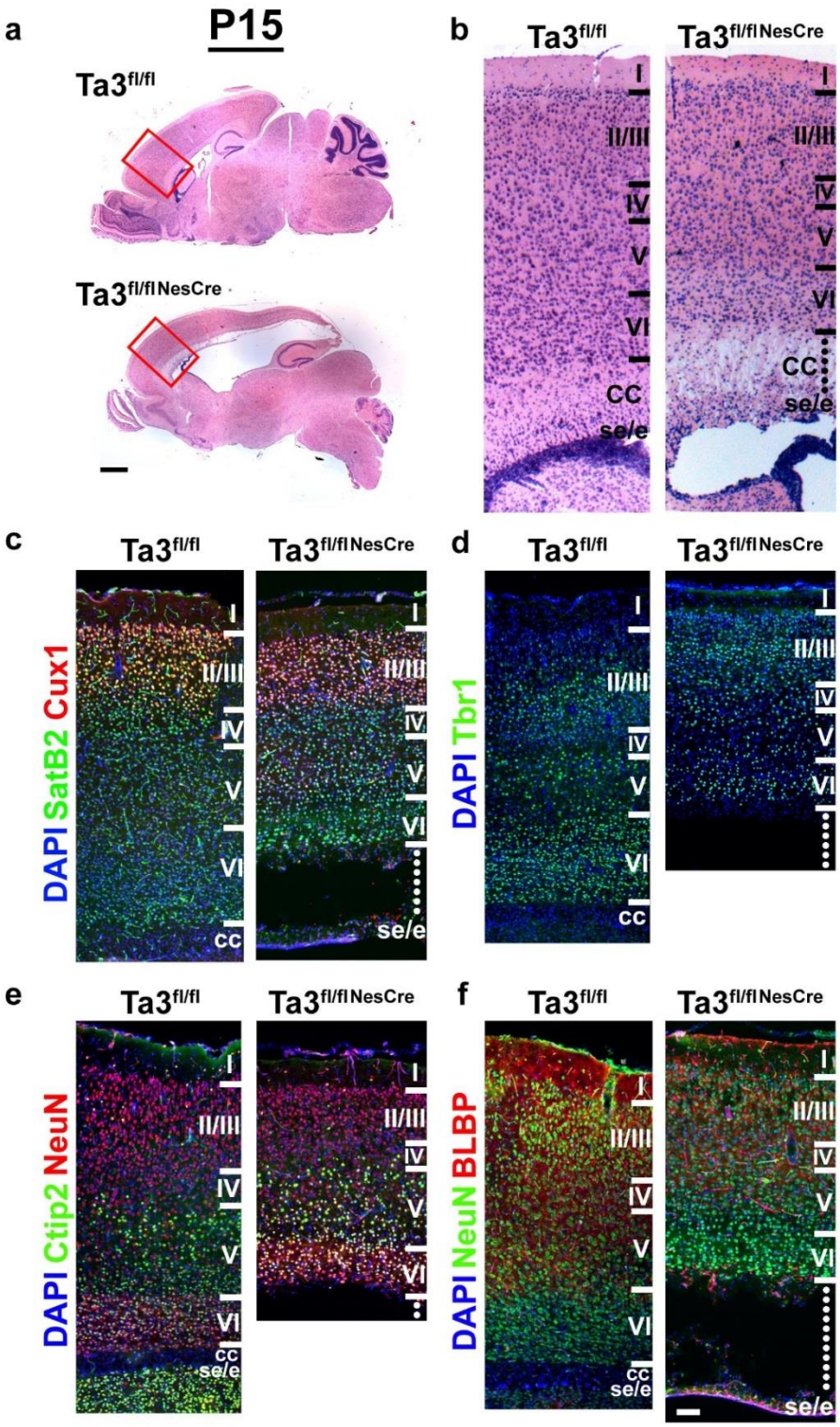

Figure 5.7 P15 *Ta3* mutant cortices have defects in deep layers.

(a) P15 sagittal sections stained with hematoxylin and eosin with red box indicating motor cortex selected for higher magnification. (b) Mutant cortex has loss of integrity in the corpus callosum (dotted line) and a faint band of eosin in deep layer VI. (c) Control and mutant have a similar distribution of Cux1+ neurons in layers II/III (red) but mutants have a compressed band of Satb2 in layer VI (green). (d) Mutants have a striking loss of Tbr1+ neurons in deep layer VI and migration of neuron to the boundary of layer I/II. (e) Control and mutant have a similar distribution of Ctip2 (green) but mutants show a lower density of neurons. Mutants also show a compression of mature NeuN+ neurons (red) in layer VI. (f) Mutants have a compression in deep NeuN+ neurons (green) but the distribution of control and mutant BLBP+ glia (red) is very comparable between control and mutant. Roman numeral indicate cortical layers. CC, corpus callosum, se/e, subependymal/ependymal layer. Scale 1mm (a), 100µm (b-f).

5.2.6 P15 *Ta3* mutant mice lack cortical primary cilia

The *NesCre* deleter is known to cause recombination throughout the postnatal cortex but it is still important to confirm the effect on primary cilia due to loss of *Ta3*. P15 brains were labelled with ACIII and in control nearly all cortical cells exhibited a primary cilia approximately 5 µm in length. In contrast, mutants exhibited nearly complete loss of cilia in all cortical regions examined (Fig 5.8a,b). Even superficial regions, which have limited cortical phenotype, had near complete loss of cilia.

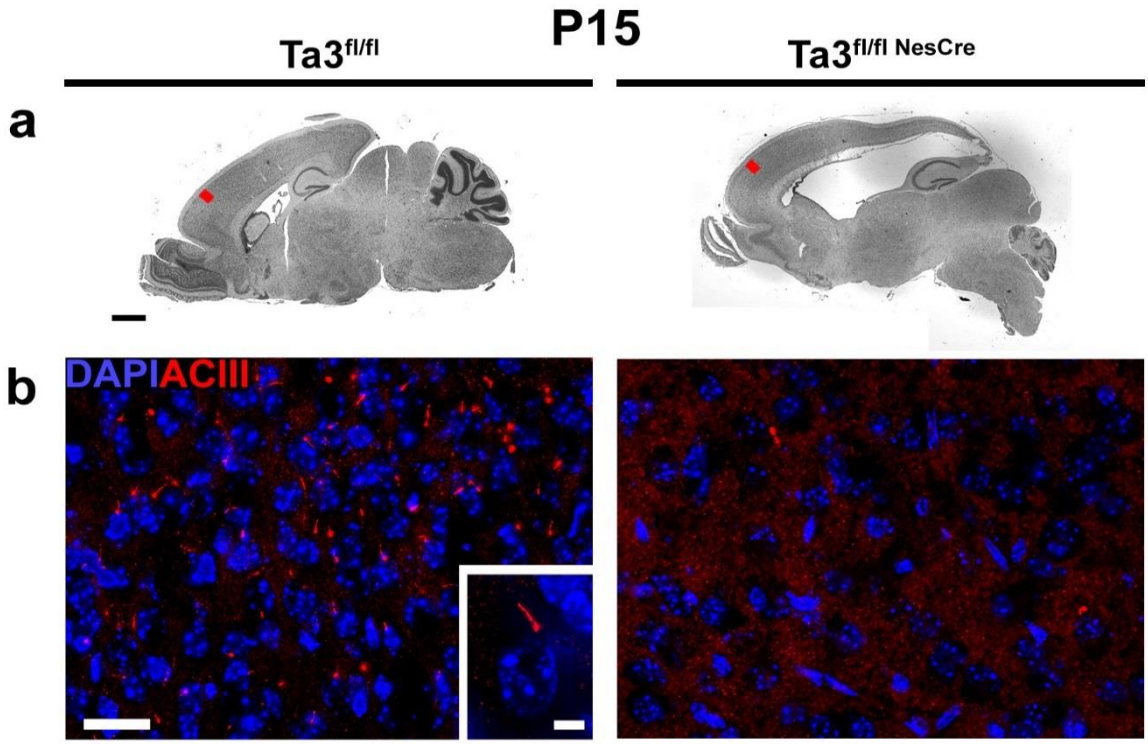

Figure 5.8 *Ta3* mutant cortices exhibits near complete loss of primary cilia
(a) Whole sagittal sections with red box indicating region of motor cortex shown in (b). (b) Labelling of primary cilia using ACIII in superficial layers II/III. In all control cortical regions nearly every cell exhibits primary cilium, boxed inset shows higher magnification image. Mutants exhibit near complete loss of primary cilia in all cortical regions. Scale, 1mm (a), 25 µm (b), 5 µm (boxed inset).

5.2.7 P5 and P15 *Ta3* mutant mice have defective Shh signalling

To better assess the molecular basis causing the cortical phenotypes, tissues were collected for RNA and protein analysis at P5 and P15. For this section all experimental mice were bred, dissected and genotyped by the author however, due to time constraints, qPCR and western blot experiments were completed by Ross Ferguson (Research assistant, Subramanian Laboratory).

Analysis of *Gli1*, *Gli2* and *Ptc1* mRNA expression found that control levels dropped by approximately half between P5 and P15 demonstrating that later cortical stages have a reduced level of Shh signalling (Fig 5.9a). The expression of *Gli1* in P5 mutants was reduced by 75% compared to control and in P15 mutants it was reduced by 80% compared to control. The expression of *Gli2* in P5 mutants was also reduced by 25% compared to control but the difference was negligible at P15. Comparison of *Gli3* expression in both ages also showed a small but significant reduction in mutants when compared to control. In addition to *Gli1*, *Ptc1* expression is a key indicator of Shh pathway activation. P5 Mutants exhibited a 75% reduction in *Ptc1* compared to control and P15 mutants had a 50% reduction compared to control. There was no difference in *Smo* expression between control and mutant at either age. These results clearly demonstrated that at both P5 and P15 mutants have an overall reduction in their response to Shh signalling.

Protein analysis showed that in control both Gli1 and Gli2 levels were halved between P5 and P15 consistent with the trend in mRNA expression and confirming the reduced level of Shh signalling in later stages (Fig 5.9b,c). Analysis of samples taken from three mutant mice allowed quantification of protein levels relative to gapdh (Fig 5.9c). In mutant P5 cortex the levels of Gli1 and Gli2a were significantly reduced by 37% and 27% respectively when compared to control (Fig 5.9c). In contrast, P15 mutant mice showed no difference in Gli1 or Gli2A protein levels compared to control. Gli2R was undetectable in both of the ages analysed. Gli3 was found to be present in low levels in both P5 and P15 control cortex. In P5 control cortex the full length Gli3A protein was most evident with undetectable levels of Gli3R. Conversely, in P15 cortex the smaller Gli3R was more prominent. Quantitation of band intensity demonstrated that, at P5, Gli3A levels were 25% higher in mutant compared to control. This increase was much less notable at P15 and, although it was not significant, mutant cortex had a small but consistent increase in both Gli3A and Gli3R.

These results confirm that the mutant cortex has a reduced overall response to Shh signalling. However, despite seeing a decrease in mutant *Gli3* mRNA expression at P5 the relative protein levels of Gli3A were higher than control suggesting altered processing of this important transcription factor.

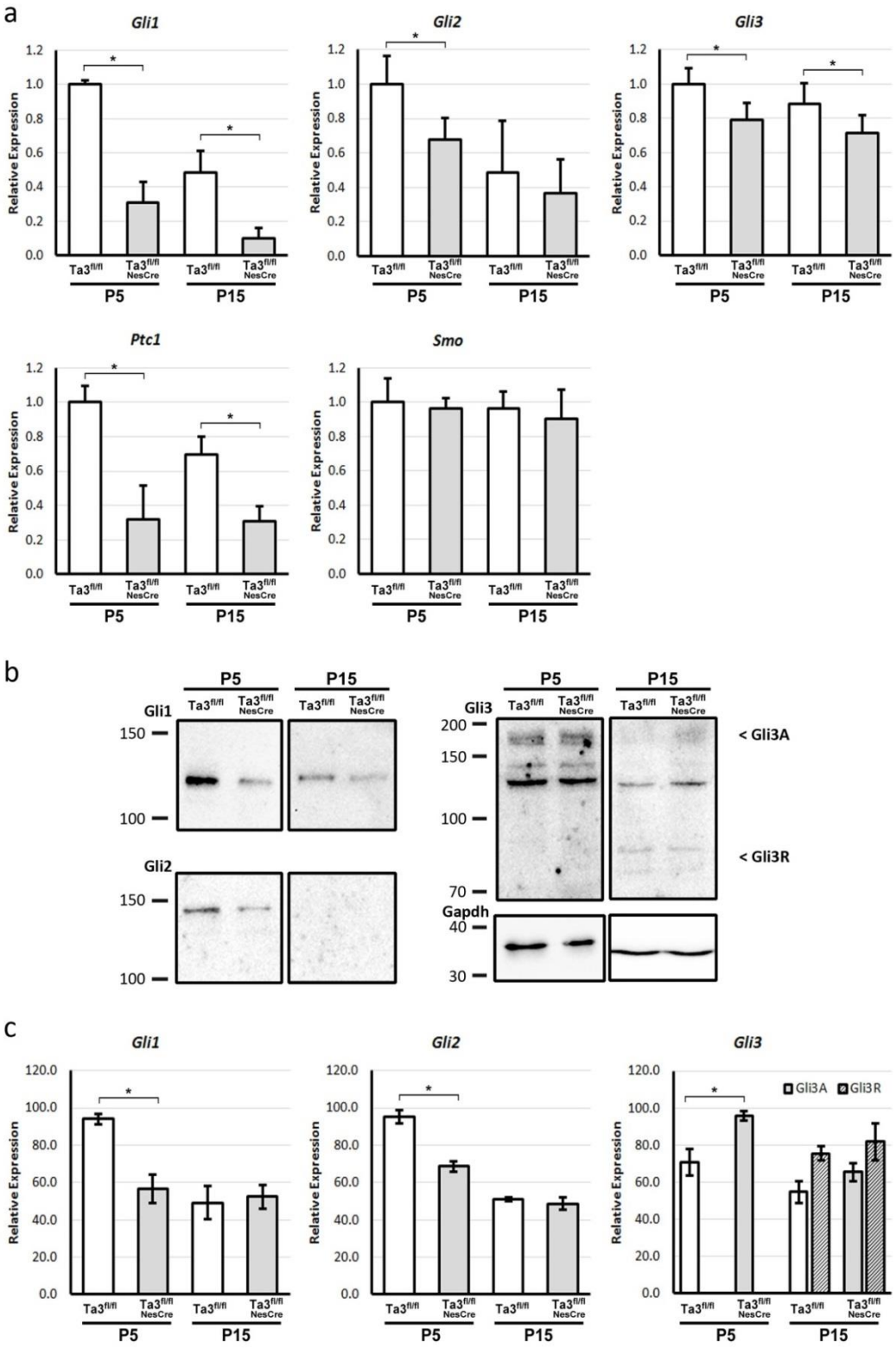

Figure 5.9 *Ta3* mutants have reduction in Shh pathway activation and altered Gli3 processing

(All Breeding, dissections and genotyping were completed by the author but qPCR and Western blot experiments and figures were kindly completed by Ross Ferguson (Research Assistant, Subramanian lab). (a) qPCR for hedgehog pathway components in the cortex, mean results from four cortices of each genotype and age relative to gapdh and actb. Both P5 and P15 mutants have a significant reduction in *Gli1* expression compared to control. P5 mutants have a significant reduction in *Gli2* expression. P5 and P15 mutants have a significant reduction in *Gli3* and *Ptc1* expression. (b) Representative western blots for Gli1, Gli2 and Gli3 in control and mutant cortices at P5 and P15. (c) Quantification of western blots from three cortices of each genotype and age relative to gapdh. P5 mutants have a significant reduction in Gli1 and Gli2 protein but a significant increase in Gli3A. Error bars (a) s.e.m (n = 4), (b) s.e.m (n = 3), * P≤0.05, (one tailed Students-t test).

5.7 Discussion

The cortical phenotype of *Ta3*$^{fl/fl;NesCre}$ mice has been presented here at three key stages. E18.5 mutant mice are similar to control in their gross cortical phenotype, however, closer analysis demonstrated subtle defects in deep layers. By P5 the deep layer defects became more prominent with a notable loss of both Tbr1-positive and Ctip2-positive neurons. Also evident at this stage was a reduction in subplate neurons and a loss of integrity in the corpus callosum. The phenotype became more prominent by P15 with the loss of neurons most noticeable in the Tbr1 and Ctip2 population. NeuN and Satb2 neurons also showed a compressive phenotype in deep mutant layers which seemed more attributable to the effects of hydrocephaly. Analysis of the mechanistic causes confirmed that postnatal mice exhibit a striking loss of primary cilia in the cortex. In addition, analysis of mRNA and protein demonstrated that mutants exhibited a reduced response to Shh in the postnatal cortex and altered Gli3 processing compared to control.

Understanding the cortical phenotype in mice with loss of primary cilia depends on the time of recombination. Constitutive primary cilia mutants display striking defects which are often attributed to early problems specifying the dorso-ventral axis (Besse et al., 2011). The knock-on effect of this broad patterning defect makes analysis of later phenotypes difficult to interpret. Investigating the roles of primary cilia after dorso-ventral patterning relies on conditional deletion, however this interpretation is not without difficulties due to hydrocephaly having a confounding effect on nearby structures.

Many human ciliopathy patients with disruption of primary cilia present with callosal defects including Joubert, Meckel, Ofd and BBS (Valente et al., 2014, Edwards et al., 2014). Little description of the corpus callosum has been made in investigations of mice with conditional loss of primary cilia. On first impression, the degeneration and detachment of the corpus callosum could be attributed to stretching of the cortical wall due to the hydrocephaly. Intriguingly, Shh has been shown to be expressed in the corpus callosum (Machold et al., 2003) and it is possible to attribute the callosal defects to defective signalling.

In the brain, most oligodendrocytes derive from ventral regions. However, oligodendrocytes which populate the corpus callosum derive from an *Emx1*-positive lineage

demonstrating they are of cortical origin (Gorski et al., 2002). Conditional loss of *Smo* (*Smo*$^{fl/-;NesCre}$) causes a phenotype with reduced oligodendrocyte precursors and degeneration of the corpus callosum (Machold et al., 2003). In the study Machold and colleagues hypothesised that Shh has an active role in the maintenance or survival of the corpus callosum oligodendrocytes, rather than their specification in the ventral neural tube. Conditional mutants in Gli3 (*Gli3*$^{fl/fl;NesCre}$) have also been shown to have a hypoplastic corpus callosum (Wang et al., 2011). Interestingly, earlier loss of Gli3 from E10.5 using a different *Cre* deleter (*Gli3*$^{fl/fl;Emx1Cre}$) (Amaniti et al., 2013) or hypomorphic loss (*Gli3*$^{Pdn/Pdn}$) (Magnani et al., 2014) results in an even more severe phenotype with agenesis of the corpus callosum. The increase in severity is thought to be due to an earlier role of Gli3 in the regulation of axonal pathfinding in callosal projection neurons. This early patterning role regulates levels of Wnt7b/8b and Fgf8 in the midline at E12.5 and is important for positioning of astroglia which produce signals required for axonal pathfinding (Wang et al., 2011). The defects seen in the *Ta3*$^{fl/fl;NesCre}$ corpus callosum more closely resembles the defects seen in *Smo*$^{fl/-;NesCre}$ and *Gli3*$^{fl/fl;NesCre}$ mice suggesting that degeneration of the corpus callosum is due to oligodendrocyte defects rather than axon pathfinding caused by disruption of the Shh signal transduction. Interestingly, conditional loss of Fgfr1 using the same *Nestin-Cre* deleter (*Fgfr1*$^{fl/fl;NesCre}$) resulted in complete agenesis of callosal projections (Smith et al., 2006) . This suggests that loss of primary cilia in *Ta3*$^{fl/fl;NesCre}$ mice does not affect Fgf1 signalling.

The superficial cortical layers appeared largely unaffected in the *Ta3*$^{fl/fl;NesCre}$ mutant mice. These neurons are the latest born cortical neurons and migrate through the cortical plate in an inside-out manner. This suggested the birth and normal migration of superficial Cux1-positive neurons does not require primary cilia. Deep cortical layers, however, appeared compressed at later postnatal stages consistent with increasing outward pressure from the lateral ventricles. Distinct from this compressive phenotype, deep layer Tbr1-positive and Ctip2-positive neurons had a conspicuous reduction in number. At E18.5 the loss was less noticeable but still evident in the deepest region of the cortical plate. Although not statistically significant, PH3 staining appeared to show a reduction in proliferation of the intermediate zone. Quantification of a greater number of mutant mice may have helped to demonstrate a genuine difference. Nonetheless, a proliferative defect such as this, is

unlikely to be responsible for the loss of Tbr1 or Ctip2 neurons which are some of the earliest born in the cortex (Hevner et al., 2001, Leid et al., 2004).

The defect does not appear to be affected by increased levels of apoptosis at E18.5 or P5. Based on these findings it is likely that the loss of Tbr1 and Ctip2 neurons is due to events earlier in development which may include a reduction in birth, survival or even fate specification. An interesting point to consider is that the Tbr1 and Ctip2 defects in mutant cortex appeared more severe the defect observed in subplate marker Nurr1. Subplate neurons are some of the earliest born cortical neurons and so if the loss of deep layer neurons was due to survival defects it would be reasonable to expect a greater loss of subplate neurons. Further studies looking at younger embryonic *Ta3*$^{fl/fl;NesCre}$ mice will be important in understanding the cause of the deep layer defects.

Studies investigating the loss of the basal body component Stumpy using the *NesCre* deleter strain (*Stumpy*$^{fl/fl;NesCre}$*)* do not describe the cortical phenotype (Town et al., 2008, Breunig et al., 2008). *Stumpy*$^{fl/fl;NesCre}$ mice were observed to have a thinner cortex but the research focussed on describing the more prominent phenotypes. In stark contrast, loss of anterograde motor protein, Kif3a, using the same *NesCre* deleter (*Kif3α*$^{fl/fl;NesCre}$) resulted in a severe phenotype and death of pups within hours of birth (Wilson et al., 2012). *Kif3α*$^{fl/fl;NesCre}$ brains were enlarged and the cortices showed ~1.75x increase in size. The group demonstrated that mice have loss of primary cilia and progenitors exhibited a reduced cell cycle time with increased cell divisions. They attributed the defect to an increased ratio of Gli3A:Gli3R resulting in elevated *CyclinD* expression.

Although *Ta3*$^{fl/fl;NesCre}$, *Stumpy*$^{fl/fl;NesCre}$ and *Kif3α*$^{fl/fl;NesCre}$ mice all lack primary cilia the phenotypes between the basal body proteins and IFT motor are quite different. It is probable that the proliferative defect is due to a difference in the processing of Gli3. *Kif3α*$^{fl/fl;NesCre}$ mice were analysed at E12.5 and protein analysis demonstrated a significant increase in the ratio of Gli3A:Gli3R resulting in an increased overall response to Shh as shown by an increase in Ptc1 and CyclinD protein levels. In contrast, the current study shows that *Ta3*$^{fl/fl;NesCre}$ cortices also have an increase in Gli3A levels but importantly the Shh response is reduced as shown by lower expression of *Gli1* and *Ptc1* mRNA. This is similar to the processing of Gli3 described in the hippocampus of *Stumpy*$^{fl/fl;NesCre}$ mice (Breunig et al., 2008). Although the hippocampus is a distinct brain region it has a number of similarities as

both develop from the dorsal telencephalon. Breunig and colleagues show that *Stumpy*$^{fl/fl;NesCre}$ mice have an elevated level of Gli3A in the hippocampus but the difference is only marginal. Importantly, they too show a reduced overall response in the Shh pathway shown by lower *Gli1* expression. Although the comparison between the three studies is difficult due to the different ages and tissues used, there is a clear difference in the overall Shh response. This difference in Shh signal transduction is likely to be due to the loss of IFT component, in the case of *Kif3a* mutants versus the loss of basal body components in *Ta3* and *Stumpy* mutants. While disruption of Kif3a or Ta3 both prevent the formation of primary cilia, it is possible that Kif3a could have other roles in the cell which affect Gli processing.

Conditional mouse mutants with earlier loss of primary cilia have more significant defects in the developing cortex. Constitutive loss of *Arl13b* (*Arl13b*$^{hnn/hnn}$) results in impaired function rather than complete loss of primary cilia (Caspary et al., 2007). Mice exhibit a phenotype where the early radial glial scaffold loses polarity and becomes reversed forming an inverted cortex in an outside-in manner (Higginbotham et al., 2013). In this thorough study, Higginbotham and colleagues demonstrate that time of recombination is crucial for development of the phenotype. Using a *Foxg1-Cre* deleter (*Arl13b*$^{hnn/fl;Foxg1Cre}$), which deletes from E9.5, they were able to recreate the inverted cortical phenotype. However, use of *NesCre* and *hGFAP-Cre* developed normal polarity. This time dependency was confirmed by inducible recombination using a tamoxifen responsive Cre to show that deletion before E10.5 was required to develop polarity defects. Although not described in detail, the subtle defects seen in the *Arl13b*$^{fl/fl;NesCre}$ cortex appear to be consistent with those seen in the *Ta3*$^{fl/fl;NesCre}$ cortex. This provides an explanation as to why a more distinct cortical phenotypes were not observed in *Ta3*$^{fl/fl;NesCre}$ mice.

In the *Ta3*$^{fl/fl;NesCre}$ cortex the radial migration of postmitotic pyramidal neurons appeared largely unaffected. This is consistent with the phenotype of mutants with loss of Arl13b specifically in pyramidal neurons using the *Nex-Cre* deleter (*Arl13b*$^{fl/fl;NexCre}$) (Higginbotham et al., 2012). In *Arl13b*$^{fl/fl;NexCre}$ cortex pyramidal neurons migrated to correct layers suggesting primary cilia are dispensable for their migration. They did note a reduction of fibres in the internal capsule which also reflects the *Ta3*$^{fl/fl;NesCre}$ phenotype presented previously in Chapter 3 (Fig 3.4c). When disrupting primary cilia in the VGE and MGE using

Dlx-Cre or *Nkx2.1-Cre* deleter strains the group showed defects in tangential migration of interneurons into the cortex resulting in altered cortical interneuron placement (Higginbotham et al., 2012, Baudoin et al., 2012). These studies used slice cultures and time lapse imaging to investigate the roles of Arl13b, Kif3a and IFT88; all of which showed defects in the placement of GABAergic cortical interneurons. Interestingly both studies independently observed that, when migrating, the mutant neurons travelled at comparable speeds to control neurons but they paused more often and for longer periods. This is a phenotype which is reminiscent of the aberrant migration described in mutant *Ta3* fibroblasts which moved with less directionality (Bangs et al., 2011) in addition to *talpid*^{3} mutant chick limb mesenchyme cells (Ede and Flint, 1975).

The placement of interneurons was analysed in the P5 *Ta3*$^{fl/fl;NesCre}$ cortex by quantifying the number of GABAergic interneurons in the different layers however no significant difference was observed. There are a few possible explanations for this; firstly the *NesCre* may cause a different level of recombination in the VGE or MGE compared to the *Dlx-Cre* or *Nkx2.1-Cre* used in the other studies. Another difference between the studies is that in the slice cultures, migration of the mutant cortical interneurons was tracked using a Cre-driven fluorescent reporter. The number of GABAergic and Cre-positive cells were used for quantification providing a more accurate measure of interneurons originating from the VGE and MGE that had also undergone recombination. The current study was limited to quantifying the total GABAergic cells which may have obscured subtle differences in placement of distinct VGE or MGE populations. The final consideration why differences were not seen in the placement of *Ta3*$^{fl/fl;NesCre}$ GABAergic interneurons was that recordings were taken from the motor cortex, which is located at the anterior of the brain. The tangential distance which interneurons migrate would be relatively smaller in anterior vs. posterior locations so migration defects may have been less pronounced.

Considering signalling pathways which act through primary cilia, Shh has been shown to be important in the development of the cerebral cortex (Komada et al., 2008, Machold et al., 2003). Loss of *Smo* using the *NesCre* deleter causes a severe phenotype with lethality around P10 (Machold et al., 2003). The most significant defect is evident in the MGE where mutants exhibit a reduction in size and often fusion with the LGE. Despite this, mutants show no difference in the numbers of GABAergic interneurons present in the cortex. They

do, however, show a loss of oligodendrocytes with a 30% reduction in myelinated structures. At P15 Shh is broadly expressed in a number of cortical structures, especially in proliferative zones such as the SVZ. *Smo*$^{fl/-;NesCre}$ mice exhibit a loss of proliferation and increased apoptosis in these regions. This phenotype appears similar to but more severe than *Ta3*$^{fl/fl;NesCre}$ mice. At E18.5 *Ta3*$^{fl/fl;NesCre}$ the possible defects in proliferation were limited to the intermediate zone and no difference was observed in the VZ or SVZ.

Although the study of *Smo*$^{fl/-;NesCre}$ mice looks at proliferation, the cortical layers were not identified (Machold et al., 2003). Loss of Shh signalling at earlier stages shows a more dramatic phenotype with disruption of early patterning (Komada et al., 2008). Loss of *Smo* using the *Emx1-Cre* deleter also causes a smaller telencephalon and mice have increased apoptosis at E13.5 and decrease in basal progenitors from E15.5 (Komada et al., 2008). The intermediate zone is almost lost entirely and defects are observed in the subplate. Specifically in *Smo*$^{fl/fl;Emx1Cre}$ cortex Tbr1 is not detected in the subplate region and fewer neurons are present. The loss of deep layer neurons in *Ta3*$^{fl/fl;NesCre}$ cortex appears to reflect a mild version of this *Smo*$^{fl/fl;Emx1Cre}$ phenotype. It is likely that Shh is also required for the survival of these early born, deep layer neurons in mid-gestation.

Loss of *Gli3* using the *NesCre* results in a different cortical phenotype to that seen in *Smo*$^{fl/-;NesCre}$ cortex (Wang et al., 2011). By birth dating neurons at E13.5 or E15.5 they demonstrated that Gli3R was required for determining cortical neuronal fate with complete loss of Gli3 causing a gain of deep Ctip2-positive neurons at the expense of superficial Cux1-positive neurons. They also showed that loss of Gli3 caused a reduction in mitotic divisions at E16.5 in the SVZ. The *Ta3*$^{fl/fl;NesCre}$ cortex exhibits some similarity with this phenotype but a loss of deep layer neurons rather than a gain. This highlights the importance of Gli3A:Gli3R ratio, and suggests a scenario where the *Ta3*$^{fl/fl;NesCre}$ cortex has sufficient Gli3R to specify superficial Cux1-positive neurons but insufficient levels of Shh pathway activation to achieve normal Tbr1-positive and Ctip2-positive populations.

The interpretation of Shh gradients relies on the functional ratio of GliA:GliR and it is important to consider that this response drives both expression of GliA targets but also removes the repression imposed by GliR. The interaction of Shh at the primary cilium is required for Gli processing and so loss of primary cilia can result in complex phenotypes representing either gain or loss of Shh function due to loss of GliR and GliA coupled with the

requirement of the tissue. Here, many of the phenotypes in *Tα3*$^{fl/fl;NesCre}$ cortex can be related to defects in Shh signal transduction.

Considering other pathways in the developing cortex, Wnt is also a key signal able to regulate the size of the brain. Canonical signalling through β-catenin can influence the balance between self-renewal and differentiation. Stabilized beta-catenin causes an enlargement of embryonic brains, not through a simple mitotic effect but due to an increased tendency to maintain the progenitor pool instead of undergoing differentiation (Chenn and Walsh, 2002). Wnt signalling is evident in the E13.5 VZ (Woodhead et al., 2006) and is down regulated in cells as they leave the VZ between E14.5-E15.5. Loss of β-catenin at this stage results in premature neuronal differentiation. The phenotype of the *Tα3*$^{fl/fl;NesCre}$ cortex does not resemble the phenotype of either gain or loss of canonical Wnt signalling, suggesting this signalling pathway isn't significantly affected in mutant cortex.

On first inspection the cortical phenotype of *Tα3*$^{fl/fl;NesCre}$ mice was relatively inconspicuous compared to the major defects seen in other brain regions. The phenotype was also approached cautiously taking into account the close association of the expanded lateral ventricles with the cortical wall. By utilising key developmental stages defects were identified in deep cortical layers which appeared independent of the hydrocephaly. Instead, defects resulted from a loss of primary cilia and the response to Shh and Gli processing was shown to be significantly disrupted in mutant mice.

Chapter 6 – Hippocampal phenotype of *Tα3*$^{fl/fl;NesCre}$ mice

6.1 Introduction

The dentate gyrus of the hippocampus is one of the few regions of the CNS which continues neurogenesis into adulthood (Zhao et al., 2008). Defects in the hippocampus are associated with age-related disease processes such as Alzheimer's disease and vascular disease. In addition, defects in the hippocampus also influence conditions which commonly develop during adolescence such as Schizophrenia and depression (Small et al., 2011). Better understanding how this structure develops will be key to studying stem cell biology and these important disease processes.

The dorsal hippocampus exhibits a complex developmental sequence which was neatly described in studies by Altman and Bayer (1990). During embryogenesis the medial neuroepithelium of the lateral ventricle houses three distinct progenitor populations aligned in a dorso-ventral sequence; those destined to form the pyramidal neurons of Ammon's horn (Ammonic neuroepithelium), those which will form the dentate gyrus (primary dentate neuroepithelium) and those which will form the fimbrial germinal matrix (fimbrial glioepithelium) (Altman and Bayer, 1990b). The formation of Ammon's horn occurs mainly prenatally whereas the majority of dentate gyrus is formed peri- and postnatally.

The pyramidal cells of Ammon's horn are the first identifiable hippocampal structure which are born between in the embryonic neuroepithelium and migrate radially through the intermediate zone to the cortical plate from E14.5 (Nakahira and Yuasa, 2005). At this point, the majority of cortical plate neurons in the neocortex are radially orientated however those destined to form the hippocampus are positioned horizontally and thought to migrate laterally to form the arcing structure of Ammon's horn. Pyramidal neurons which will form the CA3 region are born first, followed by those which will form CA1 yet the final migration and morphogenesis of CA1 is complete far before that of CA3 (Altman and Bayer, 1990a). Whilst this is occurring the initial wave of dentate progenitors are formed in the neuroepithelium around E16.5, these migrate away making a path across the top of the fimbriae and forming a secondary zone of proliferation. The earliest born granule progenitors migrate in a subpial direction, forming an arc or shell outside of the presumptive granule cell layer (GCL), the so-called subpial zone (SPZ). Recent studies have identified the SPZ as an important neurogenic niche that contributes to the early cells of the

GCL and fate mapping has suggested the progenitors also migrate inwards and populate the outer edge of the hilus to form the subgranular zone (SGZ). This process is known as the SPZ-to-hilar transition (Li et al., 2009). The later born granule progenitors provide the majority of granule neurons in the dentate gyrus and it is the SGZ which is responsible for the ongoing neurogenesis into adulthood (Altman and Bayer, 1990b). A summary of dorsal hippocampal development is illustrated in Figure 5.2.

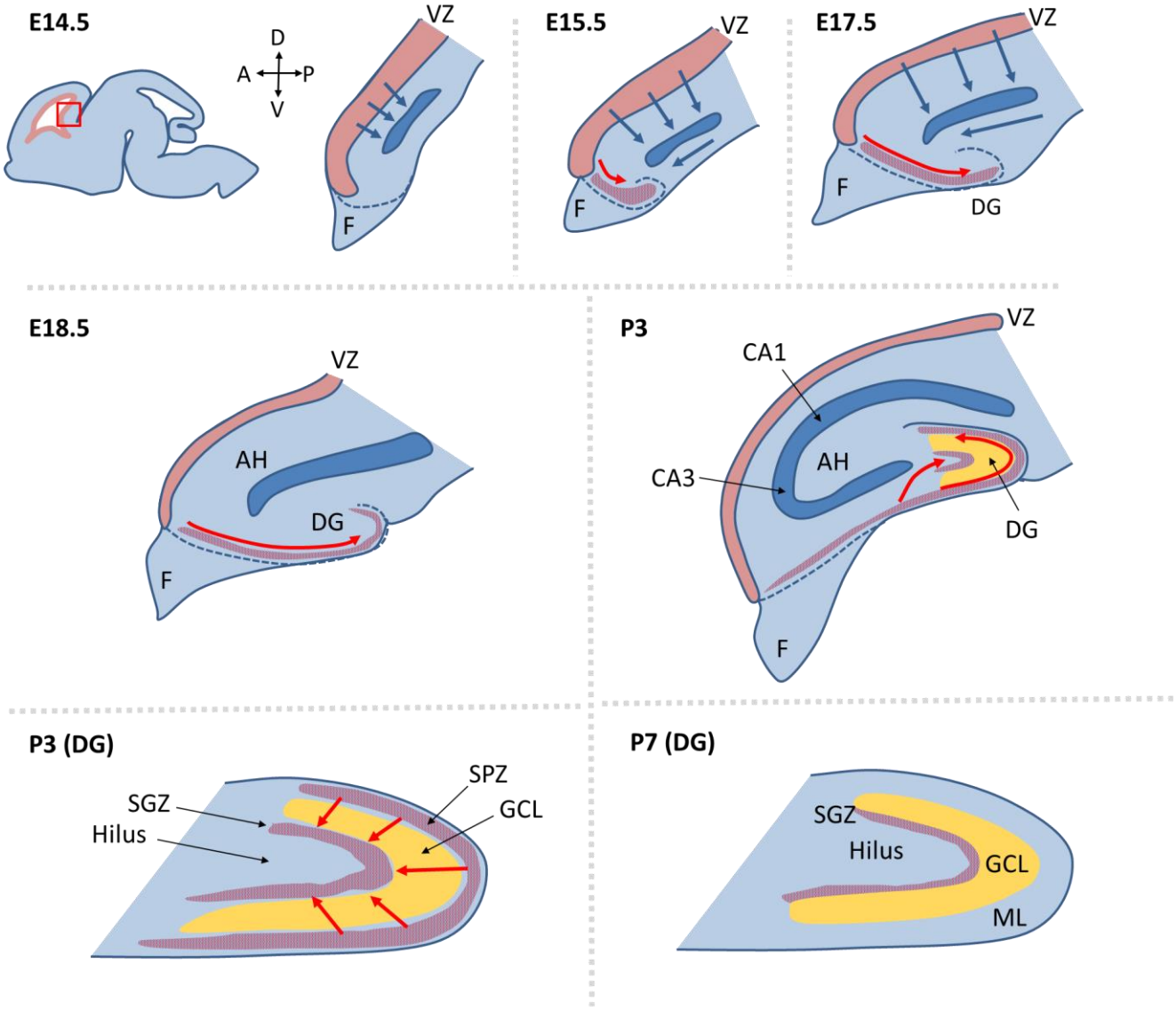

Figure 6.1 Summary of dorsal hippocampus development

Neurons born at E14.5 in ventricular zone (VZ) populate the cortical plate. They then migrate laterally to form Ammon's horn (AH) (navy arrows). E15.5 granule progenitors originating from the VZ and migrate past the fimbrial germinal matrix (F) towards to presumptive dentate gyrus (DG) (red arrows). By E18.5 granule progenitors are present in the dentate gyrus both in the hilus and the outer edge, forming the proliferative sub-pial zone (SPZ). After birth the SPZ progenitors migrate inwards towards SGZ in SPZ-to-hilar transition (red arrows). This is complete by P10. Neurogenesis in the SGZ continues throughout adult life to contribute to the granule cell layer (GCL). Solid red band indicates the VZ, interrupted red indicates dentate granule progenitors, dark blue band indicates pyramidal neurons of AH, yellow band indicates GCL. Compass indicates axis orientation (A, anterior, D, dorsal, P, posterior, V, ventral). Images adapted from (Altman and Bayer 1990) and (Li et al .,2009)

Neurogenesis in the SGZ follows a well characterised process where radial glia-like (type 1) and non-radial glia-like (type 2a) progenitors give rise to intermediate progenitors (type 2b) which proliferate to form neuroblasts (type 3) (Ming and Song, 2011). As these granule neurons mature they move into the GCL and extend dendrites radially into the ML where they make contact with terminal axons of the entorhinal perforant pathway. The granule neurons extend mossy fibres through the hilus to connect with neurons in the nearby CA3 field. In the dorsal hippocampus this pathway is particularly important in spatial memory, whereas the ventral hippocampus has an emerging role regulating emotion and anxiety (Bannerman et al., 2014).

There are a myriad of signals which are proposed to regulate the development of the dentate gyrus. Wnt signalling is required for early hippocampal development with Wnt3a expressed specifically in the cortical hem between 9.75-11 dpc and having an essential role in progenitor proliferation (Lee et al., 2000). Other effectors of the Wnt pathway such as Lef (Galceran et al., 2000) and LRP6 (Zhou et al., 2004) have also been shown to have essential proliferative roles. Shh has also been shown to be required for the proliferation of granule progenitors (Machon et al., 2003) and its transduction through the primary cilium has been shown to be important for hippocampal development (Breunig et al., 2008, Han et al., 2008). The role of both Wnt and Shh continues into adulthood where studies have demonstrated their involvement in proliferation *in vitro* and *in vivo* (Lai et al., 2003, Ahn and Joyner, 2005, Lie et al., 2005).

Here we identify prominent developmental defects in the hippocampus of $Ta3^{fl/fl;NesCre}$ mutant mice. Using a series of peri- and postnatal stages the developmental defects have been described in detail. At E18.5 the hippocampus is very comparable between control and mutant but by early postnatal stages mutants exhibit a loss of proliferation in the dentate gyrus. We further describe the presence of mislocalised progenitors in the GCL and suggest a causative role of the disrupted glial scaffold affecting cellular migration pathway and resulting in defective SPZ-to-hilar transition.

6.2 Results

6.2.1 *Ta3* mutant hippocampus is misshapen with defects in the dentate gyrus

On first inspection the sagittal structure of P15 mutant hippocampus was more elliptical and squashed compared to control, presumably as a secondary consequence of the hydrocephaly (Fig 6.2a). Despite this, mutant mice exhibited a comparable gross organisation of the dentate gyrus and Ammon's horn. Upon closer inspection, the dentate gyrus appeared smaller with a reduced number of cells (Fig 6.2b,c). Measurements of layer thicknesses taken from three control and three mutant mice at P15 demonstrated a 26% and 29% reduction in size of both the GCL and proliferative SGZ respectively (Fig 6.2d). In sections stained with hematoxylin and eosin, mutants exhibited a reduced number of darkly pigmented cells in the SGZ (Fig 6.2b,c) which have previously been identified as a progenitor population (Seri et al., 2001, Han et al., 2008). The region below the SGZ also consistently exhibited a loss of tissue integrity which often resulted in tearing of the section (Fig 6.2b,c).

The mature axonal tracts were identified by labelling for neurofilament (165kDa). In P15 horizontal sections the mutant hippocampus was also more elliptical than control (Fig 6.3a), consistent with observations in the sagittal axis. The mutant dentate gyrus was also clearly smaller; although the GCL displayed a characteristic 'U' shape, the width was reduced compared to control. Despite the reduced size of the mutant dentate gyrus, both CA1 and CA3 fields were comparable in size to the control (Fig 6.3a). Structures caudal to the hippocampus such as the presubiculum (PrS) and parasubiculum (PaS) were also smaller in mutant (Fig 6.3a).

P15 was the latest time point investigated in *Ta3* mutant hippocampus due to the postnatal lethality. To understand the phenotype in greater detail key time points were observed between E18.5 and P15. The earliest stage when the different regions can be easily identified is E18.5. By P5 the pyramidal neurons of Ammon's horn have finished their migration and the SPZ-hilar transition is nearing completion. The structures mature towards P10 and P15 alongside the continued growth in the dentate gyrus SGZ. After this time the proliferation reduces allowing the granule progenitors to slowly maintain the structure into adulthood.

Many of the key axonal connections in the hippocampus have been established by P5. To assess this, mature axons were also labelled for neurofilament (165kDa) in P5 sagittal

sections (Fig 6.3b). The ML above the GCL is the region where axons from the perforant path terminate. Both control and mutant showed a similar density and branching of axonal tracts (Fig 6.3c). Radial axons of the CA1, likely to be pyramidal neurons, were also very comparable between control and mutant (Fig 6.3d). This suggested that pyramidal neurons and connections both in/out of the hippocampus appeared to develop normally, however the dentate gyrus still appeared smaller and underdeveloped.

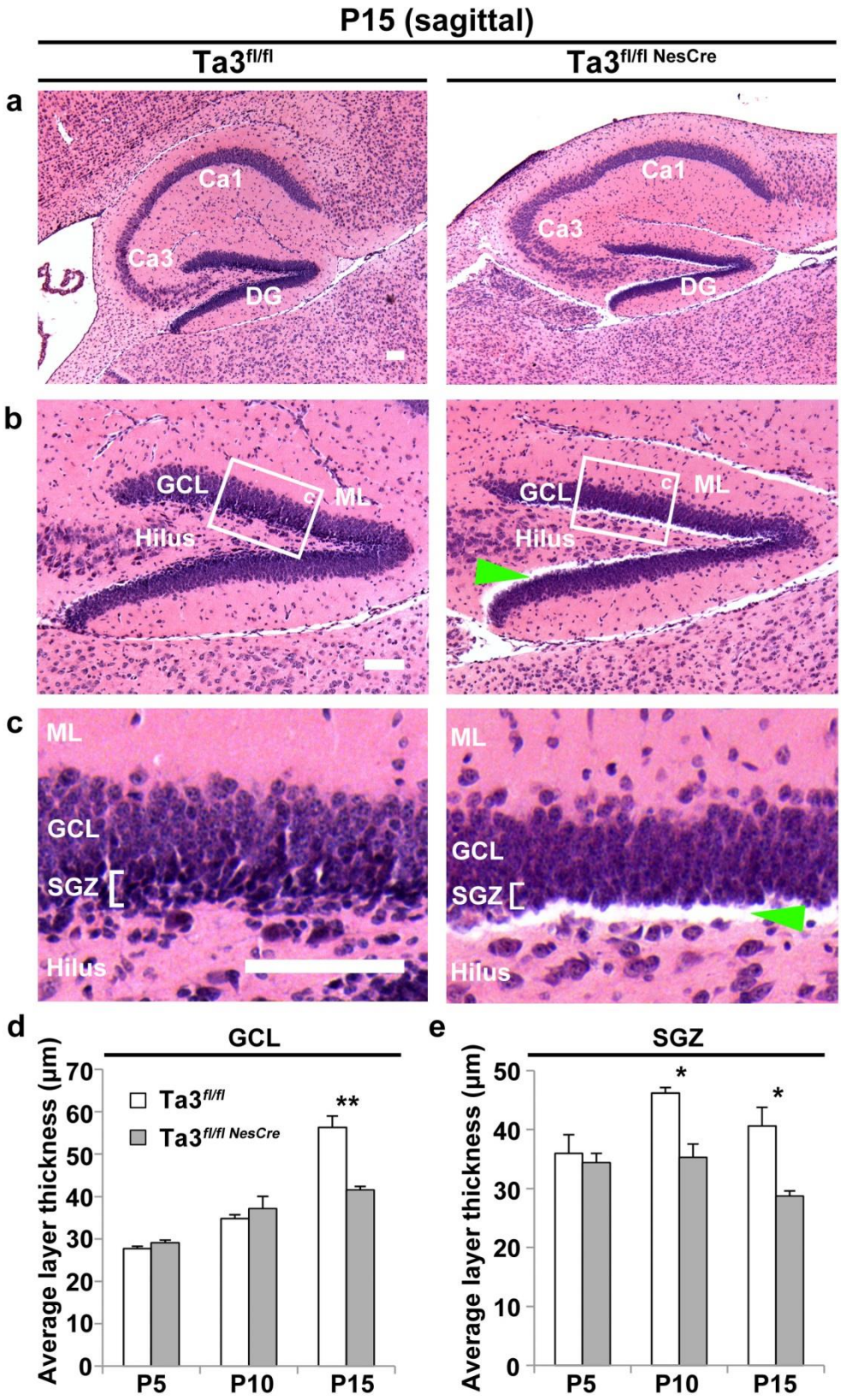

Figure 6.2 *Ta3* mutant hippocampi have comparable gross organisation but thinner SGZ and GCL

(a) Sagittal sections labelled with hematoxylin and eosin showing the dorsal hippocampus. Mutants have a more elliptical shape but gross organisation of Ammon's horn and the dentate gyrus (DG) is similar to control. (b) Higher magnification of DG. Mutants have a thinner granule cell layer (GCL) and a loss of tissue integrity at the subgranular zone (SGZ)/hilus boundary. (c) Higher magnification of GCL. Mutants have a loss of darkly pigmented cells in the SGZ. (d) Quantification of GCL thickness for P5, P10, P15 mice. P15 mutants show a reduction in GCL thickness. (e) Quantification of SGZ thickness for P5, P10, P15 mice. P10 and P15 mutants show a reduction in GCL thickness. Green arrow indicates loss of tissue integrity. Scale; 100µm (a-d). Error bars: (d,e) s.e.m (n = 3), ** P≤0.01, * P≤0.05 (two tailed Students-t test).

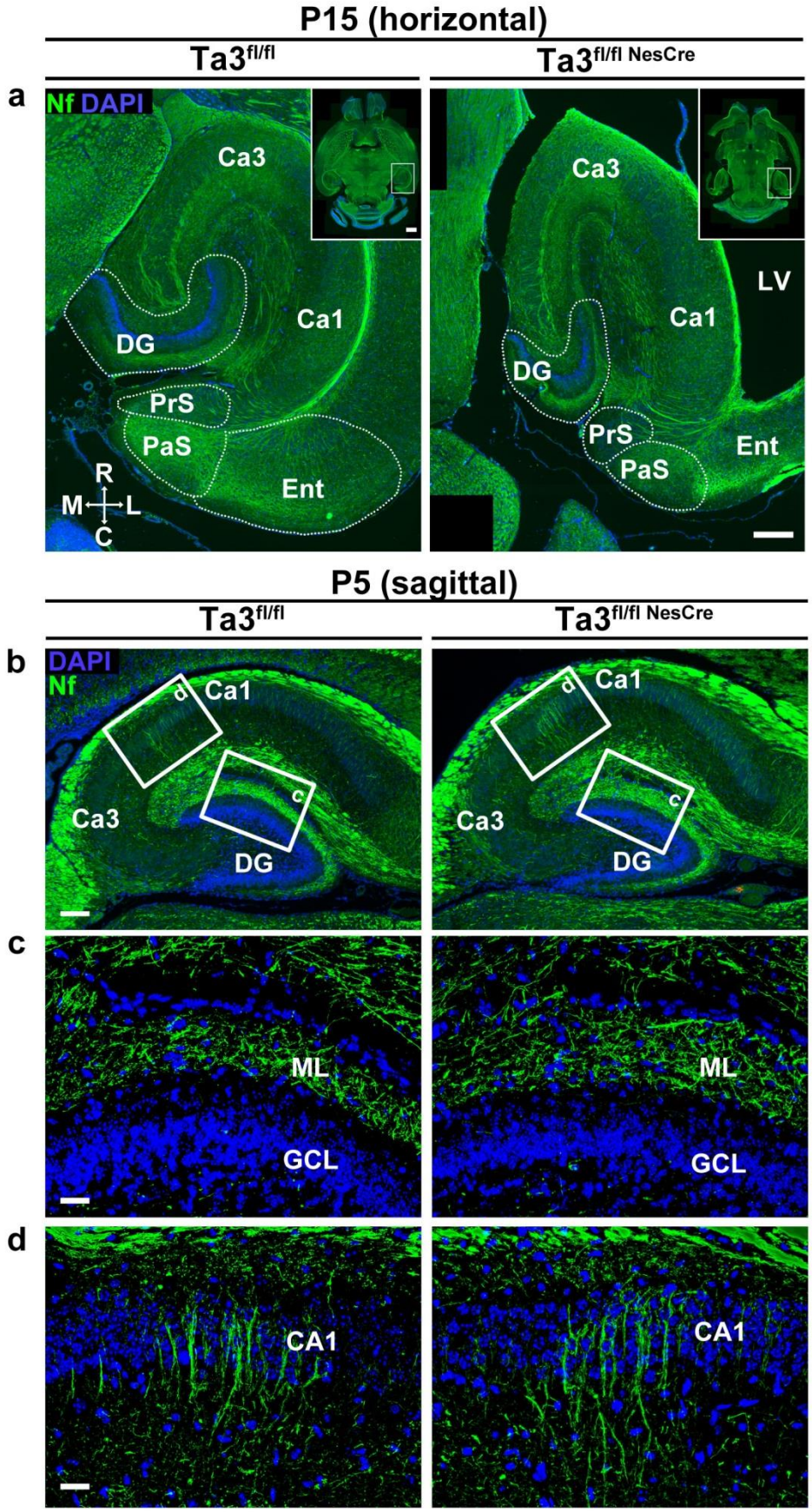

Figure 6.3 Ta3 mutant hippocampi are misshapen but with similar axonal organisation

(a) Horizontal P15 sections labelled for neurofilament (165kDa). Mutant hippocampus is elliptical with a smaller dentate gyrus. The presubiculum (PrS) and parasubiculum (PaS) are reduced in size. Compass indicates orientation; C, caudal, L, lateral, M, medial, R, Rostral. (b) Sagittal P5 sections labelled for neurofilament. White boxes indicate regions of higher magnification. (c) Axons of the performant pathway terminating in the ML and (d) radial axons of the CA1 field are similar between control and mutant. Scale; 250µm (a), 100 µm (b), 25 µm (c, d)

6.2.2 *Ta3* mutant hippocampus lacks primary cilia

As the defect in mutant mice appeared localised to the dentate gyrus, to demonstrate the consequences of Ta3 loss we stained for ACIII in three control and three mutant mice and repeated this at two different ages (Fig 6.4). At E18.5 the hilus, GCL and SPZ were identifiable by their organisation in the dentate gyrus (Fig 6.4a). Primary cilia were visible at this stage and, in control, the majority of ciliated cells were present in the SPZ (Fig 6.4b). In contrast, mutant hippocampus showed a striking loss of primary cilia. In P15 control dentate gyrus, the majority of the predominantly quiescent GCL exhibited primary cilia (Fig 6.4c). This was dramatically reduced in mutants with a 70% decrease in the percentage of ciliated cells (Fig 6.4d). Many of the cells in the SGZ are dividing progenitors and therefore fewer exhibit primary cilia which were often smaller in length. Despite this, a significant reduction of 80% in ciliated cells was also measured in the mutant SGZ.

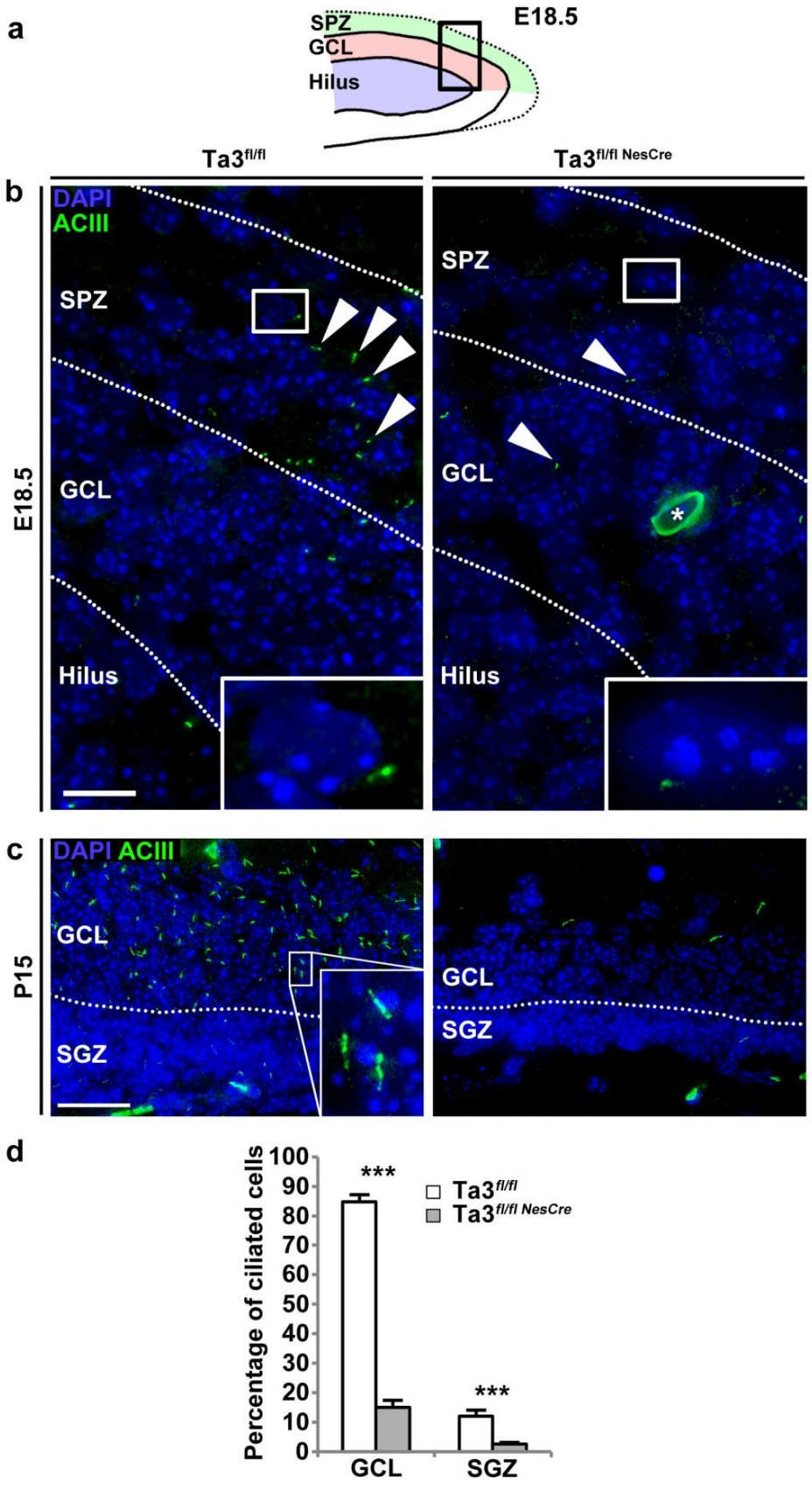

Figure 6.4 *Ta3* mutant dentate gyri have loss of primary cilia

(a) Illustration of 18.5 dentate gyrus with box indicating field of view in (b). (b) E18.5 dentate gyrus labelled with ACIII (green). Control primary cilia are found primarily in the SPZ. Mutants have a striking loss of primary cilia in all regions. (c) P15 dentate gyrus labelled with ACIII (green). Control primary cilia are found primarily in the granule cell layer (GCL). Mutant has a striking loss of primary cilia. (d) Quantification of ciliated cells in the subgranular zone (SGZ) and GCL. Mutant has a significant reduction in both regions. Scale 25µm (b,c). Error bars: (d) s.e.m (n = 3), *** P≤0.001 Students T-test. Single asterisk in (b) indicates autofluorescence.

6.2.3 Progenitors and mature neurons are mislocalised in *Ta3* mutant hippocampus

Progenitors and mature neurons were identified throughout the development of the dentate gyrus at ages E18.5, P5, P10 and P15 by staining for Pax6 and NeuN respectively (Fig 6.5). Interestingly, the outer boundary of the mutant GCL had reduced definition and a 2.4 fold increase in the number NeuN-positive cells mislocalised in the ML (Fig 6.5b). Quantitation from three control and three mutant mice demonstrated a significant increase in mislocalised mature neurons from P10 onwards (Fig 6.5d). Mutants also had a reduced number of Pax6-positive progenitors in the forming SGZ (Fig 6.5b) and quantitation revealed a significant reduction of 37% and 34% at P10 and P15 respectively (Fig 6.5c). The other surprising observation was the presence of ectopic Pax6-positive progenitors in the mutant GCL (Fig 6.5b). At younger stages between E18.5-P5 there are high numbers of progenitors present in the control GCL, reflecting the cell migration in the SPZ-to-hilar transition (Li et al., 2009) (Illustrated in Fig 6.1). Quantification from three control and three mutant mice revealed that by P15, mutants had a 6.1 fold higher number of Pax6-positive progenitors in the GCL compared to control (Fig 6.5c). Mutants also appeared to have an increased in the number of Pax6-positive progenitors in the GCL compared to control however this was not statistically significant.

Intermediate progenitors (type 2b) and proliferating cells were identified by labelling for Tbr2 and PCNA respectively in the P10 dentate gyrus (Fig 6.6a). It is likely that proliferating cells which are PCNA-positive but Tbr2-negative are RGC (type-1) or non-radial glial progenitors (type-2a). Mutant dentate gyrus showed a reduction in glial progenitors and intermediate progenitors, particularly evident in the SGZ. Mutants also showed ectopic progenitors of both types in the GCL consistent with the observations in Pax6 staining. To look at the level of cycling cells, BrdU was administered to mice two hours before sacrifice of P15 mice. Identification of incorporated BrdU demonstrated that mutants had a reduction of 70% in the number of cycling cells in the SGZ (Fig 6.6b,c). At this age, only a low number of BrdU-positive cells were identified in both control or mutant GCL and a significant difference was not observed (Fig 6.6c).

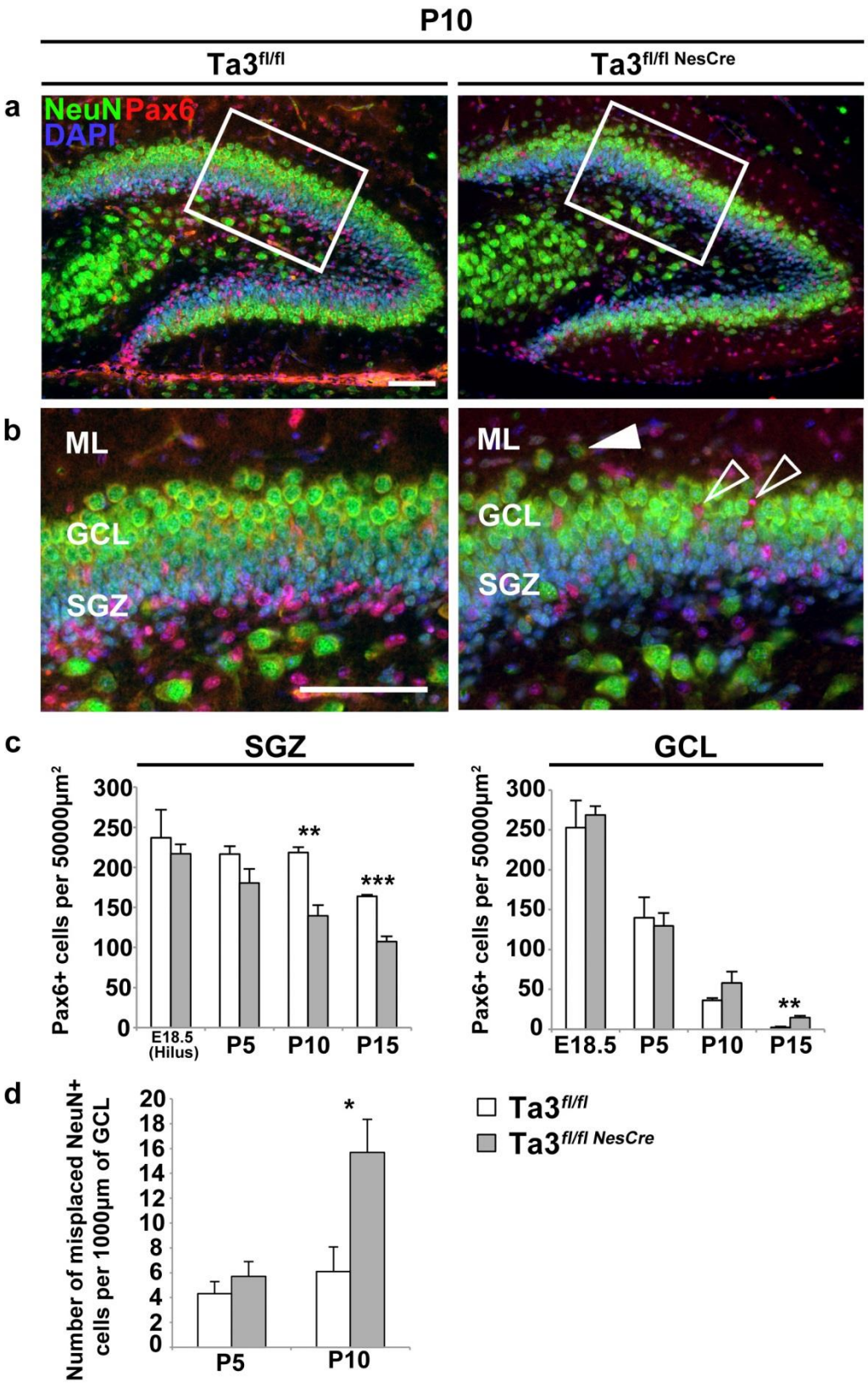

Figure 6.5 *Ta3* mutant hippocampi have reduced SGZ progenitors, misplaced GCL progenitors and ectopic mature neurons. (a) P10 dentate gyrus labelled with NeuN (green) and Pax6 (red). Box indicates region of higher magnification in (b). Mutants exhibit a loss of Pax6+ progenitors in the subgranular zone (SGZ) but an increase in the granule cell layer (GCL) (hollow arrows). Mutants also have ectopic NeuN+ neurons mislocalised outside of the GCL (white arrow). (c) Quantification of Pax6 progenitors in the SGZ and GCL. Mutant SGZ progenitors are significantly reduced from P10 onwards. Mutant GCL progenitors are significantly at P15. (d) Quantification of NeuN neurons mislocalised outside the GCL. Mutants have a significant increase from P10 onwards. Scale, 75µm (a, b). Error bars: (c,d) s.e.m (n = 3), * P≤0.05, ** P≤0.01, *** P≤0.001 Students T-test.

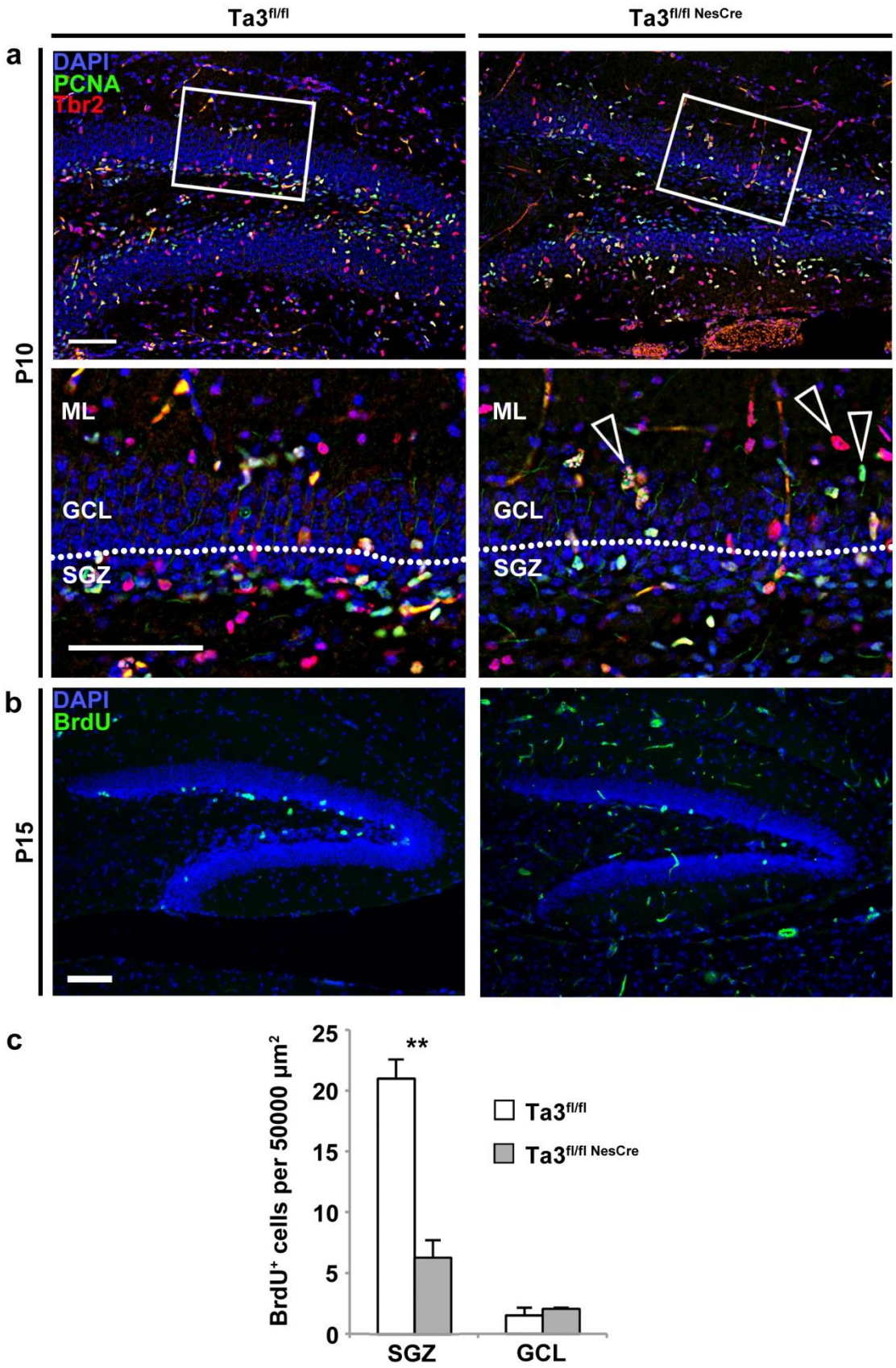

Figure 6.6 P15 *Ta3* mutant SGZ has fewer radial glia cells and intermediate progenitors

(a) P10 mutant dentate gyrus labelled for PCNA (green) and Tbr2 (red). Mutant has a loss of progenitors in the SGZ and ectopic progenitors in the SGZ (arrows). (b) BrdU was administered to P15 mice two hours before euthanasia. Immunohistochemical identification of BrdU incorporation in the dentate gyrus. BrdU positive cells were easily identifiable in the subgranular zone (SGZ) but few were visible in the granule cell layer (GCL). (c) Quantitation of BrdU+ cells demonstrated that mutants had a significant reduction in the SGZ. Scale, 75 µm (a), 100µm (b). Error bars: (b) s.e.m (n = 3), *** P≤0.001 Students T-test.

6.2.4 *Ta3* mutant hippocampus has loss of glial progenitors and intermediate progenitors

The progenitor defects were better identified by co-labelling cells for proliferating and quiescent precursor marker MCM2 and for proliferation marker Ki67. At E18.5, quantitation from three control and three mutant mice showed no significant difference in the number of MCM2-positive or Ki67-positive cells in the dentate gyrus (Fig 6.7a). Quantification in the SPZ (Fig 6.7b,c) and in the primitive GCL or the forming hilus below (Fig 6.8d,e) was unable to identify a statistical difference in any of the regions.

The similarity between control and mutant progenitors was confirmed by labelling E18.5 dentate gyrus for additional proliferative markers PCNA and PH3 (Fig 6.7d). Consistent with previous observations, the density of cycling cells and their level of proliferation was very comparable. Closer analysis of slides stained with Pax6 and NeuN also exhibited little difference between control and mutant, with progenitors clearly visible in the SPZ and GCL with the initial compaction of mature neurons in the presumptive GCL (Fig 6.7e). This demonstrates that, despite having loss of primary cilia at E18.5 (Fig 6.4d), the mutant hippocampus proliferates normally and defects occur only postnatally.

Staining for MCM2 and Ki67 was also completed at P5, P10, P15 and the number of cells quantified (Figure 6.8a-e). Mutants exhibited a significant decrease of 51% in the total number of proliferating Ki67-positive cells in P5 SGZ but no reduction was seen in the number of MCM2-positive progenitors when compared to control (Fig 6.8a,d,e). The total number of proliferative cells were significantly reduced by 45% in P10 mutant SGZ and although not significant there also appeared to be a reduction in the number of MCM2-positive progenitors. This difference in the SGZ became more apparent by P15 with mutants exhibiting a 63% reduction in MCM2-positive progenitors and 71% reduction in Ki67-positive proliferating cells compared to control (Fig 6.8b-e).

To better assess the progenitor population the number of cells single- or double-labelled for MCM2 and Ki67 were quantified. Compared to control, mutants were found to have a greater proportion of SGZ progenitors that were not dividing (MCM2-positive, Ki67-negative) and this was evident as a 10%, 5% and 14% increase at ages P5, P10 and P15 respectively, however the percentage change at P10 was not found to be statistically significant (Fig 6.9a). This meant that in addition to having fewer MCM2-positive progenitors in the SGZ, fewer of them were actively proliferating thus acting to deplete the progenitor pool.

GFAP is a marker of radial- and non-radial glial progenitors (type 1 and 2a), however it is also present in astrocytes present in the dentate gyrus. By double labelling for GFAP and Ki67 it is possible to preferentially identify the proliferating glial-progenitor population (Fig 6.9c,d). Quantification of the proportion of Ki67-positive progenitors that were GFAP-positive or GFAP–negative demonstrated that there was no statistical difference between the proportions of glial- and non-glial progenitors in the P15 SGZ when comparing control and mutant (Fig 6.9e). Given the total number of Ki67-positive cells was reduced, this leads us to the conclusion that in the SGZ there is a decline in the number of both glial progenitors and intermediate progenitors. This depletion is the likely cause of the hypoplasia seen in the GCL at later stages.

Despite the progressive depletion of progenitors seen in the mutant SGZ, the total number of MCM2-positive and Ki67-positive cells appeared to show a slight increase from P10 onwards (Fig 6.8d,e). Although these data were not significantly different they follow the same trend seen with the level of Pax6-positive cells also observed in the mutant GCL at this age (Fig 6.5c). By P15 the total levels of MCM2-positive and Ki67-positive cells in the control and mutant GCL had reduced to lower levels, however, mutants still appeared to show a higher number of cells, with there being significantly more MCM2-positive cells compared to control (Fig 6.8d,e).

Although the numbers of cells were low, analysis of single- and double-positive cells showed that, compared to P5 and P10, P15 control GCL has a greater proportion of proliferating cells which are MCM2-negative (Ki67-positive, MCM2-negative) (Fig 6.9b). This marks a shift in the type of proliferating cell present in the GCL and indicates the completion of the SPZ-to-hilar transition. In comparison, mutant P15 GCL has a 25% higher proportion of proliferating cells which are MCM2-positive (Ki67-positive, MCM2-positive) compared to the control P15 GCL (Fig 6.9b). Interestingly, the proportions of ectopic cells seen in the P15 mutant GCL more closely resembles those seen in the P15 SGZ (Fig 6.9a,b). Furthermore, a high percentage of the proliferating cells in mutant GCL are also GFAP-positive which suggests the ectopic progenitors found in the mutant GCL are mislocalised glial-progenitors (Fig 6.9f).

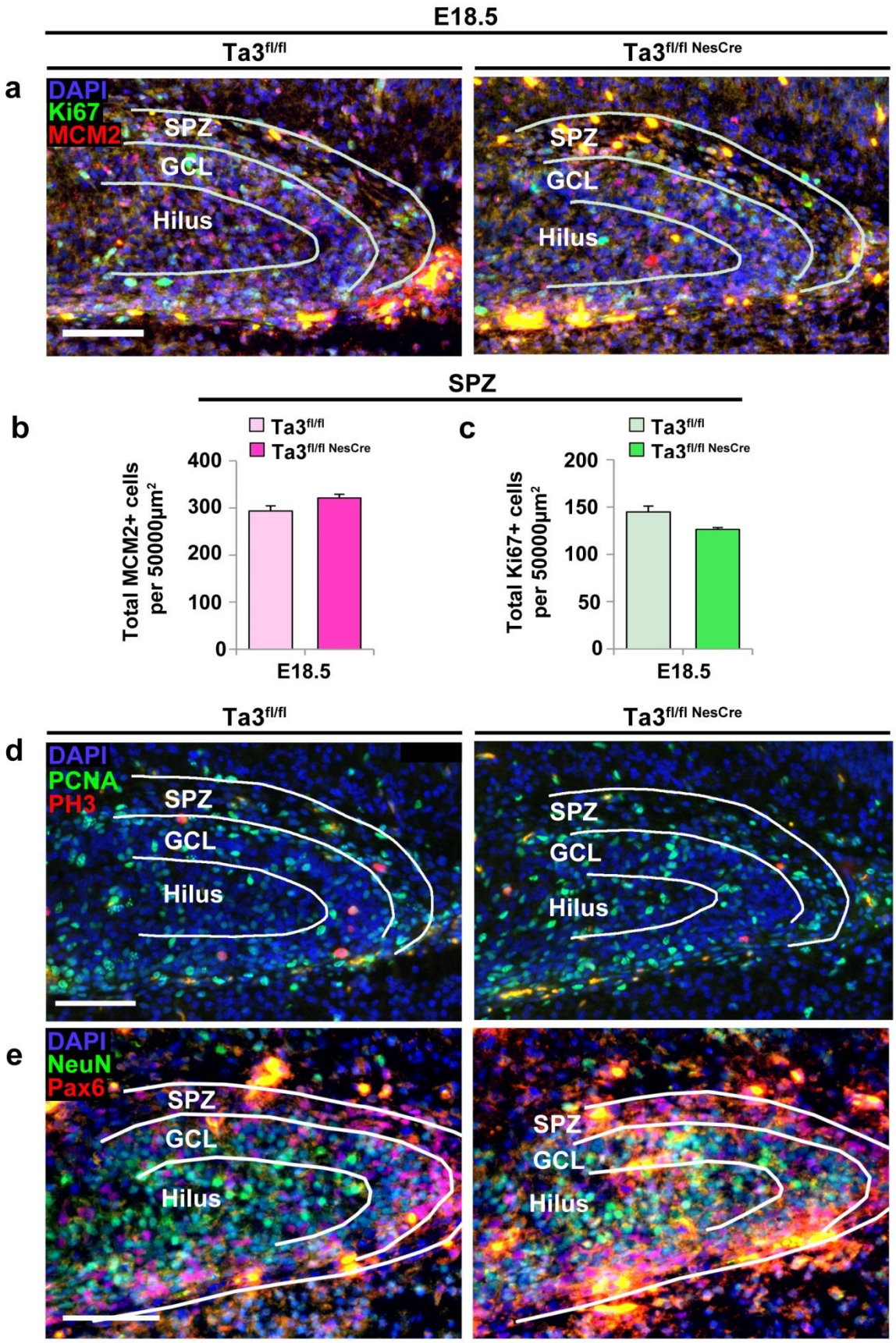

Figure 6.7 E18.5 *Ta3* mutant mice have normal dentate gyrus

(a) E18.5 dentate gyrus labelled for Ki67 (green) and MCM2 (red). (b) Quantification of total MCM2+ progenitors in the subpial zone (SPZ). (c) Quantification of total Ki67+ progenitors in the SPZ. Mutants show no difference in number of MCM2+ or Ki67+ progenitors. (d) E18.5 dentate gyrus labelled for PCNA (green) and PH3 (red). (e) E18.5 dentate gyrus labelled for NeuN (green) and Pax6 (red). Control and mutant show a comparable distribution of proliferating cells, progenitors and mature neurons. GCL, granule cell layer. Scale, 75µm (a,e). Error bars: (b) s.e.m (n = 3).

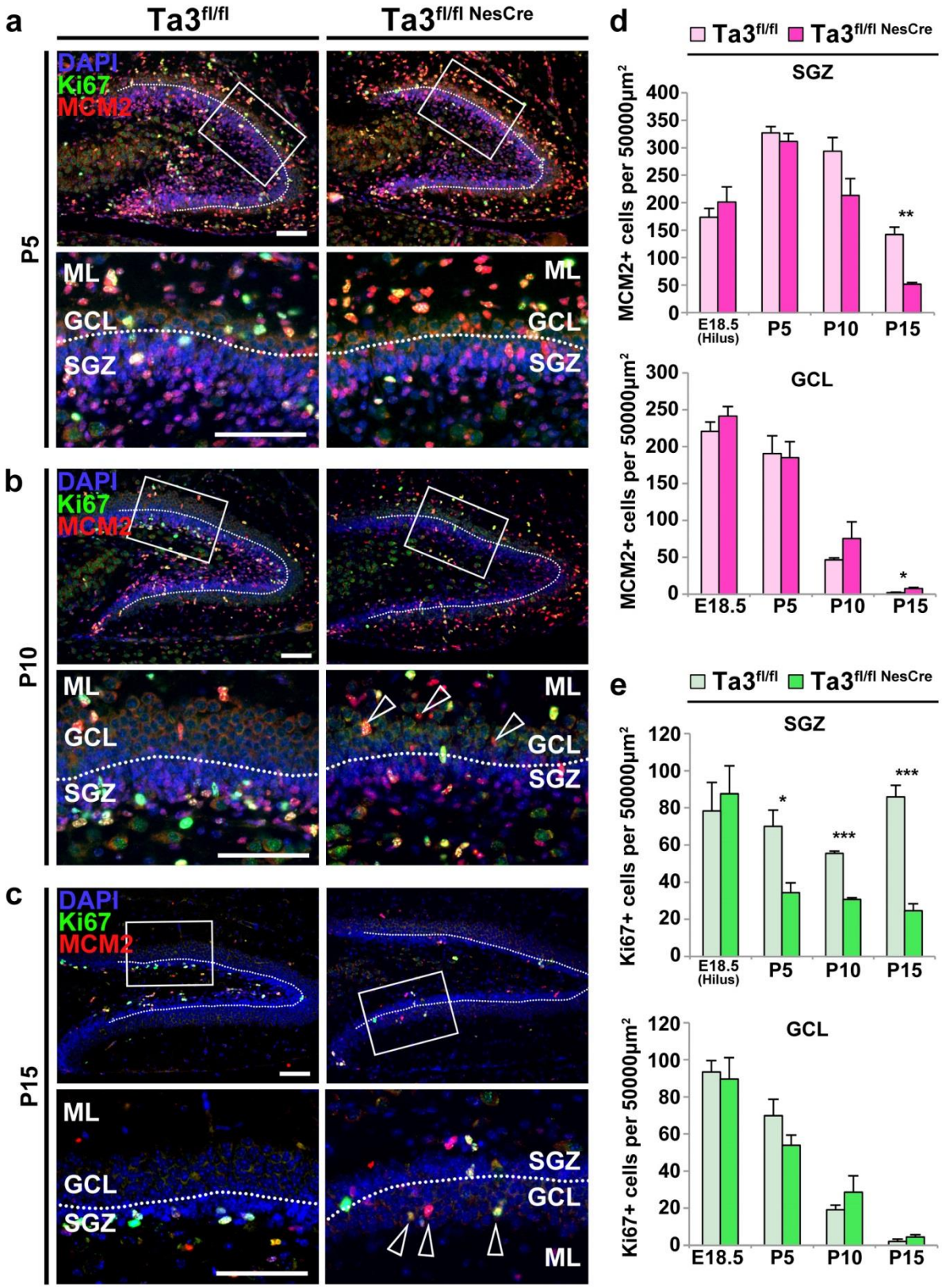

Figure 6.8 *Ta3* mutant mice have loss of SGZ progenitors and ectopic GCL progenitors

Dentate gyrus labelled for Ki67 (green) and MCM2 (red) at P5 (a), P10 (b) and P15 (c). White boxes indicate regions of higher magnification. Hollow arrows indicate ectopic progenitors in the mutant GCL. Note that in (c) area of higher magnification is on lower blade of DG resulting in reversed order of subgranular zone (SGZ), granule cell layer (GCL) and ML (ML). (d) Quantification of total MCM2+ progenitors. Mutants show significant loss in the SGZ and significant gain in the GCL at P15. (e) Quantification of total Ki67+ progenitors. Mutants show significant loss in the SGZ from P5 onwards. Scale, 75µm (a-c). Error bars: (d,e) s.e.m (n = 3), * P≤0.05, ** P≤0.01, *** P≤0.001 Students T-test.

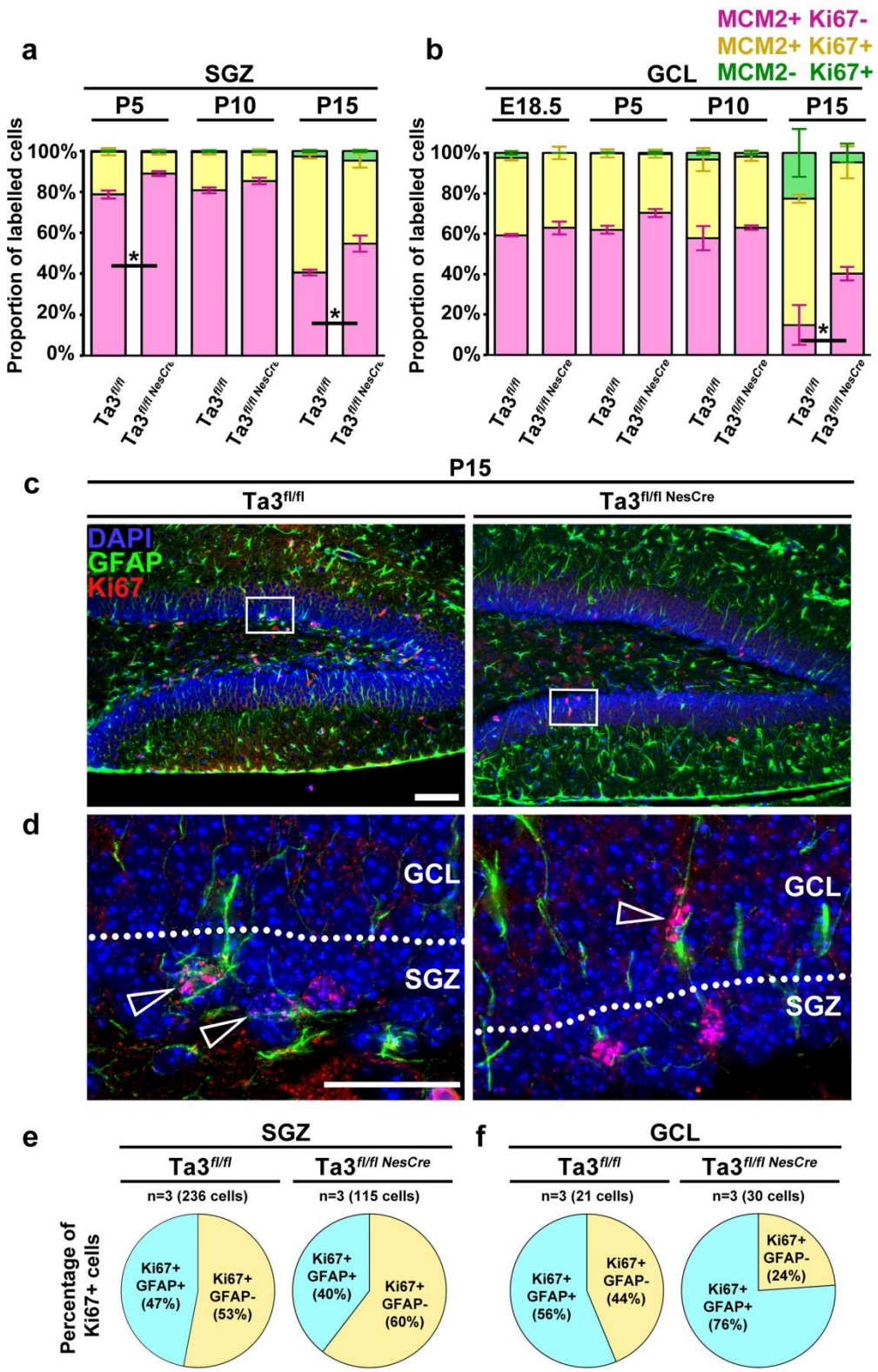

Figure 6.9 *Ta3* mutant SGZ has a lower proportion of proliferating progenitors

(a) Proportion of cells labelled for MCM2, Ki67 or both in the SGZ. At P5 and P15 Mutants have a significant increase in the proportion of MCM2-positive progenitors which are Ki67 negative (red). (b) Proportion of cells labelled for MCM2, Ki67 or both in the GCL. At E18.5, P5 and P10 mutants have similar proportions of progenitors in the GCL. At P15 control has an increase in the number of proliferating cells which are MCM2 negative (green). Mutants have a distribution more similar to that seen in the SGZ. (c) P15 dentate gyrus labelled for GFAP (green) and Ki67 (red). White box indicates region of higher magnification shown in (d). (e) Proportion of Ki67-positive cells which are likely to be RGC-progenitors (Ki67-positive, GFAP-positive, blue) in the P15 SGZ. Control and mutant have a similar proportion of cells. (f) Proportion of RGC-progenitors (Ki67-positive, GFAP-positive, blue) in the GCL. Mutant have a greater proportion of RGC-progenitors. Due to low cell numbers in control, statistical tests were not completed on this condition. Scale, 75µm (a-c). Error bars: (a,b) s.e.m (n = 3), * P≤0.05, ** P≤0.01, *** P≤0.001 Students T-test.

6.2.5 Mislocalised progenitors correlate with poorly formed cellular scaffolds

Doublecortin (Dcx) is a cytoskeleton component closely associated with neurogenesis and migration (Francis et al., 1999, Brown et al., 2003). To try and explain the presence of misplaced progenitors and mature neurons in the mutant dentate gyrus, the distribution of Dcx was analysed throughout ages E18.5 to P15 (fig 6.10a-c). At E18, expression of Dcx in the control dentate gyrus were very low and hard to detect immunohistochemically. The levels increased by P5 and in the control dentate gyrus the strongest expression was evident at the boundary of the GCL and ML (fig 6.10a). At this stage, little difference was observed between control and mutant Dcx expression. By P10, the control dentate gyrus exhibited an increase in the level of Dcx in the SGZ (Fig 6.10b). Dcx-positive fibres were also seen stretching through the GCL towards the ML. This increase was not observed in the mutant SGZ or GCL yet, despite this, both the ML and hilus appeared to have relatively normal expression levels of Dcx compared to control. By P15, the level of Dcx in control increased further and was now evident as a thick band labelling the SGZ (Fig 6.10c). The fibres stretching through the GCL were also more obvious and many could be traced from SGZ through to the ML. Mutants showed a striking absence of the thick Dcx band in the P15 SGZ and this correlated with the loss of tissue integrity (indicated by solid line, Fig6.10c). Dcx fibres stretching through the P15 mutant GCL were also far less distinct. Although the distribution of mutant Dcx demonstrated a prominent phenotype, it seemed to correlate more with the loss of progenitors in the SGZ. Given the ectopic progenitors seen in the mutant GCL, it could even be reasonable to expect increased Dcx fibres however this was not observed at later stages.

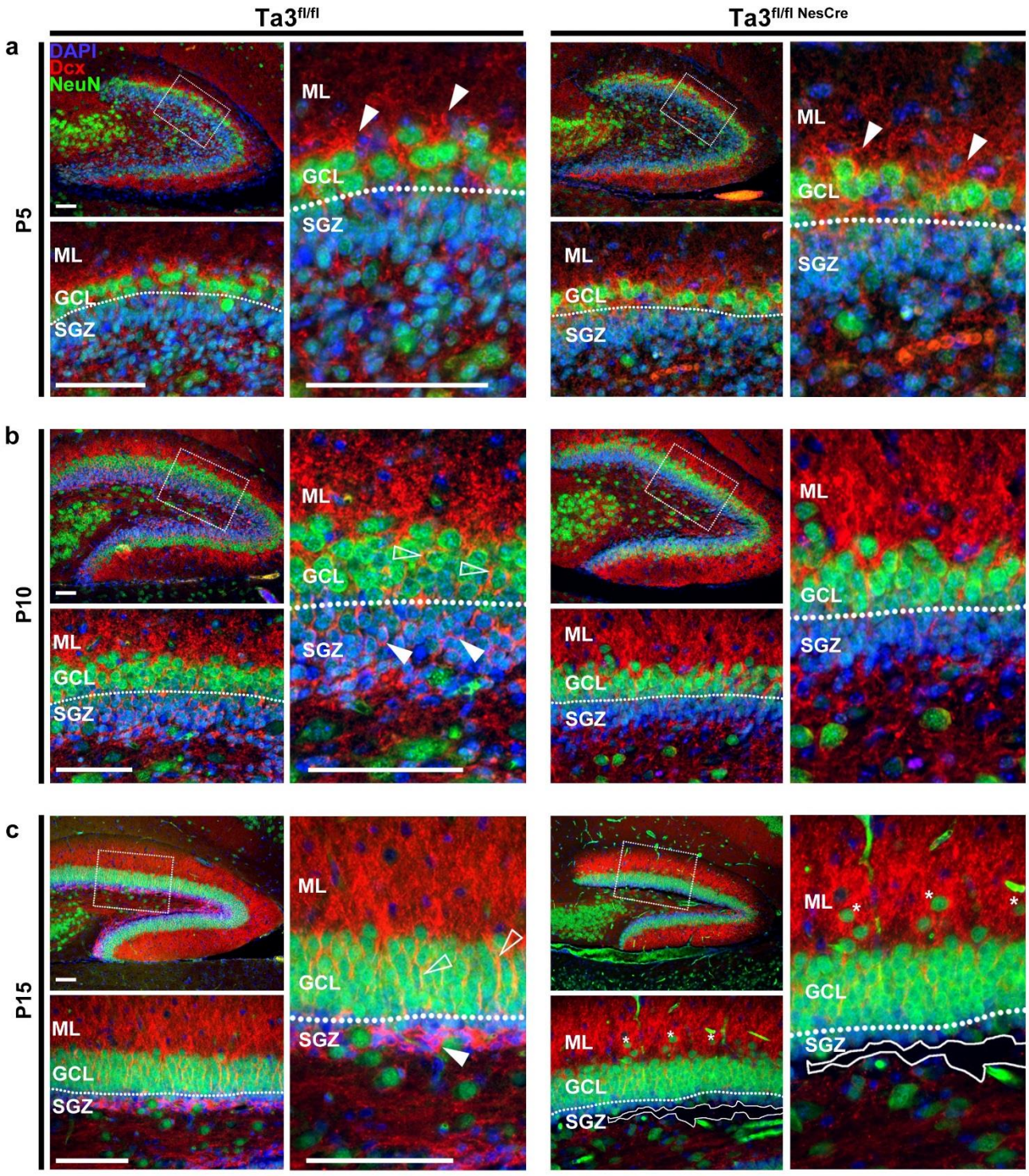

Figure 6.10 *Ta3* mutant dentate gyri have loss of Dcx in the SGZ and GCL

Dentate gyrus labelled for Dcx (red) and NeuN (green). (a) In P5 dentate gyrus the majority of Dcx is found at the boundary of the granule cell layer (GCL) and ML (ML) (white arrows). Control and mutant show a comparable level of Dcx. (b) P10 control dentate gyrus has increased levels of Dcx with fibres found in the SGZ (white arrows) and GCL (hollow arrows). This increase is far less evident in mutant SGZ and GCL. (c) P15 control dentate gyrus has thick band of Dcx in SGZ (white arrow) with fibres stretching throughout the GCL (hollow arrows). Mutants have a striking loss of Dcx in both regions. Loss of tissue integrity indicated by white line. Asterisks indicate mature neurons mislocalised in the ML (ML). Scale, 75µm (a-c).

Many of the cell movements in the developing hippocampus are thought to be directed by glial-guided migration along radial fibres. The glial scaffold was assessed at P5 by co-labelling for GFAP and nestin where double-positive cells represent glial-progenitors (type 1 and type 2a) (Encinas and Enikolopov, 2008) (Fig 6.11a). In the control dentate gyrus both GFAP-positive and nestin-positive fibres extended radially through the GCL and then branched extensively throughout the ML. There were two general types of fibre; thicker primary fibres with simple radial organisation which then bifurcate into thin diffuse fibres with widespread branching. Under close examination, all visible fibres shared some colocalisation of both GFAP and nestin (Fig 6.11b). In the thicker primary fibres, GFAP had a more continuous distribution whereas nestin was often intermittent along the length of the fibre. This high level of colocalisation is a result of the large number of glial-progenitors present at this age. The mutant dentate gyrus had a dramatic loss of both types of fibre (Fig 6.11b). Most obvious was the loss of fine branches present in the ML. Mutants also had fewer primary fibres which appeared thickened. The reduction of primary fibres is likely to represent a loss of RGC progenitors, however the distinct loss of fine branching suggests a defect in the glial cell morphology.

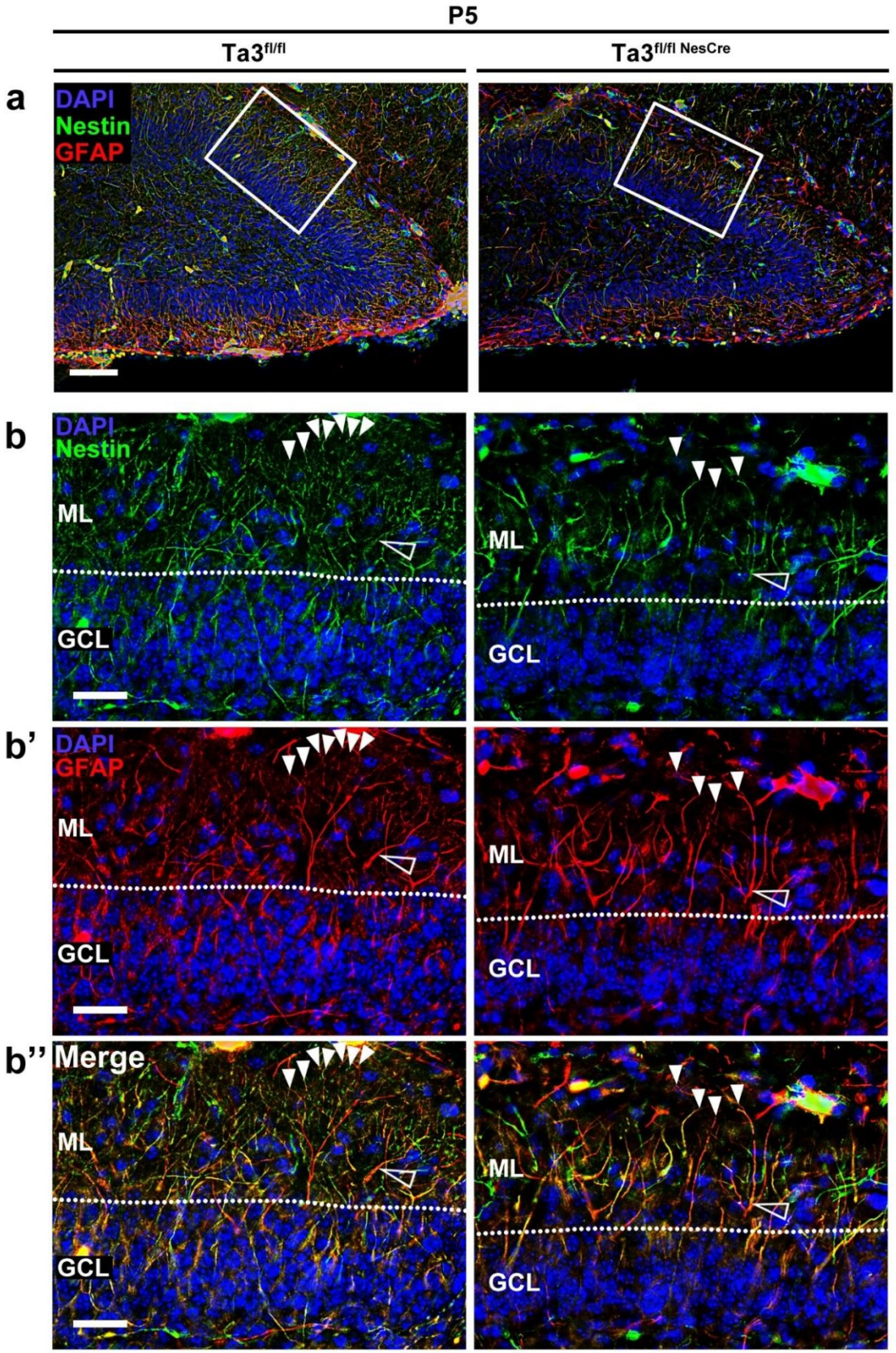

Figure 6.11 *Ta3* mutant dentate gyri have a defective glial scaffold

P5 dentate gyrus labelled for nestin (green) and GFAP (red). (a) Image of whole dentate gyrus with boxed region indicating region of higher magnification. (b) nestin expression, (b') GFAP expression, (b'') merge. Mutant has a loss of fine widely branched fibres (white arrows) and primary fibres which appear thickened (hollow arrow). In all fibres, GFAP and nestin show regions of colocalisation representing the high level of RGC progenitors at this age. Scale, 75 µm (a), 25 µm (b).

It is possible that the glial defect contributed to the ectopic progenitors seen in the mutant GCL. To test this, sections were colabelled for GFAP and progenitor marker Pax6. At E18.5, control exhibited a dense network of GFAP-positive fibres in the SPZ with a small number of fibres present in both the hilus and presumptive GCL (Fig 6.12a). In mutant there was also a dense GFAP network in the SPZ where there appeared to be a very subtle reduction in the density of fibres. Pax6-positive progenitors were comparable between control and mutant at E18.5 (Fig 6.12a), consistent with earlier observations (Fig 6.7c).

In the P5 dentate gyrus, consistent with earlier observations, the mutant dentate gyrus exhibited a striking reduction in glial fibres and extent of branching but no difference in the number of progenitors present in the GCL was evident (Fig 6.12b). When comparing the progenitors migrating through the GCL many of the mutant cells were not obviously associated with glial fibres. In a similar experiment, type 1 and type-2b progenitors were identified by Sox2 labelling in addition to GFAP (Fig 6.13a-c). Interestingly, many of the mutant glial fibres appeared overloaded with many progenitors on a single fibre (Fig 6.13c). This was in contrast to control where, despite having a similar number of progenitors, they appeared to have better distribution across the glial scaffold. It is possible that the disrupted scaffold in mutant dentate gyrus limits access to glial fibres or restricts their pathway to the SGZ. This in-turn could delay or inhibit their SPZ-to-hilar transition resulting in ectopic progenitors evident in the GCL from P10.

Another important factor in the migration of hippocampal neurons and their dendritic branching is Reelin, an extracellular protein expressed by Cajal-Retzius cells in the ML (Niu et al., 2004). Reelin has been shown to be important in the movement of progenitors away from the SPZ towards the SGZ (Li et al., 2009). It has also been demonstrated that Reelin is required for the correct formation of the RGC scaffold (Weiss et al., 2003, Frotscher et al., 2003) and is required for the correct migration of postmitotic granule neurons born in the SGZ (DelRio et al., 1997, Teixeira et al., 2012). In control P5 dentate gyrus, Reelin producing cells can clearly be seen at the outer edge of the ML (Fig 6.14). Mutant dentate gyrus still had Reelin producing cells at the edge of the layer and they displayed the simple characteristic morphology. However, there appeared to be a slight reduction in the number of Reelin-positive cells which was most evident in posterior region above the dorsal blade of the dentate gyrus (Fig 6.14). This slight defect could be a

contributing factor to the disrupted migration seen by granule progenitors or postmitotic granule neurons.

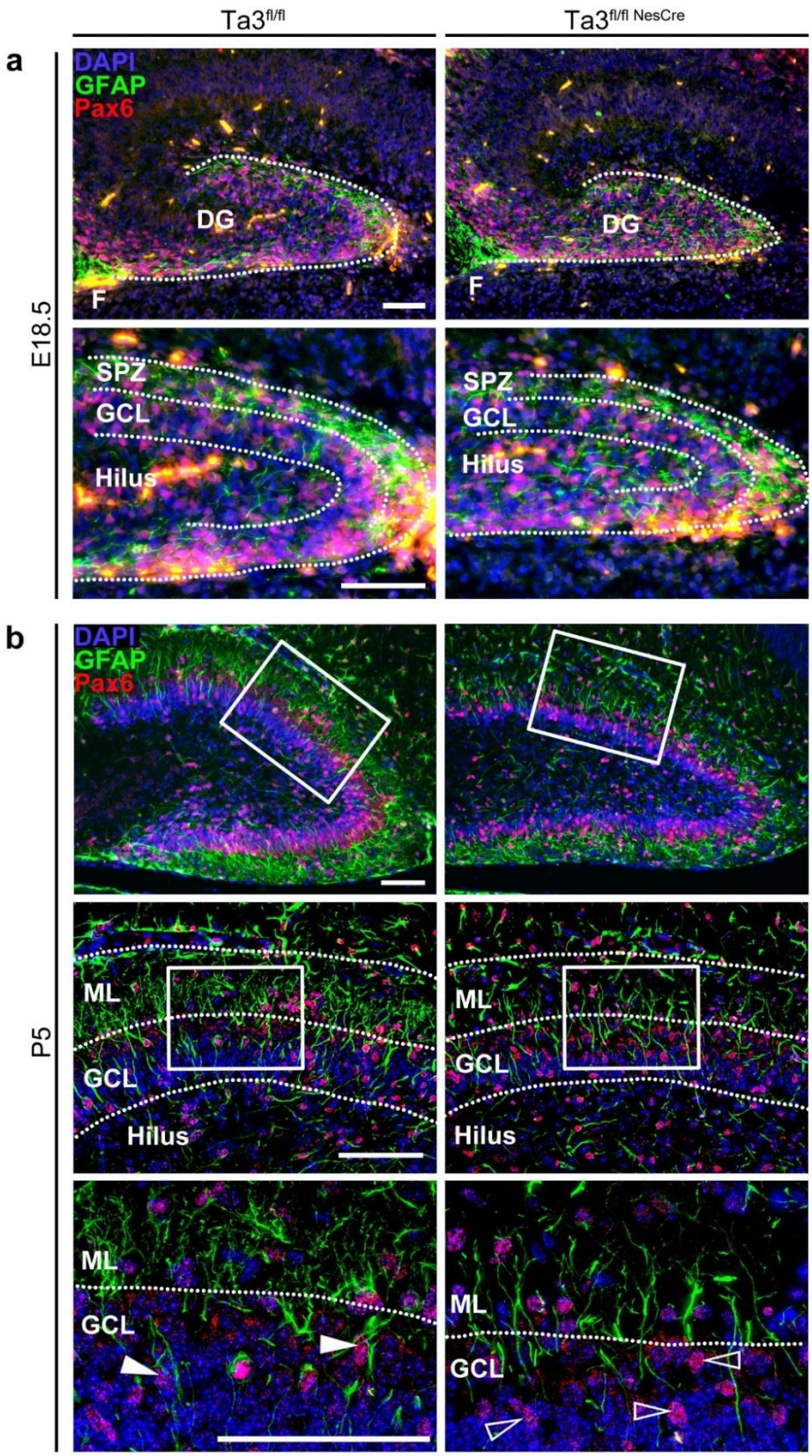

Figure 6.12 Fewer P5 *Ta3* mutant progenitors are associated with GFAP fibres

(a) E18.5 dentate gyrus labelled for GFAP (green) and Pax6 (red). Control and mutant both have dense fibres in the SPZ however mutant has a subtle reduction. (b) P5 dentate gyrus labelled for GFAP and Pax6. Mutant has a striking reduction in branches throughout the ML and fewer progenitors are seen associated with glial fibres. White boxes indicate regions of higher magnification. Progenitors associated with glial fibres (white arrows) and without glial fibres (hollow arrows). Scale, 75µm (a-b).

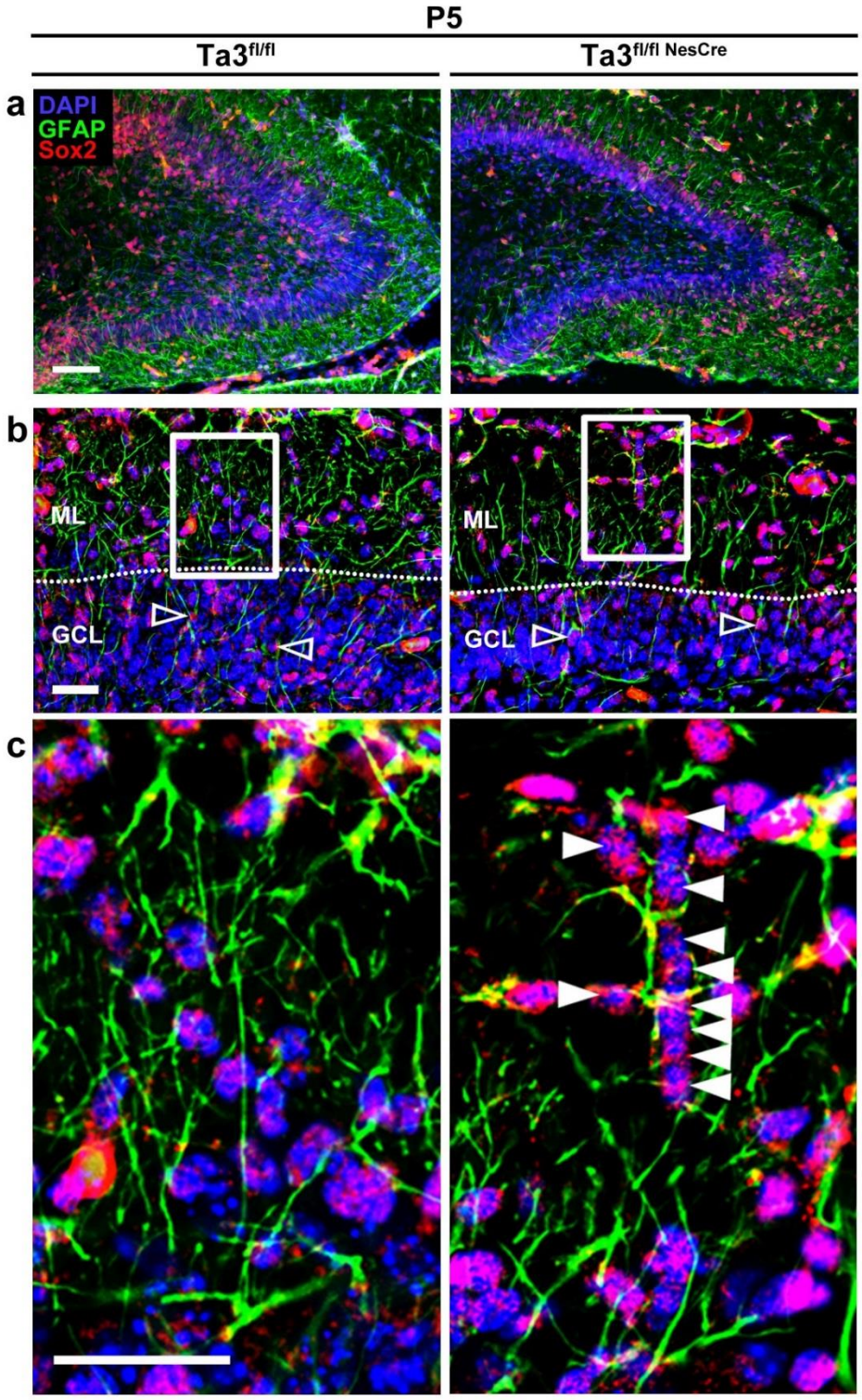

Figure 6.13 *Ta3* mutant glial scaffolds are insufficient for progenitor migration

(a-c) P5 dentate gyrus labelled for GFAP (green) and Sox2 (red). Mutant has a loss of GFAP fibres in the ML (ML) and radial fibres stretching through the granule cell layer (GCL). Control Sox2+ progenitors have an even distribution across the glial scaffold however many mutant progenitors are found clustered on the same fibre (white arrow). White box indicates region of higher magnification. Scale, 75µm (a), 25µm (b,c)

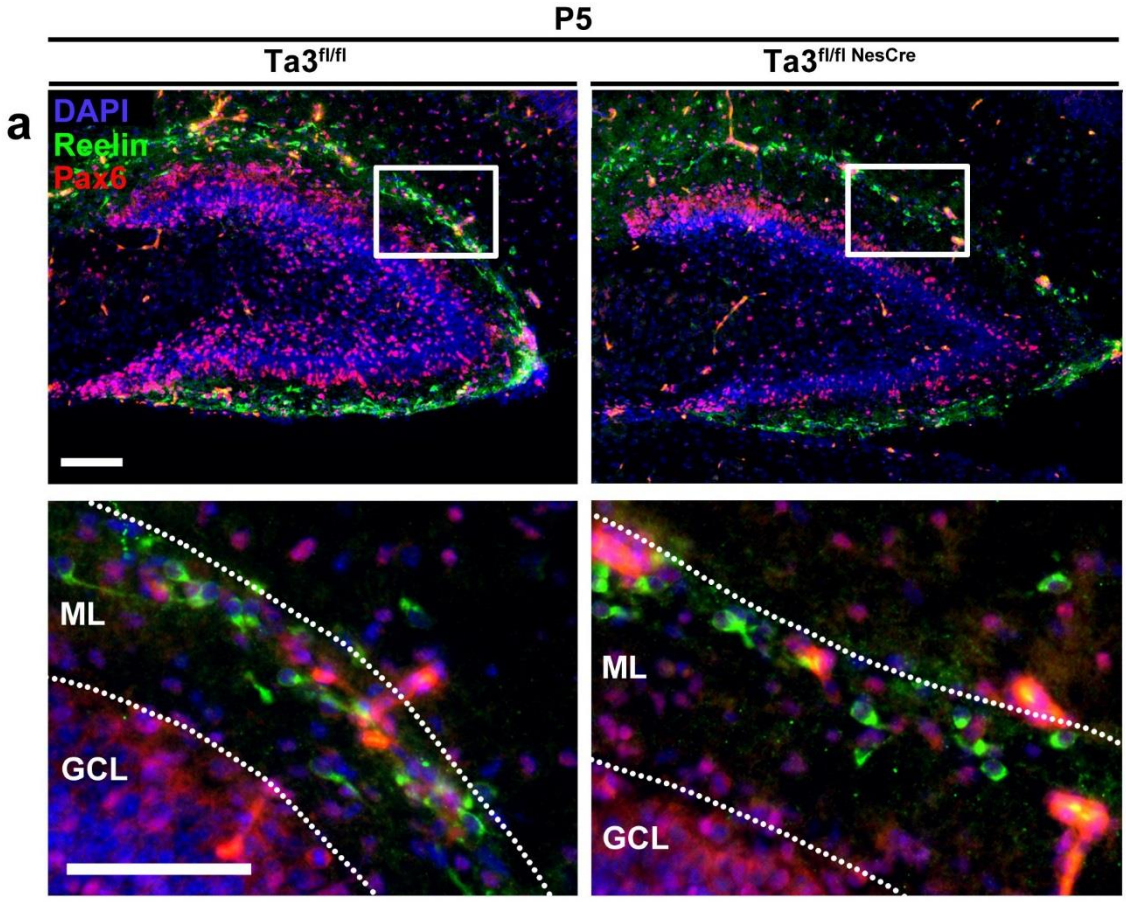

Figure 6.14 *Ta3* mutant dentate gyri have slight reduction in Reelin producing cells
(a) P5 dentate gyrus labelled for Reelin (green) and Pax6 (red). Both control and mutant have a band of Reelin-positive cells lining the outer edge of the ML. Mutant cells have a similar morphology but appear reduced in number. Scale, 75µm (a).

6.3 Discussion

Here the *Ta3* mutant phenotype has been investigated in the dorsal hippocampus; a structure which, like the cerebral cortex, derives from the embryonic telencephalon. At P15 mutants were found to have predominant defects in the dentate gyrus. Assessment of key late-embryonic and early-postnatal stages demonstrated that just prior to birth at E18.5, control and mutant hippocampi were very comparable. Mutants subsequently showed loss of progenitors in the SGZ whilst also exhibiting mislocalisation of progenitors in the GCL. These ectopic progenitors correlated with aberrant formation of the underlying glial scaffold. To date, relatively few studies have investigated the roles of primary cilia in hippocampal formation. For the first time we suggest that defects occur in the SPZ-to-hilar transition in addition to the proliferative defects described previously.

The $Ta3^{fl/fl;NesCre}$ hippocampus has a gross organisation which is relatively normal; this is perhaps unsurprising considering the cortex also has a grossly normal organisation of layers (discussed in Chapter 5). Closer analysis of the dentate gyrus revealed an interesting phenotype caused by defective proliferation and aberrant progenitor localisation. The phenotype is similar to that described in the $Stumpy^{fl/fl;NesCre}$ hippocampus (Breunig et al., 2008). In the study, the youngest stage that Breunig and colleagues investigate is P0, where they show that mice already have a significantly smaller dentate gyrus with reduced proliferation. In the current study just twenty four hours earlier, at E18.5, $Ta3^{fl/fl;NesCre}$ dentate gyrus is normal suggesting that P0 is the earliest stage of dentate gyrus development requiring primary cilia. In contrast, loss of Kif3a using the *hGFAP-Cre* deleter ($Kif3a^{fl/fl;hGFAPCre}$) resulted in a smaller dentate gyrus with reduced proliferation at E18.5 (Han et al., 2008). Both control and mutant are shown to be comparable at E16.5 indicating that loss of Kif3a causes an earlier hippocampal phenotype compared to loss of Ta3. Both *NesCre* and *hGFAP-Cre* deleters have been shown to cause widespread recombination from midgestation onwards (Tronche et al., 1999, Heffner et al., 2012, Zhuo et al., 2001), however there is evidence to suggest that some *NesCre* progenitors may escape recombination until perinatal stages (Liang et al., 2012). It is possible that an earlier defect in $Ta3^{fl/fl;NesCre}$ dentate gyrus was not observed because of slightly different onset of recombination between *hGFAP-Cre* and *NesCre* deleter strains. However, it is also tempting

to speculate about the differing roles of Ta3 and Kif3a. As discussed in Chapter 5, loss of either Ta3 or Kif3a causes loss of primary cilia but with apparently profound differences in the levels of Gli3A and Gli3R, demonstrated by the opposite cortical phenotype using the same deleter *Cre* (Wilson et al., 2012). It is plausible that the earlier phenotype seen in *Kif3a*$^{fl/fl;hGFAPCre}$ dentate gyrus compared to the *Ta3*$^{fl/fl;NesCre}$ and *Stumpy*$^{fl/fl;NesCre}$ dentate gyrus is due to a cilia-independent role of Kifa3a in the processing of Gli3. However, this does not reconcile the enlarged cortex seen in *Kif3a*$^{fl/fl;NesCre}$ mice but reduced dentate gyrus seen in *Kif3a*$^{fl/fl;hGFAPCre}$ (Wilson et al., 2012, Han et al., 2008).

Aside from the time of onset, defects in the dentate gyrus of *Ta3*$^{fl/fl;NesCre}$, *Stumpy*$^{fl/fl;NesCre}$ and *Kif3a*$^{fl/fl;hGFAPCre}$ consistently show a reduction in the level of proliferation (Breunig et al., 2008, Han et al., 2008). Han and colleagues extended this further also showing a reduction in proliferation of a hypomorphic IFT88 mutant (*IFT88*$^{orpk/orpk}$) and Ftm$^{-/-}$ mice in the dentate gyrus. Through double labelling experiments the *Ta3*$^{fl/fl;NesCre}$ dentate gyrus was shown to have both a loss of RGC (type 1), non-radial glial progenitors (type 2a) and intermediate progenitors (type 2b) resulting in a depletion of the progenitor pool. This effect was also observed in birth dating studies of *Stumpy*$^{fl/fl;NesCre}$ which showed a loss of slow cycling progenitors and greater exit from the cell cycle (Breunig et al., 2008).

In both Stumpy and Kif3a studies the defect in proliferation was attributed to loss of Shh signalling. This is consistent with a loss of proliferation seen in *Smo*$^{fl/-;NesCre}$ dentate gyrus (Machold et al., 2003). However, the phenotype in *Smo*$^{fl/-;NesCre}$ dentate gyrus was more prominent with increased hypoplasia in the GCL. Even more severe was the phenotype of *Gli3*$^{fl/fl;Emx1Cre}$ mice where the initial blade of the dentate gyrus failed to form by E18.5 (Hasenpusch-Theil et al., 2012). Firstly this finding demonstrates the importance of Gli3 in the development of dentate gyrus and supports the idea that differences in the time of onset between *Kif3a*$^{fl/fl;hGFAPCre}$ and *Ta3*$^{fl/fl;NesCre}$ could be due to differences in Gli3 processing. Secondly it provides an explanation as to why loss of Smo results in a more severe phenotype than loss of Ta3. Western blot data taken from *Ta3* mutant cortex demonstrated aberrant processing of Gli3 which resulted in an increase in Gli3a protein, despite having a lower overall response to Shh. If this observation were also true in the *Ta3* mutant hippocampus it could suggest why the phenotype was less severe when compared to the *Smo* mutant which would have experienced a loss of Gli3a. Due to the small size of the dentate gyrus, protein analysis was not completed in the current study. Future work

utilising hippocampal neurosphere cultures will be vital in assessing the Gli processing in the *Ta3* mutant hippocampus.

Many other signals, in addition to Shh, are able to act as prominent mitogens in the developing dentate gyrus; a limited number have also been implicated to act through the primary cilium. Wnts are highly expressed in the cortical hem which is a transient structure at E12.5, forming at the boundary between the developing hippocampus and cerebral cortex (Grove et al., 1998). Canonical Wnt signalling is also evident in the closely associated fimbrial germinal matrix (Galceran et al., 2000). Between E12-E15.5 these Wnt molecules boost proliferation of progenitors destined for the SPZ and SGZ proliferative zones (Galceran et al., 2000, Lie et al., 2005). Constitutive loss of the Wnt effector ($Lef1^{-/-}$) or co-receptor ($LRP6^{-/-}$) result in a lack of granule neurons and complete absence of the dentate gyrus (Zhou et al., 2004, Galceran et al., 2000). Conditional loss from E10.5 using the *D6-Cre* deleter resulted in a phenotype of reduced severity but importantly both dentate gyrus and Ammon's horn were affected (Machon et al., 2003). β-Catenin has also been functionally disrupted using the *NesCre* deleter however the phenotype was not investigated beyond E14.5 (Backman et al., 2005). The study described an expansion of dorsal markers in the ventral subpallium but provided little comparison with the current study. In $Ta3^{fl/fl;NesCre}$ brains the fimbria appeared normal and the SPZ progenitors were unaffected at E18.5. As Wnt signalling has a key role in the early development of the hippocampus it is likely that any alterations in signalling would cause a phenotype by E18.5. However it cannot be ruled out that subtle modulation of the Wnt pathway contributed to the reduced granule proliferation in $Ta3^{fl/fl;NesCre}$ hippocampus.

The $Ta3^{fl/fl;NesCre}$ dentate gyrus had ectopic progenitors in the GCL, despite having a reduction in the total number of proliferating cells. This mislocalisation of granule progenitors is reminiscent of aberrant progenitor migration seen in the mutant cerebellum described in Chapter 4. Both $Stumpy^{fl/fl;NesCre}$ and $Kif3a^{fl/fl;hGFAPCre}$ dentate gyri exhibited ectopic progenitors and demonstrated a loss of RGCs with a disrupted glial scaffold (Breunig et al., 2008, Han et al., 2008). Here, for the first time, we draw a causal link between the two phenotypes and suggest that progenitors are mislocalised as a direct result of the defective glial scaffold. Fewer progenitors were associated with radial fibres and those that were appeared overloaded. The observations suggested that the glial network was insufficient to

provide adequate scaffold for SPZ-to-hilar migration. It is important to note, however, that between the ages of P10 and P15 mutant still showed a reduction in the number of ectopic progenitors in the GCL. This suggests that it may be a delayed or ineffective migration rather than a complete block. The ectopic progenitors in the P10 mutant GCL were often quite evenly dispersed despite showing signs of cell cycle proliferation; if migration was completely blocked it could be expected that ectopic progenitors would form clusters of cells in the GCL.

Although we suggest a link between the glial scaffold and defective progenitor migration, the exact contribution of radial glia in progenitor migration is still unclear. Studies specifically targeting the glial scaffold in precise time windows during development are still required to explicitly show their requirement for SPZ-to-hilar transition. Another consideration in the mutant dentate gyrus phenotype is whether loss of *Ta3* affected the glial branching directly of whether it is simply due to the reduction in the number of glial progenitors. Further studies looking at glial behaviour *in vitro* will help determine whether Ta3 is directly required for glial scaffold formation.

The severe hydrocephaly and ataxia seen in $Ta3^{fl/fl;NesCre}$ mice precluded the study of the dentate gyrus at later stages. It would be interesting to study the prolonged development of the $Ta3^{fl/fl;NesCre}$ hippocampus, using a more restricted *Cre* deleter, to see if the progenitors 'catch-up' in their migration or maintain their ectopic position in the GCL. In the current study, many of the GFAP fibres are likely to originate from progenitors, which is reflected in their widespread colocalisation with Nestin. In later stages and adulthood astrocytes constitute a greater proportion of the GFAP-positive pool due to the gradual reduction in glial progenitors. It would also be interesting to see how the glial scaffold develops as the mice age.

Reelin is a secreted protein which is well known to influence the migration of neurons in the hippocampus. $Ta3^{fl/fl;NesCre}$ dentate gyrus showed a subtle reduction in the number of Reelin-positive cells in the ML. Mice with constitutive loss of Reelin, the so-called 'Reeler' mice, have a disruption of hippocampus with aberrant radial glial scaffold (Weiss et al., 2003, Frotscher et al., 2003) and failure of the SPZ-to-hilar transition (Li et al., 2009). Loss of Reelin signalling has also been shown to cause ectopic localisation of postmitotic granule neurons both in the hilus and ML (DelRio et al., 1997, Teixeira et al., 2012). Reeler

mutant mice also have a thinner entorhinal performant pathway termination zone in the ML (DelRio et al., 1997). Studies of other primary cilia mutants have described relatively normal presence of Reelin-positive cells in the marginal zone of the cortex of *Kif3a*$^{fl/fl;hGFAPCre}$ (Wilson et al., 2012), *Arl13b*$^{hnn/hnn}$ (Higginbotham et al., 2013) and hypomorphic *Ift88*$^{cbs/cbs}$ (Willaredt et al., 2008). The wide spanning defects seen in mutants with complete loss of Reelin makes interpreting the subtle reduction of Reelin-positive cells difficult in *Ta3*$^{fl/fl;NesCre}$ hippocampus. It would be interesting to further investigate the level of Reelin protein and mRNA in mutant hippocampus to provide supporting evidence to confirm whether there is a genuine loss of Reelin producing cells.

Another interesting phenotype in the *Ta3*$^{fl/fl;NesCre}$ dentate gyrus is the presence of ectopic postmitotic granule neurons in the ML. Cells of the GCL were also more dispersed in *Stumpy*$^{fl/fl;NesCre}$ mice (Breunig et al., 2008). Disc1 is a protein known to interact with the basal body and loss of Disc1 has been shown to cause loss of primary cilia in cultured cells (Marley and von Zastrow, 2010). Interestingly, loss of DISC1 results in aberrant placement of granule neurons in the adult hippocampus (Kvajo et al., 2008, Duan et al., 2007). In this study addition of shRNA targeting Disc1 into adult hippocampus caused aberrant migration of granule neurons beyond the GCL and into the ML (Duan et al., 2007). Loss of Disc1 through shRNA *in utero* electroporation at E15.5 also reduces the ability of cells to migrate from the adjacent ventricular zone into the dentate gyrus (Meyer and Morris, 2009). This appears to reveal two different roles for Disc1 both in the early migration of dentate progenitors and in the migration of postmitotic granule neurons in the GCL. Interestingly, mice showed no difference in proliferation or cell survival of the progenitor population (Meyer and Morris, 2009). Although the presence of primary cilia was not demonstrated alongside the migratory defects, it brings into question what roles of the basal body are dependent on primary cilia; particularly in the case of neuronal migration.

Many of the phenotypes described in the *Ta3*$^{fl/fl;NesCre}$ hippocampus are part of complex interactions between proliferation, migration and the underlying scaffold. Trying to unravel these phenotypes in what is a relatively small brain region is a challenging task, often with limited material available. Trying to distinguish the temporal contributions of each cell lineage would require a plethora of *Cre* deleters to begin to pinpoint the role of

Ta3 in each cell type. This effect is coupled with the wide ranging effect loss of primary cilia can have on cell biology. One method of simplifying the system to better examine the molecular mechanisms is to study hippocampal neurons *in vitro*. This is discussed further in chapter 7.

Chapter 7 – *In vitro* models to study *Ta3* loss in hippocampal neurospheres

7.1 Introduction

Culturing neurons *in vitro* is an excellent way to study their cellular behaviour in a controlled environment. *Ta3*$^{fl/fl;NesCre}$ mutant mice exhibit defects in proliferation, migration and glial scaffolds in the postnatal hippocampus. Ta3 is known to have roles in the formation of primary cilia but its interaction with key centrosomal proteins also suggest it could have functions independent of primary cilia function. Investigating the recombination of *Ta3 in vitro* may help to dissect any distinct cellular roles.

Culture of neurons from embryonic brains was first demonstrated over 100 years ago (Harrison, 1910, Keshishian, 2004). However, it was not until many years later that sufficient understanding and techniques were available to utilise neuronal cell culture to its full potential. In 1990 Reynolds and Weiss (1992) demonstrated that neural stem cells isolated form adult mice could be grown in suspension and form aggregates of cells termed 'neurospheres'. They showed that epidermal growth factor (EGF) and basic fibroblast growth factor (bFGF/FGF2) were required to maintain their growth and proliferation (Reynolds and Weiss, 1992, Vescovi et al., 1993). Since then, the neurosphere culture assay has developed into a popular and versatile system where spheres can be passaged by being disassociated into single cells, pooled, frozen or differentiated into neurons, astrocytes and oligodendrocytes (Seaberg et al., 2005).

Due to the popularity of the neurosphere culture assay a number of detailed protocols have been published describing isolation of multipotent neural precursors from adult mice (Pacey et al., 2006, Brewer and Torricelli, 2007, Azari et al., 2010, Guo et al., 2012). Despite nearly 20 years of neurosphere culture there are still variations in the exact method employed. Currently unpublished work from the Subramanian laboratory has set to optimise the neurosphere culture assay using neural stem cells obtained from either adult or postnatal whole brain tissue. This provides an excellent framework with which to investigate the loss of *Ta3* in a defined *in vitro* environment.

The use of the *NesCre* deleter strain described in previous chapters caused recombination in the population of neural progenitors. This provided a fixed spatial and temporal control of *Ta3* recombination. Whilst this deleter strain was able to achieve robust and highly reproducible results *in vivo*, it would be more versatile to be able to control the

exact time of recombination *in vitro*. One advantage of the Cre-LoxP system is the wide variety of *Cre* deleter strains available. Several inducible strains have been developed which either use tamoxifen or tetracyclin to cause activation of the Cre recombinase enzyme. These have been refined further by using different promoters to drive the inducible *Cre* expression in define tissues providing both spatial and temporal control of recombination.

Tamoxifen is by far the most common molecule used for inducible *Cre* deleter strains, one such deleter is the ubiquitously expressed tamoxifen-inducible Cre (*UbcCreER^{T2}*) designed by Ruzankina et al (2007). The transgene has a *ubiquitin C* promoter driving the ubiquitous expression of a Cre recombinase which is fused to a modified estrogen receptor (ER^{T2}). The receptor is only activated in the presence of the synthetic compound 4-hydroxytamoxifen (4-OHT) but not endogenous estrogen (Feil et al., 1997). The prodrug tamoxifen can be administered to mice after which it is converted into the active form (4-OHT) by the cytochrome P450 enzyme (Desta et al., 2004). Alternatively 4-OHT can be administered directly to cultured cells *in vitro*. The *UbcCreER^{T2}* strain is an attractive system to conditionally delete the function of *Ta3* in a temporally defined way and better understand its functional roles *in vitro*. The *UbcCreER^{T2}* system is illustrated in figure 7.1.

The current chapter seeks to answer some of the questions raised from the hippocampal phenotype of *Ta3$^{fl/fl;NesCre}$* mice. Firstly, the neurosphere culture method was optimised for use with postnatal hippocampal tissue isolated from *Ta3$^{fl/fl;UbcCre}$* mice. Addition of tamoxifen was then shown to cause robust excision in *Ta3* ultimately resulting in a loss of primary cilia. Neurospheres with loss of *Ta3* were smaller in size yet differentiated cells showed a similar phenotype with comparable early cell fate decisions and intermediate filament organisation. Cells with loss of *Ta3* did however show disruption of the actin cytoskeleton and defective migration using the neurosphere migration assay. This begins to address some of the questions answered and forms an excellent *in vitro* system for further research into the functional consequence of *Ta3* loss.

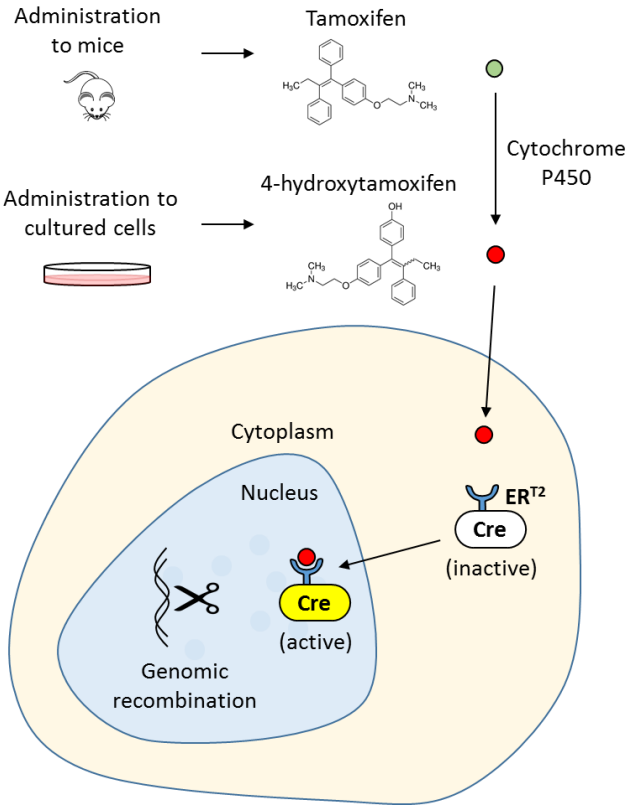

Figure 7.1 The mechanism of *UbcCreER^{T2}* activation by tamoxifen

Tamoxifen administered to mice is converted to its active form, 4-hydroxytamoxifen (4-OHT), by the cytochrome P450 enzyme. 4-OHT is administered directly to cell cultures. Cre recombinase fused to modified estrogen receptor (*CreER^{T2}*) is ubiquitously expressed by the *ubiquitin C* promoter. *CreER^{T2}* is activated in the presence of 4-OHT and causes genomic recombination of LoxP sequences.

7.2 Results

7.2.1 Hippocampal neurosphere culture to study Ta3 function

The neurosphere culture methodology had previously been established in the Subramanian laboratory using whole postnatal brains as a starting material (data not shown). In order to make the methodology more targeted to analyse the hippocampal phenotype, the technique was adapted using smaller volumes and more suitable plastic-ware to achieve efficient cell yields from dissected P5 dorsal hippocampus (Table 7.1, Fig 7.2a).

Initially both whole brain and hippocampal neurospheres lines were established to compare isolation and growth methodologies. The hippocampal neurospheres were found to grow in much the same way as those isolated from whole brains, albeit with a smaller starting number of cells. In order to find the optimum conditions to disassociate dissected tissues into a single cell suspension the duration of papain digestion was varied. It was found that an incubation of 15 minutes produced a homogenous suspension of single cells with the minimal level of cell death.

Cells were grown for seven days and efficiently formed spheres of consistent shape and size (Fig 7.2b). After the first week of growth, hippocampal cells were found to have a much higher survival rate compared to whole brain cultures, this was presumably due to the relatively higher proportion of progenitors present in the dissected hippocampal tissue (Table 7.1). Neurospheres were disassociated into single cells to allow further growth and obtain sufficient cells for experimental analysis. Disassociation using an acid/alkali method as published previously (Sen and Kallos 2004) was compared to commercially available enzymatic treatment Accutase®. No difference was observed in the ability of the techniques to disassociate neurospheres and both gave a high yield of viable cells (data not shown). Previous work in the Subramanian laboratory had found that cells split using the acid/alkali method exhibited a greater proliferative lifespan (>10 passages) compared to other methods (unpublished). For this reason, this method was selected for all hippocampal neurosphere disassociation into single cells.

To generate hippocampal neurospheres lines postnatal P5 mice were obtained by breeding males of genotype $Ta3^{fl/fl;UbcCre}$ to females of genotype $Ta3^{fl/fl}$. Each line was

created using a single mouse and throughout the course of the project 13 hippocampal neurosphere lines of *Ta3*$^{fl/fl;UbcCre}$ and *Ta3*$^{fl/fl}$ genotype were generated (Table 7.1). Neurosphere lines were expanded, disassociated and frozen. This allowed all experiments to be completed from frozen stocks using cells of identical passage number. In total 3 independent neurosphere lines of genotype *Ta3*$^{fl/fl;UbcCre}$ were selected for experimental analysis (designated '#1, 2, 3'). In addition, neurosphere lines from *Ta3*$^{fl/fl}$ mice were also used to act as controls in some of the experiments. All experiments described hereafter use hippocampal neurospheres lines.

Initial experiments found that two doses of 4-OHT during neurosphere growth, one immediately after disassociation (0d) and one three days later (3d) was able to cause robust recombination of *Ta3*. This was demonstrated by taking neurospheres after seven days growth and analysing the genomic DNA using PCR. Reactions to detect the first *LoxP* site (described in Section 3.2.1) produced bright bands at 470 bp for all three *Ta3*$^{fl/fl;UbcCre}$ neurosphere lines. Upon administration of 4-OHT, these bands were markedly reduced suggesting a high level of *Ta3* recombination had occurred (Fig 7.3a). A second PCR was completed using an alternative reverse primer designed to exon 13 which only creates a product following *Ta3* recombination (Bangs et al., 2011). *Ta3*$^{fl/fl;UbcCre}$ cells showed no visible band but following administration of 4-OHT all three neurosphere lines showed bright bands of 273 bp (Fig 7.3b). Together these results support a consistently high level of recombination caused by 4-OHT administration. These form the basis to better study the consequence of *Ta3* loss from postnatal hippocampal progenitors. The experimental plan is illustrated in Fig 7.2c.

Table 7.1 Summary of isolated neurospheres lines

All cells were isolated from P5 postnatal mice. Mice were acquired by breeding *Ta3*$^{fl/fl;UbcCre}$ males with *Ta3*$^{fl/fl}$ females or through stock breeding of outbred CD1 mice. One mouse was used to generate one neurosphere line either using whole brains or dissected dorsal hippocampi (hip). For isolation of single cells the optimum digestion time was found to be 15min at 37°C followed by mechanical disruption. Recovery states the mean total number of cells isolated (± standard deviation) Use of ~ indicates approximation of viable cell number during experiment. Use of new batch of hFGF dramatically improved cell growth as shown by the increase in split ratio. † indicates neurosphere lines selected for experimental analysis.

Number of neurospheres lines isolated (genotype)	Brain region	Digest time (min)	Mean recovery of cells per mouse (±SD)	Survival after 7 days (% of starting cell number)	Split ratio for subsequent passages	Comments
1 (1 x *Ta3*$^{fl/fl}$)	Whole brain	30	High levels of cell death	n/a	n/a	- mEGF
4 (3 x *Ta3*$^{fl/fl}$) (1 x *Ta3*$^{fl/fl;UbcCre}$)	Whole brain	15	8.9 x 10^6 cells (± 2.1 x 10^5)	73%	1:3	- mEGF
2 (CD1)	Whole brain	10	Incomplete digestion	n/a	n/a	- switch from mEGF > hEGF
2 (CD1)	Whole brain	15	Optimum digestion	n/a	n/a	- hEGF
5 (3 x *Ta3*$^{fl/fl}$) (2 x *Ta3*$^{fl/fl;UbcCre}$)	Hip	15	1.0 x 10^5 cells (± 3.9 x 10^4)	133% (after 6 days)	1:3	- hEGF
3† (3 x *Ta3*$^{fl/fl;UbcCre}$)	Hip	15	~ 1.0 x 10^5 cells	~ 145%	1:10	- new hFGF - hEFG
2† (5 x *Ta3*$^{fl/fl}$) (4 x *Ta3*$^{fl/fl;UbcCre}$)	Hip	15	~ 1.0 x 10^5 cells	~ 145%	1:10	- new hFGF - hEGF
9† (5 x *Ta3*$^{fl/fl}$) (4 x *Ta3*$^{fl/fl;UbcCre}$)	Hip	15	~ 1.0 x 10^5 cells	~ 145%	1:10	- new hFGF - hEGF

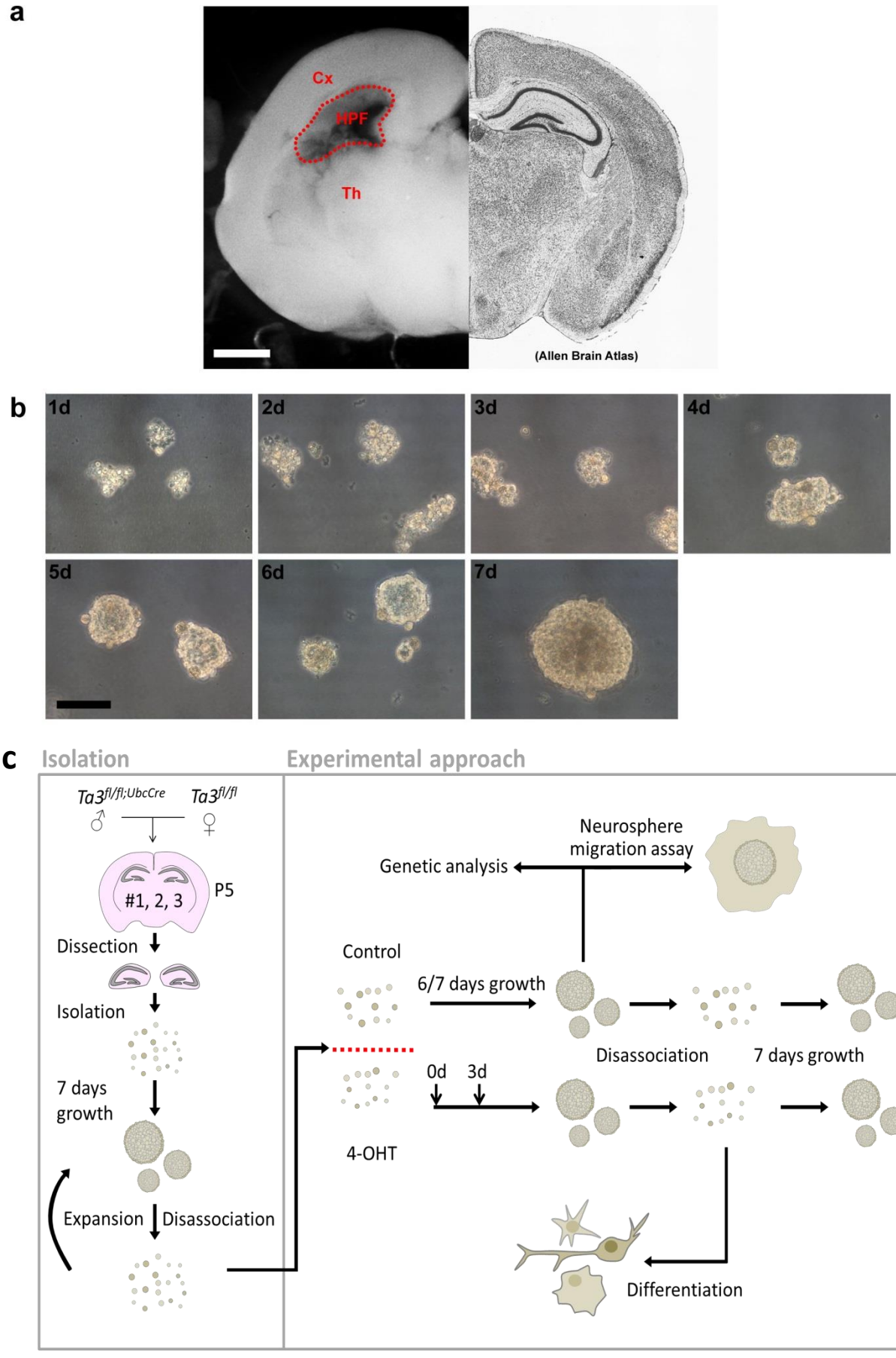
a
Cx
HPF
Th
(Allen Brain Atlas)
b
1d
2d
3d
4d
5d
6d
7d
c
Isolation
Experimental approach
Ta3fl/fl;UbcCre
Ta3fl/fl
♂
♀
#1, 2, 3
P5
Dissection
Isolation
7 days growth
Expansion
Disassociation
Genetic analysis
Neurosphere migration assay
Control
6/7 days growth
Disassociation
7 days growth
0d
3d
4-OHT
Differentiation

Figure 7.2 Generation of hippocampal neurosphere cultures

a) left: Image of coronal brain slice following removal of dorsal hippocampal formation (HPF), right: representative coronal brain slice taken from Allen Brain atlas. (b) Representative images of isolated cells forming neurospheres throughout seven day growth period. (c) Schematic diagram showing isolation and experimental approach. Isolation: cells were isolated from P5 dorsal HPF and grown for seven days. Cell numbers were expanded by disassociation into single cells followed by further growth into neurospheres. Experimental approach: Neurospheres were disassociated into single cells, separated and recombination induced by administration of tamoxifen (4-OHT) immediately (0d) and after three days (3d). After 6/7 days growth neurospheres were used for genetic analysis or migration assay or disassociated into single cells. Single cells were either allowed to grow further or differentiated for 6 days. Abbreviations, Cx, Cortex, Th, Thalamus. Scale, 1 mm (a), 100 µm (b). Image taken from Allen Brain Atlas [Internet]. Available from: www.brain-map.org.

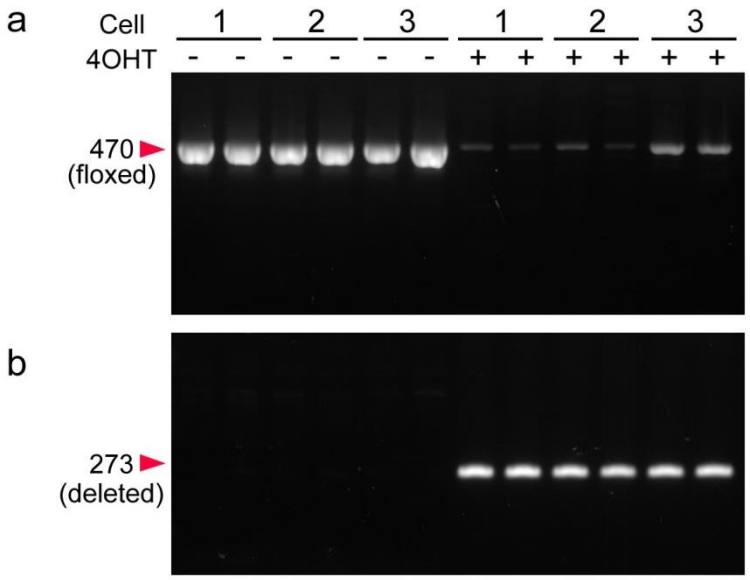

Figure 7.3 Tamoxifen administration causes robust recombination in *Ta3*$^{fl/fl;UbcCre}$ cells

PCR analysis performed on gDNA isolated in replicates from 3 *Ta3*$^{fl/fl;UbcCre}$ neurosphere lines (#1, 2, 3) after 7 days growth either control (-) or with Tamoxifen (4OHT) administrated at day 0 and day 3 (+). (a) PCR reaction amplifying sequence spanning first *LoxP* site of *Ta3* to produce product of 470 bp. 4OHT-administered cells had a substantial reduction in band intensity compared to control. (b) PCR reaction amplifying sequence only present after recombination has occurred to produce a product 273 bp. Control cells have no visible band but 4OHT-administered cells have high level of recombination.

7.2.2 Cells cultured *in vitro* with loss of *Ta3* have reduced colony size

In vivo the *Ta3* mutant hippocampus exhibits a profound loss of proliferating progenitors. To assess the consequence of *Ta3* loss in the neurospheres lines it was first important to monitor the growth of neurospheres. Due to the simple experimental design the same starting dilution of cells could be used for experiments with the only difference due to addition of 4-OHT. After seven days growth it was evident that loss of *Ta3* resulted in smaller neurosphere size across all of the neurosphere lines (Fig 7.4a).

One drawback of the neurosphere culture method is that the free-floating conditions can also lead to the fusion of neurospheres due to factors which are often hard to control such as movement of the dish and consistent distribution of cells/spheres. This can result in heterogeneous sizes of neurospheres. To limit this effect and study the cell growth in greater detail cells were plated in tissue culture treated 96-well plates. This allowed adherence of cells to the culture surface with few signs of differentiation. When plated at clonal density, cells grew as round colonies with a similar approximate size to neurospheres except each colony was likely to have originated from a single cell (Fig 7.4b). Once more, cultures treated with 4-OHT showed a smaller colony size and measurements of colonies from multiple wells demonstrated that loss of *Ta3* resulted in significant reduction in median colony area (#1=58%, #2=45%, #3=61% reduction) when comparing treated and untreated controls (Fig7.4c). An important control included the use of $Ta3^{fl/fl}$ cells with and without 4-OHT administration which showed no difference in colony size. This confirms that the defect is due to loss of *Ta3* rather than administration of 4-OHT. To assess the longer term effect of *Ta3* loss, neurospheres cultured with and without 4-OHT administration were disassociated after seven days and plated on 96-well tissue cultures plates (named 'passage +1') (Fig7.4c). These cells did not have any further addition of 4-OHT yet colonies consistently showed a significant reduction in median colony size (#1=54%, #2=64%, #3=73% reduction) when comparing treated and untreated controls. This suggests an intrinsic and permanent defect caused by loss of *Ta3*.

Another important consideration is the proportion of cells which successfully form colonies after plating. To investigate this, the number of colonies (>30 μm) formed after seven days growth was quantified and compared to the number of cells inputted into each well to calculate the colony forming efficiency (Fig 7.4d). Each neurosphere line used the same starting dilution to ensure an identical number of inputted cells for each comparison.

Interestingly, no significant difference was identified in any of the neurosphere lines treated with 4-OHT when compared to their untreated controls (Fig 7.4d). This suggests the ability of cells treated with 4-OHT to form colonies is not affected but their growth over the seven day period is.

BrdU was added to seven day neurosphere cultures two hours prior to fixation to better assess their proliferation (Fig 7.5a). Surprisingly, little difference was observed in the number of BrdU-positive cells in 4-OHT treated cultures (Fig 7.5a). To confirm this immunolabelled neurospheres were squash-mounted and the proportion of BrdU-positive cells quantified (Fig 7.5b). In control, 15-20% of cells were BrdU-positive but no statistical difference was observed between treated and untreated cultures. This confounding result suggests, at this time point, the proportion of actively proliferating cells was comparable following loss of *Ta3*. This is surprising because *in vivo Ta3* mutant mice exhibit a loss of proliferation which is assumed to be due to reduced Shh signalling through the primary cilium. With this in mind, it is possible that the current technique used to assess proliferation *in vitro* was not sensitive enough to detect a meaningful difference in proliferation.

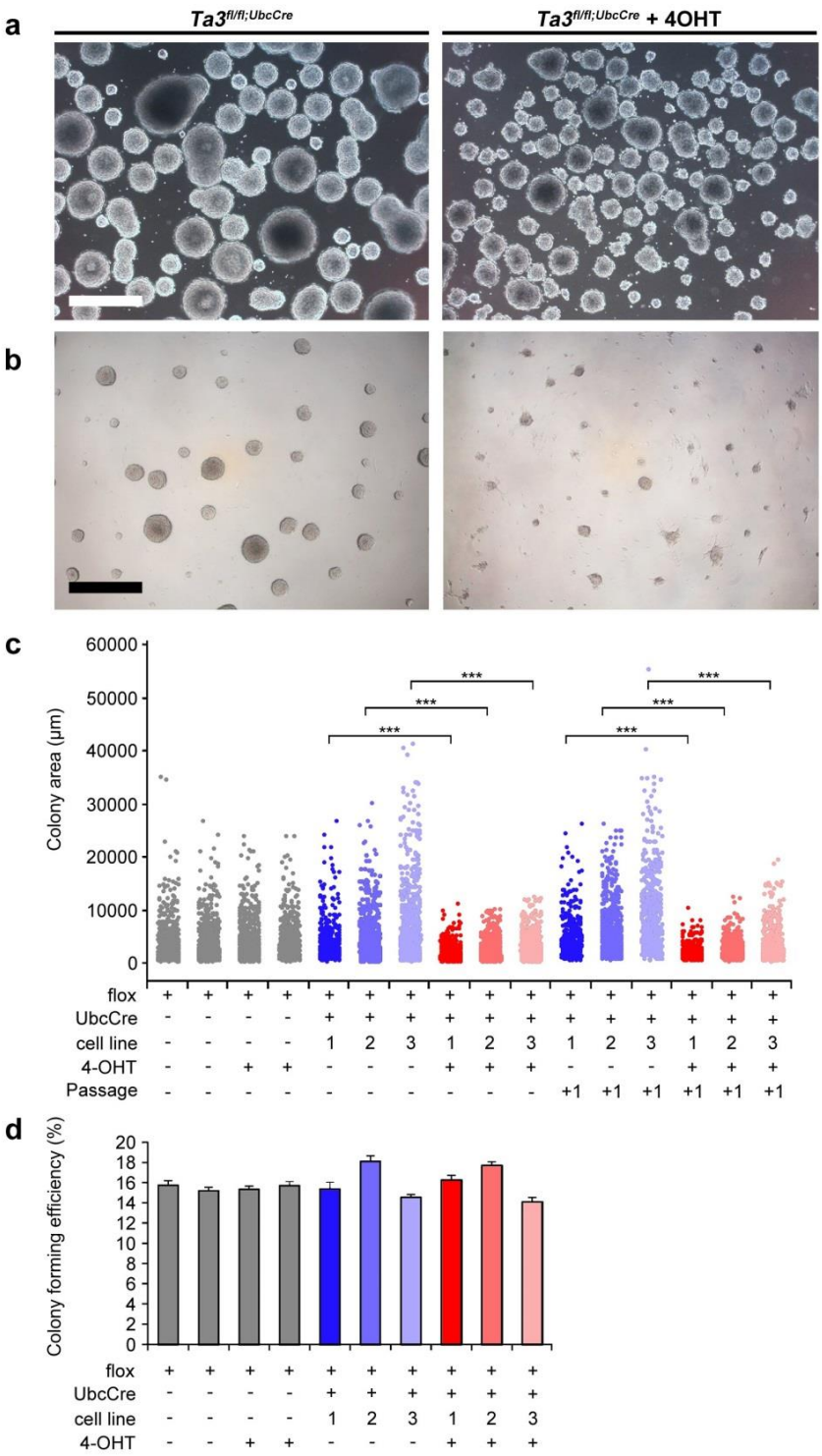

Figure 7.4 Loss of *Ta3* causes smaller colony size but comparable colony forming efficiency.

(a) representative image of control and tamoxifen (4-OHT) administered neurospheres after 7 days growth. 4-OHT treated cultures have smaller neurosphere size. (b) control and tamoxifen (4-OHT) administered cells grown as adherent colonies. 4-OHT treated cultures have smaller colony size. (c) Dot blot showing individual colony area measurements. Control $Ta3^{fl/fl}$ cells grown with and without 4-OHT have no difference in colony size (grey dots). Control $Ta3^{fl/fl;UbcCre}$ cells without 4-OHT administration (blue dots). $Ta3^{fl/fl;UbcCre}$ cells with 4-OHT administration (red dots) have a significant reduction in colony area. After 4-OHT administration neurospheres were passaged and replated as adherent cultures without any further 4-OHT administration (Passage +1). Treated neurospheres consistently showed significant reduction in colony area. (d) Quantification of colony forming efficiency. 4-OHT administration causes no significant difference in any conditions. Scale, 500µm (a, b). Statistical comparisons were made between the same neurosphere lines. Error bars: (c) dot blot: > 500 colony measurements per condition. *** P<0.001, two tailed Mann-Whitney test. (d) s.e.m (n = 12), no significant differences (two tailed Students-t test).

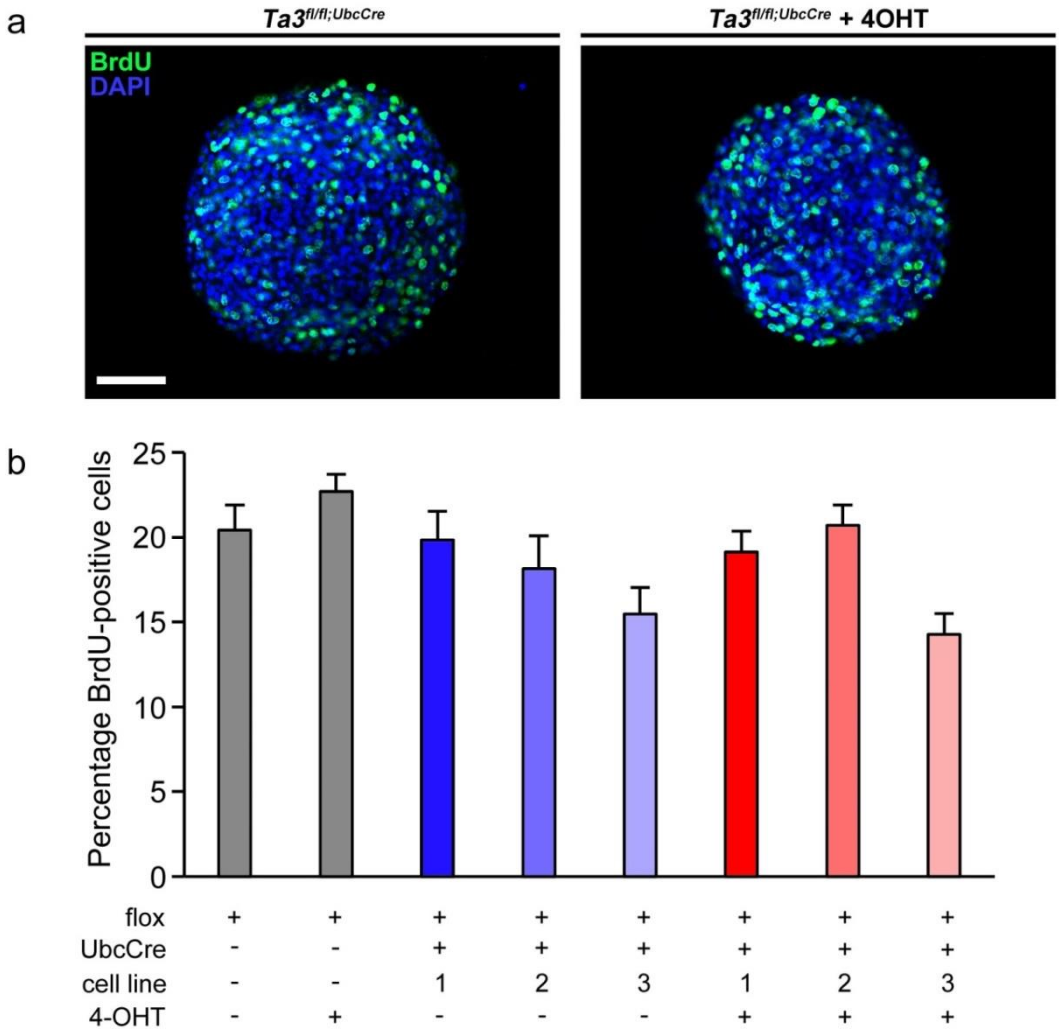

Figure 7.5 Loss of *Ta3* does not cause a significant difference in BrdU incorporation. Neurospheres after 7 days growth were administered BrdU 2 hours before fixation. (a) Representative images of BrdU identification in whole mount neurospheres with and without tamoxifen (4-OHT) administration. Loss of Ta3 does not cause a difference in BrdU incorporation. (b) Quantification of BrdU incorporation for $Ta3^{fl/fl}$ (grey) and $Ta3^{fl/fl;UbcCre}$ cells with (blue) and without (red) 4-OHT administration using squash-mounted neurospheres . BrdU incorporation expressed as a percentage of total cell number shows no significant difference in following loss of Ta3. Scale, 75 µm (a). Error bars (b) s.e.m (n = 12). Comparisons were only made between the same neurosphere lines, no significant difference (two tailed Students-t test).

7.2.3 Recombination of *Ta3* in differentiated cells causes loss of cilia, disrupted actin cytoskeleton but little defect in fate choice or cell morphology

The ability of neural precursors to differentiate was also investigated following loss of *Ta3*. Neurospheres grown with or without 4-OHT administration were disassociated to single cells after six days and transferred to differentiating conditions for a further six days. This utilised a different media composition previously shown in the laboratory to induce differentiation. It limited proliferation by removal of EGF and reduced FGF which, at low levels, has been shown to have a beneficial effect improving survival and neuronal differentiation (Vicario-Abejon et al., 1995). Cells were also plated on coverslips coated with Matrigel®, a well-documented basement membrane material known to improve attachment, survival and neural differentiation (Hadley et al., 1985, Uemura et al., 2010, Ma et al., 2008).

After 24 hours growth cells had a flattened morphology with multipolar shape and radial processes extending around the central nucleus (Fig 7.6a). At this early stage there was no visible difference between treated and untreated cultures. As the differentiation continued the cell network increased in complexity, many of the cells resembled astroglia and only a very limited number extended elongated processes resembling neuronal processes. Cells were fixed after six days of differentiation and firstly, it was important to assess the consequence of *Ta3* loss on primary cilia. Cells were immunolabelled for ACIII and acetylated α-tubulin and it was clearly evident that cells with loss of *Ta3* exhibited fewer primary cilia (Fig 7.6b). Quantification demonstrated that, in untreated cultures, primary cilia were detected on 61% of cells whereas loss of *Ta3* resulted in a 6.8 fold reduction with primary cilia detected on only 9% of cells (Fig 7.6c). This confirmed that recombination of *Ta3* had occurred in a high number of cells and was sufficient to cause loss of primary cilia. Further analysis of the acetylated α-tubulin staining was unable to detect any difference in the distribution or organisation of the microtubule cytoskeleton between treated and untreated cultures.

Previous reports have suggested that loss of *Ta3* causes defects in the actin cytoskeleton (Yin et al., 2009, Bangs et al., 2011). Fluorescently labelled phalloidin was used to detect stabilised F-actin in differentiated cells (Fig 7.7a). Analysis of several coverslips showed a reduction in the number of stress fibres in cells with loss of *Ta3* (Fig 7.7b). Importantly, however, increased levels of actin in the ruffled membrane or filopodia were not observed in these cells.

Using the current culture conditions few cells displayed morphological characteristics indicative of mature neurons. To confirm this, differentiated cells were immunolabelled for mature neuronal markers neurofilament (165 kDa) and β III tubulin but no immunoreactivity was detected (data not shown). The intermediate filaments, nestin and GFAP, however, were expressed at high levels (Fig 7.8a). Coimmunolabelling identified three main cell types, those that were predominantly nestin positive and likely to have a neuronal fate, those that were both nestin and GFAP positive are likely to represent glial-progenitors and those that were predominantly GFAP positive having a more mature glial fate. To see if loss of *Ta3* affected the early fate decision of these differentiated cells, the relative proportions were quantified (Fig 7.8c). Nestin-positive and double nestin- and GFAP-positive cells were the most abundant cell types averaging 46% and 47% respectively. Proportions were found to be highly consistent between treated and untreated cultures suggesting that loss of *Ta3* during neurosphere culture did not affect the early cell fate choice or differentiation. The GFAP scaffold was also assessed using high power microscopy to see if cells exhibit loss of branching or fibres as described *in vivo* (Fig 7.8b). Interestingly, all treated and untreated cultures showed a very similar distribution and organisation of GFAP- fibres both in the single and double-positive cells (Fig 7.8b). This suggests that the intrinsic ability of cells to form the cellular intermediate filament scaffold of is unaffected by loss of *Ta3*.

The differentiation presented here appears to still resemble a relatively immature state. To confirm this finding, the presence of Pax6 was investigated and found to have widespread expression in many of the cells (Fig 7.8d). The extensive Pax6 distribution showed little difference between treated and untreated cultures at this early stage of maturation.

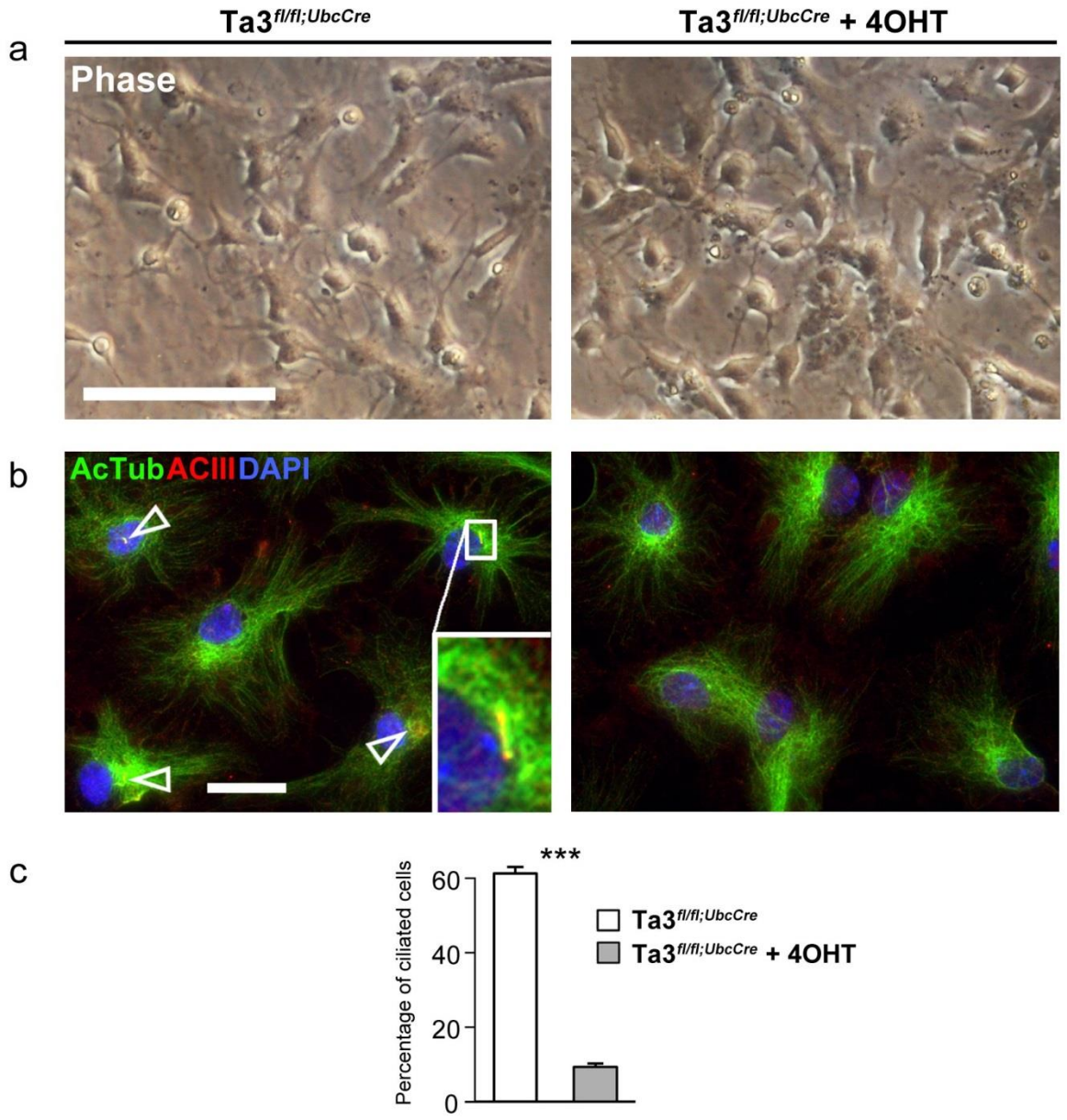

Figure 7.6 Differentiated cells lacking Ta3 have loss of primary cilia

(a) Representative phase contrast images of disassociated cells differentiated on matrigel for 24 hours following tamoxifen administration to neurospheres. (b) Cells differentiated for 6 days immunolabelled for adenylyl cyclase III (red) and acetylated α-tubulin (green). Cultures with loss of Ta3 have a loss of primary cilia but no apparent difference in microtubule organisation. (c) Quantification shows that loss of Ta3 causes a significant reduction in the percentage of ciliated cells. Scale, 25 µm (a, b). Error bars (c) s.e.m (n = 12) *** P≤0.001, (one tailed Students-t test).

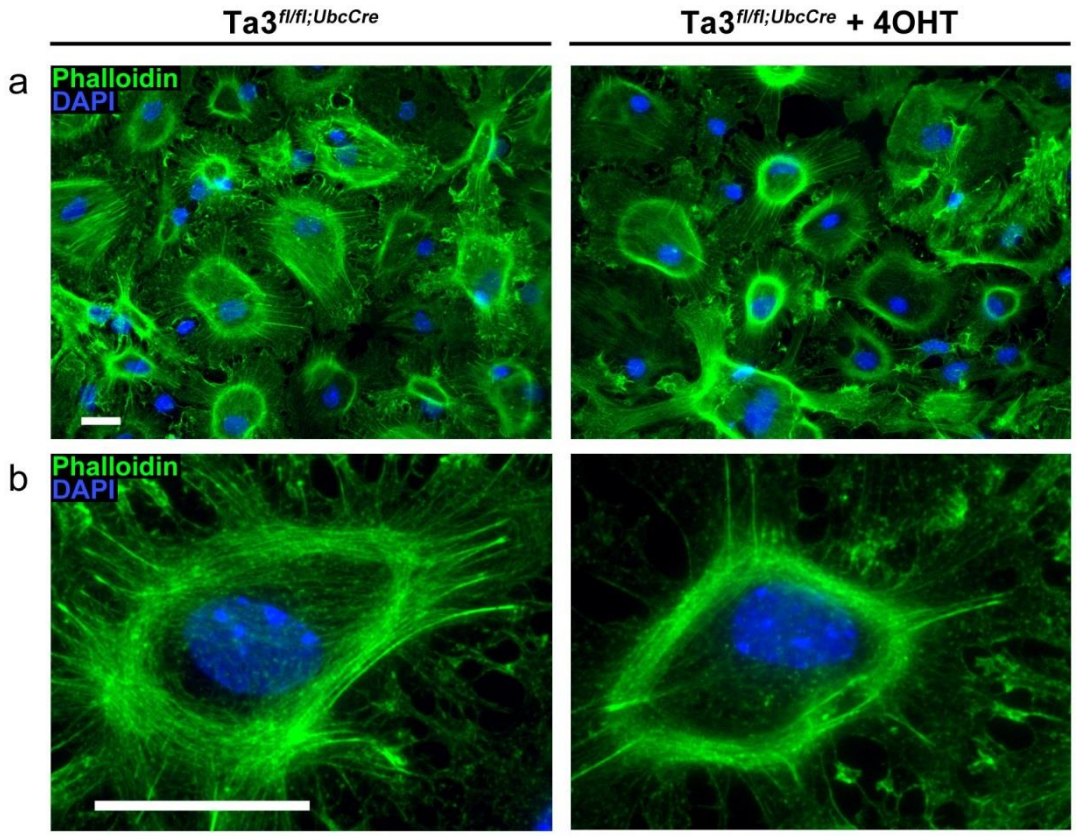

Figure 7.7 Loss of *Ta3* causes reduction of F-actin stress fibres

(a, b) Identification of f-actin using fluorescently labelled palloidin (green). Loss of Ta3 causes a disruption of actin cytoskeleton with fewer stress fibres. No difference in F-actin was observed at ruffled membrane in filopodia. Scale, 25 µm (a,b).

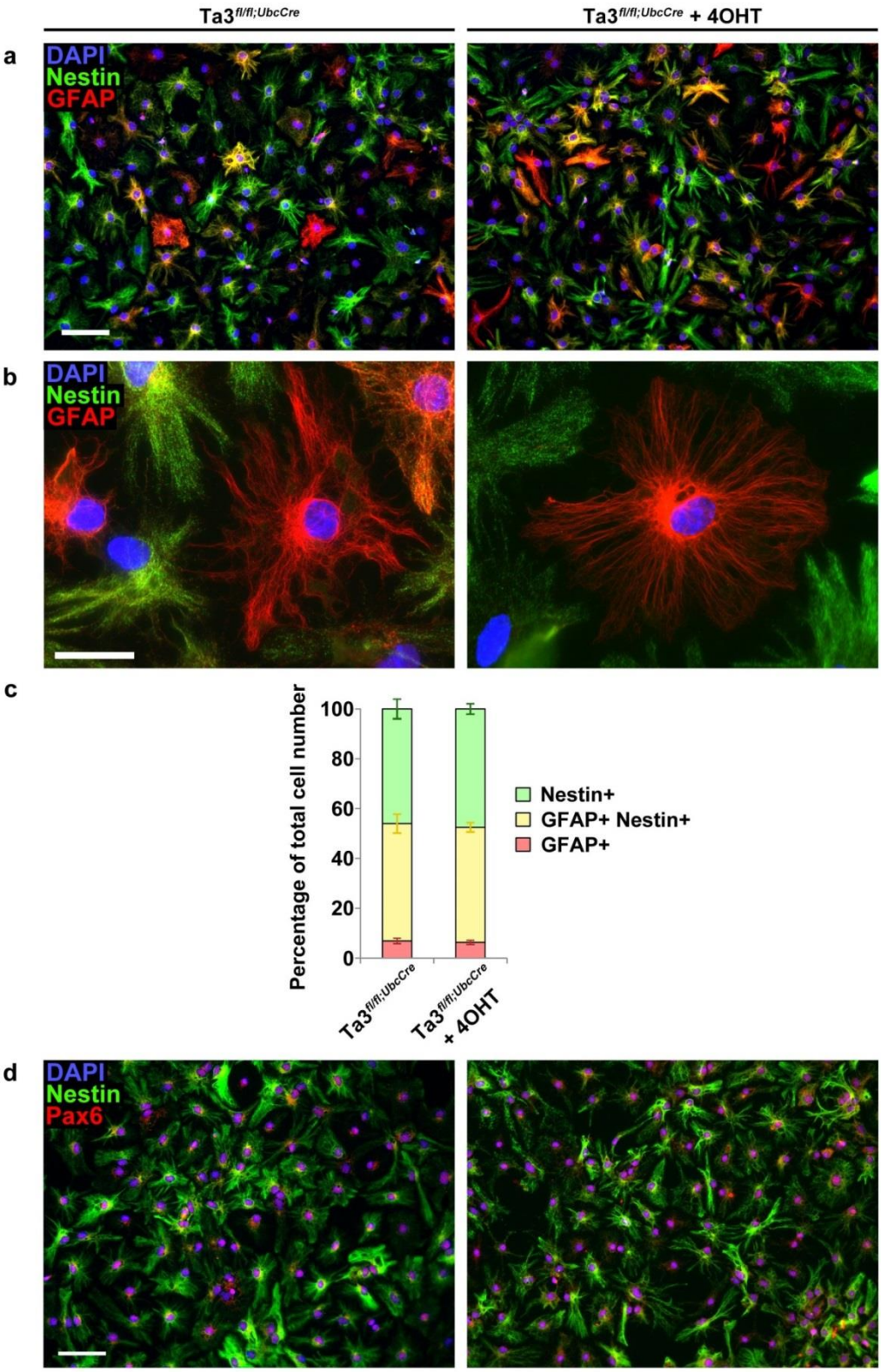

Figure 7.8 Loss of *Ta3* does not affect cell fate choice or glial scaffold formation

Representative images of cells differentiated on matrigel for 6 days following tamoxifen administration to neurospheres. (a,b) Immunolabelling for nestin (green) and gfap (red). Cells exhibit a range of cell shapes but no observable difference following loss of Ta3. GFAP-positive glia show no apparent defect in branching or cell shape following loss of Ta3. (c) Quantification of the proportion of single- or double- positive cells. Loss of Ta3 does not affect the early fate choice of differentiated cells. (d) Immunolabelling of nestin (green) and Pax6 (red) shows a high proportion of progenitors indicating only early level of neural maturation. Loss of Ta3 does not affect the extent of maturation in cell culture. Scale, 75 µm (a, d), 25 µm (b). Error bars (c) s.e.m (n = 12), no significant differences (two tailed Students-t test).

7.2.4 Loss of *Ta3* causes a reduction in neurosphere migration

An effective way to monitor the capacity of neural cells to migrate is using the neurosphere migration assay (Durbec et al., 2008, Kong et al., 2008, Ishido and Suzuki, 2010, Brennand et al., 2015). In this paradigm, neurospheres of equal size are transferred to individual wells coated with Matrigel® and containing differentiation media. Migration of cells away from the neurosphere is monitored over the course of seventy-two hours to provide a quantitative readout of neural migration (Fig 7.9a). Due to the nature of this assay it is a useful system to monitor the fundamental ability of cells to migrate, rather than in response to signals or soluble gradients.

Both treated and untreated seven-day neurospheres from all three neurosphere lines were measured after two, twenty four, forty eight and seventy-two hours. In all stages, treated cells had migrated significantly less distance than the untreated controls (Fig 7.9b). In addition to the smaller radial area, after forty-eight hours the leading edge of the treated cultures had a lower density of cells (Fig7.9c). This effect was also consistent after seventy-two hours (Fig 7.9d).

Fibroblasts lacking *Ta3* have previously been described as moving with less directionality in the scratch assay (Bangs et al., 2011). Positioning of the trans-golgi-network is an excellent marker to determine the direction of the cell because it is known to orientate itself relative to the nucleus in the direction of cell motility (Kupfer et al., 1983, Nabi, 1999, Yadav et al., 2009). To determine whether cell direction was the cause of aberrant neurosphere migration, cells were fixed after seventy-two hours and immunolabelled for trans-golgi-network marker TGN46 (Fig 7.10). In untreated cultures the central core of cells had a random orientation however at the leading edge (region of ~250 µm) cells were preferentially pointed in a radial direction (Fig 7.10a,b). To see if any difference in cell direction was evident in cultures with loss of *Ta3*, cells at the leading edge were quantified according to their direction. To ensure equal comparison ROIs (250 µm x 320 µm) were taken from opposite sides of the migrational circumference and then rotated to face the same direction (the right direction was chosen as an arbitrary 0°). Untreated cultures showed a clear preference for radial orientation showing a characteristic 'bell curve' in the relative frequency distribution (Fig 7.10c). Surprisingly, treated cultures showed an almost indistinguishable distribution (Fig 7.10c). This suggests at the leading edge of the neurosphere migration assay the directionality of the cells is unaffected by loss of *Ta3*.

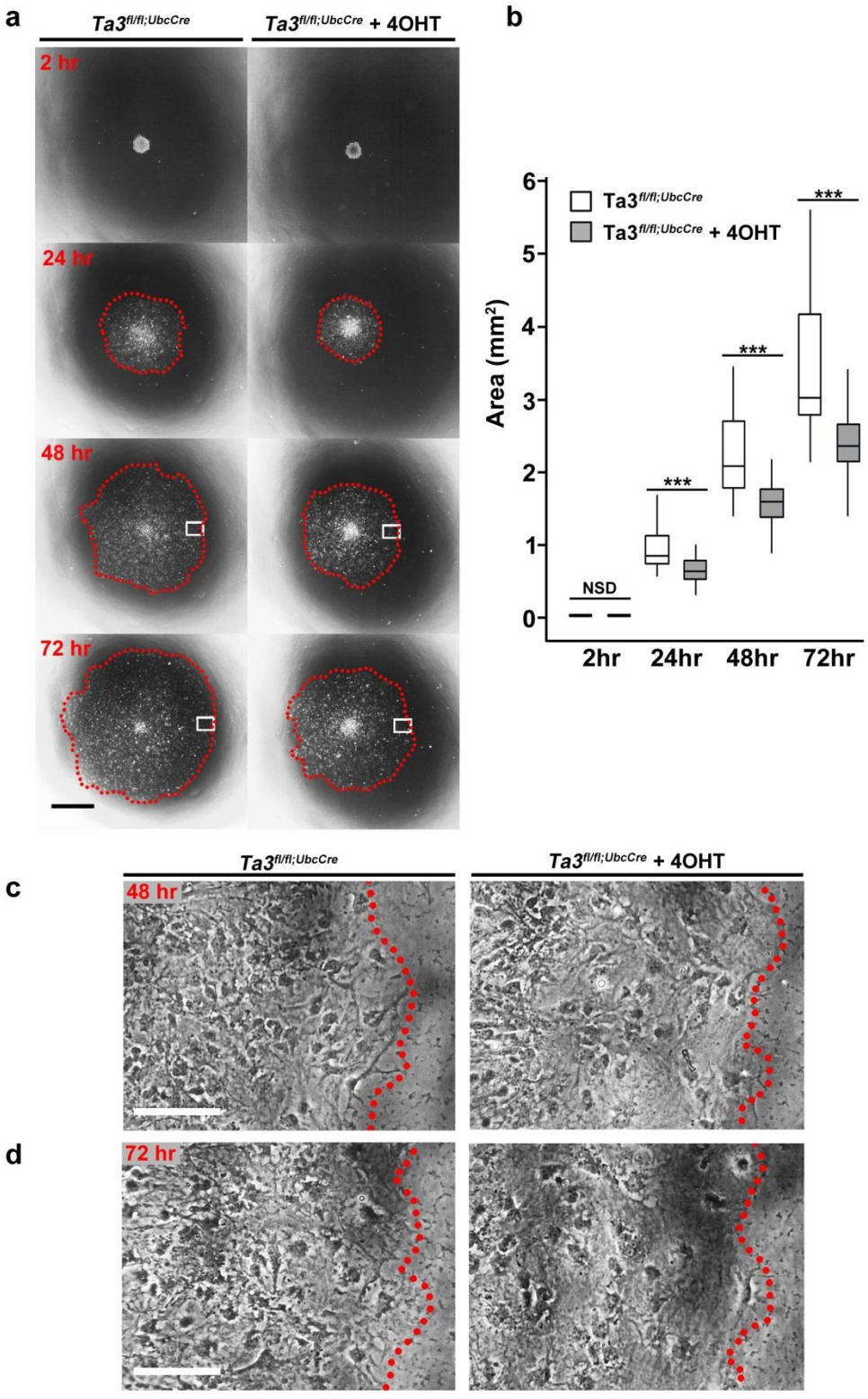

Figure 7.9 Loss of *Ta3* causes a reduction in migration distance

(a) Representative images of neurosphere migration assay where 7day neurospheres (with or without tamoxifen administration) are plated on matrigel and their migration monitored over 72 hours. Red line indicates maximum extent of migration at 72 hours. White box indicates location of higher magnification shown in (c, d). (b) Quantification of migration areas shows that loss of Ta3 results in a reduced migration distance 24, 48 and 72 hours after plating. After (c) 48 hours and (d) 72 hours, cells at the outer edge appear more diffuse following loss of Ta3. Scale, 500 µm (a), 100 µm (c, d). Error bars, box plot (control; n = 36, 4OHT; n=35) *** P<0.001 (one tailed Mann-Whitney test).

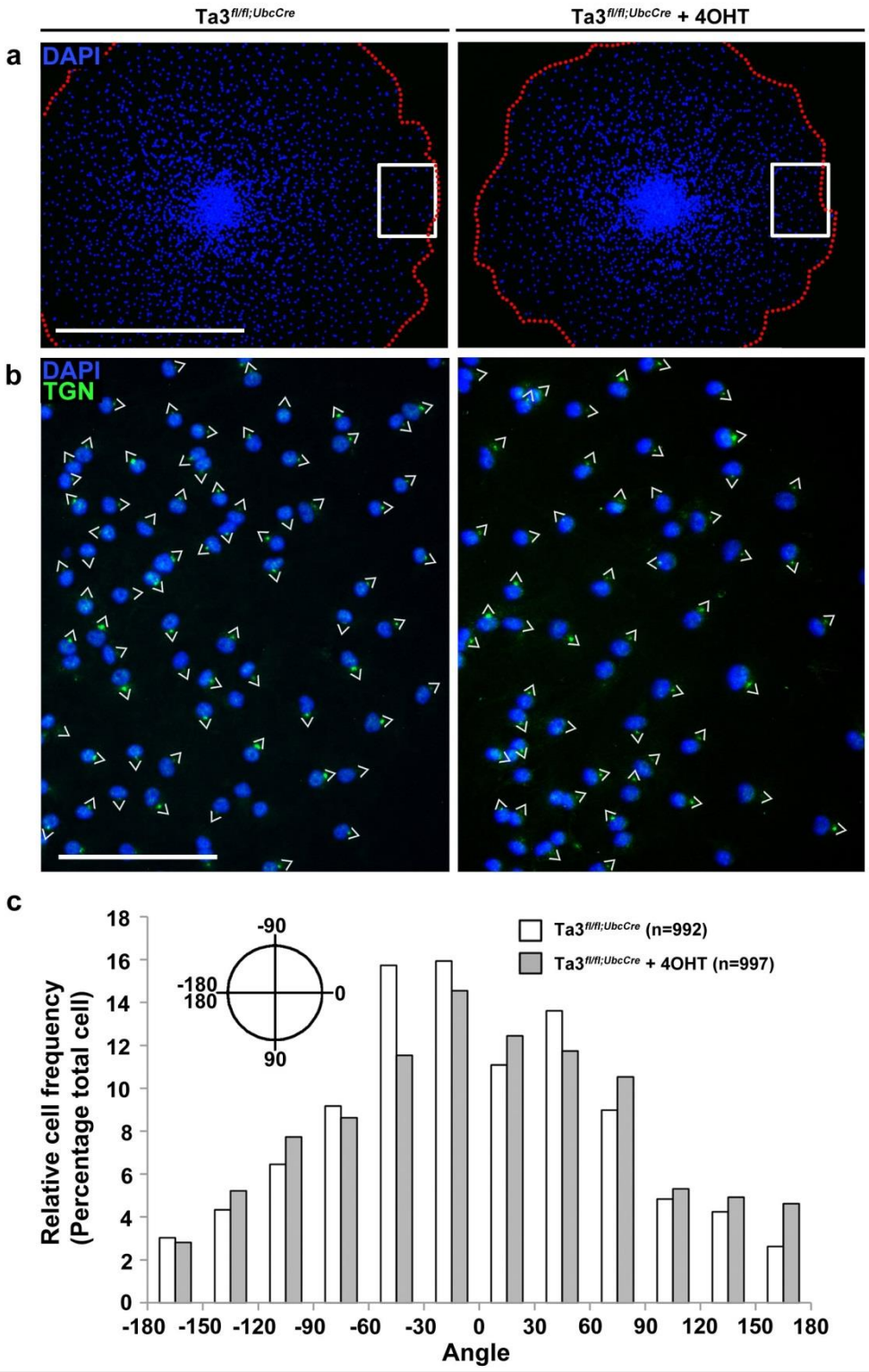

Figure 7.10 Leading edge migrating cell direction is unaffected by loss of *Ta3*

(a) Low power magnification of neurosphere migration after 72 hours. White box indicates 250 x 320 µm ROI used to quantify cell orientation shown in (b). (b) Immunostaining for trans-golgi network marker TGN46 (green). Cell orientation was determined the position of TGN staining relative to the nucleus (Indicated by white arrows). (c) Relative frequency histogram of outer cell orientations following rotation of ROIs to the right of the neurosphere. Cells orientated radially in an outward direction had an angle of 0°. Cells orientated perpendicular had an angle of either 90° (down) or -90° (up). The majority of cells exhibited a radial orientation and this distribution was very comparable in following loss of Ta3. Measurements were taken from 12 neurospheres for each condition and a total of 992 cells (control) and 997 cells (4OHT) measured.

7.3 Discussion

An *in vitro* approach was taken to begin to address the questions arising from the *Ta3*$^{fl/fl;NesCre}$ mouse hippocampal phenotype. Firstly, existing neurosphere methodology from the Subramanian laboratory was optimised for use with cells isolated from dorsal hippocampal tissue. The use of *Ta3*$^{fl/fl;UbcCre}$ mice as a starting material allowed the conditional deletion of *Ta3* after neurosphere isolation and addition of 4-OHT was shown to cause robust recombination in the cells. Loss of Ta3 function caused a reduction in colony size after seven days growth but no change was seen in the colony forming efficiency or BrdU incorporation. Treated cells differentiated for six days were shown to have a significant reduction in primary cilia with a disruption of the actin cytoskeleton. The differentiating conditions were unable to induce formation of mature neurons but early cell fate choices could still be determined through the presence of intermediate filaments. Cells with loss of *Ta3* showed no difference in cell fate choice and still exhibited a high proportion of progenitors consistent with untreated controls. Treated cells did, however, show a marked decrease in migration as shown by the neurosphere migration assay. Fewer cells were apparent at the leading edge but despite previously publish observations (Bangs et al., 2011) cell orientation appeared unaffected.

The level of recombination was measured by taking samples of neurosphere cultures which were prepared for PCR using direct cell lysis. Whilst this created adequate template for PCR reactions, DNA concentration could not be accurately quantified due to other contaminants and degradation of high molecular weight DNA. This meant that comparisons between samples relied on approximately the same number of cells being collected in each neurosphere sample. Despite this potential source of error, qualitative assessment of the PCR product showed that treated cultures had a substantial increase in the presence of the deleted product (273bp) at the expense of a decrease in floxed product (470bp). To strengthen these conclusions it would have been preferable to include an additional PCR reaction of a standard housekeeping gene, such as GAPDH, to act as a DNA loading control.

Perhaps the more critical assessment of homozygous *Ta3* recombination was the absence of primary cilia on differentiated cultures. Treated cultures showed a 6.8 fold reduction in ciliated cells. The fact that some ciliated cells still remained in 4-OHT treated

cultures suggested that the induction system did not affect every cell. As experimental cells were isolated from mice genotyped to be positive for *Ta3*$^{fl/fl;UbcCre}$, all cultured cells should have been carrying the *UbcCre* transgene. Ta3 has also been shown to be essential for cilia formation (Bangs et al., 2011, Yin et al., 2009) and it is highly unlikely that cilia were still present in the absence of functional Ta3. Together these data suggest that the remaining cilia present on treated cultures were due to incomplete recombination of the *Ta3*^{fl} allele. Preliminary studies trying to optimise the recombination in *Ta3*$^{fl/fl;UbcCre}$ cells *in vitro* found low levels of intact *Ta3*^{fl} when administering lower doses of 4-OHT (data not shown). The same effect was also found *in vivo* when administering tamoxifen to live mice (data not shown). This demonstrated that the dose of 4-OHT *in vitro* was critical to achieving sufficient levels of recombination. Previously published studies using the same *UbcCreER*^{T2} in neurosphere lines have used final concentrations of 0.2 µm (Thiel et al., 2010), 0.5 µm (Singh et al., 2013, Ragland et al., 2013) and 1 µm (Leguillier et al., 2012). In this study the dose of 4-OHT was increased to match the highest published doses of 1 µm and these were given on two separate occasions to try and cause homozygous recombination of the *floxed Ta3* allele. One of the important considerations in the experimental design was causing a sufficiently high level of recombination of *Ta3* without excessive levels of 4-OHT causing an adverse effect on the cells. Rather than solely relying on published information, an improvement to the approach would have been to complete our own tests to determine the toxic doses of 4-OHT.

Although genetic analyses suggested a sufficiently high level of recombination in the experimental cells it still appeared insufficient to cause complete recombination. It is likely that cells with cilia remaining only underwent heterozygous recombination of *Ta3*, or avoided it altogether. Mice with heterozygous loss of *Ta3* show no overt phenotype either in *Ta3*$^{fl/wt;NesCre}$ mice or constitutive *Ta3*$^{+/-}$ mice generated previously (Bangs et al., 2011). An improvement to the current approach would have been to breed *Ta3*$^{+/-}$ and *Ta3*$^{fl/fl;UbcCre}$ mice together, followed by intercrossing of offspring to isolate neurospheres from postnatal mice of genotype *Ta3*$^{fl/-;UbcCre}$. This would have effectively halved the number of recombination events required to achieve homozygous loss of *Ta3* and may have resulted in an even more efficient system.

An alternative explanation for the persistence of cilia, which has largely remained unstudied, could be due to low turnover of ciliary components in the cell. In a study looking at postnatal cilia loss, *Kif3a*$^{fl/fl;Z/EG}$ mice were injected with an adenovirus which contained a *Cre* construct (Tong et al., 2014). Interestingly the group showed that after 30 days, despite the occurrence of recombination, cilia were still present on many cells. They further demonstrated that only after 40 days had most of the cells lost their cilia and suggested that it may be related to low turnover of essential proteins or may be associated with the quiescent population neural stem cells (Tong et al., 2014). Although this poses an interesting concept it leaves a number of unanswered questions, especially why other cilia mutants do not experience this delay. Nonetheless it raises the intriguing possibility of whether the cells in the current study did in fact undergo recombination but the time period was insufficient to see complete loss of cilia. Analysis of the Ta3 protein present within the treated cells would begin to address this question.

Despite the difficulties achieving the best level of recombination in the current study caused a striking loss of primary cilia. This still allowed further study of the cells to better analyse the loss of *Ta3* and interpret the *in vivo* phenotype. One of the consequences of *Ta3* loss in neurospheres lines was a smaller colony size. This suggested a reduction in progenitor proliferation consistent with the loss of dividing progenitors seen in the *Ta3*$^{fl/fl;NesCre}$ hippocampus. To try and demonstrate this, BrdU incorporation was assessed to quantify the number of cycling cells. Surprisingly, despite neurospheres exhibiting an incorporation in 15-20% of cells, treated cultures with loss of *Ta3* showed no difference in BrdU incorporation. This result was unexpected given that *Ta3* mutant hippocampus shows proliferative defects *in vivo*. It is possible that, at this stage, the test was not sensitive enough to observe a significant reduction. It is likely that the cells exhibited changeable growth kinetics over the seven day period however a study of adherent cultures of neural progenitors suggests that they reach their exponential growth phase after approximately 7 days (Sun et al., 2011). It is possible that differences in the neurospheres and colony size arose due to changes in growth across the whole seven day period. It may be that single point analysis after seven days missed critical differences which arose due to a cumulative effect. To test this idea further more complex proliferation analysis could be completed at multiple time points. One approach to more accurately compare cell cycle dynamics would be to use a short BrdU incorporation followed by propidium iodide staining and FACS

analysis as described previously (Savatier et al., 2002). This procedure is able to accurately identify the percentage of cells in G1, S and G2/M phase of the cell cycle and would provide useful information not easily acquired *in vivo*. An alternative approach could utilise multiple BrdU analogues such as Chlorodeoxyuridine (CldU) or Iodouridine (IdU). An interesting idea could be to label cycling cells prior to 4-OHT administration followed by additional of a different label after administration similar to that described previously (Lim et al., 2012). Analysis of the proportion of double labelled cells would allow the number of cells re-entering the cell cycle to be assessed following loss of *Ta3*.

Considering other reasons for reduced colony size, the current study did not rule out the contribution of increased apoptosis or necrosis. The demonstration that treated cells exhibited the same colony forming efficiency as untreated cells indicated that cell survival was unaffected. In addition the number of pyknotic cells still appeared comparably low in treated cultures. Nevertheless, it could still remain a causative factor of smaller neurosphere and colony size across the seven-day period. This factor will need to be addressed either by staining for active caspase3 or terminal deoxynucleotidyl transferase dUTP nick end labelling (TUNEL) to identify apoptotic cells.

Assessing the growth phenotype using adherent culture had the distinct advantage of ensuring clonal colony growth. Free-floating cultures showed evidence of neurosphere fusion during optimisation of the technique, which was a confounding variable for assessing neurosphere size. This is not an uncommon feature of neurosphere culture and is an important consideration when selecting culture methodology (Jessberger et al., 2007). Both free-floating and adherent cultures have been shown to allow growth of neural precursors with similar characteristic, but neurosphere culture is reported to improve consistency of growth properties over multiple passages (Sun et al., 2011). The combined use of these techniques worked well in the current study and utilised the strengths of each to compare the loss of *Ta3*.

It is likely that the smaller colony size seen *in vitro* and the reduction of hippocampal progenitors seen *in vivo* are regulated by the same mechanism following loss of *Ta3* and primary cilia. The cells which were isolated and propagated from the P5 mice are the progenitor cells which are rapidly dividing to populate the growing hippocampus. At this age the bulk of proliferation in the hippocampus occurs within the dentate gyrus and so they are

highly likely to represent the progenitors of the SGZ and SPZ. The small colony size seen in the current chapter reflects the smaller size of SGZ and SPZ seen *in vivo*. Although we were unable to demonstrate proliferative defects *in vitro* the results are in agreement with the overall reduction in the total number of progenitors (MCM2-positive) and the level of proliferating cells (Ki67-positive) seen *in vivo*.

The current *in vitro* system provides a great opportunity to investigate the mechanistic cause and future experiments will provide valuable information on the proliferative phenotype in hippocampal cells. To date there have been limited studies looking at loss of primary cilia in hippocampal cultures. Breunig and colleagues (2008) showed that, in slice cultures, loss of primary cilia rendered hippocampal progenitors unable to respond to exogenous Shh. In a different study, cultures isolated from the perinatal SVZ demonstrated that neurospheres require cooperation between Shh and EGF signalling to regulate their formation and growth (Palma and Altaba, 2004). Under similar culture conditions used in the current study, the Hh inhibitor, cyclopamine, was able to reduce neurosphere proliferation indicating the occurrence of autocrine or paracrine Hh signalling within neurospheres. Given the known roles of hippocampal Shh *in vivo* (Machold et al., 2003, Breunig et al., 2008, Han et al., 2008), the signalling pathway is a prime candidate influencing the growth of hippocampal neurospheres following loss of *Ta3*.

In addition to Shh there are numerous other candidate signals which could be regulating the colony size following loss of *Ta3*. EGFR has been shown to localise at the primary cilium in the kidney neurosphere line (LLC-PK_1) where it has a role influencing polycystin2 function (Ma et al., 2005). It has yet to be demonstrated whether EGFR localises on primary cilia in other cell types but, given that EGF is one of the key mitogens driving the *in vitro* neurosphere culture, it is possible that loss of primary cilia could affect the transduction of EGF signalling. Inhibition of glycogen synthase kinase 3β (gsk3β) is able to potentiate canonical Wnt signalling. Addition of gsk3β inhibitors to embryonic hippocampal cultures has been shown to cause an increase in the size and number of neurospheres (Holowacz et al., 2013). Although the role of Wnt signalling through primary cilia is controversial, many groups suggest that loss of primary cilia results in potentiated Wnt responsiveness (Corbit et al., 2008, Gerdes et al., 2007). As this scenario would produce increased proliferation it seems unlikely that modulation of Wnt due to loss of primary cilia

is the cause of smaller colony size.

When considering the phenotype *in vivo*, study of the affected signalling pathways proved difficult due to the small size of the dentate gyrus and limited tissue available for genetic or proteomic analyses. It will be important for further work to investigate which signalling pathways are affected in neurospheres with loss of *Ta3* and what mitogenic signals they are still capable of responding to. This may help shed new light on the pathways affected in the mouse dentate gyrus.

The differentiation of disassociated neurospheres is a useful paradigm to look at the maturation of neural cell types. Immunodetection of the acetylated α-tubulin scaffold demonstrated that, apart from lacking primary cilia, cells with loss of Ta3 had no visible microtubule disruption. In contrast, treated cells had fewer F-actin stress fibres compared to untreated controls. These observations are consistent with cytoskeletal phenotypes seen in other Ta3 deficient cell types including *talpid*^{3} chick neural tube, cultured *talpid*^{3} chick limb cells (Yin et al., 2009) and *Ta3*$^{flfl;PrrxCre}$ mouse limb fibroblasts (Bangs et al., 2011). Actin defects are not unique to Ta3 disruption and are likely to be due to loss of primary cilia. Loss of IFT88 and basal body proteins BBS4, BBS6, Mks3 have also been shown to disrupt the actin cytoskeleton (Jones et al., 2011, Hernandez-Hernandez et al., 2013, Dawe et al., 2009). The extent of which the disruption of actin contributes to the *Ta3*$^{fl/fl;NesCre}$ hippocampal phenotype is unclear but it could well contribute to alterations in cell behaviours, especially defective migration. Further analyses of the actin *in vivo*, or even *ex vivo* techniques such as slice culture may allow live imaging of actin dynamics in a more representative system.

The *Ta3*$^{fl/fl;NesCre}$ dentate gyrus exhibited a loss of progenitors with an associated reduction in the branching of the GFAP scaffold. Identification of intermediate filaments nestin and GFAP provided an indication of the early cell fate choice made by the differentiated progenitors in culture. Despite many of the cells having a similar flattened morphology, proportional analysis of the discernible cell types clearly demonstrated a heterogeneous mix of cells with the three probable fates being neuronal, astroglial and glial. No difference in the cell proportions was observed following loss of *Ta3*. One explanation for this is that cell fates had already been determined prior to loss of *Ta3*. Whilst this is plausible, it has been demonstrated that fate can be determined during neurosphere

culture for example by inhibiting notch signalling (Ma et al., 2014). In the study administration of γ-secretase inhibitor N-(N-(3,5-Difluorophenacetyl-L-alanly))-S-phenylglycine-t-Butyl Ester (DAPT) to embryonic hippocampal neurospheres was able to increase the proportion of neuronal fate as determined by Tuj1+ neurons. Although the current study only assesses intermediate filaments it is tempting to speculate that early cell fate decisions in postnatal hippocampal progenitors are unaffected by loss of primary cilia. Further experiments utilising cells grown from clonal origins would prove interesting in understanding the heterogeneity seen in the hippocampal cultures and the importance of primary cilia on cell fate.

Another important observation from the intermediate filament staining was that the GFAP scaffold appeared unaffected in cells with loss of *Ta3*. Filaments had a comparable organisation with equal levels of spreading and branching between treated and untreated cells. When considering the glial phenotype *in vivo,* cells of the dentate gyrus often had fewer branches and Bergmann glia of the cerebellum were disorganised and misshapen. The *in vitro* data suggests that the glial defects seen *in vivo* are not inherent cellular defects and that under culture conditions at least they appear to develop a normal structure. It suggests that the *in vivo* glial defect could be due to extrinsic defects such as transduction of signals guiding their structure or their maturation. They could even be secondary to other defects, for example the loss of granule progenitors may affect the glial maturation through a reduction in cellular interaction.

One aspect of the current study which would benefit from improvement would be differentiation of cells into a more mature state. Most differentiation protocols remove mitogenic stimulation to induce quiescence and allow differentiation. In the current study, differentiation was sufficient to induce quiescence as demonstrated by presence of primary cilia. Despite this, cells still maintained expression of Pax6, indicating an immature state. In terms of the cellular morphology, may of the cells were flattened with a spread out appearance most similar to astroglia. It has been reported that adult hippocampal cultures grown as neurospheres have a greater tendency to differentiate towards glial lineages (Oh et al., 2014). This effect has also been reported after extended passages of neurosphere cultures from other brain regions (Seaberg et al., 2005). Given the heterogeneity of differentiated cultures in the current study and lack of GFAP expression in a number of cells this does not appear to be the cause of the loss of mature neuronal phenotypes. Instead it

may be that further optimisation of the existing differentiation media such as removal of serum or FGF may improve mature neuronal fate in hippocampal culture. An alternative approach could be the use of co-culture systems to provide soluble factors to enhance neuronal differentiation. One alternative described previously (Kawasaki et al., 2000) and already in use in use in the Subramanian laboratory (Subramanian et al., 2008) is the co-culture of cells with the stromal cell line (PA6). In embryonic stem cells (Kawasaki et al., 2000), embryonic carcinoma cells (Subramanian et al., 2008), and in whole brain postnatal neurosphere culture (unpublished data) this system has been proven to be a very effective inducer of mature neuronal fate.

Ectopic neurons and progenitors are evident in *Ta3*$^{fl/fl;NesCre}$ dentate gyrus and this is hypothesised to be a result of defective cell migration. *In vivo*, cells were seen to accumulate in GCL due to a defect in SPZ-to-hilar transition and this correlated with defects in the underlying glial scaffold. In this current chapter, data are presented showing defects in the cellular migration which are independent of the underlying scaffold. Hippocampal neurospheres with a loss of *Ta3* showed a reduction in migration distance using the neurosphere migration assay. Fewer cells were seen at the leading edge suggesting that loss of *Ta3* caused more cells to remain in the neurosphere core. As the assay utilised neurospheres of the same size and differentiating medium lacking mitogens, the difference is unlikely to be caused by altered proliferation. Another interesting feature of the assay is that it does not establish any gradients of soluble molecules which drive the direction of the radial migration. Instead, migration differences in this assay are likely to be the result of intrinsic defects in the ability of cells to move, rather than their ability to orientate themselves towards a soluble signal. This is perhaps illustrated by treated and untreated controls showing the same relative frequency of cells with radial orientation. This is in contrast to other 2D migration assays such as the scratch assay where cells lacking *Ta3* were described as having less directionality (Bangs et al., 2011). It cannot be ruled out, however, that the analysis of cells at the leading edge could have preferentially selected those which had better migration ability and escaped homozygous recombination. Due to the random of orientation of cells inside of the leading edge, orientation could not be compared. These data suggest that, in the *in vivo* hippocampal phenotype, defects in both the migrating cells and the underlying glial scaffolds contribute towards the migratory defect and failure of

SPZ-to-hilar transition.

To our knowledge this is the first example of the neurosphere migration assay being used to compare cells with loss of primary cilia. Scratch assays have been used to compare other cilial components in different cell types including endothelial cells and MEFs with hypomorphic loss of IFT88 (Jones et al., 2011, Clement et al., 2013) and kidney cells lacking BBS4 or BBS6 (Hernandez-Hernandez et al., 2013). In all cases, cells with loss of cilia were shown to have reduced migration ability. MEFs have been shown to require primary cilia to transduce PDGFα signalling required for directional cell movement (Schneider et al., 2010). It has been further shown that loss of IFT88 influences PDGFα signalling which has a resultant effect on MEK1/2 – Erk1/2 pathway and ultimately affecting actin distribution at the lamellipodia of migrating fibroblasts (Clement et al., 2013). This mechanism appears important in cell directionality because, in the scratch assay, cells are acting to fill a gap and presumably detect soluble molecules originating from the opposite side of the scratch. In contrast the neurosphere migration assay starts with cells present on a central island and explore the radial acellular environment. It is currently unclear the extent to which PDGFα acts in this system but analysis has shown that cells isolated from whole hippocampus do express factors of the PDGFα signalling pathway (Gilley et al., 2011). This relationship provides an interesting area for further research and will be important to investigate *in vivo*.

One question which remains unanswered is why only specific cell types in the *Tα3*$^{fl/fl;NesCre}$ dentate gyrus appear to have migration defects. It could be that these cells are guided by different directional signals transduced by the primary cilia or it could also be due to their mode of migration and substrate which they attach to. Migration defects in response to soluble signals are better studied using different *in vitro* paradigms such as the microfluidics chambers used by Higginbotham and colleagues (2012) to study Arl13b function. The interaction with ECM following loss of primary cilia is an interesting consideration and something which could be further investigated using the neurosphere migration assay. Integrins, the transmembrane structural unit which connect the actin cytoskeleton to the ECM, have been found to localise in primary cilia in chondrocytes (McGlashan et al., 2006), airway smooth muscle cells (Wu et al., 2009) and vascular smooth muscle cells (Lu et al., 2008). As cells with loss of *Tα3* have disruption in the actin cytoskeleton *in vitro* it would be interesting to see there is any link between the migration defects and their interaction with the ECM. It is possible that certain cell types, which may

utilise different integrin subunits, or the different substrates which cells migrate on *in vivo* could influence the severity of phenotype. To consider this in a more complex organisation it would be fascinating to assess the migration deficiencies in co-culture systems such as on glial monolayers.

In the current chapter some of the questions arising from the *in vivo* $Ta3^{fl/fl;NesCre}$ phenotype have started to be addressed. These key *in vitro* observations include the smaller colony size, the normal formation of glial scaffold and the defect in cell migration. All of these provide additional information supporting the *in vivo* hippocampal phenotype. The use of this culture system has also established a firm foundation for which further studies can be completed to try and answer the mechanistic consequences of *Ta3* loss. Given the small size of the hippocampus, molecular experiments using dissected material are both challenging and limited by small tissue available. Here, an excellent system with expandable cultured cells is presented to continue work assessing the cellular hippocampal phenotype following loss of *Ta3*.

Chapter 8 – Discussion

This project investigated the roles of Ta3 in the developing brain. We have presented a detailed characterisation of the phenotype of mice with conditional loss of *Ta3* using the *NesCre* deleter strain. Mutant mice developed ataxia, hydrocephaly and distinct defects in the cerebellum, cortex and hippocampus. The mechanistic cause was shown to be a result of loss of primary cilia and many of the defects could be attributed to defective transduction of the Shh signalling pathway. To date, only a limited number of studies have conditionally removed cilial components throughout the developing nervous system and fewer still have targeted basal body proteins. Here the detailed analysis provides greater detail as to the emerging neural roles of Ta3 and primary cilia.

Throughout the study the $Ta3^{fl/fl;NesCre}$ mutant phenotype resembled the neural defects seen in cases of human ciliopathies. For the first time we present data that demonstrates mutations in *TA3* in a clinical case of Joubert Syndrome (JS). Combined with phenotypes shown in constitutive loss of *Ta3*, such as polydactyly (Bangs et al., 2011), we present a wide spectrum of defects associated with this condition. Furthermore we describe defects in brain regions such as the cortex and hippocampus which to date have received relatively little attention in clinical investigations of JS. The $Ta3^{fl/fl;NesCre}$ mutant mouse represents a valuable model system to study the neural defects in JS and begin to understand the mechanistic cause of a rare but clinically relevant condition.

Throughout the project there are a number of key cellular phenotypes which appear in similar ways throughout the different regions of the brain. These reoccurring defects provide the greatest insight into the neural role of Ta3. A reduction in the size of the progenitor population was seen most notably in the cerebellum and hippocampus. The resultant effect was the smaller size of mature structures. In both cases the smaller progenitor population was accompanied by a reduction in the number of proliferating cells. Due to the fact that the cerebellar and hippocampal progenitors produce both neurons and more progenitors it is probable that the loss of proliferation caused a knock-on effect of fewer progenitors which in-turn resulted in the further reduction of proliferation. Ultimately this resulted in fewer mature neurons in these two brain structures. Interestingly, this proliferative defect does not appear to be a universal phenotype in the *Ta3* mutant brain as

proliferative defects in the cortex were not immediately obvious in the time points investigated. Furthermore the overall size of the brain was not uniformly reduced as seen in cases of microcephaly, which can be caused by defects in some centrosomal proteins (Mochida and Walsh 2001). This distinction demonstrates that Ta3 is unlikely to have a role in the actual process of proliferation but instead influences the cellular decision of whether to proliferate or not. This finding is highly consistent with the known roles of Ta3 in the formation of primary cilia and its transduction of important mitotic signals but is a previously undescribed role of Ta3 in the developing brain (Yin et al., 2009, Bangs et al., 2011).

Another key feature described in the cerebellum and hippocampus was a disruption of the radial glial scaffold normally formed by the RGC progenitor population. Whilst this would have been affected by the reduced progenitor population the structure of the scaffolds seemed less organised with fewer branches. The *in vitro* studies suggested that, for the hippocampus at least, the mutant glial cells were still able to form comparably similar glial structures under culture conditions. This demonstrated that the defects in the glial scaffold appeared to be context dependent. This could be due to a secondary effect of the reduced interaction with mature neurons preventing their correct maturation or a loss of signal transduction which normally guides their structural organisation. The latter explanation further highlights the role of Ta3 in allowing the transduction of signals required for glial maturation which are likely to be transduced through the primary cilium. Although the exact reason for the aberrant glial structure is still in question, the consequence appeared to result in migratory defects due to a loss of the substratum normally used to both attach and guide migrating neurons. To our knowledge this is the first description of this type of defect in mutants with loss of primary cilia. This was evident in the cerebellum with granule progenitors trapped in the disorganised molecular layer and also in the hippocampus with the failure of SPZ-to-hilar transition. In both cases the failure to reach their end destination resulted in ectopic progenitors and mature neurons localised in the wrong place. This mislocalisation of neurons in the brain is similar to that described in the somites of *Talpid*^{3} chick mutants (Davey et al., 2006).

Another fascinating finding is the defective migration of hippocampal progenitors seen in the neurosphere migration assay; the first time mutant neurons with loss of cilia have been examined in this way. Here, neurons lacking functional Ta3 migrated less

distance than control neurons at all stages examined. The interesting point is that the design of the assay does not test their migration towards a diffusible signal and is independent of the attachment substratum. Instead, it suggests that there may be inherent defects in the ability of *Ta3* mutant neurons to migrate. To date, there have been limited studies looking at neuronal migration and primary cilia. Those that look at the tangential migration of interneurons attribute the defects seen in migration path and cortical placement to aberrant signal transduction. Whilst this is likely to play a role in the current study it is also possible that defects in the mutant cytoskeleton may contribute to the migratory defects. The cilium and basal body are microtubule based structures however the actin cytoskeleton is closely associated around the basal body and both can be influenced by proteins present in the basal body (Hernandez-Hernandez et al., 2013). The actin cytoskeleton is essential for generating the driving force in migrating cells where it is responsible for attaching cells to the extracellular matrix in addition to generating the morphological changes seen in migrating cells. In the current study we show defects in the actin cytoskeleton of mutant neurons consistent with previously described data (Yin et al., 2009, Bangs et al., 2011). Based on the *in vitro* data it is tempting to speculate that neurons with loss of Ta3 also exhibit migrational defects caused by deficiencies in the mutant cytoskeleton. This idea is supported further by additional observations, which are not described in the current study, where loss of Ta3 results in loss of focal adhesions and increased actin at the ruffled membrane of migrating cells (Yin et al., 2009, Bangs et al., 2011). It is likely that cytoskeletal defects act in tandem with the loss of cilia-related signal transduction and aberrant glial scaffolds which all contribute to the migratory defects seen in *Ta3* mutant neurons. This is a novel finding of the role of Ta3 in neural migration.

Ultimately the disruption of proliferation and migration seen the *Ta3* mutant brain caused a disorganised phenotype which had varying severity in different regions of the postnatal structure. This is likely to be due to the time at which these structures develop; for example the cortex, which exhibited a relatively mild phenotype, develops early during brain development whereas the cerebellum and hippocampus, which show much more striking defects, are structures which predominantly develop postnatally. Importantly, it also demonstrates that not all regions are reliant on cilia-dependent events in the latter half of brain development. It shows that there are a range of cellular mechanisms which are employed to direct the development of such a complex structure.

8.1 Primary cilia and Shh are essential for brain development

Ta3 has previously been shown to be required for primary cilia formation (Yin et al., 2009, Bangs et al., 2011). Understandably, many of the phenotypes described in the *Ta3* mutant mice can be attributed to loss of primary cilia and, more specifically, loss of Hedgehog signalling which is known to be transduced through this organelle. Shh is a morphogen with a crucial requirement in early patterning events of the brain between E8.5-E14.5, however, after this point it has a more specific role maintaining proliferation, cell maturation and migration (Traiffort et al., 2010). The *NesCre* deleter has been reported to cause excision from E11.5 onwards (Tronche et al., 1999, Heffner et al 2012) however it has been suggested that complete recombination may not occur until later in embryogenesis (Liang et al., 2012). The $Ta3^{fl/fl;NesCre}$ mutant mouse correctly specifies the CNS and establishes a gross regional organisation comparable to control mice at E14.5. As only one embryo was investigated at this stage it is unclear whether the $Ta3^{fl/fl;NesCre}$ mutant mice exhibit more discrete patterning defects at this stage. However, given the time of recombination caused by the *NesCre* deleter it is probable that loss of cilia occurs after the early role of Shh establishing the broad regional identities.

Consistent with the later roles of Shh in neural development one of the recurring cellular phenotypes in *Ta3* mutant mice was a loss of proliferation. This was most notable in the cerebellar GNPS and also the hippocampal and cortical progenitors. Furthermore, increased apoptosis was seen in the cerebellum and the smaller size of neurospheres suggests a likely reduction in cell proliferation and/or survival. These roles are highly consistent with those of Shh, which is known to activate transcription of *CyclinD1* and *N-Myc* which promote progression through the cell cycle (Oliver et al., 2003). It is possible that the loss of proliferation alone is a contributing factor to some of the phenotypes seen in the *Ta3* mutant brain. For example, the laminar disorganisation of the cerebellum or the loss of glial fibres in the hippocampus are likely to be a direct result of fewer cells being present in the correct location. With this in mind, future experiments which target postmitotic populations of cells need to be performed to determine other functions of Ta3.

The loss of *Ta3* throughout the developing CNS using the *NesCre* deleter provided an excellent starting point to assess the neural requirement of Ta3. Many of the studies which

investigate the function of basal body proteins *in vivo* have used constitutive mutagenesis to target protein function. These include Ftm, Ofd1, Mks1 and Ta3 (Vierkotten et al., 2007, Besse et al., 2011, Ferrante et al., 2006, Weatherbee et al., 2009, Bangs et al., 2011) but whilst they provide valuable information about early roles of these proteins, embryonic lethality prevents study at later stages. Basal body proteins such as Cep290 and Ahi1 have also been targeted to model JS *in vivo* and these mutant mice survive to adulthood however they show relatively modest phenotypes (Lancaster et al., 2011b). Here we have been able to extend the life expectancy of mice with conditional loss of Ta3 allowing its study in the late embryonic and early postnatal brain.

A distinct advantage of using the *NesCre* deleter is its widespread availability. From the limited number of conditional mutants mice targeting basal body and IFT components, many have also used the *NesCre* deleter making comparisons with the $Ta3^{fl/fl;NesCre}$ mice far more applicable. The conditional primary cilia mutants that have been described include basal body components $Stumpy^{fl/fl;NesCre}$, $Cep120^{fl/-;NesCre}$ (Town et al., 2008, Breunig et al., 2008, Wu et al., 2014), IFT components $Kif3a^{fl/fl;NesCre}$, $IFT88^{fl/fl;NesCre}$ (Wilson et al., 2012, Chizhikov et al., 2007) and also functional component $Arl13b^{fl/fl;NesCre}$ (Higginbotham et al., 2013). Furthermore, many components of signalling pathways such as Shh or Wnt which are associated with the primary cilium have also been targeted using the *NesCre* deleter.

A particularly valuable comparison commented on throughout the project is between $Ta3^{fl/fl;NesCre}$ mice and either *Smo* or *Gli3* mutants. An interesting finding is that in nearly all phenotypes loss of *Smo* results in a more severe phenotype that loss of *Ta3.* This highlights that the defects seen in $Ta3^{fl/fl;NesCre}$ mice are not caused by a simple loss of Shh transduction but also a disruption of Gli processing. Gli2A has recently been demonstrated to require cilia for its correct function (Liu et al., 2015). A knock-in approach demonstrated that endogenous Gli2 which does not localise at the cilium was unable to interact with Smo which meant that it was not released from the inhibitory action of Sufu (Liu et al., 2015). Proteolytic processing of Gli3 into Gli3R also requires intact cilia (Huangfu and Anderson, 2005). To add to the complexity, it has also recently been shown that both Gli3A and Gli3R are degraded in different ways, with Gli3R being more stable than Gli3A (Wen et al., 2010). This means that following loss or disruption of primary cilia it is reasonable to expect a loss of Gli2A function which, as a predominant activator in the pathway, would result in decreased expression of target genes *Gli1*, *Ptc1, CyclinD* and *N-myc*. The other feature

would be a loss of processing of Gli3 into the short repressor form Gli3R and an increase in Gli3A which could still allow transcription of some Shh targets. It is this loss of repression which is thought to make cilial mutant phenotypes less severe than Shh mutant phenotypes. The general understanding is based on embryos with constitutive loss of cilial components. Western blot has shown elevated Gli3A and reduced Gli3R in E10.5 embryos with hypomorphic loss of IFT88 ($IFT88^{hypo}$), complete loss of IFT88 ($IFT88^{-/-}$) (Liu et al., 2005), E11.5 embryos with loss of IFT88 (*Tg737*$^{\Delta 2-3\beta\text{-}gal}$)(Haycraft et al 2005) or Ftm (Vierkotten et al., 2007) and E12.5 telencephalon with loss of Ftm (Besse et al., 2011). Furthermore in the *talpid*^{3} chicken mutant both limbs and trunk show an increase in Gli3A and loss of Gli3R (Davey et al., 2006).

In the current study loss of *Ta3* appeared to have different effects on Gli processing when comparing the mutant cortex and mutant cerebellum. Overall both tissues showed a loss of Shh pathway activation as shown by decreased expression of *Gli1* and *Ptc1* mRNA. Consistent with this finding, both tissues also showed a reduction in Gli2A protein levels. When comparing Gli3 however, the mutant cortex had increased levels of Gli3A but there was no measureable differences in Gli3R. This *Ta3*$^{fl/fl;NesCre}$ cortical phenotype is relatively consistent with the expected Gli3 processing following loss of cilia. In contrast, the *Ta3*$^{fl/fl;NesCre}$ mutant cerebellum had almost undetectable levels of Gli3A but an apparent increase was seen in Gli3R. This unexpected cerebellar phenotype may be due to reduced levels of Shh signalling towards the end of cerebellar development.

Although increased Gli3R does not agree with the general trend in cilial mutants there are a limited number of studies report similar findings. A mouse model targeting Cep290, which is known to interact with Ta3, has previously demonstrated a reduction in the Shh response (Hynes et al., 2014). In adult kidney they further showed that mutants have an increased level of Gli3R. Humans with mutations in the cilial transition zone protein in Tectonic3 (TCTN3) result in a Mohr-Majewski syndrome, a ciliopathy condition with similar phenotypes to MKS and OFD (Thomas et al., 2012). Although rudimentary cilia are still intact, Shh processing defects were evident in *TCTN3* mutant fibroblasts which were shown to result in an increase level in Gli3R. Interestingly both the kidney or fibroblasts studied are not classically associated with Shh signalling which raises the question of whether the Gli3 processing defect seen in *Ta3*$^{fl/fl;NesCre}$ mutant mice could be due to the tissue having reduced levels of signalling in the control environment. Analysis of younger P5

stages, consistent with the experiments completed on *Ta3* mutant cortex, would further investigate this discrepancy between the Gli3 processing in the two tissue types.

When comparing the Gli processing phenotype of *Ta3*$^{fl/fl;NesCre}$ mice to other conditional mutants there are limited data available. In *Stumpy*$^{fl/fl;NesCre}$ mice, Gli3 levels were assessed in P5 hippocampus and a possible increase in Gli3A was detected however protein levels were extremely low and Gli3R was not shown making the results difficult to interpret with confidence (Breunig et al., 2008). The other conditional mutant where Gli processing was addressed was the *Kif3a*$^{fl/fl;NesCre}$ mice. Here mice show an overgrowth phenotype which is in striking contrast to the *Ta3*$^{fl/fl;NesCre}$ cortex. In the study Wilson and colleagues (2012) investigate the Gli3 processing in E12.5 *Kif3a*$^{fl/fl;NesCre}$ telencephalon and demonstrate that *Kif3a* mutants show a predominant increase of Gli3A but little difference in Gli3R.

Although the *Kif3a*$^{fl/fl;NesCre}$ mutants and *Ta3*$^{fl/fl;NesCre}$ mutants have been analysed at different ages, it suggests both tissues follow a similar trend in disrupted Gli processing. However, this does not reconcile the striking phenotypic difference between the *Kif3a* and *Ta3* mutant cortices. The authors suggest that the overgrowth phenotype of *Kif3a* mutants is due to the exceptionally high level of Gli3A causing an increase in the rate of cell cycle progression. Although both *Kif3a* and *Ta3* mutants lack primary cilia, it raises the intriguing question of whether the processing of Gli3 is different between the two mutants. This idea is plausible based on their different roles in the cilium. Ta3 has predominantly been associated with docking of the basal body with the plasma membrane and Kif3a is responsible for the anterograde IFT transport along microtubules. However, loss of *Kif3a* has also been shown to result in centrosomal defects including loss of subdistal appendages (Kodani et al., 2013) which is not the case in other IFT mutants such as Ift88 (Kodani et al., 2013) or *Ta3* mutant centrioles (Kobayashi et al., 2014). In summary, many of the defects described in *Ta3*$^{fl/fl;NesCre}$ mutant mice can be attributed to a disruption of Shh signal transduction. The specific defects in Gli3 processing appear to be consistent with the expected role of cilia but comparison with other conditional primary cilia mutants suggests that differing cortical phenotypes could be due to differences in Gli3 processing.

8.2 Effects on other signalling pathways in primary cilia

Numerous signalling pathways, in addition to Hedgehog, have been implicated at the primary cilium. These include: canonical Wnt (Lancaster et al., 2011, Simons et al., 2005), the PCP pathway (Jones et al., 2008), tyrosine kinase receptors (Christensen et al., 2012), notch receptors (Ezratty et al., 2011), serotonin receptors (Brailov et al., 2000), and somatostatin receptors (Handel et al., 1999). One of the approaches used in the current study to detect pathway defects was to try and identify traits in *Ta3* mutants which phenocopy those seen in mutants of other signalling pathways. No defects were described in *Ta3* mutants which could be uniquely linked to signalling pathways other than Shh. A challenging aspect of this was that many of the *Ta3* mutant phenotypes were dominated by the loss of Shh signalling. This often risked the masking of more subtle phenotypes caused by different pathways. Analysis of mRNA expression in the cerebellum tried to address this question further, at least in the case of the Wnt and Notch pathways, but no difference in known target genes were identified.

During the project P5 cerebellar tissue was collected with the intention of completing whole transcriptome sequencing. Unfortunately due to unforeseen circumstances the analysis is yet to be completed. Having this type of data would be invaluable in helping to establish the link between different signalling pathways and primary cilia. In the study *Wnt7a* was shown to have lower expression in *Ta3* mutants but due to the lack of change in the *Axin2* target gene it was suggested it may be due to the deficit in the number of granule cell number or their maturation. Having whole transcriptome data would allow powerful analysis of a large number of genes which may help strengthen links with other signalling pathways. This work is currently on-going and the results are eagerly awaited.

Here we have shown that Ta3 is essential for the correct cellular morphology of Purkinje cells, Bergman glia and glial progenitors. There are a number of factors which are likely to contribute to these defects seen in mutant mice. In the cerebellum Shh is thought to have a role in the maturation of Bergmann glia (Dahmane and Altaba, 1999). Secondary effects such as the loss of proliferation could also have contributed to the morphology of these cell types (Otero et al., 2014). In the current study we showed that the spreading of GFAP-positive fibres in *Ta3* mutant cells *in vitro* appeared unaffected. This would suggest that the morphological defects in the glia are context dependent. When considering the

Purkinje cells however there is evidence showing that dendritic aborisation is severely disrupted in neurons with dysfunctional primary cilia (Guadiana et al., 2013). In the study by Guadiana and colleagues, disruption of cilia was achieved by overexpression of somatostatin or serotonin receptors but it was unclear whether the phenotype was directly due to these pathways or a general disruption of cilial function. For this reason, loss of primary cilia cannot be eliminated as a cause of the disrupted cellular morphology. Further *in vitro* studies using isolated cell types will be essential in understanding morphological defects caused by loss of primary cilia.

8.3 Cilia independent roles for Ta3

One of the exciting yet challenging aspects of this project was trying to identify novel roles of Ta3 which are independent of primary cilia. As a centrosomal component Ta3 has been shown to interact with a number of essential proteins involved in protein trafficking (Kobayashi et al), centriole duplication (Wu et al., 2014) and docking of centrosomes with the plasma membrane (Bangs et al., 2011). It is therefore quite possible that Ta3 may have other cellular roles. Through detailed characterisation of the phenotype following loss of *Ta3 in vivo* and *in vitro* we attempted to identify aspects which may be distinct from cilia.

A consistent defect seen in the $Ta3^{fl/fl;NesCre}$ mutant was incomplete or aberrant migration. In the cerebellum this was evident in misorientated granule neurons many of which failed to reach the IGL. In the hippocampus ectopic progenitors were also present in the GCL and mature granule neurons were located outside of the GCL. In support of these observations the *in vitro* neurosphere assay demonstrated reduced migration which suggested a defect inherent in the cell itself rather than a lack of signal transduction. It is intriguing then why only certain cell types appear to show migration defects in *Ta3* mutant brains. One assumption is that morphogen gradients, such as Shh, may not be correctly transduced, preventing cells from detecting the 'correct' migrational path. An alternative explanation was that the scaffold on which cells migrate was disorganised and insufficient for the cells to move along the 'correct' path. Evidence is presented to support this idea, showing the correlation of poor granule migration with disoriented glial scaffolds in both the cerebellum and hippocampus. However, as neither explains the reduced migration *in vitro* they are unlikely to be the sole causes of the migration defect.

The neurosphere migration assay provides a unique paradigm where cells are not migrating towards a signal and the underlying scaffold is uniform. Migration defects of *talpid*^{3} mutants cells *in vitro* were first described in explant culture of chick limb mesenchymal cells (Ede and Flint, 1975). The saltatory migration of *talpid*^{3} mutant cells had greater periods of rest rather than defective migrational speed. Work by Yin and colleagues (2009) provided a mechanistic explanation for this, showing that *talpid*^{3} mutant cells *in vitro* exhibit slower microtubule regrowth. Presumably this is a result of the centriole function as the key microtubule organising centre in the cell. These data would support the migrational defects seen in neurosphere migration assay in addition to the ectopic cells seen *in vivo*. A scenario is possible in the *Ta3* mutant cerebellum and hippocampus where slow moving cells simply become trapped in the rapidly developing matrix. For the first time here we have presented migration defects in neural cells lacking *Ta3*. These appear consistent with migration defects seen in the limb and suggest that Ta3 has an important role in the correct movement of cells.

8.4 *Ta3*$^{fl/fl;NesCre}$ as a model for Joubert syndrome

The gross neural defects and cerebellar malformation of *Ta3*$^{fl/fl;NesCre}$ mutant mice, presented in Chapters 3 and 4, closely resembled the traits seen in humans with known ciliopathy conditions. Mice exhibited progressive ataxia with a severely hypoplastic cerebellum. Mutant cerebella also had a reduced vermis and defects were evident in the decussation of the cerebellar peduncles. Through collaboration with clinical investigators we were able to identify one case of JS with mutations in the *TA3* gene. Despite there being 27 genes identified as causative for JS (OMIM), the molecular defect in over half of JS cases is unidentified. The finding of clinically significant mutations in *TA3* is a positive outcome for helping to improve diagnoses and identify causes behind human ciliopathy conditions. Furthermore it gives the *Ta3* mutant phenotype a greater precedence as a model to study a rare but clinically relevant condition.

An interesting consideration is the difference in severity between the described case of JS and the embryonic lethality described in mice with constitutive loss of *Ta3* (Bangs et al., 2011). The compound heterozygous mutations found in human *TA3* correspond to one

allele having a premature stop codon at exon 5 and the other a disrupted splice site preceding exon 11. Together these are likely to result in truncated a *Ta3* transcript and one where exon 11 is skipped. The fact that this combination is not lethal during embryogenesis suggests that some functional protein is being produced. The added observation that the patient does not present with polydactyly also supports the idea that there is incomplete loss of *TA3* function. This is the first evidence that hypomorphic alleles of *Ta3* exist and these may prove essential in understanding its function.

To date a number of tagged domain constructs have been designed to identify functional regions of the Ta3 protein (Yin et al., 2009, Kobayashi et al., 2014). The key functional domain is consistently identified as the conserved coiled-coil domain at exons 11 and 12 (Davey et al., 2006, Yin et al., 2009, Bangs et al., 2011, Kobayashi et al., 2014, Wu et al., 2014). Despite this, relatively little is known about the remaining protein function or its genetic regulation. Further investigating of the clinical mutations in *TA3* and particularly trying to understand the residual function remaining in the exon11-skipped transcript may prove vital in understanding the molecular behaviour of Ta3.

In terms of better understanding JS, the $Ta3^{fl/fl;NesCre}$ mice present and excellent model to study the disease. To date a number of studies have generated mouse models to study JS but these display a great deal of phenotypic variation and often present contrasting causative mechanisms. Better known alleles of JS have been targeted such as *Ahi1* or *Cep290* however the mutant mice showed a relatively mild phenotype (Lancaster et al., 2011). *Ahi1* and *Cep290* mutant mice also show no change in Shh signalling and instead, defects were attributed to loss of the canonical Wnt response. In contrast, a different model targeting *Cep290* using a genetrap mutant ($Cep290^{LacZ/LacZ}$) shows a prominent reduction in Shh signalling but the research mainly focuses on the kidney phenotype (Hynes et al., 2014). The wide spectrum of phenotypes in human ciliopathies is reflected in the variation seen in associated mouse models. Here we present a useful addition to the growing resource available to study this developmental condition.

The $Ta3^{fl/fl;NesCre}$ mice recapitulate some of more severe aspects reported in of JS. They even show phenotypic overlap with MKS including hydrocephaly and severe malformation of the cerebellum (Szymanska et al., 2014). MKS also results in embryonic lethality and this is reflected in constitutive mouse models targeting causative alleles such as

Ftm/Rpgrip1l (Vierkotten et al 2007., Besse et al., 2011). The phenotype of *Ftm*$^{-/-}$ embryos is not unlike those with constitutive loss of *Ta3* (Bangs et al., 2011). This suggests that defects in *TA3* could even contribute to a wider range of human ciliopathy conditions.

When modelling JS, the severe aspects in the *Ta3*$^{fl/fl;NesCre}$ mutant mouse phenotype can be viewed as a positive feature to uncover less striking clinical defects which may be otherwise overlooked. For example, patients with JS can present with severely reduced cognitive ability (Maria et al., 1999). Some cases of JS can be associated with polymicrogyria or loss of the corpus callosum but this is not always the case (Giordano et al., 2009, Dixon-Salazar et al., 2004). To our knowledge the deep layer defects described in *Ta3*$^{fl/fl;NesCre}$ cortex are a previously uncharacterised feature. It is quite possible that more subtle defects of this nature could be a contributing factor to the reduced cognitive ability seen in cases of JS. This highlights the use of this model system to better understand the disease process and developmental defects in such a heterogeneous spectrum of conditions.

8.5 Future work

The study of the *Ta3* mutant mouse has laid the foundation for further research into the role of Ta3 and primary cilia in the brain. It has also identified a number of questions which will be important to answer in the future. In particular, which cells types in the cerebellar, hippocampal and cortical phenotype are most affected by loss of *Ta3*? Also, what cellular phenotypes are a due to inherent defects of the cells rather than secondary consequences of the surrounding environment? Finally, what is the significance of the clinical JS mutations discovered in *TA3* and how do they affect its function?

Thanks to the versatility of the Cre/LoxP system the effect of *Ta3* recombination can easily be studied in more detail by using different *Cre* deleter strains. The use of the *NesCre* deleter in this study was not without its difficulties; being on the same chromosome as *Ta3*, the disagreement in published literature about the exact time of recombination and mosaicism in the level of distribution. Despite there still being strong positive arguments for the use of *NesCre*, especially its widespread use allowing excellent comparison with other mutants, there are also alternative pan-neural deleter strains which could be used. The *foxg1Cre* deleter targets specifically to the telencephalon from E9.5 (Hébert and McConnell, 2000) and *EmxCre* deleter targets from E10.5 onwards (Gorski et al., 2002). Another alternative is the *GFAPCre* deleter which targets the embryonic brain from E13.5 (Zhuo et

al., 2001). Although these mice are not without their own caveats, study of alternative pan-neural deleters which target the developing brain from slightly different times of onset, would provide a more complete picture of the general role of *Ta3* in the developing brain and strengthen the findings described in the current study.

A question of greater importance is to better understand the role each cell type plays in the formation of the complex phenotype described in this project. The use of *Cre* deleter strains to target more restricted cell lineages will provide a better understanding of the root cause of the phenotype described here. In particular the cerebellum is one of the more straightforward structures to study and there are a number of specific *Cre* lines which could be employed. Targeting of Purkinje neurons could be achieved using the *Purkinje cell protein (PCP) Cre* strain (Zhang et al., 2004), Granule precursors using the *Math1-Cre* (Matei et al., 2005) and Bergmann glia could also be targeted by the tamoxifen inducible *Glast-CreER*^{T2} (Slezak et al., 2007). The combined use of these cell-specific *Cre* strains would provide a detailed understanding of how each lineage contributes to the complex phenotype described in Chapter 4. The use of tamoxifen inducible strains in general could also help to further investigate the temporal requirement of Ta3 in the developing brain. By optimising an inducible system, the onset of recombination could be induced at intervals throughout embryonic development to better understand the exact points when cells require Ta3.

Secondly, more thorough analysis of *Ta3* loss *in vitro* will be essential in gaining a deeper understanding of its function. It will allow isolated cell types to be studied in highly control environments to try and further identify intrinsic cellular defects. The establishment of the hippocampal neurosphere culture model provides a useful system to study the defects evident in the *Ta3* mutant dentate gyrus. This needs to be optimised further to achieve better maturation of neuronal subtypes. In addition, isolation of different cell types will help to answer targeted questions, for example whether the formation of Purkinje cell dendrites is a primary defect following cilia disruption.

Migration is also a feature which can be easily studied in culture with the easy addition of small molecule inhibitors or genetic constructs to modify their function. One experiment of particular interest is the live cell monitoring of the neurosphere migration assay. As the system was established using multi-well plates there is the exciting potential to

monitor the cultures using high content imaging and analysis. By transfecting cells with fluorescent reporters their migration could be monitored and tracked over the course of the experiment. By tracking single cells and multiple cultures simultaneously powerful data could be acquired to better understand the defect in the migrating neurons lacking Ta3 function.

Live cell imaging using culture of brain slices is also now routinely used in many laboratories with protocols widely available (Simioni and Yu, 2006). This type of experiment would prove fascinating in the context of Ta3 loss and would allow detailed study of the organisation and migrational defect in live brain tissues. In this context mutant mice which also carry fluorescent reporters to indicate recombination can be used to study cell behaviour where recombination has taken place. Another interesting concept is the use of co-culture systems to assess how different cells interact (Rio et al., 1997), specifically how granule neurons migrate and interact when cultured on glial monolayers. This type of experiment would also allow the interesting opportunity to see whether defects lie in migrating cells or the underlying substrate which could be achieved by culturing different combinations of wild type and *Ta3* mutant cells.

Finally, better understanding the genetic regulation of *Ta3* will be essential for study of clinical ciliopathy conditions. Whilst the existing $Ta3^{fl/fl;NesCre}$ model does represent a useful model to study JS it still has a number of limitations. The conditional nature of the mouse mutant does not take into account the early embryonic role of Ta3. This is highlighted by the embryonic lethality seen in mice with a constitutive form of the defect (Bangs et al,. 2011) and the postnatal lethality seen in the current study. These results suggest that the removal of the conserved coiled-coil domains is too severe a defect to model the clinical syndromes affecting TA3 described so far. Furthermore the $Ta3^{fl/fl;NesCre}$ model does not allow the study of non-neural defects often associated with JS such as obesity, polydactyly and hepatic disease. Development of mouse models which replicate the clinical mutations seen in humans will be the next logical priority in studying Ta3-related ciliopathies. Whilst the *NesCre* model represents the more severe end of the spectrum, which can be useful in some contexts, more subtle genetic alterations will be essential to understand its true contribution in clinical conditions.

Both mouse and human *TA3* have a number of splice variants which have currently received little attention. Investigating the functional significance of these variants in

addition to the specific clinical *TA3* mutations will improve the current understanding of how the protein functions and how it is regulated at a molecular level. The recent development of RNA-guided Cas9 nuclease systems, which utilise clustered regularly interspaced short palindromic repeats (CRISPR) (Ran et al 2013), will help to recreate the clinical *TA3* mutations in endogenous gene loci. This will show the significance of these genetic defects and may provide further information as to the function of Ta3. In addition with the advent of induced pluripotent stem cells (iPSCs) (Takahashi et al., 2007), the technologies are becoming available to maintain *in vitro* cultures of patient specific cells which are capable of differentiating into any neural cell type.

8.6 Concluding remarks

The characterisation of the *Ta3* mutant mice is a useful and informative starting point to understand the function of Ta3 and primary cilia it the developing brain. Here we have demonstrated that mice with loss of *Ta3* in the developing CNS show a predominant phenotype in late embryonic and early postnatal stages. Postnatally, they develop severe ataxia with progressive hydrocephaly. *Ta3* mutant mice exhibit hypoplasia of the cerebellum with gross laminar disorganisation and a loss of proliferation. Cerebellar defects also include defective migration of granule neurons with malformed Purkinje cells and Bergmann glia. The cortex shows a notable phenotype with disruption of deep cortical layers. The dorsal hippocampus also shows a distinct phenotype with loss of progenitors and both migrational and glial scaffold defects. Analysis of mechanistic causes consistently demonstrates a loss of primary cilia and disruption of the Hh signalling pathway. Finally, neurosphere culture methodology was optimised to maintain postnatal hippocampal cells *in vitro*. This provided an excellent opportunity to begin to understand the underlying mechanisms. It also presents a promising platform to facilitate further work.

Appendices

Appendix 1 Recipes and solutions

1.1 Lysis buffer:

Tris-HCl 50 mM pH7.5, Ethylenediaminetetraacetic acid (EDTA) 50 mM, NaCl 100 mM, SDS 1% (w/v).

1.2 TE buffer:

Tris-HCl 10 mM pH8, EDTA 1 mM.

1.3 TBE buffer (0.5X):

Tris-borate 45 mM, EDTA 1 mM.

1.4 DNA loading buffer (6X):

Ficoll 15% (w/v), bromophenol blue 0.25% (w/v), xylene cyanol 0.25% (w/v)

1.5 Chrome-alum solution:

Gelatin 6 g/L, chromium potassium sulphate 0.6 g/L

1.6 Antigen retrieval solution

Trisodium citrate 10 mM adjusted with HCl to pH6, Tween-20 0.1% (v/v)

1.7 Blocking buffer (for immunohistochemistry)

Fetal calf serum 0.1% (v/v), gelatin 0.1% (w/v), Triton X-100 0.5% (v/v)

1.8 Mowiol mountant

Mowiol 4-88 was dissolved in glycerol and water was added to final concentration of Mowiol (20% w/v) and glycerol (50% v/v). To prevent fading of fluorescence 1,4-Diazobicyclo-(2,2,2)-octane (DABCO) was added to final concentration of 2.5% (w/v). Mountant was stored frozen at -20°C until required.

1.9 Sample denaturing buffer (for RNA)

TBE 0.5 X, deionised formamide 50% (v/v), formaldehyde 6.66% (v/v), ethidium bromide 40 µg/ml

1.10 Sample lysis buffer (for protein extraction)

Tris-HCl 50mM pH6.8, SDS 2% (w/v)

1.11 Resolving gel composition (for Western blot)

Bis/acrylamide 7% (w/v), Tris pH 8.8 375 mM, SDS 0.1% (w/v), ammonium persulfate 0.1% (w/v), TEMED 0.08% (v/v)

1.12 Stacking gel composition (for Western blot)

Bis/acrylamide 5% (w/v), Tris pH 6.8 125 mM, SDS 0.1% (w/v), ammonium persulfate 0.1% (w/v) and TEMED 0.1% (v/v)

1.13 Protein loading dye (1X, for Western blot)

Tris-HCl pH 6.8 60 mM, SDS 2% (w/v), glycerol 10% (v/v), dithiothreitol 100 mM and bromophenol blue (0.01% w/v)

1.14 Running buffer (for Western blot)

Tris-HCl 25 mM, glycine 250 mM, SDS 0.1% (w/v)

1.15 Transfer buffer (for Western blot)

Tris-HCl pH8.3 25 mM, glycine 192 mM, 20% methanol (v/v)

1.16 Ponceau Red stain (for Western blot)

Ponceau-S 0.1% (w/v), acetic acid 5% (v/v)

1.17 Coomassie blue stain (for Western blot)

(Coomassie Brilliant Blue R250 0.25% w/v, methanol 45% v/v, acetic acid 10% v/v)

1.18 Destain (for Western blot)

(methanol 45% v/v, acetic acid 10% v/v)

1.19 Amido black stain (for Western blot)

Amido black 0.1% (w/v, methanol 40% (v/v), acetic acid 10% (v/v)

1.20 Blocking buffer (for Western blot)

PBS, milk powder 5% (w/v, Marvel), Tween-20 0.1% (v/v)

1.21 ECL reagent (for Western blot)

Dimethyl sulfoxide (DMSO) stocks of Luminol and 4-iodophenylboronic acid (4-IPBA) were added to a final concentration of Tris-HCl pH8 (100 mM), Luminol (1.25 mM), 4-IPBA (2 mM) followed by hydrogen peroxide 0.015% (v/v). Recipe taken from (Haan and Behrmann 2006).

1.22 Dissecting solution

PBS, glucose 0.6% (w/v)

1.23 Digestion solution

PBS, glucose 0.6% (w/v), Papain 1 mg/ml, L-cysteine 0.25 mg/ml, EDTA 1.1 mM, Pen-Strep (1X)

1.24 Neurosphere culture medium

DMEM/F-12, B27 without vitA 2% (v/v, Gibco, UK), Heparin 2 µg/mL, hFGF-2 20 ng/mL (Peprotech, UK), hEGF 20 ng/ml (Peprotech, UK), methylcellulose 0.5% (w/v), Pen-Strep 1X. Media was sterilised by passing through 0.2 µm filter. Stock methylcelluose solution 5% (w/v) was made by suspending powder in 1/3 volume of 80°C PBS whilst stirring, once homogenous 2/3 cool PBS was mixed and allowed to cool and dissolve overnight at 4°C. Methylcellulose was autoclaved, mixed and cooled to 4°C before use.

1.25 Alkaline DMEM/F12 (pH11.6)

NaOH (400 µL, 1N) was added to DMEM/F12 (10ml). pH was checked using pH paper and sterilised by passing through 0.2 µm filter.

1.26 Acid DMEM/F12 (pH2)

HCl (500 µL, 1N) was added to DMEM/F12 (10ml). pH was checked using pH paper and sterilised by passing through 0.2 µm filter.

1.27 Cryostorage media

DMEM/F-12, DMSO 10% (v/v), fetal bovine serum 50% (v/v)

1.28 PBT-block

PBS, BSA 0.5% (w/v), Tween 0.5% (v/v)

1.29 Alkaline lysis reagent (HotSHOT lysis)

Water (25 ml), NaOH (62.5 µl, 10N), EDTA (10 µl, 0.5M)

1.30 Neutralisation reagent (HotSHOT lysis)

Water (24 ml), Tris-HCl (1 ml, 1 M)

1.31 Differentiation media

DMEM/F12, B27 2%, Heparin 2 µg/µl, FBS 2.5% (v/v), FGF 1 ng/µl

1.32 Attachment media

Conditioned neurosphere culture media 50% (v/v), DMEM/F12 47.5% (v/v), FBS 2.5% (v/v)

1.33 Developing solution

1.25% w/v hydroquinone, 0.02% w/v silver nitrate, 0.625% w/v gum mastic, 25% ethanol v/v

Appendix 2 *Ta3* and *NesCre* are both on chromosome 12

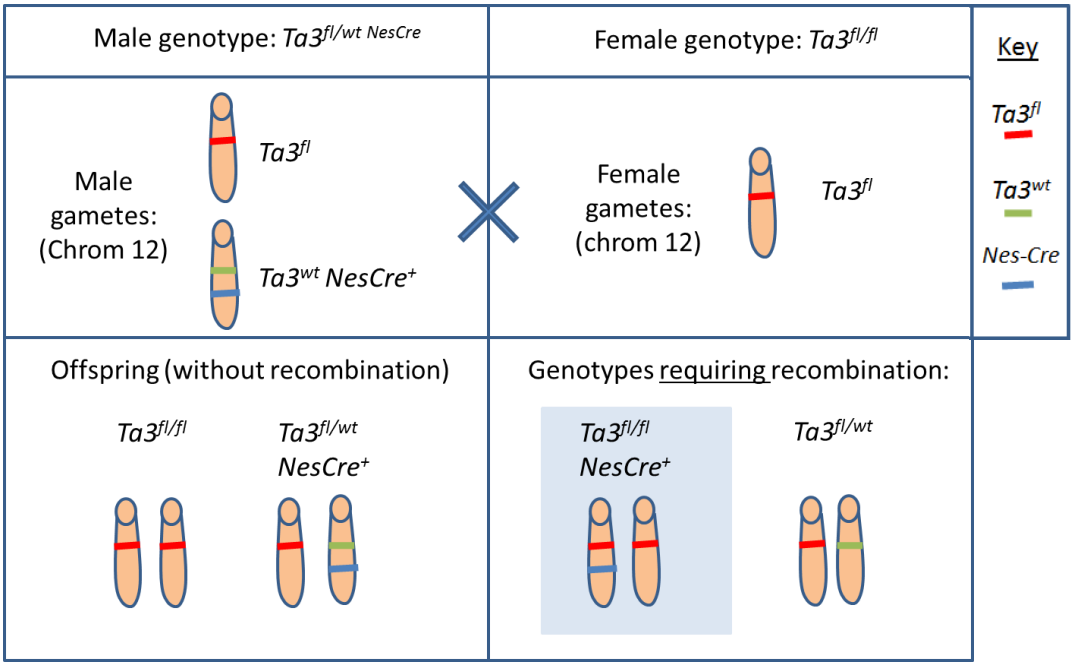

Appendix 2.1 Illustration showing the linkage on chromosome 12 between Ta3 and NesCre. Top row indicates experimental crosses between Stud males (*Ta3*$^{fl/wt;NesCre}$) and Ta3 females (*Ta3*$^{fl/fl}$). Bottom row indicates offspring generated from experimental crosses. Bottom left shows genotypes not requiring translocation. Bottom right shows genotypes requiring translocation. Genotype of mutant mice are indicated in blue box. Chromosome 12 (orange) in illustrated for each genotype with *floxed* (red), *wildtype* (green) alleles and *NesCre* (blue) transgene.

Appendix 3 Mutations in *TA3* and Joubert Syndrome

Supplementary Table 3.1

List of Genes analysed for mutations in the Joubert syndrome patient cohort by targeted capture and NGS. Four patients found to be negative for mutations in the 27 genes.

Gene	Reference sequence/s	% Coverage (30x)
AHI1	NM_**001134831**.1 NM_001134832.1	88.5
ARL13B	NM_182896.2	85.4
B9D1	NM_015681.3 NM_001243473.1 NM_001243475.1	100
C2CD3	NM_015531.4	98.6
C5ORF42	NM_023073.3	96.9
CC2D2A	NM_001080522.2 NM_020785.2 NM_001164720.1	97.7
CEP290	NM_025114.3	86.7
CEP41	NM_018718.2 NM_001257160.1	94.1
CSPP1	NM_024790.6	95.6
INPP5E	NM_019892.3	99.4
KIF7	NM_198525.2	98.1
MKS1	NM_017777.3 NM_001165927.1	99.8
NPHP1	NM_000272.3	97.4
OFD1	NM_003611.2	96.9
PDE6D	NM_002601.2	100
POC1B	NM_172240.2	92.1
RPGRIP1L	NM_015272.2	96.3
TCTN1	NM_001082538.2 NM_001173975.1 NM_001173976.1 NM_024549.5	93.5
TCTN2	NM_024809.4	96.1
TCTN3	NM_015631.5	99.8
TMEM138	NM_016464.4	100
TMEM216	NM_001173991.2	100
TMEM231	NM_001077416.1 NM_001077418.1	100
TMEM237	NM_001044385.1 NM_152388.3	96.2
TMEM67	NM_153704.5 NM_001142301.1	90.7
TTC21B	NM_024753.4	92.4
ZNF423	NM_015069.3	100

a

```
SP|Q9BVV6|TALD3_HUMAN   NNKQKANDIFISQYTMGQKDALRTVLKQ-------------------------------- 121
SP|Q9BVV6-2|TALD3_HUMAN NNKQKANDIFISQYTMGQKDALRTVLKQ-------------------------------- 136
SP|Q9BVV6-3|TALD3_HUMAN NNKQKANDIFISQYTMGQKDALRTVLKQNVSLCLTGWSDHSGVITTHCSLYLLRLMRSSH 180
SP|Q9BVV6-4|TALD3_HUMAN NNKQKANDIFISQYTMGQKDALRTVLKQNVSLCLTGWSDHSGVITTHCSLYLLRLMRSSH 83
                        ***************************

SP|Q9BVV6|TALD3_HUMAN   ----------KAQSMPVFKEVKVHLLEDAGIEKDAVTQETRISPSGIDSATTVAAATAAAI 172
SP|Q9BVV6-2|TALD3_HUMAN ----------KAQSMPVFKEVKVHLLEDAGIEKDAVTQETRISPSGIDSATTVAAATAAAI 187
SP|Q9BVV6-3|TALD3_HUMAN LSLPSSWDYRAQSMPVFKEVKVHLLEDAGIEKDAVTQETRISPSGIDSATTVAAATAAAI 240
SP|Q9BVV6-4|TALD3_HUMAN LSLPSSWDYRAQSMPVFKEVKVHLLEDAGIEKDAVTQETRISPSGIDSATTVAAATAAAI 143
                          :************************************************

SP|Q9BVV6|TALD3_HUMAN   ATAAPLIKVQSDLEAKVNSVTELLSKLQETDKHLQRVTEQQTSIQRKQEKLHCHDHEKQM 232
SP|Q9BVV6-2|TALD3_HUMAN ATAAPLIKVQSDLEAKVNSVTELLSKLQETDKHLQRVTEQQTSIQRKQEKLHCHDHEKQM 247
SP|Q9BVV6-3|TALD3_HUMAN ATAAPLIKVQSDLEAKVNSVTELLSKLQETDKHLQRVTEQQTSIQRKQEKLHCHDHEKQM 300
SP|Q9BVV6-4|TALD3_HUMAN ATAAPLIKVQSDLEAKVNSVTELLSKLQETDKHLQRVTEQQTSIQRKQEKLHCHDHEKQM 203
                        ************************************************************

SP|Q9BVV6|TALD3_HUMAN   NVFMEQHIRHLEKLQQQQIDIQTHFISAALKTSSFQPVSMPSSRAVEKYSVKPEHPNLGS 292
SP|Q9BVV6-2|TALD3_HUMAN NVFMEQHIRHLEKLQQQQIDIQTHFISAALKTSSFQPVSMPSSRAVEKYSVKPEHPNLGS 307
SP|Q9BVV6-3|TALD3_HUMAN NVFMEQHIRHLEKLQQQQIDIQTHFISAALKTSSFQPVSMPSSRAVEKYSVKPEHPNLGS 360
SP|Q9BVV6-4|TALD3_HUMAN NVFMEQHIRHLEKLQQQQIDIQTHFISAALKTSSFQPVSMPSSRAVEKYSVKPEHPNLGS 263
                        ************************************************************

SP|Q9BVV6|TALD3_HUMAN   CNPSLYNTFASKQAPLKEVEDTSFDKQKSPLETPAPRRFAPVPVSRDDELSKRENLLEEK 352
SP|Q9BVV6-2|TALD3_HUMAN CNPSLYNTFASKQAPLKEVEDTSFDKQKSPLETPAPRRFAPVPVSRDDELSKRENLLEEK 367
SP|Q9BVV6-3|TALD3_HUMAN CNPSLYNTFASKQAPLKEVEDTSFDKQKSPLETPAPRRFAPVPVSRDDELSKRENLLEEK 420
SP|Q9BVV6-4|TALD3_HUMAN CNPSLYNTFASKQAPLKEVEDTSFDKQKSPLETPAPRRFAPVPVSRDDELSKRENLLEEK 323
                        ************************************************************

SP|Q9BVV6|TALD3_HUMAN   ENMEVSCHRGNVRLLEQILNNNDSLTRKSESSNTTSLTRSKIGWTPEKTNRFPSCEELET 412
SP|Q9BVV6-2|TALD3_HUMAN ENMEVSCHRGNVRLLEQILNNNDSLTRKSESSNTTSLTRSKIGWTPEKTNRFPSCEELET 427
SP|Q9BVV6-3|TALD3_HUMAN ENMEVSCHRGNVRLLEQILNNNDSLTRKSESSNTTSLTRSKIGWTPEKTNRFPSCEELET 480
SP|Q9BVV6-4|TALD3_HUMAN ENMEVSCHRGNVRLLEQILNNNDSLTRKSESSNTTSLTRSKIGWTPEKTNRFPSCEELET 383
                        ************************************************************

SP|Q9BVV6|TALD3_HUMAN   TKVTMQKSDDVLKDLGQMEKETKSMVQPKESLSMLKLPDLPQNSVKLQTTNTTRSVLKDA 472
SP|Q9BVV6-2|TALD3_HUMAN TKVTMQKSDDVLKDLGQMEKETKSMVQPKESLSMLKLPDLPQNSVKLQTTNTTRSVLKDA 487
SP|Q9BVV6-3|TALD3_HUMAN TKVTMQKSDDVLKDLGQMEKETKSMVQPKESLSMLKLPDLPQNSVKLQTTNTTRSVLKDA 540
SP|Q9BVV6-4|TALD3_HUMAN TKVTMQKSDDVLKDLGQMEKETKSMVQPKESLSMLKLPDLPQNSVKLQTTNTTRSVLKDA 443
                        ************************************************************

SP|Q9BVV6|TALD3_HUMAN   EKILRGVQNNKKVLEENLEAIIRAKDGAAMYSLINALSTNREMSEKIRIRKTVDEWIKTI 532
SP|Q9BVV6-2|TALD3_HUMAN EKILRGVQNNKKVLEENLEAIIRAKDGAAMYSLINALSTNREMSEKIRIRKTVDEWIKTI 547
SP|Q9BVV6-3|TALD3_HUMAN EKILRGVQNNKKVLEENLEAIIRAKDGAAMYSLINALSTNREMSEKIRIRKTVDEWIKTI 600
SP|Q9BVV6-4|TALD3_HUMAN EKILRGVQNNKKVLEENLEAIIRAKDGAAMYSLINALSTNREMSEKIRIRKTVDEWIKTI 503
                        ************************************************************

SP|Q9BVV6|TALD3_HUMAN   SAEIQDELSRTDYEQKRFDQKNQRTKKGQNMTKDIRTNTQDKTVNKSVIPRKHSQKQIEE 592
SP|Q9BVV6-2|TALD3_HUMAN SAEIQ---------------------------------------------------- 552
SP|Q9BVV6-3|TALD3_HUMAN SAEIQDELSRTDYEQKRFDQKNQRTKKGQNMTKDIRTNTQDKTVNKSVIPRKHSQKQIEE 660
SP|Q9BVV6-4|TALD3_HUMAN SAEIQDELSRTDYEQKRFDQKNQRTKKGQNMTKDIRTNTQDKTVNKSVIPRKHSQKQIEE 563
                        *****
```

b

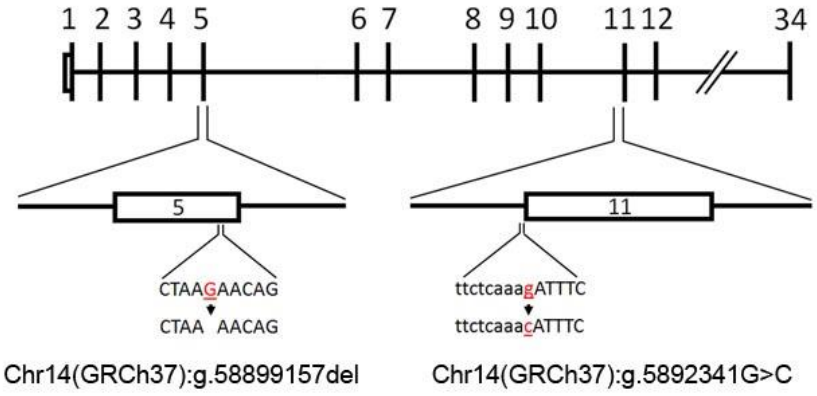

Supplementary Figure 3.1. Key features of the TALPID 3 protein
Part of the TALPID 3 protein showing Exon 5, Exon11, Exon 12, Blue: centrosomal localization region, Boxed area: coiled coil domains. Protein sequence of major transcripts obtained from http://www.uniprot.org/uniprot/Q9BVV6#. Q9BVV6-1 is the canonical sequence and transcript ID is KIAA0586-001.

References

ABBOTT, U. K., TAYLOR, L. W. & ABPLANALP, H. 1960. STUDIES WITH TALPID2, AN EMBRYONIC LETHAL OF THE FOWL. *Journal of Heredity,* 51**,** 195-202.

AGUILAR, A., MEUNIER, A., STREHL, L., MARTINOVIC, J., BONNIERE, M., ATTIE-BITACH, T., ENCHA-RAZAVI, F. & SPASSKY, N. 2012. Analysis of human samples reveals impaired SHH-dependent cerebellar development in Joubert syndrome/Meckel syndrome. *Proceedings of the National Academy of Sciences of the United States of America,* 109**,** 16951-16956.

AHN, S. & JOYNER, A. L. 2005. In vivo analysis of quiescent adult neural stem cells responding to Sonic hedgehog. *Nature,* 437**,** 894-897.

ALCAMO, E. A., CHIRIVELLA, L., DAUTZENBERG, M., DOBREVA, G., FARINAS, I., GROSSCHEDL, R. & MCCONNELL, S. K. 2008. Satb2 regulates callosal projection neuron identity in the developing cerebral cortex. *Neuron,* 57**,** 364-77.

ALTMAN, J. & BAYER, S. A. 1990a. Migration and Distribution of 2 Populations of Hippocampal Granule Cell Precursors during the Perinatal and Postnatal Periods. *Journal of Comparative Neurology,* 301**,** 365-381.

ALTMAN, J. & BAYER, S. A. 1990b. Mosaic Organization of the Hippocampal Neuroepithelium and the Multiple Germinal Sources of Dentate Granule Cells. *Journal of Comparative Neurology,* 301**,** 325-342.

ALTMAN, J. & DAS, G. D. 1965. Autoradiographic and Histological Evidence of Postnatal Hippocampal Neurogenesis in Rats. *Journal of Comparative Neurology,* 124**,** 319-&.

ALVAREZ RETUERTO, A. I., CANTOR, R. M., GLEESON, J. G., USTASZEWSKA, A., SCHACKWITZ, W. S., PENNACCHIO, L. A. & GESCHWIND, D. H. 2008. Association of common variants in the Joubert syndrome gene (AHI1) with autism. *Human Molecular Genetics,* 17**,** 3887-3896.

AMANITI, E. M., HASENPUSCH-THEIL, K., LI, Z. W., MAGNANI, D., KESSARIS, N., MASON, J. O. & THEIL, T. 2013. Gli3 is required in Emx1(+) progenitors for the development of the corpus callosum. *Developmental Biology,* 376**,** 113-124.

AMANN-ZALCENSTEIN, D., AVIDAN, N., KANYAS, K., EBSTEIN, R. P., KOHN, Y., HAMDAN, A., BEN-ASHER, E., KARNI, O., MUJAHEED, M., SEGMAN, R. H., MAIER, W., MACCIARDI, F., BECKMANN, J. S., LANCET, D. & LERER, B. 2007. AHI1, a pivotal neurodevelopmental gene, and C6orf217 are associated with susceptibility to schizophrenia (vol 14, pg 1111, 2006). *European Journal of Human Genetics,* 15**,** 387-387.

ANDERSON, R. G. 1972. The three-dimensional structure of the basal body from the rhesus monkey oviduct. *J Cell Biol,* 54**,** 246-65.

ANDERSON, S. A., EISENSTAT, D. D., SHI, L. & RUBENSTEIN, J. L. 1997. Interneuron migration from basal forebrain to neocortex: dependence on Dlx genes. *Science,* 278**,** 474-6.

ANDERSON, S. A., MARIN, O., HORN, C., JENNINGS, K. & RUBENSTEIN, J. L. R. 2001. Distinct cortical migrations from the medial and lateral ganglionic eminences. *Development,* 128**,** 353-363.

ANGEVINE, J. B., JR. & SIDMAN, R. L. 1961. Autoradiographic study of cell migration during histogenesis of cerebral cortex in the mouse. *Nature,* 192**,** 766-8.

APPS, R. & GARWICZ, M. 2005. Anatomical and physiological foundations of cerebellar information processing. *Nature Reviews Neuroscience,* 6**,** 297-311.

ARIMATSU, Y., ISHIDA, M., KANEKO, T., ICHINOSE, S. & OMORI, A. 2003. Organization and development of corticocortical associative neurons expressing the orphan nuclear receptor Nurr1. *Journal of Comparative Neurology,* 466**,** 180-196.

ARELLANO, J., GUADIANA, SM., BREUNIG, JJ., RAKIC, P., SARKISIAN M. 2012. Development and distribution of neuronal cilia in mouse neocortex. J Comp Neurol., 2012, 520, 848-73.

ARLOTTA, P., MOLYNEAUX, B. J., CHEN, J., INOUE, J., KOMINAMI, R. & MACKLIS, J. D. 2005. Neuronal subtype-specific genes that control corticospinal motor neuron development in vivo. *Neuron,* 45**,** 207-221.

AZARI, H., RAHMAN, M., SHARIFIFAR, S. & REYNOLDS, B. A. 2010. Isolation and expansion of the adult mouse neural stem cells using the neurosphere assay. *J Vis Exp*.

BAALA, L., AUDOLLENT, S., MARTINOVIC, J., OZILOU, C., BABRON, M. C., SIVANANDAMOORTHY, S., SAUNIER, S., SALOMON, R., GONZALES, M., RATTENBERRY, E., ESCULPAVIT, C., TOUTAIN, A., MORAINE, C., PARENT, P., MARCORELLES, P., DAUGE, M. C., ROUME, J., LE MERRER, M., MEINER, V., MEIR, K., MENEZ, F., BEAUFRERE, A. M., FRANCANNET, C., TANTAU, J., SINICO, M., DUMEZ, Y., MACDONALD, F., MUNNICH, A., LYONNET, S., GUBLER, M. C., GENIN, E., JOHNSON, C. A., VEKEMANS, M., ENCHA-RAZAVI, F. & ATTIE-BITACH, T. 2007. Pleiotropic effects of CEP290 (NPHP6) mutations extend to Meckel syndrome. *American Journal of Human Genetics,* 81**,** 170-179.

BACKMAN, M., MACHON, O., MYGLAND, L., VAN DEN BOUT, C. J., ZHONG, W. M., TAKETO, M. M. & KRAUSS, S. 2005. Effects of canonical Wnt signaling on dorso-ventral specification of the mouse telencephalon. *Developmental Biology,* 279**,** 155-168.

BANGS, F., ANTONIO, N., THONGNUEK, P., WELTEN, M., DAVEY, M. G., BRISCOE, J. & TICKLE, C. 2011. Generation of mice with functional inactivation of talpid3, a gene first identified in chicken. *Development,* 138**,** 3261-3272.

BANIZS, B., PIKE, M. M., MILLICAN, C. L., FERGUSON, W. B., KOMLOSI, P., SHEETZ, J., BELL, P. D., SCHWIEBERT, E. M. & YODER, B. K. 2005. Dysfunctional cilia lead to altered ependyma and choroid plexus function, and result in the formation of hydrocephalus. *Development,* 132**,** 5329-5339.

BANNERMAN, D. M., SPRENGEL, R., SANDERSON, D. J., MCHUGH, S. B., RAWLINS, J. N. P., MONYER, H. & SEEBURG, P. H. 2014. Hippocampal synaptic plasticity, spatial memory and anxiety. *Nature Reviews Neuroscience,* 15**,** 181-192.

BAPTISTA, C. A., HATTEN, M. E., BLAZESKI, R. & MASON, C. A. 1994. Cell-Cell Interactions Influence Survival and Differentiation of Purified Purkinje-Cells in-Vitro. *Neuron,* 12**,** 243-260.

BARRAL, D. C., GARG, S., CASALOU, C., WATTS, G. F. M., SANDOVAL, J. L., RAMALHO, J. S., HSU, V. W. & BRENNER, M. B. 2012. Arl13b regulates endocytic recycling traffic. *Proceedings of the National Academy of Sciences of the United States of America,* 109**,** 21354-21359.

BARZI, M.,BERENGUER, J., MENENDEZ, A., ALVAREZ-RODRIGUEZ, R., PONS, S., (2010). Sonic-hedgehog-mediated proliferation requires the localization of PKA to the cilium base. J. Cell Sci. 123, 62–69.

BAUDOIN, J. P., VIOU, L., LAUNAY, P. S., LUCCARDINI, C., GIL, S. E., KIYASOVA, V., IRINOPOULOU, T., ALVAREZ, C., RIO, J. P., BOUDIER, T., LECHAIRE, J. P., KESSARIS, N., SPASSKY, N. & METIN, C. 2012. Tangentially Migrating Neurons Assemble a Primary Cilium that Promotes Their Reorientation to the Cortical Plate. *Neuron,* 76**,** 1108-1122.

BEN, J., ELWORTHY, S., NG, A. S. M., VAN EEDEN, F. & INGHAM, P. W. 2011. Targeted mutation of the talpid3 gene in zebrafish reveals its conserved requirement for ciliogenesis and Hedgehog signalling across the vertebrates. *Development,* 138**,** 4969-4978.

BENARIE, N., BELLEN, H. J., ARMSTRONG, D. L., MCCALL, A. E., GORDADZE, P. R., GUO, Q. X., MATZUK, M. M. & ZOGHBI, H. Y. 1997. Math1 is essential for genesis of cerebellar granule neurons. *Nature,* 390**,** 169-172.

BENRAISS, A., CHMIELNICKI, E., LERNER, K., ROH, D. & GOLDMAN, S. A. 2001. Adenoviral brain-derived neurotrophic factor induces both neostriatal and olfactory neuronal recruitment from endogenous progenitor cells in the adult forebrain. *Journal of Neuroscience,* 21**,** 6718-6731.

BESSE, L., NETI, M., ANSELME, I., GERHARDT, C., RUTHER, U., LACLEF, C. & SCHNEIDER-MAUNOURY, S. 2011. Primary cilia control telencephalic patterning and morphogenesis via Gli3 proteolytic processing. *Development,* 138**,** 2079-2088.

BETLEJA, E. & COLE, D. G. 2010. Ciliary Trafficking: CEP290 Guards a Gated Community. *Current Biology,* 20**,** R928-R931.

BETTENCOURT-DIAS, M., RODRIGUES-MARTINS, A., CARPENTER, L., RIPARBELLI, M., LEHMANN, L., GATT, M. K., CARMO, N., BALLOUX, F., CALLAINI, G. & GLOVER, D. M. 2005. SAK/PLK4 is required for centriole duplication and flagella development. *Current Biology,* 15**,** 2199-2207.

BIJLSMA, M. F., DAMHOFER, H. & ROELINK, H. 2012. Hedgehog-Stimulated Chemotaxis Is Mediated by Smoothened Located Outside the Primary Cilium. *Science Signaling,* 5.

BISHOP, G. A., BERBARI, N. F., LEWIS, J. & MYKYTYN, K. 2007. Type III adenylyl cyclase localizes to primary cilia throughout the adult mouse brain. *Journal of Comparative Neurology,* 505**,** 562-571.

BLAESS, S., CORRALES, J. D. & JOYNER, A. L. 2006. Sonic hedgehog regulates Gli activator and repressor functions with spatial and temporal precision in the mid/hindbrain region. *Development,* 133**,** 1799-1809.

BLOCK, M., ZECCA, L., HONG, J., 2007. Microglia-mediated neurotoxicity: uncovering the molecular mechanisms. Nature Reviews Neuroscience, 8, 57-69.

BRAILOV, I., BANCILA, M., BRISORGUEIL, M. J., MIQUEL, M. C., HAMON, M. & VERGE, D. 2000. Localization of 5-HT6 receptors at the plasma membrane of neuronal cilia in the rat brain. *Brain Research,* 872**,** 271-275.

BRAVO, R. & MACDONALD-BRAVO, H. 1987. Existence of two populations of cyclin/proliferating cell nuclear antigen during the cell cycle: association with DNA replication sites. Journal of Cell Biology, 105, 1549-54.

BRENNAND, K., SAVAS, J. N., KIM, Y., TRAN, N., SIMONE, A., HASHIMOTO-TORII, K., BEAUMONT, K. G., KIM, H. J., TOPOL, A., LADRAN, I., ABDELRAHIM, M., MATIKAINEN-ANKNEY, B., CHAO, S. H., MRKSICH, M., RAKIC, P., FANG, G., ZHANG, B., YATES, J. R. & GAGE, F. H. 2015. Phenotypic differences in hiPSC NPCs derived from patients with schizophrenia. *Molecular Psychiatry,* 20**,** 361-368.

BREUNIG, J. J., SARKISIAN, M. R., ARELLANO, J. I., MOROZOV, Y. M., AYOUB, A. E., SOJITRA, S., WANG, B., FLAVELL, R. A., RAKIC, P. & TOWN, T. 2008. Primary cilia regulate hippocampal neurogenesis by mediating sonic hedgehog signaling. *Proceedings of the National Academy of Sciences of the United States of America,* 105**,** 13127-13132.

BREWER, G. J. & TORRICELLI, J. R. 2007. Isolation and culture of adult neurons and neurospheres. *Nature Protocols,* 2**,** 1490-1498.

BRITANOVA, O., AKOPOV, S., LUKYANOV, S., GRUSS, P. & TARABYKIN, V. 2005. Novel transcription factor Satb2 interacts with matrix attachment region DNA elements in a tissue-specific manner and demonstrates cell-type-dependent expression in the developing mouse CNS. *Eur J Neurosci,* 21**,** 658-68.

BROWN, J. P., COUILLARD-DESPRES, S., COOPER-KUHN, C. M., WINKLER, J., AIGNER, L. & KUHN, H. G. 2003. Transient expression of doublecortin during adult neurogenesis. *Journal of Comparative Neurology,* 467**,** 1-10.

BULFONE, A., MARTINEZ, S., MARIGO, V., CAMPANELLA, M., BASILE, A., QUADERI, N., GATTUSO, C., RUBENSTEIN, J. L. R. & BALLABIO, A. 1999. Expression pattern of the Tbr2 (Eomesodermin) gene during mouse and chick brain development. *Mechanisms of Development,* 84**,** 133-138.

BULFONE, A., SMIGA, S. M., SHIMAMURA, K., PETERSON, A., PUELLES, L. & RUBENSTEIN, J. L. 1995. T-brain-1: a homolog of Brachyury whose expression defines molecularly distinct domains within the cerebral cortex. *Neuron,* 15**,** 63-78.

CAJANEK, L. & NIGG, E. A. 2014. Cep164 triggers ciliogenesis by recruiting Tau tubulin kinase 2 to the mother centriole. *Proceedings of the National Academy of Sciences of the United States of America,* 111**,** E2841-E2850.

CARTER, C. S., VOGEL, T. W., ZHANG, Q. H., SEO, S., SWIDERSKI, R. E., MONINGER, T. O., CASSELL, M. D., THEDENS, D. R., KEPPLER-NOREUIL, K. M., NOPOULOS, P., NISHIMURA, D. Y., SEARBY, C. C., BUGGE, K. & SHEFFIELD, V. C. 2012. Abnormal development of NG2(+)PDGFR-alpha(+) neural progenitor cells leads to neonatal hydrocephalus in a ciliopathy mouse model. *Nature Medicine,* 18**,** 1797-+.

CASPARY, T., LARKINS, C. E. & ANDERSON, K. V. 2007. The graded response to sonic hedgehog depends on cilia architecture. *Developmental Cell,* 12**,** 767-778.

CHAKI, M., AIRIK, R., GHOSH, A. K., GILES, R. H., CHEN, R., SLAATS, G. G., WANG, H., HURD, T. W., ZHOU, W. B., CLUCKEY, A., GEE, H. Y., RAMASWAMI, G., HONG, C. J., HAMILTON, B. A., CERVENKA, I., GANJI, R. S., BRYJA, V., ARTS, H. H., VAN REEUWIJK, J., OUD, M. M., LETTEBOER, S. J. F., ROEPMAN, R., HUSSON, H., IBRAGHIMOV-BESKROVNAYA, O., YASUNAGA, T., WALZ, G., ELEY, L., SAYER, J. A., SCHERMER, B., LIEBAU, M. C., BENZING, T., LE CORRE, S., DRUMMOND, I., JANSSEN, S., ALLEN, S. J., NATARAJAN, S., O'TOOLE, J. F., ATTANASIO, M., SAUNIER, S., ANTIGNAC, C., KOENEKOOP, R. K., REN, H. N., LOPEZ, I., NAYIR, A., STOETZEL, C., DOLLFUS, H., MASSOUDI, R., GLEESON, J. G., ANDREOLI, S. P., DOHERTY, D. G., LINDSTRAD, A., GOLZIO, C., KATSANIS, N., PAPE, L., ABBOUD, E. B., AL-RAJHI, A. A., LEWIS, R. A., OMRAN, H., LEE, E. Y. H. P., WANG, S. H., SEKIGUCHI, J. M., SAUNDERS, R., JOHNSON, C. A., GARNER, E., VANSELOW, K., ANDERSEN, J. S., SHLOMAI, J., NURNBERG, G., NURNBERG, P., LEVY, S., SMOGORZEWSKA, A., OTTO, E. A. & HILDEBRANDT, F. 2012. Exome Capture Reveals ZNF423 and CEP164 Mutations, Linking Renal Ciliopathies to DNA Damage Response Signaling. *Cell,* 150**,** 533-548.

CHAVALI, P. L., PUTZ, M. & GERGELY, F. 2014. Small organelle, big responsibility: the role of centrosomes in development and disease. *Philosophical Transactions of the Royal Society B-Biological Sciences,* 369.

CHEN, Z. H., INDJEIAN, V. B., MCMANUS, M., WANG, L. Y. & DYNLACHT, B. D. 2002. CP110, a cell cycle-dependent CDK substrate, regulates centrosome duplication in human cells. *Developmental Cell,* 3**,** 339-350.

CHENN, A. 2008. Wnt/beta-catenin signaling in cerebral cortical development. *Organogenesis,* 4**,** 76-80.

CHENN, A. & WALSH, C. A. 2002. Regulation of cerebral cortical size by control of cell cycle exit in neural precursors. *Science,* 297**,** 365-369.

CHI, C. L., MARTINEZ, S., WURST, W. & MARTIN, G. R. 2003. The isthmic organizer signal FGF8 is required for cell survival in the prospective midbrain and cerebellum. *Development,* 130**,** 2633-2644.

CHIZHIKOV, V. V., DAVENPORT, J., ZHANG, Q., SHIH, E. K., CABELLO, O. A., FUCHS, J. L., YODER, B. K. & MILLEN, K. J. 2007. Cilia proteins control cerebellar morphogenesis by promoting expansion of the granule progenitor pool. *Journal of Neuroscience,* 27**,** 9780-9789.

CHRISTENSEN, S. T., CLEMENT, C. A., SATIR, P. & PEDERSEN, L. B. 2012. Primary cilia and coordination of receptor tyrosine kinase (RTK) signalling. *Journal of Pathology,* 226**,** 172-184.

CLEMENT, D. L., MALLY, S., STOCK, C., LETHAN, M., SATIR, P., SCHWAB, A., PEDERSEN, S. F. & CHRISTENSEN, S. T. 2013. PDGFR alpha signaling in the primary cilium regulates NHE1-dependent fibroblast migration via coordinated differential activity of MEK1/2-ERK1/2-p90(RSK) and AKT signaling pathways. *Journal of Cell Science,* 126**,** 953-965.

COLE, R. K. 1942. THE "TALPID LETHAL" IN THE DOMESTIC FOWL. *Journal of Heredity,* 33**,** 83-86.

COPPIETERS, F., LEFEVER, S., LEROY, B. P. & DE BAERE, E. 2010. CEP290, a Gene with Many Faces: Mutation Overview and Presentation of CEP290base. *Human Mutation,* 31**,** 1097-1108.

CORBIT, K. C., AANSTAD, P., SINGLA, V., NORMAN, A. R., STAINIER, D. Y. R. & REITER, J. F. 2005. Vertebrate Smoothened functions at the primary cilium. *Nature,* 437**,** 1018-1021.

CORBIT, K. C., SHYER, A. E., DOWDLE, W. E., GAULDEN, J., SINGLA, V., CHEN, M. H., CHUANG, P. T. & REITER, J. F. 2008. Kif3a constrains beta-catenin-dependent Wnt signalling through dual ciliary and non-ciliary mechanisms (vol 10, pg 70, 2008). *Nature Cell Biology,* 10**,** 497-497.

CORRALES, J. D., BLAESS, S., MAHONEY, E. M. & JOYNER, A. L. 2006. The level of sonic hedgehog signaling regulates the complexity of cerebellar foliation. *Development,* 133**,** 1811-1821.

CRAIGE, B., TSAO, C. C., DIENER, D. R., HOU, Y., LECHTRECK, K. F., ROSENBAUM, J. L. & WITMAN, G. B. 2010. CEP290 tethers flagellar transition zone microtubules to the membrane and regulates flagellar protein content. *J Cell Biol,* 190**,** 927-40.

CUNNINGHAM, F., AMODE, M. R., BARRELL, D., BEAL, K., BILLIS, K., BRENT, S., CARVALHO-SILVA, D., CLAPHAM, P., COATES, G., FITZGERALD, S., GIL, L., GIRON, C. G., GORDON, L., HOURLIER, T., HUNT, S. E., JANACEK, S. H., JOHNSON, N., JUETTEMANN, T., KAHARI, A. K., KEENAN, S., MARTIN, F. J., MAUREL, T., MCLAREN, W., MURPHY, D. N., NAG, R., OVERDUIN, B., PARKER, A., PATRICIO, M., PERRY, E., PIGNATELLI, M., RIAT, H. S., SHEPPARD, D., TAYLOR, K., THORMANN, A., VULLO, A., WILDER, S. P., ZADISSA, A., AKEN, B. L., BIRNEY, E., HARROW, J., KINSELLA, R., MUFFATO, M., RUFFIER, M., SEARLE, S. M. J., SPUDICH, G., TREVANION, S. J., YATES, A., ZERBINO, D. R. & FLICEK, P. 2015. Ensembl 2015. *Nucleic acids research,* 43**,** D662-9.

DAFINGER, C., LIEBAU, M. C., ELSAYED, S. M., HELLENBROICH, Y., BOLTSHAUSER, E., KORENKE, G. C., FABRETTI, F., JANECKE, A. R., EBERMANN, I., NURNBERG, G., NURNBERG, P., ZENTGRAF, H., KOERBER, F., ADDICKS, K., ELSOBKY, E., BENZING, T., SCHERMER, B. & BOLZ, H. J. 2011. Mutations in KIF7 link Joubert syndrome with Sonic Hedgehog signaling and microtubule dynamics. *Journal of Clinical Investigation,* 121**,** 2662-2667.

DAHMANE, N. & ALTABA, A. R. I. 1999. Sonic hedgehog regulates the growth and patterning of the cerebellum. *Development,* 126**,** 3089-3100.

DAHMANE, N., SANCHEZ, P., GITTON, Y., PALMA, V., SUN, T., BEYNA, M., WEINER, H. & ALTABA, A. R. I. 2001. The Sonic Hedgehog-Gli pathway regulates dorsal brain growth and tumorigenesis. *Development,* 128**,** 5201-5212.

DAI, P., AKIMARU, H., TANAKA, Y., MAEKAWA, T., NAKAFUKU, M. & ISHII, S. 1999. Sonic hedgehog-induced activation of the Gli1 promoter is mediated by GLI3. *Journal of Biological Chemistry,* 274**,** 8143-8152.

DAMMERMANN, A. & MERDES, A. 2002. Assembly of centrosomal proteins and microtubule organization depends on PCM-1. *Journal of Cell Biology,* 159**,** 255-266.

DANILOV, A. I., GOMES-LEAL, W., AHLENIUS, H., KOKAIA, Z., CARLEMALM, E. & LINDVALL, O. 2009. Ultrastructural and Antigenic Properties of Neural Stem Cells and Their Progeny in Adult Rat Subventricular Zone. *Glia,* 57**,** 136-152.

DAVEY, M. G., PATON, I. R., YIN, Y., SCHMIDT, M., BANGS, F. K., MORRICE, D. R., SMITH, T. G., BUXTON, P., STAMATAKI, D., TANAKA, M., MUENSTERBERG, A. E., BRISCOE, J., TICKLE, C. & BURT, D. W. 2006. The chicken talpid(3) gene encodes a novel protein essential for Hedgehog signaling. *Genes & Development,* 20**,** 1365-1377.

DAWE, H. R., ADAMS, M., WHEWAY, G., SZYMANSKA, K., LOGAN, C. V., NOEGEL, A. A., GULL, K. & JOHNSON, C. A. 2009. Nesprin-2 interacts with meckelin and mediates ciliogenesis via remodelling of the actin cytoskeleton. *J Cell Sci,* 122**,** 2716-26.

DELOUS, M., BAALA, L., SALOMON, R., LACLEF, C., VIERKOTTEN, J., TORY, K., GOLZIO, C., LACOSTE, T., BESSE, L., OZILOU, C., MOUTKINE, I., HELLMAN, N. E., ANSELME, I., SILBERMANN, F., VESQUE, C., GERHARDT, C., RATTENBERRY, E., WOLF, M. T. F., GUBLER, M. C., MARTINOVIC, J., ENCHA-RAZAVI, F., BODDAERT, N., GONZALES, M., MACHER, M. A., NIVET, H., CHAMPION, G., BERTHELEME, J. P., NIAUDET, P., MCDONALD, F., HILDEBRANDT, F., JOHNSON, C. A., VEKEMANS, M., ANTIGNAC, C., RUTHER, U., SCHNEIDER-MAUNOURY, S., ATTIE-BITACH, T. & SAUNIER, S. 2007. The ciliary gene RPGRIP1L is mutated in cerebello-oculo-renal syndrome (Joubert syndrome type B) and Meckel syndrome. *Nature Genetics,* 39**,** 875-881.

DELRIO, J. A., HEIMRICH, B., BORRELL, V., FORSTER, E., DRAKEW, A., ALCANTARA, S., NAKAJIMA, K., MIYATA, T., OGAWA, M., MIKOSHIBA, K., DERER, P., FROTSCHER, M. & SORIANO, E. 1997. A role for Cajal-Retzius cells and reelin in the development of hippocampal connections. *Nature,* 385**,** 70-74.

DESTA, Z., WARD, B. A., SOUKHOVA, N. V. & FLOCKHART, D. A. 2004. Comprehensive evaluation of tamoxifen sequential biotransformation by the human cytochrome P450 system in vitro: Prominent roles for CYP3A and CYP2D6. *Journal of Pharmacology and Experimental Therapeutics,* 310**,** 1062-1075.

DING, Q., FUKAMI, S. I., MENG, X., NISHIZAKI, Y., ZHANG, X., SASAKI, H., DLUGOSZ, A., NAKAFUKU, M. & HUI, C. C. 1999. Mouse Suppressor of fused is a negative regulator of Sonic hedgehog signaling and alters the subcellular distribution of Gli1. *Current Biology,* 9**,** 1119-1122.

DINGEMAN, K. P. 1969. Relation between Cilia and Mitoses in Mouse Adenohypophysis. *Journal of Cell Biology,* 43**,** 361-&.

DIXON-SALAZAR, T., SILHAVY, J. L., MARSH, S. E., LOUIE, C. M., SCOTT, L. C., GURURAJ, A., AL-GAZALI, L., AL-TAWARI, A. A., KAYSERILI, H., SZTRIHA, L. & GLEESON, J. G. 2004. Mutations in the AHI1 gene, encoding Jouberin, cause Joubert syndrome with cortical polymicrogyria. *American Journal of Human Genetics,* 75**,** 979-987.

DOETSCH, F., CAILLE, I., LIM, D. A., GARCIA-VERDUGO, J. M. & ALVAREZ-BUYLLA, A. 1999. Subventricular zone astrocytes are neural stem cells in the adult mammalian brain. *Cell,* 97**,** 703-716.

DOXSEY, S. J., STEIN, P., EVANS, L., CALARCO, P. D. & KIRSCHNER, M. 1994. Pericentrin, a Highly Conserved Centrosome Protein Involved in Microtubule Organization. *Cell,* 76**,** 639-650.

DUAN, X., CHANG, J. H., GE, S., FAULKNER, R. L., KIM, J. Y., KITABATAKE, Y., LIU, X. B., YANG, C. H., JORDAN, J. D., MA, D. K., LIU, C. Y., GANESAN, S., CHENG, H. J., MING, G. L., LU, B. & SONG, H. 2007. Disrupted-In-Schizophrenia 1 regulates integration of newly generated neurons in the adult brain. *Cell,* 130**,** 1146-58.

DURBEC, P., FRANCESCHINI, I., LAZARINI, F. & DUBOIS-DALCQ, M. 2008. In vitro migration assays of neural stem cells. *Methods Mol Biol,* 438**,** 213-25.

EDE, D. A. & FLINT, O. P. 1975. Cell movement and adhesion in the developing chick wing bud: studies on cultured mesenchyme cells from normal and talpid mutant embryos. *J Cell Sci,* 18**,** 301-13.

EDE, D. A. & KELLY, W. A. 1964a. DEVELOPMENTAL ABNORMALITIES IN HEAD REGION OF TALPID3 MUTANT OF FOWL. *Journal of Embryology and Experimental Morphology,* 12**,** 161-&.

EDE, D. A. & KELLY, W. A. 1964b. DEVELOPMENTAL ABNORMALITIES IN TRUNK + LIMBS OF TALPID3 MUTANT OF FOWL. *Journal of Embryology and Experimental Morphology,* 12**,** 339-&.

EDWARDS, T. J., SHERR, E. H., BARKOVICH, A. J. & RICHARDS, L. J. 2014. Clinical, genetic and imaging findings identify new causes for corpus callosum development syndromes. *Brain,* 137**,** 1579-1613.

ENCINAS, J. M. & ENIKOLOPOV, G. 2008. Identifying and, quantitating neural stem and progenitor cells in the adult brain. *Fluorescent Proteins, Second Edition,* 85**,** 243-+.

ENGLUND, C., FINK, A., LAU, C., PHAM, D., DAZA, R. A. M., BULFONE, A., KOWALCZYK, T. & HEVNER, R. F. 2005. Pax6, Tbr2, and Tbr1 are expressed sequentially by radial glia, intermediate progenitor cells, and postmitotic neurons in developing neocortex. *Journal of Neuroscience,* 25**,** 247-251.

ERIKSSON, P. S., PERFILIEVA, E., BJORK-ERIKSSON, T., ALBORN, A. M., NORDBORG, C., PETERSON, D. A. & GAGE, F. H. 1998. Neurogenesis in the adult human hippocampus. *Nature Medicine,* 4**,** 1313-1317.

EZRATTY, E. J., STOKES, N., CHAI, S., SHAH, A. S., WILLIAMS, S. E. & FUCHS, E. 2011. A Role for the Primary Cilium in Notch Signaling and Epidermal Differentiation during Skin Development. *Cell,* 145**,** 1129-1141.

FEIL, R., WAGNER, J., METZGER, D. & CHAMBON, P. 1997. Regulation of Cre recombinase activity by mutated estrogen receptor ligand-binding domains. *Biochemical and Biophysical Research Communications,* 237**,** 752-757.

FERLAND, R. J., EYAID, W., COLLURA, R. V., TULLY, L. D., HILL, R. S., AL-NOURI, D., AL-RUMAYYAN, A., TOPCU, M., GASCON, G., BODELL, A., SHUGART, Y. Y., RUVOLO, M. & WALSH, C. A. 2004. Abnormal cerebellar development and axonal decussation due to mutations in AHI1 in Joubert syndrome (vol 36, pg 1008, 2004). *Nature Genetics,* 36**,** 1126-1126.

FERRANTE, M. I., ZULLO, A., BARRA, A., BIMONTE, S., MESSADDEQ, N., STUDER, M., DOLLE, P. & FRANCO, B. 2006. Oral-facial-digital type I protein is required for primary cilia formation and left-right axis specification. *Nature Genetics,* 38**,** 112-117.

FISH, J. L., KOSODO, Y., ENARD, W., PAABO, S. & HUTTNER, W. B. 2006. Aspm specifically maintains symmetric proliferative divisions of neuroepithelial cells. *Proceedings of the National Academy of Sciences of the United States of America,* 103**,** 10438-10443.

FONTE, V. G., SEARLS, R. L. & HILFER, S. R. 1971. Relationship of Cilia with Cell Division and Differentiation. *Journal of Cell Biology,* 49**,** 226-&.

FRANCIS, F., KOULAKOFF, A., BOUCHER, D., CHAFEY, P., SCHAAR, B., VINET, M. C., FRIOCOURT, G., MCDONNELL, N., REINER, O., KAHN, A., MCCONNELL, S. K., BERWALD-NETTER, Y., DENOULET, P. & CHELLY, J. 1999. Doublecortin is a developmentally regulated, microtubule-associated protein expressed in migrating and differentiating neurons. *Neuron,* 23**,** 247-256.

FREMEAU, R. T., TROYER, M. D., PAHNER, I., NYGAARD, G. O., TRAN, C. H., REIMER, R. J., BELLOCCHIO, E. E., FORTIN, D., STORM-MATHISEN, J. & EDWARDS, R. H. 2001. The expression of vesicular glutamate transporters defines two classes of excitatory synapse. *Neuron,* 31**,** 247-260.

FROTSCHER, M., HAAS, C. A. & FORSTER, E. 2003. Reelin controls granule cell migration in the dentate gyrus by acting on the radial glial scaffold. *Cerebral Cortex,* 13**,** 634-640.

GALCERAN, J., MIYASHITA-LIN, E. M., DEVANEY, E., RUBENSTEIN, J. L. R. & GROSSCHEDL, R. 2000. Hippocampus development and generation of dentate gyrus granule cells is regulated by LEF1. *Development,* 127**,** 469-482.

GARVEY, W., BIGELOW, F. & CARPENTER, B. 1999. Rapid and economical silver impregnation technique to demonstrate nerve fibers, axons, neurons, and senile plaques and neurofibrillary tangles of Alzheimer's disease. *Journal of Histotechnology,* 22**,** 37-41.

GERDES, J. M., DAVIS, E. E. & KATSANIS, N. 2009. The Vertebrate Primary Cilium in Development, Homeostasis, and Disease. *Cell,* 137**,** 32-45.

GERDES, J. M., LIU, Y., ZAGHLOUL, N. A., LEITCH, C. C., LAWSON, S. S., KATO, M., BEACHY, P. A., BEALES, P. L., DEMARTINO, G. N., FISHER, S., BADANO, J. L. & KATSANIS, N. 2007. Disruption of the basal body compromises proteasomal function and perturbs intracellular Wnt response. *Nat Genet,* 39**,** 1350-60.

GILLEY, J. A., YANG, C. P. & KERNIE, S. G. 2011. Developmental Profiling of Postnatal Dentate Gyrus Progenitors Provides Evidence For Dynamic Cell-Autonomous Regulation. *Hippocampus,* 21**,** 33-47.

GIORDANO, L., VIGNOLI, A., PINELLI, L., BRANCATI, F., ACCORSI, P., FARAVELLI, F., GASPAROTTI, R., GRANATA, T., GIACCONE, G., INVERARDI, F., FRASSONI, C., DALLAPICCOLA, B., VALENTE, E. M. & SPREAFICO, R. 2009. Joubert Syndrome With Bilateral Polymicrogyria: Clinical and Neuropathological Findings in Two Brothers. *American Journal of Medical Genetics Part A,* 149A**,** 1511-1515.

GOETZ, S. C. & ANDERSON, K. V. 2010. The primary cilium: a signalling centre during vertebrate development. *Nature Reviews Genetics,* 11**,** 331-344.

GOETZ, S. C., LIEM, K. F. & ANDERSON, K. V. 2012. The Spinocerebellar Ataxia-Associated Gene Tau Tubulin Kinase 2 Controls the Initiation of Ciliogenesis. *Cell,* 151**,** 847-858.

GOODRICH, L. V., JOHNSON, R. L., MILENKOVIC, L., MCMAHON, J. A. & SCOTT, M. P. 1996. Conservation of the hedgehog/patched signaling pathway from flies to mice: Induction of a mouse patched gene by Hedgehog. *Genes & Development,* 10**,** 301-312.

GORDEN, N. T., ARTS, H. H., PARISI, M. A., COENE, K. L. M., LETTEBOER, S. J. F., VAN BEERSUM, S. E. C., MANS, D. A., HIKIDA, A., ECKERT, M., KNUTZEN, D., ALSWAID, A. F., OZYUREK, H., DIBOOGLU, S., OTTO, E. A., LIU, Y. F., DAVIS, E. E., HUTTER, C. M., BAMMLER, T. K., FARIN, F. M., DORSCHNER, M., TOPCU, M., ZACKAI, E. H., ROSENTHAL, P., OWENS, K. N., KATSANIS, N., VINCENT, J. B., HILDEBRANDT, F., RUBEL, E. W., RAIBLE, D. W., KNOERS, N. V. A. M., CHANCE, P. F., ROEPMAN, R., MOENS, C. B., GLASS, I. A. & DOHERTY, D. 2008. CC2D2A Is Mutated in

Joubert Syndrome and Interacts with the Ciliopathy-Associated Basal Body Protein CEP290. *American Journal of Human Genetics,* 83**,** 559-571.

GORIVODSKY, M., MUKHOPADHYAY, M., WILSCH-BRAEUNINGER, M., PHILLIPS, M., TEUFEL, A., KIM, C., MALIK, N., HUTTNER, W. & WESTPHAL, H. 2009. Intraflagellar transport protein 172 is essential for primary cilia formation and plays a vital role in patterning the mammalian brain. *Developmental Biology,* 325**,** 24-32.

GORSKI, J. A., TALLEY, T., QIU, M., PUELLES, L., RUBENSTEIN, J. L. & JONES, K. R. 2002. Cortical excitatory neurons and glia, but not GABAergic neurons, are produced in the Emx1-expressing lineage. *The Journal of neuroscience,* 22**,** 6309-6314.

GRASER, S., STIERHOF, Y. D., LAVOIE, S. B., GASSNER, O. S., LAMLA, S., LE CLECH, M. & NIGG, E. A. 2007. Cep164, a novel centriole appendage protein required for primary cilium formation. *Journal of Cell Biology,* 179**,** 321-330.

GREIG, L. C., WOODWORTH, M. B., GALAZO, M. J., PADMANABHAN, H. & MACKLIS, J. D. 2013. Molecular logic of neocortical projection neuron specification, development and diversity. *Nat Rev Neurosci,* 14**,** 755-69.

GROVE, E. A., TOLE, S., LIMON, J., YIP, L. W. & RAGSDALE, C. W. 1998. The hem of the embryonic cerebral cortex is defined by the expression of multiple Wnt genes and is compromised in Gli3-deficient mice. *Development,* 125**,** 2315-2325.

GRUBER, R., ZHOU, Z. W., SUKCHEV, M., JOERSS, T., FRAPPART, P. O. & WANG, Z. Q. 2011. MCPH1 regulates the neuroprogenitor division mode by coupling the centrosomal cycle with mitotic entry through the Chk1-Cdc25 pathway. *Nature Cell Biology,* 13**,** 1325-U100.

GUADIANA, S. M., SEMPLE-ROWLAND, S., DAROSZEWSKI, D., MADORSKY, I., BREUNIG, J. J., MYKYTYN, K. & SARKISIAN, M. R. 2013. Arborization of Dendrites by Developing Neocortical Neurons Is Dependent on Primary Cilia and Type 3 Adenylyl Cyclase. *Journal of Neuroscience,* 33**,** 2626-2638.

GUO, W. X., PATZLAFF, N. E., JOBE, E. M. & ZHAO, X. Y. 2012. Isolation of multipotent neural stem or progenitor cells from both the dentate gyrus and subventricular zone of a single adult mouse. *Nature Protocols,* 7**,** 2005-2012.

HAAN, C. & BEHRMANN, I. 2007. A cost effective non-commercial ECL-solution for Western blot detections yielding strong signals and low background. *J Immunol Methods,* 318**,** 11-9.

HABEDANCK, R., STIERHOF, Y. D., WILKINSON, C. J. & NIGG, E. A. 2005. The Polo kinase Plk4 functions in centriole duplication. *Nat Cell Biol,* 7**,** 1140-6.

HADLEY, M. A., BYERS, S. W., SUAREZQUIAN, C. A., KLEINMAN, H. K. & DYM, M. 1985. Extracellular-Matrix Regulates Sertoli-Cell Differentiation, Testicular Cord Formation, and Germ-Cell Development Invitro. *Journal of Cell Biology,* 101**,** 1511-1522.

HAN, Y. G., SPASSKY, N., ROMAGUERA-ROS, M., GARCIA-VERDUGO, J. M., AGUILAR, A., SCHNEIDER-MAUNOURY, S. & ALVAREZ-BUYLLA, A. 2008. Hedgehog signaling and primary cilia are required for the formation of adult neural stem cells. *Nature Neuroscience,* 11**,** 277-284.

HANDEL, M., SCHULZ, S., STANARIUS, A., SCHREFF, M., ERDTMANN-VOURLIOTIS, M., SCHMIDT, H., WOLF, G. & HOLLT, V. 1999. Selective targeting of somatostatin receptor 3 to neuronal cilia. *Neuroscience,* 89**,** 909-926.

HARRISON, R. G. 1910. The outgrowth of the nerve fiber as a mode of protoplasmic movement. *Journal of Experimental Zoology,* 9**,** 787-846.

HASENPUSCH-THEIL, K., MAGNANI, D., AMANITI, E. M., HAN, L., ARMSTRONG, D. & THEIL, T. 2012. Transcriptional Analysis of Gli3 Mutants Identifies Wnt Target Genes in the Developing Hippocampus. *Cerebral Cortex,* 22**,** 2878-2893.

HAYCRAFT, C. J., BANIZS, B., AYDIN-SON, Y., ZHANG, Q., MICHAUD, E. J. & YODER, B. K. 2005. Gli2 and Gli3 localize to cilia and require the intraflagellar transport protein polaris for processing and function. *PLoS Genet,* 1**,** e53.

HE, M., SUBRAMANIAN, R., BANGS, F., OMELCHENKO, T., LIEM, K. F., KAPOOR, T. M. & ANDERSON, K. V. 2014. The kinesin-4 protein Kif7 regulates mammalian Hedgehog signalling by organizing the cilium tip compartment. *Nature Cell Biology,* 16**,** 663-+.

HEFFNER, C. S., PRATT, C. H., BABIUK, R. P., SHARMA, Y., ROCKWOOD, S. F., DONAHUE, L. R., EPPIG, J. T. & MURRAY, S. A. 2012. Supporting conditional mouse mutagenesis with a comprehensive cre characterization resource. *Nature Communications,* 3.

HERBERT, J., MCCONNELL, S., 2000. Targeting of cre to the Foxg1 (BF-1) Locus Mediates loxP Recombination in the Telencephalon and Other Developing Head Structures. *Developmental Biology*, 222, 296–306.

HERNANDEZ-HERNANDEZ, V., PRAVINCUMAR, P., DIAZ-FONT, A., MAY-SIMERA, H., JENKINS, D., KNIGHT, M. & BEALES, P. L. 2013. Bardet-Biedl syndrome proteins control the cilia length through regulation of actin polymerization. *Human Molecular Genetics,* 22**,** 3858-3868.

HEVNER, R. F., DAZA, R. A. M., ENGLUND, C., KOHTZ, J. & FINK, A. 2004. Postnatal shifts of interneuron position in the neocortex of normal and reeler mice: Evidence for inward radial migration. *Neuroscience,* 124**,** 605-618.

HEVNER, R. F., SHI, L., JUSTICE, N., HSUEH, Y., SHENG, M., SMIGA, S., BULFONE, A., GOFFINET, A. M., CAMPAGNONI, A. T. & RUBENSTEIN, J. L. 2001. Tbr1 regulates differentiation of the preplate and layer 6. *Neuron,* 29**,** 353-66.

HIGGINBOTHAM, H., EOM, T. Y., MARIANI, L. E., BACHLEDA, A., HIRT, J., GUKASSYAN, V., CUSACK, C. L., LAI, C., CASPARY, T. & ANTON, E. S. 2012. Arl13b in Primary Cilia Regulates the Migration and Placement of Interneurons in the Developing Cerebral Cortex. *Developmental Cell,* 23**,** 925-938.

HIGGINBOTHAM, H., GUO, J. M., YOKOTA, Y., UMBERGER, N. L., SU, C. Y., LI, J. J., VERMA, N., HIRT, J., GHUKASYAN, V., CASPARY, T. & ANTON, E. S. 2013. Arl13b-regulated cilia activities are essential for polarized radial glial scaffold formation. *Nature Neuroscience,* 16**,** 1000-U44.

HOERDER-SUABEDISSEN, A., WANG, W. Z., LEE, S., DAVIES, K. E., GOFFINET, A. M., RAKIC, S., PARNAVELAS, J., REIM, K., NICOLIC, M., PAULSEN, O. & MOLNAR, Z. 2009. Novel Markers Reveal Subpopulations of Subplate Neurons in the Murine Cerebral Cortex. *Cerebral Cortex,* 19**,** 1738-1750.

HOLOWACZ, T., ALEXSON, T. O., COLES, B. L., DOBLE, B. W., KELLY, K. F., WOODGETT, J. R. & VAN DER KOOY, D. 2013. The responses of neural stem cells to the level of GSK-3 depend on the tissue of origin. *Biology Open,* 2**,** 812-821.

HOOVER, A. N., WYNKOOP, A., ZENG, H. Q., JIA, J. P., NISWANDER, L. A. & LIU, A. M. 2008. C2cd3 is required for cilia formation and Hedgehog signaling in mouse. *Development,* 135**,** 4049-4058.

HUANGFU, D. & ANDERSON, K. V. 2005. Cilia and Hedgehog responsiveness in the mouse. *Proc Natl Acad Sci U S A,* 102**,** 11325-30.

HUANGFU, D. W., LIU, A. M., RAKEMAN, A. S., MURCIA, N. S., NISWANDER, L. & ANDERSON, K. V. 2003. Hedgehog signalling in the mouse requires intraflagellar transport proteins. *Nature,* 426**,** 83-87.

HUARD, J. M. T., FORSTER, C. C., CARTER, M. L., SICINSKI, P. & ROSS, M. E. 1999. Cerebellar histogenesis is disturbed in mice lacking cyclin D2. *Development,* 126**,** 1927-1935.

HYNES, A. M., GILES, R. H., SRIVASTAVA, S., ELEY, L., WHITEHEAD, J., DANILENKO, M., RAMAN, S., SLAATS, G. G., COLVILLE, J. G., AJZENBERG, H., KROES, H. Y., THELWALL, P. E., SIMMONS, N. L., MILES, C. G. & SAYER, J. A. 2014. Murine Joubert syndrome reveals Hedgehog signaling defects as a potential therapeutic target for nephronophthisis. *Proceedings of the National Academy of Sciences of the United States of America,* 111**,** 9893-9898.

IBANEZ-TALLON, I., PAGENSTECHER, A., FLIEGAUF, M., OLBRICH, H., KISPERT, A., KETELSEN, U. P., NORTH, A., HEINTZ, N. & OMRAN, H. 2004a. Dysfunction of axonemal dynein heavy chain Mdnah5 inhibits ependymal flow and reveals a novel mechanism for hydrocephalus formation. *Hum Mol Genet,* 13**,** 2133-41.

INAMURA, N., KIMURA, T., TADA, S., KURAHASHI, T., YANAGIDA, M., YANAGAWA, Y., IKENAKA, K. & MURAKAMI, F. 2012. Intrinsic and Extrinsic Mechanisms Control the Termination of Cortical Interneuron Migration. *Journal of Neuroscience,* 32**,** 6032-6042.

INGASON, A., SIGMUNDSSON, T., STEINBERG, S., SIGURDSSON, E., HARALDSSON, M., MAGNUSDOTTIR, B. B., FRIGGE, M. L., KONG, A., GULCHER, J., THORSTEINSDOTTIR, U., STEFANSSON, K., PETURSSON, H. & STEFANSSON, H. 2007. Support for involvement of the AHI1 locus in schizophrenia. *European Journal of Human Genetics,* 15**,** 988-991.

ISHIDO, M. & SUZUKI, J. 2010. Inhibition by rotenone of mesencephalic neural stem-cell migration in a neurosphere assay in vitro. *Toxicology in Vitro,* 24**,** 552-557.

JESSBERGER, S., CLEMENSON, G. D. & GAGE, F. H. 2007. Spontaneous fusion and nonclonal growth of adult neural stem cells. *Stem Cells,* 25**,** 871-874.

JHO, E. H., ZHANG, T., DOMON, C., JOO, C. K., FREUND, J. N. & COSTANTINI, F. 2002. Wnt/beta-catenin/Tcf signaling induces the transcription of Axin2, a negative regulator of the signaling pathway. *Molecular and Cellular Biology,* 22**,** 1172-1183.

JIN, H., WHITE, S. R., SHIDA, T., SCHULZ, S., AGUIAR, M., GYGI, S. P., BAZAN, J. F. & NACHURY, M. V. 2010. The Conserved Bardet-Biedl Syndrome Proteins Assemble a Coat that Traffics Membrane Proteins to Cilia. *Cell,* 141**,** 1208-U198.

JOHANSON, C. E., DUNCAN, J. A., 3RD, KLINGE, P. M., BRINKER, T., STOPA, E. G. & SILVERBERG, G. D. 2008. Multiplicity of cerebrospinal fluid functions: New challenges in health and disease. *Cerebrospinal Fluid Res,* 5**,** 10.

JOHNSON, D. R. 1967. Extra-Toes - a New Mutant Gene Causing Multiple Abnormalities in Mouse. *Journal of Embryology and Experimental Morphology,* 17**,** 543-&.

JOHNSTON, M., ZAKHAROV, A., PAPAICONOMOU, C., SALMASI, G. & ARMSTRONG, D. 2004. Evidence of connections between cerebrospinal fluid and nasal lymphatic vessels in humans, non-human primates and other mammalian species. *Cerebrospinal Fluid Res,* 1**,** 2.

JONES, C., ROPER, V. C., FOUCHER, I., QIAN, D., BANIZS, B., PETIT, C., YODER, B. K. & CHEN, P. 2008. Ciliary proteins link basal body polarization to planar cell polarity regulation. *Nature Genetics,* 40**,** 69-77.

JONES, T. J., ADAPALA, R. K., GELDENHUYS, W. J., BURSLEY, C., NAULI, S. & THODETI, C. K. 2011. Primary cilia regulates the directional migration and barrier integrity of endothelial cells through the modulation of hsp27 dependent actin cytoskeletal organization. *Faseb Journal,* 25.

JOO, K., KIM, C. G., LEE, M. S., MOON, H. Y., LEE, S. H., KIM, M. J., KWEON, H. S., PARK, W. Y., KIM, C. H., GLEESON, J. G. & KIM, J. 2013. CCDC41 is required for ciliary vesicle docking to the mother centriole. *Proceedings of the National Academy of Sciences of the United States of America,* 110**,** 5987-5992.

KAMIYA, A., TAN, P. L., KUBO, K. I., ENGELHARD, C., ISHIZUKA, K., KUBO, A., TSUKITA, S., PULVER, A. E., NAKAJIMA, K., CASCELLA, N. G., KATSANIS, N. & SAWA, A. 2008. Recruitment of PCM1 to the centrosome by the cooperative action of DISC1 and BBS4 - A candidate for psychiatric illnesses. *Archives of General Psychiatry,* 65**,** 996-1006.

KAWASAKI, H., MIZUSEKI, K., NISHIKAWA, S., KANEKO, S., KUWANA, Y., NAKANISHI, S., NISHIKAWA, S. I. & SASAI, Y. 2000. Induction of midbrain dopaminergic neurons from ES cells by stromal cell-derived inducing activity. *Neuron,* 28**,** 31-40.

KEMP, C., WILLEMS, E., ABDO, S., LAMBIV, L. & LEYNS, L. 2005. Expression of all Wnt genes and their secreted antagonists during mouse blastocyst and postimplantation development. *Developmental Dynamics,* 233**,** 1064-1075.

KENNEY, A. M., COLE, M. D. & ROWITCH, D. H. 2003. Nmyc upregulation by sonic hedgehog signaling promotes proliferation in developing cerebellar granule neuron precursors. *Development,* 130**,** 15-28.

KESHISHIAN, H. 2004. Ross Harrison's "The outgrowth of the nerve fiber as a mode of protoplasmic movement". *Journal of Experimental Zoology Part A: Comparative Experimental Biology,* 301A**,** 201-203.

KIM, J., KRISHNASWAMI, S. R. & GLEESON, J. G. 2008. CEP290 interacts with the centriolar satellite component PCM-1 and is required for Rab8 localization to the primary cilium. *Human Molecular Genetics,* 17**,** 3796-3805.

KIM, K. H., KIM, J. M., CHOI, Y. L., SHIN, Y. K., LEE, H. C., SEONG, I. O., KIM, B. K., CHAE, S. W., CHUNG, Y. S. & KIM, S. H. 2009. Expression of Sonic hedgehog signaling molecules in normal, hyperplastic and carcinomatous endometrium. *Pathology International,* 59**,** 279-287.

KOBAYASHI, T., KIM, S., LIN, Y. C., INOUE, T. & DYNLACHT, B. D. 2014. The CP110-interacting proteins Talpid3 and Cep290 play overlapping and distinct roles in cilia assembly. *Journal of Cell Biology,* 204**,** 215-229.

KODANI, A., SIREROL-PIQUER, M. S., SEOL, A., GARCIA-VERDUGO, J. M. & REITER, J. F. 2013. Kif3a interacts with Dynactin subunit p150(Glued) to organize centriole subdistal appendages. *Embo Journal,* 32**,** 597-607.

KOH, Y. Y., SUN, Y. H., MIN, Y. G., CHI, J. G. & KIM, C. K. 2003. Chemotaxis of blood neutrophils from patients with primary ciliary dyskinesia. *Journal of Korean Medical Science,* 18**,** 36-41.

KOMADA, M., SAITSU, H., KINBOSHI, M., MIURA, T., SHIOTA, K. & ISHIBASHI, M. 2008. Hedgehog signaling is involved in development of the neocortex. *Development,* 135**,** 2717-2727.

KOMURO, H., YACUBOVA, E., YACUBOVA, E. & RAKIC, P. 2001. Mode and tempo of tangential cell migration in the cerebellar external granular layer. *Journal of Neuroscience,* 21**,** 527-540.

KONG, H., FAN, Y., XIE, J., DING, J., SHA, L., SHI, X., SUN, X. & HU, G. 2008. AQP4 knockout impairs proliferation, migration and neuronal differentiation of adult neural stem cells. *J Cell Sci,* 121**,** 4029-36.

KUMAMOTO, N., GU, Y., WANG, J., JANOSCHKA, S., TAKEMARU, K. I., LEVINE, J. & GE, S. 2012. A role for primary cilia in glutamatergic synaptic integration of adult-born neurons. *Journal of Neurochemistry,* 123**,** 39-39.

KUPFER, A., DENNERT, G. & SINGER, S. J. 1983. Polarization of the Golgi-Apparatus and the Microtubule-Organizing Center within Cloned Natural-Killer Cells Bound to Their Targets. *Proceedings of the National Academy of Sciences of the United States of America-Biological Sciences,* 80**,** 7224-7228.

KVAJO, M., MCKELLAR, H., ARGUELLO, P. A., DREW, L. J., MOORE, H., MACDERMOTT, A. B., KARAYIORGOU, M. & GOGOS, J. A. 2008. A mutation in mouse Disc1 that models a schizophrenia risk allele leads to specific alterations in neuronal architecture and cognition. *Proceedings of the National Academy of Sciences of the United States of America,* 105**,** 7076-7081.

LAI, K., KASPAR, B. K., GAGE, F. H. & SCHAFFER, D. V. 2003. Sonic hedgehog regulates adult neural progenitor proliferation in vitro and in vivo. *Nature Neuroscience,* 6**,** 21-27.

LANCASTER, M. A., SCHROTH, J. & GLEESON, J. G. 2011. Subcellular spatial regulation of canonical Wnt signalling at the primary cilium. *Nature Cell Biology,* 13**,** 700-U173.

LANCASTER, M. A., GOPAL, D. J., Kim, J., SALEEM, S., SILHAVY, J. L., LOUIE, C. M., THACKER, B. E., WILLIAMS, Y., ZAKI, M., GLEESON, J. G. 2011b. Defective Wnt-dependent cerebellar midline fusion in a mouse model of Joubert syndrome. *Nature Medicine,* 17, 726–731.

LAVDAS, A. A., GRIGORIOU, M., PACHNIS, V. & PARNAVELAS, J. G. 1999. The medial ganglionic eminence gives rise to a population of early neurons in the developing cerebral cortex. *J Neurosci,* 19**,** 7881-8.

LAWSON, L., PERRY, V., DRI, P., GORDON, S., 1990. Heterogeneity in the distribution and morphology of microglia in the normal adult mouse brain. Neuroscience, 39, 151–170.

LEE, J., PLATT, K. A., CENSULLO, P. & ALTABA, A. R. I. 1997. Gli1 is a target of Sonic hedgehog that induces ventral neural tube development. *Development,* 124**,** 2537-2552.

LEE, J. E., SILHAVY, J. L., ZAKI, M. S., SCHROTH, J., BIELAS, S. L., MARSH, S. E., OLVERA, J., BRANCATI, F., IANNICELLI, M., IKEGAMI, K., SCHLOSSMAN, A. M., MERRIMAN, B., ATTIE-BITACH, T., LOGAN, C. V., GLASS, I. A., CLUCKEY, A., LOUIE, C. M., LEE, J. H., RAYNES, H. R., RAPIN, I., CASTROVIEJO, I. P., SETOU, M., BARBOT, C., BOLTSHAUSER, E., NELSON, S. F., HILDEBRANDT, F., JOHNSON, C. A., DOHERTY, D. A., VALENTE, E. M. & GLEESON, J. G. 2012. CEP41 is mutated in Joubert syndrome and is required for tubulin glutamylation at the cilium. *Nature Genetics,* 44**,** 193-199.

LEE, S. M. K., TOLE, S., GROVE, E. & MCMAHON, A. P. 2000. A local Wnt-3a signal is required for development of the mammalian hippocampus. *Development,* 127**,** 457-467.

LEGUILLIER, T., VANDORMAEL-POURNIN, S., ARTUS, J., HOULARD, M., PICARD, C., BERNEX, F., ROBINE, S. & COHEN-TANNOUDJI, M. 2012. Omcg1 is critically required for mitosis in rapidly dividing mouse intestinal progenitors and embryonic stem cells. *Biology Open,* 1**,** 648-657.

LEID, M., ISHMAEL, J. E., AVRAM, D., SHEPHERD, D., FRAULOB, V. & DOLLE, P. 2004. CTIP1 and CTIP2 are differentially expressed during mouse embryogenesis. *Gene Expression Patterns,* 4**,** 733-739.

LEIDEL, S., DELATTRE, M., CERUTTI, L., BAUMER, K. & GONCZY, P. 2005. SAS-6 defines a protein family required for centrosome duplication in C. elegans and in human cells. *Nat Cell Biol,* 7**,** 115-25.

LEIN, E. S., HAWRYLYCZ, M. J., AO, N., AYRES, M., BENSINGER, A., BERNARD, A., BOE, A. F., BOGUSKI, M. S., BROCKWAY, K. S., BYRNES, E. J., CHEN, L., CHEN, L., CHEN, T. M., CHIN, M. C., CHONG, J., CROOK, B. E., CZAPLINSKA, A., DANG, C. N., DATTA, S., DEE, N. R., DESAKI, A. L., DESTA, T., DIEP, E., DOLBEARE, T. A., DONELAN, M. J., DONG, H. W., DOUGHERTY, J. G., DUNCAN, B. J., EBBERT, A. J., EICHELE, G., ESTIN, L. K., FABER, C., FACER, B. A., FIELDS, R., FISCHER, S. R., FLISS, T. P., FRENSLEY, C., GATES, S. N., GLATTFELDER, K. J., HALVERSON, K. R., HART, M. R., HOHMANN, J. G., HOWELL, M. P., JEUNG, D. P., JOHNSON, R. A., KARR, P. T., KAWAL, R., KIDNEY, J. M., KNAPIK, R. H., KUAN, C. L., LAKE, J. H., LARAMEE, A. R., LARSEN, K. D., LAU, C., LEMON, T. A., LIANG, A. J., LIU, Y., LUONG, L. T., MICHAELS, J., MORGAN, J. J., MORGAN, R. J., MORTRUD, M. T., MOSQUEDA, N. F., NG, L. L., NG, R., ORTA, G. J., OVERLY, C. C., PAK, T. H., PARRY, S. E., PATHAK, S. D., PEARSON, O. C., PUCHALSKI, R. B., RILEY, Z. L., ROCKETT, H. R., ROWLAND, S. A., ROYALL, J. J., RUIZ, M. J., SARNO, N. R., SCHAFFNIT, K., SHAPOVALOVA, N. V., SIVISAY, T., SLAUGHTERBECK, C. R., SMITH, S. C., SMITH, K. A., SMITH, B. I., SODT, A. J., STEWART, N. N., STUMPF, K. R., SUNKIN, S. M., SUTRAM, M., TAM, A., TEEMER, C. D., THALLER, C., THOMPSON, C. L., VARNAM, L. R., VISEL, A., WHITLOCK, R. M., WOHNOUTKA, P. E., WOLKEY, C. K., WONG, V. Y., et al. 2007. Genome-wide atlas of gene expression in the adult mouse brain. *Nature,* 445**,** 168-176.

LEONE, D. P., SRINIVASAN, K., CHEN, B., ALCAMO, E. & MCCONNELL, S. K. 2008. The determination of projection neuron identity in the developing cerebral cortex. *Curr Opin Neurobiol,* 18**,** 28-35.

LEWIS, K. E., DROSSOPOULOU, G., PATON, I. R., MORRICE, D. R., ROBERTSON, K. E., BURT, D. W., INGHAM, P. W. & TICKLE, C. 1999. Expression of ptc and gli genes in talpid(3) suggests bifurcation in Shh pathway. *Development,* 126**,** 2397-2407.

LEWIS, P. M., GRITLI-LINDE, A., SMEYNE, R., KOTTMANN, A. & MCMAHON, A. P. 2004. Sonic hedgehog signaling is required for expansion of granule neuron precursors and patterning of the mouse cerebellum. *Developmental Biology,* 270**,** 393-410.

LI, G. N., KATAOKA, H., COUGHLIN, S. R. & PLEASURE, S. J. 2009. Identification of a transient subpial neurogenic zone in the developing dentate gyrus and its regulation by Cxcl12 and reelin signaling. *Development,* 136**,** 327-335.

LI, Y., LUILKART, B. W., BIRNBAUM, S., CHEN, J., KWON, C. H., KERNIE, S. G., BASSEL-DUBY, R. & PARADA, L. F. 2008. TrkB Regulates Hippocampal Neurogenesis and Governs Sensitivity to Antidepressive Treatment (vol 59, pg 399, 2008). *Neuron,* 60**,** 730-730.

LIANG, H., HIPPENMEYER, S. & GHASHGHAEI, H. T. 2012a. A Nestin-cre transgenic mouse is insufficient for recombination in early embryonic neural progenitors. *Biology open,* 1**,** 1200-3.

LIE, D. C., COLAMARINO, S. A., SONG, H. J., DESIRE, L., MIRA, H., CONSIGLIO, A., LEIN, E. S., JESSBERGER, S., LANSFORD, H., DEARIE, A. R. & GAGE, F. H. 2005. Wnt signalling regulates adult hippocampal neurogenesis. *Nature,* 437**,** 1370-1375.

LIEM, K., HE, M., OCBINA, P., ANDERSON, K., 2009. Mouse Kif7/Costal2 is a cilia-associated protein that regulates Sonic hedgehog signaling. *PNAS*, 106, 13377-13382.

LIM, Y. C., ROBERTS, T. L., DAY, B. W., HARDING, A., KOZLOV, S., KIJAS, A. W., ENSBEY, K. S., WALKER, D. G. & LAVIN, M. F. 2012. A role for homologous recombination and abnormal cell-cycle progression in radioresistance of glioma-initiating cells. *Mol Cancer Ther,* 11**,** 1863-72.

LIN, Y. N., WU, C. T., LIN, Y. C., HSU, W. B., TANG, C. J., CHANG, C. W. & TANG, T. K. 2013. CEP120 interacts with CPAP and positively regulates centriole elongation. *J Cell Biol,* 202**,** 211-9.

LIU, A. M., WANG, B. L. & NISWANDER, L. A. 2005. Mouse intraflagellar transport proteins regulate both the activator and repressor functions of Gli transcription factors. *Development,* 132**,** 3103-3111.

LIU, J., ZENG, H. & LIU, A. 2015. The loss of Hh responsiveness by a non-ciliary Gli2 variant. *Development,* 142**,** 1651-60.

LIZARRAGA, S. B., MARGOSSIAN, S. P., HARRIS, M. H., CAMPAGNA, D. R., HAN, A. P., BLEVINS, S., MUDBHARY, R., BARKER, J. E., WALSH, C. A. & FLEMING, M. D. 2010. Cdk5rap2 regulates centrosome function and chromosome segregation in neuronal progenitors. *Development,* 137**,** 1907-1917.

LORENZ, A., DEUTSCHMANN, M., AHLFELD, J., PRIX, C., KOCH, A., SMITS, R., FODDE, R., KRETZSCHMAR, H. A. & SCHULLER, U. 2011. Severe alterations of cerebellar cortical development after constitutive activation of Wnt signaling in granule neuron precursors. *Mol Cell Biol,* 31**,** 3326-38.

LU, C. J., DU, H., WU, J., JANSEN, D. A., JORDAN, K. L., XU, N., SIECK, G. C. & QIAN, Q. 2008. Non-random distribution and sensory functions of primary cilia in vascular smooth muscle cells. *Kidney Blood Press Res,* 31**,** 171-84.

MA, C. Y., YAO, M. J., ZHAI, Q. W., JIAO, J. W., YUAN, X. B. & POO, M. M. 2014. SIRT1 suppresses self-renewal of adult hippocampal neural stem cells. *Development,* 141**,** 4697-4709.

MA, R., LI, W. P., RUNDLE, D., KONG, J., AKBARALI, H. I. & TSIOKAS, L. 2005. PKD2 functions as an epidermal growth factor-activated plasma membrane channel. *Molecular and Cellular Biology,* 25**,** 8285-8298.

MA, W., TAVAKOLI, T., DERBY, E., SEREBRYAKOVA, Y., RAO, M. S. & MATTSON, M. P. 2008. Cell-extracellular matrix interactions regulate neural differentiation of human embryonic stem cells. *Bmc Developmental Biology,* 8.

MACHOLD, R., HAYASHI, S., RUTLIN, M., MUZUMDAR, M. D., NERY, S., CORBIN, J. G., GRITLI-LINDE, A., DELLOVADE, T., PORTER, J. A., RUBIN, L. L., DUDEK, H., MCMAHON, A. P. & FISHELL, G. 2003a. Sonic hedgehog is required for progenitor cell maintenance in telencephalic stem cell niches. *Neuron,* 39**,** 937-950.

MACHON, O., VAN DEN BOUT, C. J., BACKMAN, M., KEMLER, R. & KRAUSS, S. 2003. Role of beta-catenin in the developing cortical and hippocampal neuroepithelium. *Neuroscience,* 122**,** 129-43.

MAGNANI, D., HASENPUSCH-THEIL, K., BENADIBA, C., YU, T., BASSON, M. A., PRICE, D. J., LEBRAND, C. & THEIL, T. 2014. Gli3 Controls Corpus Callosum Formation by Positioning Midline Guideposts During Telencephalic Patterning. *Cerebral Cortex,* 24**,** 186-198.

MARIA, B. L., BOLTSHAUSER, E., PALMER, S. C. & TRAN, T. X. 1999. Clinical features and revised diagnostic criteria in Joubert syndrome. *J Child Neurol,* 14**,** 583-90; discussion 590-1.

MARIGO, V., JOHNSON, R. L., VORTKAMP, A. & TABIN, C. J. 1996a. Sonic hedgehog differentially regulates expression of GLI and GLI3 during limb development. *Developmental Biology,* 180**,** 273-283.

MARIGO, V., SCOTT, M. P., JOHNSON, R. L., GOODRICH, L. V. & TABIN, C. J. 1996b. Conservation in hedgehog signaling: Induction of a chicken patched homolog by Sonic hedgehog in the developing limb. *Development,* 122**,** 1225-1233.

MARIN-PADILLA, M. 1978. Dual origin of the mammalian neocortex and evolution of the cortical plate. *Anat Embryol (Berl),* 152**,** 109-26.

MARLEY, A. & VON ZASTROW, M. 2010. DISC1 Regulates Primary Cilia That Display Specific Dopamine Receptors. *Plos One,* 5.

MASSINEN, S., HOKKANEN, M. E., MATSSON, H., TAMMIMIES, K., TAPIA-PAEZ, I., DAHLSTROM-HEUSER, V., KUJA-PANULA, J., BURGHOORN, J., JEPPSSON, K. E., SWOBODA, P., PEYRARD-JANVID, M., TOFTGARD, R., CASTREN, E. & KERE, J. 2011. Increased Expression of the Dyslexia Candidate Gene DCDC2 Affects Length and Signaling of Primary Cilia in Neurons. *Plos One,* 6.

MATEI, V., PAULEY, S., KAING, S., ROWITCH, D., BEISEL, K. W., MORRIS, K., FENG, F., JONES, K., LEE, J. & FRITZSCH, B. 2005. Smaller inner ear sensory epithelia in Neurog 1 null mice are related to earlier hair cell cycle exit. *Dev Dyn,* 234**,** 633-50.

MAYE, P., BECKER, S., KASAMEYER, E., BYRD, N. & GRABEL, L. 2000. Indian hedgehog signaling in extraembryonic endoderm and ectoderm differentiation in ES embryoid bodies. *Mech Dev,* 94**,** 117-32.

MCGLASHAN, S. R., JENSEN, C. G. & POOLE, C. A. 2006. Localization of extracellular matrix receptors on the chondrocyte primary cilium. *J Histochem Cytochem,* 54**,** 1005-14.

MCKENNA, W. L., BETANCOURT, J., LARKIN, K. A., ABRAMS, B., GUO, C., RUBENSTEIN, J. L. & CHEN, B. 2011. Tbr1 and Fezf2 regulate alternate corticofugal neuronal identities during neocortical development. *J Neurosci,* 31**,** 549-64.

MEYER, K. D. & MORRIS, J. A. 2009. Disc1 regulates granule cell migration in the developing hippocampus. *Human Molecular Genetics,* 18**,** 3286-3297.

MILLAR, J. K., WILSON-ANNAN, J. C., ANDERSON, S., CHRISTIE, S., TAYLOR, M. S., SEMPLE, C. A. M., DEVON, R. S., ST CLAIR, D. M., MUIR, W. J., BLACKWOOD, D. H. R. & PORTEOUS, D. J. 2000. Disruption of two novel genes by a translocation co-segregating with schizophrenia. *Human Molecular Genetics,* 9**,** 1415-1423.

MING, G. L. & SONG, H. J. 2011. Adult Neurogenesis in the Mammalian Brain: Significant Answers and Significant Questions. *Neuron,* 70**,** 687-702.

MITTELBRONN, M., DIETZ, K., SCHLUESENER, H., MEYERMANN, R., 2001. Local distribution of microglia in the normal adult human central nervous system differs by up to one order of magnitude. Acta Neuropathol. 101, 249–255.

MOLYNEAUX, B. J., ARLOTTA, P., MENEZES, J. R. & MACKLIS, J. D. 2007. Neuronal subtype specification in the cerebral cortex. *Nat Rev Neurosci,* 8**,** 427-37.

MORALES, M., FIFKOVA, E. 1991. Distribution of acetylated alpha-tubulin in brain. In situ localization and biochemical characterization. Cell Tissue Res, 265, 415-23.

MORRIS, J. A., KANDPAL, G., MA, L. & AUSTIN, C. P. 2003. DISC1 (Disrupted-In-Schizophrenia 1) is a centrosome-associated protein that interacts with MAP1A, MIPT3, ATF4/5 and NUDEL: regulation and loss of interaction with mutation. *Human Molecular Genetics,* 12**,** 1591-1608.

NABI, I. R. 1999. The polarization of the motile cell. *Journal of Cell Science,* 112**,** 1803-1811.

NACHURY, M. V., LOKTEV, A. V., ZHANG, Q., WESTLAKE, C. J., PERANEN, J., MERDES, A., SLUSARSKI, D. C., SCHELLER, R. H., BAZAN, J. F., SHEFFIELD, V. C. & JACKSON, P. K. 2007. A core complex of BBS proteins cooperates with the GTPase Rab8 to promote ciliary membrane biogenesis. *Cell,* 129**,** 1201-1213.

NADARAJAH, B. & PARNAVELAS, J. G. 2002. Modes of neuronal migration in the developing cerebral cortex. *Nature Reviews Neuroscience,* 3**,** 423-432.

NAKAHIRA, E. & YUASA, S. 2005. Neuronal generation, migration, and differentiation in the mouse hippocampal primoridium as revealed by enhanced green fluorescent protein gene transfer by means of in utero electroporation. *Journal of Comparative Neurology,* 483**,** 329-340.

NAULI, S. M., ALENGHAT, F. J., LUO, Y., WILLIAMS, E., VASSILEV, P., LIL, X. G., ELIA, A. E. H., LU, W. N., BROWN, E. M., QUINN, S. J., INGBER, D. E. & ZHOU, J. 2003. Polycystins 1 and 2 mediate mechanosensation in the primary cilium of kidney cells. *Nature Genetics,* 33**,** 129-137.

NECHIPURENKO, I. V., DOROQUEZ, D. B. & SENGUPTA, P. 2013. Primary cilia and dendritic spines: Different but similar signaling compartments. *Molecules and Cells,* 36**,** 288-303.

NEUGEBAUER, J. M., AMACK, J. D., PETERSON, A. G., BISGROVE, B. W. & YOST, H. J. 2010. FGF signalling during embryo development regulates cilia length in diverse epithelia (vol 458, pg 651, 2009). *Nature,* 463.

NIETO, M., MONUKI, E. S., TANG, H., IMITOLA, J., HAUBST, N., KHOURY, S. J., CUNNINGHAM, J., GOTZ, M. & WALSH, C. A. 2004. Expression of Cux-1 and Cux-2 in the subventricular zone and upper layers II-IV of the cerebral cortex. *J Comp Neurol,* 479**,** 168-80.

NIGG, E. A. 2002. Centrosome aberrations: Cause or consequence of cancer progression? *Nature Reviews Cancer,* 2**,** 815-825.

NIU, S., RENFRO, A., QUATTROCCHI, C. C., SHELDON, M. & D'ARCANGELO, G. 2004. Reelin promotes hippocampal dendrite development through the VLDLR/ApoER2-Dab1 pathway. *Neuron,* 41**,** 71-84.

NOVAK, A., GUO, C. Y., YANG, W. Y., NAGY, A. & LOBE, C. G. 2000. Z/EG, a double reporter mouse line that expresses enhanced green fluorescent protein upon Cre-mediated excision. *Genesis,* 28**,** 147-155.

NOVOROL, C., BURKHARDT, J., WOOD, K. J., IQBAL, A., ROQUE, C., COUTTS, N., ALMEIDA, A. D., HE, J., WILKINSON, C. J. & HARRIS, W. A. 2013. Microcephaly models in the developing zebrafish retinal neuroepithelium point to an underlying defect in metaphase progression. *Open Biology,* 3.

NOZAWA, Y. I., YAO, E., LIN, C. W., YANG, J. H., WILSON, C. W., GACAYAN, R. & CHUANG, P. T. 2013. Fused (Stk36) is a Ciliary Protein Required for Central Pair Assembly and Motile Cilia Orientation in the Mammalian Oviduct. *Developmental Dynamics,* 242**,** 1307-1319.

NUSSLEIN-VOLHARD, C., WEISCHAUS, E., 1980. Mutations affecting segment number and polarity in *Drosophila*. Nature 287:795–801

OCBINA, P. J., TUSON, M. & ANDERSON, K. V. 2009. Primary cilia are not required for normal canonical Wnt signaling in the mouse embryo. *PLoS One,* 4**,** e6839.

OH, J., DANIELS, G. J., CHIOU, L. S., YE, E. A., JEONG, Y. S. & SAKAGUCHI, D. S. 2014. Multipotent adult hippocampal progenitor cells maintained as neurospheres favor differentiation toward glial lineages. *Biotechnology Journal,* 9**,** 921-933.

OHATA, S., NAKATANI, J., HERRANZ-PEREZ, V., CHENG, J. G., BELINSON, H., INUBUSHI, T., SNIDER, W. D., GARCIA-VERDUGO, J. M., WYNSHAW-BORIS, A. & ALVAREZ-BUYLLA, A. 2014. Loss of Dishevelleds Disrupts Planar Polarity in Ependymal Motile Cilia and Results in Hydrocephalus. *Neuron,* 83**,** 558-571.

OLIVER, T. G., GRASFEDER, L. L., CARROLL, A. L., KAISER, C., GILLINGHAM, C. L., LIN, S. M., WICKRAMASINGHE, R., SCOTT, M. P. & WECHSLER-REYA, R. J. 2003. Transcriptional profiling of the Sonic hedgehog response: A critical role for N-myc in proliferation of neuronal precursors. *Proceedings of the National Academy of Sciences of the United States of America,* 100**,** 7331-7336.

OTERO, J. J., KALASZCZYNSKA, I., MICHOWSKI, W., WONG, M., GYGLI, P. E., GOKOZAN, H. N., GRIVEAU, A., ODAJIMA, J., CZEISLER, C., CATACUTAN, F. P., MURNEN, A., SCHULLER, U., SICINSKI, P. & ROWITCH, D. 2014. Cerebellar cortical lamination and foliation require cyclin A2. *Developmental Biology,* 385**,** 328-339.

PACEY, L., STEAD, S., GLEAVE, J., TOMCZYK, K. & DOERING, L. 2006. Neural Stem Cell Culture: Neurosphere generation, microscopical analysis and cryopreservation.

PAETAU, A., SALONEN, R. & HALTIA, M. 1985. Brain Pathology in the Meckel Syndrome - a Study of 59 Cases. *Clinical Neuropathology,* 4**,** 56-62.

PALMA, V. & ALTABA, A. R. I. 2004. Hedgehog-GLI signaling regulates the behavior of cells with stem cell properties in the developing neocortex. *Development,* 131**,** 337-345.

PAMPLIEGA, O., ORHON, I., PATEL, B., SRIDHAR, S., DIAZ-CARRETERO, A., BEAU, I., CODOGNO, P., SATIR, B. H., SATIR, P. & CUERVO, A. M. 2013. Functional interaction between autophagy and ciliogenesis. *Nature,* 502**,** 194-+.

PAN, Y., BAI, C. Y. B., JOYNER, A. L. & WANG, B. L. 2006. Sonic hedgehog signaling regulates Gli2 transcriptional activity by suppressing its processing and degradation. *Molecular and Cellular Biology,* 26**,** 3365-3377.

PATEL, S. & BARKOVICH, A. J. 2002. Analysis and classification of cerebellar malformations. *American Journal of Neuroradiology,* 23**,** 1074-1087.

PAZOUR, G. J., DICKERT, B. L., VUCICA, Y., SEELEYE, E. S., ROSENBAUM, J. L., WITMAN, G. B. & COLE, D. G. 2000. Chlamydomonas IFT88 and its mouse homologue, polycystic kidney disease gene Tg737, are required for assembly of cilia and flagella. *Molecular Biology of the Cell,* 11**,** 369a-369a.

PAZOUR, G. J., SAN AGUSTIN, J. T., FOLLIT, J. A., ROSENBAUM, J. L. & WITMAN, G. B. 2002. Polycystin-2 localizes to kidney cilia and the ciliary level is elevated in Tg737(orpk) mice with polycystic kidney disease. *Molecular Biology of the Cell,* 13**,** 326a-327a.

PETERSEN, P., ZOU, K., HWANG, J., JAN, Y. & ZHONG, W. 2002. Progenitor cell maintenance requires numb and numblike during mouse neurogenesis. *Nature*, 31, 929-34.

POGORILER, J., MILLEN, K., UTSET, M. & DU, W. 2006. Loss of cyclin D1 impairs cerebellar development and suppresses medulloblastoma formation. *Development,* 133**,** 3929-3937.

POLLEUX, F., WHITFORD, K. L., DIJKHUIZEN, P. A., VITALIS, T. & GHOSH, A. 2002. Control of cortical interneuron migration by neurotrophins and PI3-kinase signaling. *Development,* 129**,** 3147-60.

PRINZ, M., & PRILLER, J., 2014. Microglia and brain macrophages in the molecular age: from origin to neuropsychiatric disease. *Nature Reviews Neuroscience*, 15, 300–312

PURVES, D., FITZPATRICK, D., KATZ, L. C., LAMANTIA, A. S., MCNAMARA, J. O., WILLIAMS, S. M. & AUGUSTINE, G. J. 2001. *Neuroscience*, Sinauer Associates.

RAGLAND, R. L., PATEL, S., RIVARD, R. S., SMITH, K., PETERS, A. A., BIELINSKY, A. K. & BROWN, E. J. 2013. RNF4 and PLK1 are required for replication fork collapse in ATR-deficient cells. *Genes & Development,* 27**,** 2259-2273.

RAI, K. S., HATTIANGADY, B. & SHETTY, A. K. 2007. Enhanced production and dendritic growth of new dentate granule cells in the middle-aged hippocampus following intracerebroventricular FGF-2 infusions. *European Journal of Neuroscience,* 26**,** 1765-1779.

RALLU, M., CORBIN, J. G. & FISHELL, G. 2002. Parsing the prosencephalon. *Nature Reviews Neuroscience,* 3**,** 943-951.

RAN, F. A., HSU, P. D., WRIGHT, J., AGARWALA, V., SCOTT, D. A. & ZHANG, F. 2013. Genome engineering using the CRISPR-Cas9 system. *Nature Protocols,* 8**,** 2281-2308.

REYNOLDS, B. A. & WEISS, S. 1992. Generation of Neurons and Astrocytes from Isolated Cells of the Adult Mammalian Central-Nervous-System. *Science,* 255**,** 1707-1710.

RIBES, V. & BRISCOE, J. 2009. Establishing and Interpreting Graded Sonic Hedgehog Signaling during Vertebrate Neural Tube Patterning: The Role of Negative Feedback. *Cold Spring Harbor Perspectives in Biology,* 1.

RIEDER, C. L., FARUKI, S. & KHODJAKOV, A. 2001. The centrosome in vertebrates: more than a microtubule-organizing center. *Trends in Cell Biology,* 11**,** 413-419.

RIO, C., RIEFF, H. I., QI, P. M., KHURANA, T. S. & CORFAS, G. 1997. Neuregulin and erbB receptors play a critical role in neuronal migration (vol 19, pg 39, 1997). *Neuron,* 19**,** U11-U11.

ROHATGI, R., MILENKOVIC, L. & SCOTT, M. P. 2007. Patched1 regulates Hedgehog signaling at the primary cilium. *Science,* 317**,** 372-376.

ROSSANT, J. & NAGY, A. 1995. Genome Engineering - the New Mouse Genetics. *Nature Medicine,* 1**,** 592-594.

ROUSSEL, M. F. & HATTEN, M. E. 2011. Cerebellum: Development and Medulloblastoma. *Cancer and Development,* 94**,** 235-282.

RUZANKINA, Y., PINZON-GUZMAN, C., ASARE, A., ONG, T., PONTANO, L., COTSARELIS, G., ZEDIAK, V. P., VELEZ, M., BHANDOOLA, A. & BROWN, E. J. 2007. Deletion of the developmentally essential gene ATR in adult mice leads to age-related phenotypes and stem cell loss. *Cell Stem Cell,* 1**,** 113-26.

SALONEN, R., KESTILA, M. & BERGMANN, C. 2011. Clinical utility gene card for: Meckel syndrome. *European Journal of Human Genetics,* 19.

SANAI, N., TRAMONTIN, A. D., QUINONES-HINOJOSA, A., BARBARO, N. M., GUPTA, N., KUNWAR, S., LAWTON, M. T., MCDERMOTT, M. W., PARSA, A. T., VERDUGO, J. M. G., BERGER, M. S. & ALVAREZ-BUYLLA, A. 2004. Unique astrocyte ribbon in adult human brain contains neural stem cells but lacks chain migration. *Nature,* 427**,** 740-744.

SANSOM, S. N. & LIVESEY, F. J. 2009. Gradients in the brain: the control of the development of form and function in the cerebral cortex. *Cold Spring Harb Perspect Biol,* 1**,** a002519.

SASAKI, H., NISHIZAKI, Y., HUI, C. C., NAKAFUKU, M. & KONDOH, H. 1999. Regulation of Gli2 and Gli3 activities by an amino-terminal repression domain: implication of Gli2 and Gli3 as primary mediators of Shh signaling. *Development,* 126**,** 3915-3924.

SATO, T., ARAKI, I. & NAKAMURA, H. 2001. Inductive signal and tissue responsiveness defining the tectum and the cerebellum. *Development,* 128**,** 2461-2469.

SAUER, B. & HENDERSON, N. 1988. Site-Specific DNA Recombination in Mammalian-Cells by the Cre Recombinase of Bacteriophage-P1. *Proceedings of the National Academy of Sciences of the United States of America,* 85**,** 5166-5170.

SAVATIER, P., LAPILLONNE, H., JIRMANOVA, L., VITELLI, L. & SAMARUT, J. 2002. Analysis of the cell cycle in mouse embryonic stem cells. *Methods Mol Biol,* 185**,** 27-33.

SCHAFER, T., PUTZ, M., LIENKAMP, S., GANNER, A., BERGBREITER, A., RAMACHANDRAN, H., GIELOFF, V., GERNER, M., MATTONET, C., CZARNECKI, P. G., SAYER, J. A., OTTO, E. A., HILDEBRANDT, F., KRAMER-ZUCKER, A. & WALZ, G. 2009. Genetic and physical interaction between the NPHP5 and NPHP6 gene products (vol 17, pg 3665, 2008). *Human Molecular Genetics,* 18**,** 4226-4226.

SCHINDELIN, J., ARGANDA-CARRERAS, I., FRISE, E., KAYNIG, V., LONGAIR, M., PIETZSCH, T., PREIBISCH, S., RUEDEN, C., SAALFELD, S., SCHMID, B., TINEVEZ, J. Y., WHITE, D. J., HARTENSTEIN, V., ELICEIRI, K., TOMANCAK, P. & CARDONA, A. 2012. Fiji: an open-source platform for biological-image analysis. *Nat Methods,* 9**,** 676-82.

SCHMIDT, K. N., KUHNS, S., NEUNER, A., HUB, B., ZENTGRAF, H. & PEREIRA, G. 2012. Cep164 mediates vesicular docking to the mother centriole during early steps of ciliogenesis. *Journal of Cell Biology,* 199**,** 1083-1101.

SCHNEIDER, L., CAMMER, M., LEHMAN, J., NIELSEN, S. K., GUERRA, C. F., VELAND, I. R., STOCK, C., HOFFMANN, E. K., YODER, B. K., SCHWAB, A., SATIR, P. & CHRISTENSEN, S. T. 2010. Directional Cell Migration and Chemotaxis in Wound Healing Response to PDGF-AA are Coordinated by the Primary Cilium in Fibroblasts. *Cellular Physiology and Biochemistry,* 25**,** 279-292.

SCHNEIDER, L., CLEMENT, C. A., TEILMANN, S. C., PAZOUR, G. J., HOFFMANN, E. K., SATIR, P. & CHRISTENSEN, S. T. 2005. PDGFR alpha alpha signaling is regulated through the primary cilium in fibroblasts. *Current Biology,* 15**,** 1861-1866.

SCHULLER, U., HEINE, V., MAO, J., KHO, A., DILLON, A., HAN, Y., HUILLARD, E., SUN, T., LIGON, A., QIAN, Y., MA, Q., ALVAREZ-BUYLLA, A., MCMAHON, A., ROWITCH, D. & LIGON, K. 2008. Acquisition of granule neuron precursor identity is a critical determinant of progenitor cell competence to form Shh-induced medulloblastoma. *Cancer Cell*. 12, 123-34.

SEABERG, R. M., SMUKLER, S. R. & VAN DER KOOY, D. 2005. Intrinsic differences distinguish transiently neurogenic progenitors from neural stem cells in the early postnatal brain. *Developmental Biology,* 278**,** 71-85.

SERI, B., GARCIA-VERDUGO, J. M., MCEWEN, B. S. & ALVAREZ-BUYLLA, A. 2001. Astrocytes give rise to new neurons in the adult mammalian hippocampus. *Journal of Neuroscience,* 21**,** 7153-7160.

SHENG, G., XU, X., LIN, Y. F., WANG, C. E., RONG, J., CHENG, D., PENG, J., JIANG, X., LI, S. H. & LI, X. J. 2008. Huntingtin-associated protein 1 interacts with Ahi1 to regulate cerebellar and brainstem development in mice. *J Clin Invest,* 118**,** 2785-95.

SHIMOGORI, T., BANUCHI, V., NG, H. Y., STRAUSS, J. B. & GROVE, E. A. 2004. Embryonic signaling centers expressing BMP, WNT and FGF proteins interact to pattern the cerebral cortex. *Development,* 131**,** 5639-5647.

SILLIBOURNE, J. E., SPECHT, C. G., IZEDDIN, I., HURBAIN, I., TRAN, P., TRILLER, A., DARZACQ, X., DAHAN, M. & BORNENS, M. 2011. Assessing the localization of centrosomal proteins by PALM/STORM nanoscopy. *Cytoskeleton,* 68**,** 619-627.

SIMONI, A., YU, L., 2006. Preparation of organotypic hippocampal slice cultures: interface method. *Nature Protocols* 1, 1439–1445

SIMONS, M., GLOY, J., GANNER, A., BULLERKOTTE, A., BASHKUROV, M., KRONIG, C., SCHERMER, B., BENZING, T., CABELLO, O. A., JENNY, A., MLODZIK, M., POLOK, B., DRIEVER, W., OBARA, T. & WALZ, G. 2005. Inversin, the gene product mutated in nephronophthisis type II, functions as a molecular switch between Wnt signaling pathways. *Nature Genetics,* 37**,** 537-543.

SINGH, S. K., WILLIAMS, C. A., KLARMANN, K., BURKETT, S. S., KELLER, J. R. & OBERDOERFFER, P. 2013. Sirt1 ablation promotes stress-induced loss of epigenetic and genomic hematopoietic stem and progenitor cell maintenance. *Journal of Experimental Medicine,* 210**,** 987-1001.

SLEZAK, M., GORITZ, C., NIEMIEC, A., FRISEN, J., CHAMBON, P., METZGER, D. & PFRIEGER, F. W. 2007. Transgenic mice for conditional gene manipulation in astroglial cells. *Glia,* 55**,** 1565-76.

SMALL, S. A., SCHOBEL, S. A., BUXTON, R. B., WITTER, M. P. & BARNES, C. A. 2011. A pathophysiological framework of hippocampal dysfunction in ageing and disease. *Nat Rev Neurosci,* 12**,** 585-601.

SMITH, K. M., OHKUBO, Y., MARAGNOLI, M. E., RASIN, M. R., SCHWARTZ, M. L., SESTAN, N. & VACCARINO, F. M. 2006. Midline radial glia translocation and corpus callosum formation require FGF signaling. *Nature Neuroscience,* 9**,** 787-797.

SOROKIN, S. 1962. Centrioles and Formation of Rudimentary Cilia by Fibroblasts and Smooth Muscle Cells. *Journal of Cell Biology,* 15**,** 363-&.

SPASSKY, N., HAN, Y. G., AGUILAR, A., STREHL, L., BESSE, L., LACLEF, C., ROS, M. R., GARCIA-VERDUGO, J. M. & ALVAREZ-BUYLLA, A. 2008. Primary cilia are required for cerebellar development and Shh-dependent expansion of progenitor pool. *Developmental Biology,* 317**,** 246-259.

SPEKTOR, A., TSANG, W. Y., KHOO, D. & DYNLACHT, B. D. 2007. Cep97 and CP110 suppress a cilia assembly program. *Cell,* 130**,** 678-690.

SPENCER, M., DETWILER, P. B. & BUNTMILAM, A. H. 1988. Distribution of Membrane-Proteins in Mechanically Dissociated Retinal Rods. *Investigative Ophthalmology & Visual Science,* 29**,** 1012-1020.

STEPHEN, L. A., DAVIS, G. M., MCTEIR, K. E., JAMES, J., MCTEIR, L., KIERANS, M., BAIN, A. & DAVEY, M. G. 2013. Failure of centrosome migration causes a loss of motile cilia in talpid(3) mutants. *Developmental Dynamics,* 242**,** 923-931.

STERNBERG, N., HAMILTON, D. & HOESS, R. 1981. Bacteriophage-P1 Site-Specific Recombination .2. Recombination between Loxp and the Bacterial Chromosome. *Journal of Molecular Biology,* 150**,** 487-507.

STOTTMANN, R. W., TRAN, P. V., TURBE-DOAN, A. & BEIER, D. R. 2009. Ttc21b is required to restrict sonic hedgehog activity in the developing mouse forebrain. *Developmental Biology,* 335**,** 166-178.

STURROCK, R. R. 1980. Myelination of the mouse corpus callosum. *Neuropathol Appl Neurobiol,* 6**,** 415-20.

SUBRAMANIAN, V., CRABTREE, B. & ACHARYA, K. R. 2008. Human angiogenin is a neuroprotective factor and amyotrophic lateral sclerosis associated angiogenin variants affect neurite extension/pathfinding and survival of motor neurons. *Human Molecular Genetics,* 17**,** 130-149.

SUN, T., WANG, X. J., XIE, S. S., ZHANG, D. L., WANG, X. P., LI, B. Q., MA, W. & XIN, H. 2011. A comparison of proliferative capacity and passaging potential between neural stem and progenitor cells in adherent and neurosphere cultures. *International Journal of Developmental Neuroscience,* 29**,** 723-731.

SZYMANSKA, K., HARTILL, V. L. & JOHNSON, C. A. 2014. Unraveling the genetics of Joubert and Meckel-Gruber syndromes. *J Pediatr Genet,* 3**,** 65-78.

TAKEDA, S., YONEKAWA, Y., TANAKA, Y., OKADA, Y., NONAKA, S. & HIROKAWA, N. 1999. Left-right asymmetry and kinesin superfamily protein KIF3A: New insights in determination of laterality and mesoderm induction by kif3A(-/-) mice analysis. *Journal of Cell Biology,* 145**,** 825-836.

TAKEMOTO, D. J. & CUNNICK, J. M. 1990. Visual Transduction in Rod Outer Segments. *Cellular Signalling,* 2**,** 99-104.

TANG, Z. M., LIN, M. G., STOWE, T. R., CHEN, S., ZHU, M. Y., STEARNS, T., FRANCO, B. & ZHONG, Q. 2013. Autophagy promotes primary ciliogenesis by removing OFD1 from centriolar satellites. *Nature,* 502**,** 254-+.

TANOS, B. E., YANG, H. J., SONI, R., WANG, W. J., MACALUSO, F. P., ASARA, J. M. & TSOU, M. F. B. 2013. Centriole distal appendages promote membrane docking, leading to cilia initiation. *Genes & Development,* 27**,** 163-168.

TEILMANN, S. C. & CHRISTENSEN, S. T. 2005. Localization of the angiopoietin receptors Tie-1 and Tie-2 on the primary cilia in the female reproductive organs. *Cell Biology International,* 29**,** 340-346.

TEIXEIRA, C. M., KRON, M. M., MASACHS, N., ZHANG, H., LAGACE, D. C., MARTINEZ, A., REILLO, I., DUAN, X., BOSCH, C., PUJADAS, L., BRUNSO, L., SONG, H., EISCH, A. J., BORRELL, V., HOWELL, B. W., PARENT, J. M. & SORIANO, E. 2012. Cell-autonomous inactivation of the reelin pathway impairs adult neurogenesis in the hippocampus. *J Neurosci,* 32**,** 12051-65.

THAUVIN-ROBINET, C., LEE, J. S., LOPEZ, E., HERRANZ-PEREZ, V., SHIDA, T., FRANCO, B., JEGO, L., YE, F., PASQUIER, L., LOGET, P., GIGOT, N., ARAL, B., LOPES, C. A. M., ST-ONGE, J., BRUEL, A. L., THEVENON, J., GONZALEZ-GRANERO, S., ALBY, C., MUNNICH, A., VEKEMANS, M., HUET, F., FRY, A. M., SAUNIER, S., RIVIERE, J. B., ATTIE-BITACH, T., GARCIA-VERDUGO, J. M., FAIVRE, L., MEGARBANE, A. & NACHURY, M. V. 2014. The oral-facial-digital syndrome gene C2CD3 encodes a positive regulator of centriole elongation. *Nature Genetics,* 46**,** 905-911.

THIEL, A. T., BLESSINGTON, P., ZOU, T., FEATHER, D., WU, X. J., YAN, J. Z., ZHANG, H., LIU, Z. G., ERNST, P., KORETZKY, G. A. & HUA, X. X. 2010. MLL-AF9-Induced Leukemogenesis Requires Coexpression of the Wild-Type Mll Allele. *Cancer Cell,* 17**,** 148-159.

THOMAS, K. R. & CAPECCHI, M. R. 1990. Targeted Disruption of the Murine Int-1 Protooncogene Resulting in Severe Abnormalities in Midbrain and Cerebellar Development. *Nature,* 346**,** 847-850.

THOMAS, S., LEGENDRE, M., SAUNIER, S., BESSIERES, B., ALBY, C., BONNIERE, M., TOUTAIN, A., LOEUILLET, L., SZYMANSKA, K., JOSSIC, F., GAILLARD, D., YACOUBI, M. T., MOUGOU-ZERELLI, S., DAVID, A., BARTHEZ, M. A., VILLE, Y., BOLE-FEYSOT, C., NITSCHKE, P., LYONNET, S., MUNNICH, A., JOHNSON, C. A., ENCHA-RAZAVI, F., CORMIER-DAIRE, V., THAUVIN-ROBINET,

C., VEKEMANS, M. & ATTIE-BITACH, T. 2012. TCTN3 mutations cause Mohr-Majewski syndrome. *Am J Hum Genet,* 91**,** 372-8.

TISSIR, F., QU, Y. B., MONTCOUQUIOL, M., ZHOU, L. B., KOMATSU, K., SHI, D. B., FUJIMORI, T., LABEAU, J., TYTECA, D., COURTOY, P., POUMAY, Y., UEMURA, T. & GOFFINET, A. M. 2010. Lack of cadherins Celsr2 and Celsr3 impairs ependymal ciliogenesis, leading to fatal hydrocephalus. *Nature Neuroscience,* 13**,** 700-U71.

TONG, C., HAN, Y., SHAH, J., OBERNIER, K., GUINTO, C., ALVAREZ-BUYLLA, A. 2014.Primary cilia are required in a unique subpopulation of neural progenitors. *PNAS,* 111, 12438–12443.

TOWN, T., BREUNIG, J. J., SARKISIAN, M. R., SPILIANAKIS, C., AYOUB, A. E., LIU, X. X., FERRANDINO, A. F., GALLAGHER, A. R., LI, M. O., RAKIC, P. & FLAVELL, R. A. 2008. The stumpy gene is required for mammalian ciliogenesis. *Proceedings of the National Academy of Sciences of the United States of America,* 105**,** 2853-2858.

TRAIFFORT, E., ANGOT, E. & RUAT, M. 2010. Sonic Hedgehog signaling in the mammalian brain. *Journal of Neurochemistry,* 113**,** 576-590.

TROMBLY, D. J., WOODRUFF, T. K. & MAYO, K. E. 2009. Suppression of Notch signaling in the neonatal mouse ovary decreases primordial follicle formation. *Endocrinology,* 150**,** 1014-24.

TRONCHE, F., KELLENDONK, C., KRETZ, O., GASS, P., ANLAG, K., ORBAN, P. C., BOCK, R., KLEIN, R. & SCHUTZ, G. 1999. Disruption of the glucocorticoid receptor gene in the nervous system results in reduced anxiety. *Nature Genetics,* 23**,** 99-103.

TRUETT, G. E., HEEGER, P., MYNATT, R. L., TRUETT, A. A., WALKER, J. A. & WARMAN, M. L. 2000. Preparation of PCR-quality mouse genomic DNA with hot sodium hydroxide and tris (HotSHOT). *Biotechniques,* 29**,** 52, 54.

TSANG, W. Y., BOSSARD, C., KHANNA, H., PERAENEN, J., SWAROOP, A., MALHOTRA, V. & DYNLACHT, B. D. 2008. CP110 suppresses primary cilia formation through its interaction with CEP290, a protein deficient in human ciliary disease. *Developmental Cell,* 15**,** 187-197.

TSUKIYAMA, T. & YAMAGUCHI, T. P. 2012. Mice lacking Wnt2b are viable and display a postnatal olfactory bulb phenotype. *Neuroscience Letters,* 512**,** 48-52.

TUKACHINSKY, H., LOPEZ, L. V. & SALIC, A. 2010. A mechanism for vertebrate Hedgehog signaling: recruitment to cilia and dissociation of SuFu-Gli protein complexes. *J Cell Biol,* 191**,** 415-28.

TUSON, M., HE, M., ANDERSON, K., 2011. Protein kinase A acts at the basal body of the primary cilium to prevent Gli2 activation and ventralization of the mouse neural tube. *Development*, 138, 4921-30.

UEMURA, M., REFAAT, M. M., SHINOYAMA, M., HAYASHI, H., HASHIMOTO, N. & TAKAHASHI, J. 2010. Matrigel Supports Survival and Neuronal Differentiation of Grafted Embryonic Stem Cell-Derived Neural Precursor Cells. *Journal of Neuroscience Research,* 88**,** 542-551.

UETAKE, Y. & SLUDER, G. 2010. Prolonged Prometaphase Blocks Daughter Cell Proliferation Despite Normal Completion of Mitosis. *Current Biology,* 20**,** 1666-1671.

VALENTE, E. M., ROSTI, R. O., GIBBS, E. & GLEESON, J. G. 2014. Primary cilia in neurodevelopmental disorders. *Nature Reviews Neurology,* 10**,** 27-36.

VALENTE, E. M., SILHAVY, J. L., BRANCATI, F., BARRANO, G., KRISHNASWAMI, S. R., CASTORI, M., LANCASTER, M. A., BOLTSHAUSER, E., BOCCONE, L., AL-GAZALI, L., FAZZI, E., SIGNORINI, S., LOUIE, C. M., BELLACCHIO, E., BERTINI, E., DALLAPICCOLA, B., GLEESON, J. G. & GRP, J. S. 2006. Mutations in CEP290, which encodes a centrosomal protein, cause pleiotropic forms of Joubert syndrome. *Nature Genetics,* 38**,** 623-625.

VALENTINE, J. M. L. V. 2010. *Dicer and Nestin-Cre are linked on mouse chromosome 12* [Online]. The Jackson Laboratory, Maine. Available: http://jaxmice.jax.org/literature/003771_FISH_analysis.pdf.

VESCOVI, A. L., REYNOLDS, B. A., FRASER, D. D. & WEISS, S. 1993. Bfgf Regulates the Proliferative Fate of Unipotent (Neuronal) and Bipotent (Neuronal Astroglial) Egf-Generated Cns Progenitor Cells. *Neuron,* 11**,** 951-966.

VICARIO-ABEJON, C., JOHE, K. K., HAZEL, T. G., COLLAZO, D. & MCKAY, R. D. 1995. Functions of basic fibroblast growth factor and neurotrophins in the differentiation of hippocampal neurons. *Neuron,* 15**,** 105-14.

WALLACE, V. A. 1999. Purkinje-cell-derived Sonic hedgehog regulates granule neuron precursor cell proliferation in the developing mouse cerebellum. *Current Biology,* 9**,** 445-448.

WANG, B. L., FALLON, J. F. & BEACHY, P. A. 2000. Hedgehog-regulated processing of Gli3 produces an anterior/posterior repressor gradient in the developing vertebrate limb. *Cell,* 100**,** 423-434.

WANG, H., GE, G. N., UCHIDA, Y., LUU, B. & AHN, S. 2011. Gli3 Is Required for Maintenance and Fate Specification of Cortical Progenitors. *Journal of Neuroscience,* 31**,** 6440-6448.

WANG, V. Y. & ZOGHBI, H. Y. 2001. Genetic regulation of cerebellar development. *Nature Reviews Neuroscience,* 2**,** 484-491.

WATERS, A. M. & BEALES, P. L. 2011. Ciliopathies: an expanding disease spectrum. *Pediatric Nephrology,* 26**,** 1039-1056.

WEATHERBEE, S. D., NISWANDER, L. A. & ANDERSON, K. V. 2009. A mouse model for Meckel syndrome reveals Mks1 is required for ciliogenesis and Hedgehog signaling. *Human Molecular Genetics,* 18**,** 4565-4575.

WECHSLER-REYA, R. J. & SCOTT, M. P. 1999. Control of neuronal precursor proliferation in the cerebellum by sonic hedgehog. *Neuron,* 22**,** 103-114.

WEISS, K. H., JOHANSSEN, C., TIELSCH, A., HERZ, J., DELLER, T., FROTSCHER, M. & FORSTER, E. 2003. Malformation of the radial glial scaffold in the dentate gyrus of reeler mice, scrambler mice, and ApoER2/VLDLR-deficient mice. *Journal of Comparative Neurology,* 460**,** 56-65.

WEN, X., LAI, C. K., EVANGELISTA, M., HONGO, J. A., DE SAUVAGE, F. J. & SCALES, S. J. 2010. Kinetics of hedgehog-dependent full-length Gli3 accumulation in primary cilia and subsequent degradation. *Mol Cell Biol,* 30**,** 1910-22.

WILLAREDT, M. A., HASENPUSCH-THEIL, K., GARDNER, H. A. R., KITANOVIC, I., HIRSCHFELD-WARNEKEN, V. C., GOJAK, C. P., GORGAS, K., BRADFORD, C. L., SPATZ, J., WOLFL, S., THEIL, T. & TUCKER, K. L. 2008. A Crucial Role for Primary Cilia in Cortical Morphogenesis. *Journal of Neuroscience,* 28**,** 12887-12900.

WILSON, S. L., WILSON, J. P., WANG, C. B., WANG, B. L. & MCCONNELL, S. K. 2012. Primary cilia and Gli3 activity regulate cerebral cortical size. *Developmental Neurobiology,* 72**,** 1196-1212.

WINGATE, R. J. T. & HATTEN, M. E. 1999. The role of the rhombic lip in avian cerebellum development. *Development,* 126**,** 4395-4404.

WOODHEAD, G. J., MUTCH, C. A., OLSON, E. C. & CHENN, A. 2006. Cell-autonomous beta-catenin signaling regulates cortical precursor proliferation. *Journal of Neuroscience,* 26**,** 12620-12630.

WU, C. Q., YANG, M., LI, J., WANG, C. B., CAO, T., TAO, K. X. & WANG, B. L. 2014. Talpid3-Binding Centrosomal Protein Cep120 Is Required for Centriole Duplication and Proliferation of Cerebellar Granule Neuron Progenitors. *Plos One,* 9.

WU, J., DU, H., WANG, X., MEI, C., SIECK, G. C. & QIAN, Q. 2009a. Characterization of primary cilia in human airway smooth muscle cells. *Chest,* 136**,** 561-70.

WURST, W. & BALLY-CUIF, L. 2001. Neural plate patterning: Upstream and downstream of the isthmic organizer. *Nature Reviews Neuroscience,* 2**,** 99-108.

XIE, Z., MOY, L. Y., SANADA, K., ZHOU, Y., BUCHMAN, J. J. & TSAI, L. H. 2007. Cep120 and TACCs control interkinetic nuclear migration and the neural progenitor pool. *Neuron,* 56**,** 79-93.

XU, H. W., YANG, Y., TANG, X. T., ZHAO, M. N., LIANG, F. C., XU, P., HOU, B. K., XING, Y., BAO, X. H. & FAN, X. T. 2013. Bergmann Glia Function in Granule Cell Migration During Cerebellum Development. *Molecular Neurobiology,* 47**,** 833-844.

YADAV, S., PURI, S. & LINSTEDT, A. D. 2009. A Primary Role for Golgi Positioning in Directed Secretion, Cell Polarity, and Wound Healing. *Molecular Biology of the Cell,* 20**,** 1728-1736.

YE, X., ZENG, H. Q., NING, G., REITER, J. F. & LIU, A. M. 2014. C2cd3 is critical for centriolar distal appendage assembly and ciliary vesicle docking in mammals. *Proceedings of the National Academy of Sciences of the United States of America,* 111**,** 2164-2169.

YIN, Y. L., BANGS, F., PATON, I. R., PRESCOTT, A., JAMES, J., DAVEY, M. G., WHITLEY, P., GENIKHOVICH, G., TECHNAU, U., BURT, D. W. & TICKLE, C. 2009. The Talpid3 gene (KIAA0586) encodes a centrosomal protein that is essential for primary cilia formation. *Development,* 136**,** 655-664.

YOSHIMURA, S., EGERER, J., FUCHS, E., HAAS, A. K. & BARR, F. A. 2007. Functional dissection of Rab GTPases involved in primary cilium formation. *Journal of Cell Biology,* 178**,** 363-369.

YU, T. A., YAGUCHI, Y., ECHEVARRIA, D., MARTINEZ, S. & BASSON, M. A. 2011. Sprouty genes prevent excessive FGF signalling in multiple cell types throughout development of the cerebellum. *Development,* 138**,** 2957-2968.

YUSA, K., RAD, R., TAKEDA, J. & BRADLEY, A. 2009. Generation of transgene-free induced pluripotent mouse stem cells by the piggyBac transposon. *Nat Methods,* 6**,** 363-9.

ZHANG, X. M., NG, A. H., TANNER, J. A., WU, W. T., COPELAND, N. G., JENKINS, N. A. & HUANG, J. D. 2004. Highly restricted expression of Cre recombinase in cerebellar Purkinje cells. *Genesis,* 40**,** 45-51.

ZHAO, C., DENG, W. & GAGE, F. H. 2008. Mechanisms and functional implications of adult neurogenesis. *Cell,* 132**,** 645-60.

ZHOU, C. J., BORELLO, U., RUBENSTEIN, J. L. R. & PLEASURE, S. J. 2006. Neuronal production and precursor proliferation defects in the neocortex of mice with loss of function in the canonical Wnt signaling pathway. *Neuroscience,* 142**,** 1119-1131.

ZHOU, C. J., ZHAO, C. J. & PLEASURE, S. J. 2004. Wnt signaling mutants have decreased dentate granule cell production and radial glial scaffolding abnormalities. *Journal of Neuroscience,* 24**,** 121-126.

ZHU, D., SHI, S., WANG, H. Z. & LIAO, K. 2009. Growth arrest induces primary-cilium formation and sensitizes IGF-1-receptor signaling during differentiation induction of 3T3-L1 preadipocytes. *Journal of Cell Science,* 122**,** 2760-2768.

ZHUO, L., THEIS, M., ALVAREZ-MAYA, I., BRENNER, M., WILLECKE, K. & MESSING, A. 2001. hGFAP-cre transgenic mice for manipulation of glial and neuronal function in vivo. *Genesis,* 31**,** 85-94.

ZIMMERMAN, L., PARR, B., LENDAHL, U., CUNNINGHAM, M., MCKAY, R., GAVIN, B., MANN, J,. VASSILEVA, G., MCMAHON, A., 1994. Independent regulatory elements in the nestin gene direct transgene expression to neural stem cells or muscle precursors. *Neuron*, 12, 11−24.